BESIEGING THE BIOFILM: **POLYMER-BASED SYSTEMS TO COMBAT** PATHOGENIC BIOFILMS **RADBOUD** UNIVERSITY

Institute for Molecules and Materials

BELA BENJAMIN BERKING

Radboud Dissertation Series

Besieging the Biofilm: Polymer-based Systems to Combat Pathogenic Biofilms

Bela Benjamin Berking

Bela B. Berking

Besieging the Biofilm: Polymer-based Systems to Combat Pathogenic Biofilms

Radboud Dissertation Series

ISSN: 2950-2772 (Online); 2950-2780 (Print)

Published by RADBOUD UNIVERSITY PRESS Postbus 9100, 6500 HA Nijmegen, The Netherlands www.radbouduniversitypress.nl

Design: Proefschrift AIO | Annelies Lips

Cover: Bela B. Berking

Printing: DPN Rikken/Pumbo

ISBN: 9789465150260

DOI: 10.54195/9789465150260

Free download at: https://doi.org/10.54195/9789465150260

© 2025 Bela Benjamin Berking

RADBOUD UNIVERSITY PRESS

This is an Open Access book published under the terms of Creative Commons Attribution-Noncommercial-NoDerivatives International license (CC BY-NC-ND 4.0). This license allows reusers to copy and distribute the material in any medium or format in unadapted form only, for noncommercial purposes only, and only so long as attribution is given to the creator, see http://creativecommons.org/licenses/by-nc-nd/4.0/.

Besieging the Biofilm:

Polymer-based Systems to Combat Pathogenic Biofilms

Proefschrift ter verkrijging van de graad van doctor
aan de Radboud Universiteit Nijmegen
op gezag van de rector magnificus prof. dr. J.M. Sanders,
volgens besluit van het college voor promoties
in het openbaar te verdedigen op

maandag 17 maart 2025 om 12.30 uur precies

door

Bela Benjamin Berking

geboren op 9 december 1995 in Evanston, Verenigde Staten

Promotoren:

Prof. dr. D.A. Wilson

Prof. dr. L.A.M.P van Niftrik

Manuscriptcommissie:

Prof. dr. W.T.S. Huck

Dr. R.S. Jansen

Prof. dr. P.Y.W. Dankers (Technische Universiteit Eindhoven)

Besieging the Biofilm:

Polymer-based Systems to Combat Pathogenic Biofilms

Dissertation to obtain the degree of doctor
from Radboud University Nijmegen
on the authority of the Rector Magnificus prof. dr. J.M. Sanders,
according to the decision of the Doctorate Board
to be defended in public on

Monday, March 17, 2025 at 12.30 pm

by

Bela Benjamin Berking

born on December 9, 1995 In Evanston, United States

Supervisors:

Prof. dr. D.A. Wilson

Prof. dr. L.A.M.P. van Niftrik

Manuscript Committee:

Prof. dr. W.T.S. Huck

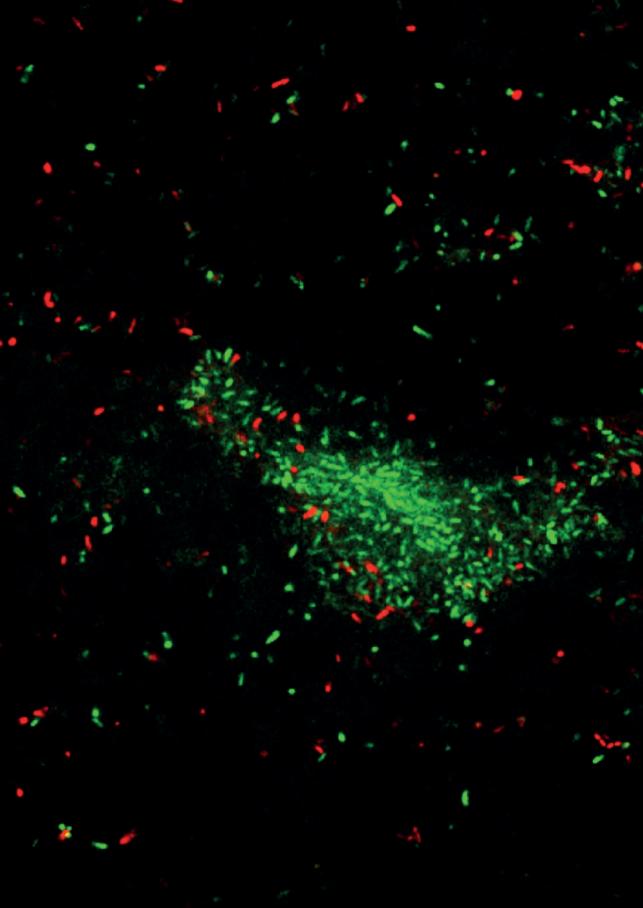
Dr. R.S. Jansen

Prof. dr. P.Y.W. Dankers (Eindhoven University of Technology)

Table of contents

Chapter 1 Bacterial Biofilms and the Many Ways to Combat them	11					
1.1 Biofilms in nature	13					
1.2 Composition of Bacterial Biofilms						
1.3 Quorum Sensing						
1.4 Stages of Biofilm Formation						
1.5 Surface coatings as Antifouling agents						
1.6 Nanoparticle-based strategies to combat biofilms						
1.7 Light-driven Molecular Rotors						
1.8 Thesis Outline						
1.9 References	34					
Chapter 2 Zwitterionic Polymeric Ylides with Minimal Charge Separation						
open a New Generation of Antifouling and Bactericidal Materials	45					
2.1 Introduction	47					
2.2 Results and Discussion	49					
2.3 Conclusion						
2.4 Acknowledgments	63					
2.5 Experimental and Supplementary Information						
2.6 References	75					
Chapter 3 Porous Polymersomes as Carriers for Silver Nanoparticles						
and Nanoclusters: Advantages of Compartmentalization for						
Antimicrobial Usage	79					
3.1 Introduction	81					
3.2 Results and Discussion						
3.3 Conclusion	90					
3.4 Materials and Methods	91					
3.5 Acknowledgements	94					
3.6 References	95					
3.7 Supplementary Information						

Chapter 4 Biofilm Disruption from Within: Light-activated Molecular					
Drill functionalized Polymersomes bridge the gap between					
Membrane Damage and Quorum Sensing mediated Cell Death	105				
4.1 Introduction	107				
4.2 Results and Discussion					
4.3 Conclusion					
4.4 Experimental Section					
4.5 References					
4.6 Supplementary Introduction	127				
Chapter 5 Quorum Sensing lights the way: Chemotactic Nanomotors					
target biofilms via quorum-quenching mechanism	135				
5.1 Introduction					
5.2 Results and Discussion					
5.4 Material and Methods					
5.5 References	148				
5.6 Supporting Information	151				
Chapter 6 Summary and Perspectives	153				
6.1 Summary					
6.2 Perspective					
6.3 References	158				
Appendices					
Acknowledgments	162				
List of Publications	164				
Research and Data management	165				
About the Author	166				



Chapter 1

Bacterial Biofilms and the Many Ways to Combat them

Bela B. Berking, Jenny Dammer, Daniela Wilson

Institude for Molecules and Materials, Radboud University, Heyendaalseweg 135, 6525 AJ, Nijmegen, Netherlands

Abstract

Bacterial Biofilms have become the leading cause of infections in hospitals, with as much as 80% of infections stemming from a biofilm. Growing on medical devices, catheters, ventilators, implants, and every surface possible, biofilms create infectious reservoirs, leading to higher mortality rates, prolonged hospital stays, and increased costs. This review focuses on highlighting important mechanisms of bacterial biofilms, discussing the composition, signaling systems, and maturation stages linked to surface adhesion, to put into perspective the many ways one can combat biofilms with tailored approaches, inhibiting communication, disrupting the building blocks, and many more. We then discuss nanoparticle-based systems, focusing on stimuli-responsive nanoparticles, which use various triggers to deploy cargo or emit antimicrobial functions, and motion-depicting systems to eradicate biofilms. By tuning the building blocks, properties, and functionalities of a system, we aim to battle biofilms using smart polymer-based systems.

1.1 Biofilms in nature

Biofilms have always accompanied humans as part of daily life, whether it is between the teeth or on the tongue, as Leeuwenhoek saw them or in aged wine, described by Pasteur, yet it was not even one hundred years ago that the term, biofilm was coined. Now, estimates range that around 90% of all microbial life resides in this organized clump of mass and cells, both in the environment and the host. Biofilms have since gained great attention in the medical field, due to their challenging treatment and difficulty to eradicate fully. Accompanying increases in antibiotic resistance have put pressure on researchers to find new solutions for efficient treatment and prevention of biofilms.

1.2 Composition of Bacterial Biofilms

Bacterial biofilms consist of bacteria embedded in their self-produced extracellular matrix (ECM). This matrix has been shown to consist of a range of biomolecules such as proteins, extracellular DNA (eDNA), polysaccharides, and active enzymes, all collectively contributing to the structural integrity of the biofilm and the protection of it from external factors such as the host immune system or bacteriophage attacks (Figure 1A and B) 1,2. Design of novel biofilm targeting strategies is therefore tasked with overcoming this multifaceted barrier. ECM production is affected by transcriptional regulators as well as external factors, making the ECM a malleable and versatile system able to adapt easily. In P. aeruginosa, ECM production has been linked to three key regulators: the guorum sensing apparatus, c-di-GMP signaling, and small non-coding RNAs, each responsible for the production and secretion of rhamnolipids and eDNA, adhesins, and exopolysaccharides or the inhibition of exopolysaccharide synthesis ^{3, 4}. All these components have various shielding effects: eDNA shielding the biofilm from antimicrobial peptides and cationic antimicrobials 5-7, exopolysaccharides like Pel protecting from enzymatic degradation of the biofilm 8 and proteins effectively repelling silver ions 9.

The importance of all these components to the structural integrity and function of the biofilm becomes evident when exploring strategies for degrading these building blocks as an approach to combat biofilms 10. By using enzymes many vital components can be degraded, such as eDNA via DNase, which has proven to significantly reduce and disperse biofilms and increase antibiotic susceptibility 11, 12. Disturbing protein-mediated cell adhesion via enzymatic protein degradation by proteases has been an effective tool in inhibiting bacterial cell adhesion but was also shown to disrupt matured biofilms and resensitize tolerant strains to antibiotics 13-15. Many different glycoside hydrolases have been investigated for their effectiveness in cleaving exopolysaccharides present in biofilms. Application of such enzymes in vivo studies degraded biofilms and even boosted the immune defense and susceptibility to Colistin. 16, 17

Bacteria residing in biofilms have come up with strategies to fortify the biofilm in various scenarios, to create the impenetrable fortress the biofilm is often compared to. One such mechanism is biofilm formation and fortification via bacterial lysis, regulated either by autolysis or prophage induction to release eDNA, which is a vital component of biofilms ¹⁸⁻²¹. This type of eDNA release has been shown to be activated under factors such as DNA-damaging agents, high-intensity light, and mechanical damage 18, 22-24. Recent advances in understanding the underlying mechanisms controlling this phenomenon have revealed these responses to be tied to quorum sensing, where the cell density-dependent signaling can control lysis events ²⁵.

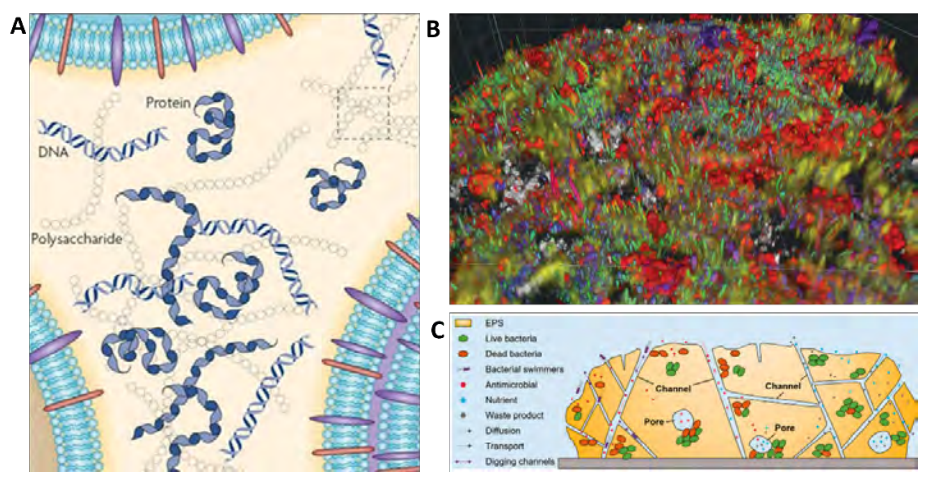


Figure 1. Complexity of biofilm components. A. Schematic overview of the most prominent building blocks, DNA, proteins, and polysaccharides, reprinted with permission 31. Copyright 2010 Springer Nature. B. Confocal microscopy of a river biofilm showcasing the heterogeneity of all the building blocks by imaging of DNA (green), phototrophic microorganisms((blue/purple), glycoconjugates (yellow), polysaccharides (white), and mineral reflections (white), reprinted with permission 32. Copyright 2022 Springer Nature, C. Schematic overview of the different channels and pores found inside biofilms with a heterogeneous population spread amongst them. Channels are facilitated by swimmer bacteria and lined with rhamnolipids to hinder the regrowth of bacteria on them, reprinted with permission ²⁷. Copyright 2021, Informa UK Limited.

All components put together create an intricate network of channels and pores to facilitate water, nutrients, and oxygen flow into the deeper layers of the biofilm ²⁶ ²⁷.

Infiltration of biofilms through these channels is mostly limited to particle sizes of around 100 nm ²⁸ ²⁹, yet large channels of up to 10 µm have been found to stretch through the ECM (Figure 1C) 30.

As the biofilm grows and expands, its population within it becomes more and more heterogeneous, with gradients throughout the biofilm being created, such as anaerobic zones and areas without nutrient availability in the center, facilitating bacterial subpopulations with a vastly different metabolic and genetic profile than those found towards the outside of the biofilm ³³ ³⁴. Other gradients include a more acidic pH as well as an increase in quorum-sensing molecules in the center of the biofilm 35, 36. Further growth and complexity require an apparatus to control the overall population.

1.3 Quorum Sensing

The dynamic processes occurring in the biofilm as well as the ever-shifting heterogeneity and growth of the biofilm population in parts is steered by a process called quorum sensing 37, 38. This process is defined as the usage of small diffusible chemical signaling molecules, referred to as autoinducers (Als), for the coordination of f.e. dispersion of the biofilm, adapting of metabolic activity, and increasing the bacterial population 39 40. Various types of guorum sensing machineries exist in different bacterial species: The homoserine-lactone system dominates in Gram-negative bacteria while autoinducing peptides prevail in Gram-positive bacteria 41. Reaching specific thresholds of these molecules leads to the control of gene expression and the henceforth up- or downregulation of target genes 42. Demonstrating the hierarchical manner in which the quorum sensing system functions, P. aeruginosa has become the model organism, where four interconnected systems, namely las, rhl, (Pseudomonas quinolone signal) pgs, and igs stand 43 44. At the top of this system stands LasR, which is activated by N-(3-oxododecanoyl)-homoserine lactone and subsequently activates rhl, pgs, and igs 45. At the next stage of the regulatory hierarchy comes RhIR, which steers the production of N-butyryl-homoserine lactone (C4-HSL) by Rhll. RhlR has an inhibitory effect on the pgs system, while LasR upregulates it (Figure 2). This puts the pqs system at an interconnective spot between the las and rhl system 46. The last signaling system, the iqs system, utilizes (2-(2-hydroxyl- phenyl)-thiazole-4carbaldehyde), synthesized by the AmbBCDE complex ⁴⁷. This system is under the control of the las regulator and can influence the activity of the pgs system.

The effects this whole interconnected apparatus has on biofilm formation, metabolic activity, and stress responses are immense. LasR has been acknowledged to be one of the main regulators in virulence factor production, by activating genes such as hemolysins, proteases, and exotoxins⁴⁸ ⁴⁹. RhIR is crucial for the production of rhamnolipids, which are key components of the biofilm and necessary for the upkeep of channels, as well as the steering of pyocyanin 50,51. PQS can induce the production of Hydrogen Cyanide, whose cyanogenic properties add to the overall virulence and induce alginate production for biofilm development 52,53.

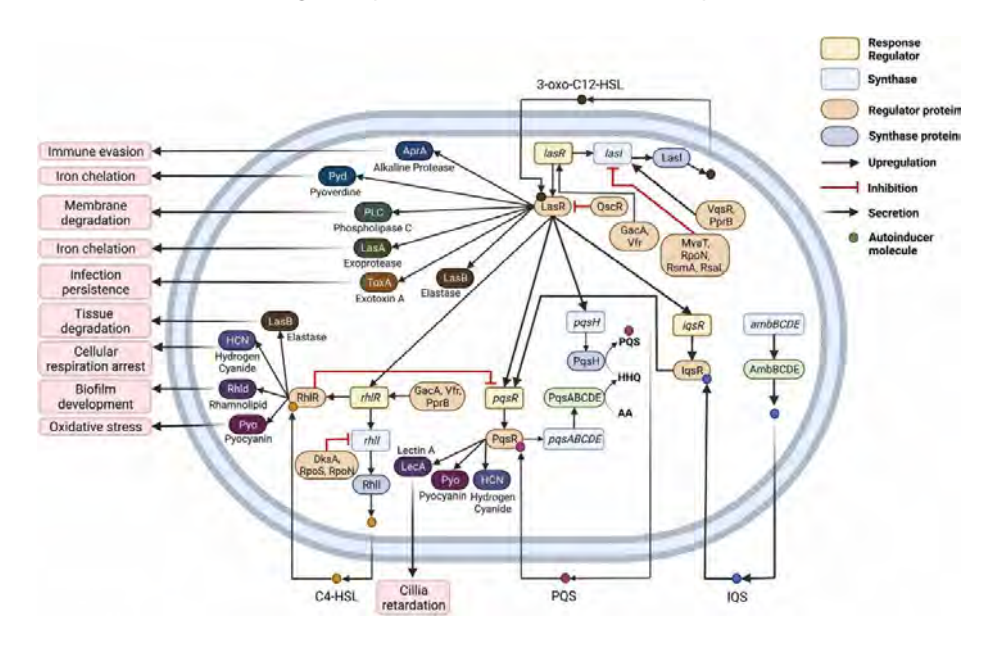


Figure 2: Hierarchical quorum sensing system in P. aeruginosa. LasR, as a key player, upregulates the Rhl, pgs, and igs system, while RhlR has an inhibitory function on pgsR. All four systems are steered by their respective autoinducing molecule, reprinted with permission ⁵⁴. Copyright (2022) Elsevier.

Quorum sensing has become one of the many approaches to tackle infectious biofilms, with three main strategies currently being investigated: inhibition of Al synthesis, degradation of Als (f.e. enzymatic degradation), or interfering and blocking signal receptors 54-56. Enzymatic degradation of Als has been extensively studied using *P. aeruginosa*, with three enzyme classes prominent in literature: AHL-acylases, AHL-lactonases, and AHL-oxidoreductase, all three of which degrade homoserine-lactone based sensing molecules ^{54, 55 57}. Since quorum quenching has been directly associated with a decrease in virulence and an increase in antibiotic susceptibility, hopes are that combining this approach with conventional antibiotics can alleviate the pressure caused by antibiotic-resistant strains 58-60.

By immobilizing the quorum quenching enzyme Acylase with a Ciprofloxacinreleasing PDA nanoparticle, the initial effects of Ciprofloxacin were enhanced, showcasing the synergistic effects of quorum quenching with antibiotics 61. In another example by Bernabè et al., the quorum-sensing inhibitor Azan-7 synergized with the antibiotic Clindamycin to restore effectiveness against methicillin-resistant Staphylococcus aureus. Incorporating quorum quenching enzymes into biofilm targeting platforms can therefore be a valuable tool to mitigate virulence factors and increase susceptibility.

1.4 Stages of Biofilm Formation

Biofilm growth has been separated into five maturation stages, with each stage displaying various phenotypes (Figure 3) 1 2. In the first stage, single cells will loosely attach to a surface, being able to reverse this attachment in case the surface is not suitable, hence the name reversible attachment 62 63. Once committed to the surface, bacteria will undergo an orientation change and lay flat on the surface losing motility and beginning with ECM production 64 65. This early stage of sessile growth has been shown to induce a multitude of genes that increase resistance to outer factors and antibiotics 66 67. Only after this step will biofilms begin to grow into a more complex three-dimensional structure, a step that is referred to as microcolony formation and is accompanied by the formation of a more heterogenous bacterial population, comprised of different levels of metabolically active cells 63 68 69. Further maturation of the biofilm can yield pillars or mushroom-like shapes and will be divided into three layers: an outer layer with planktonic cells ready to redisperse, the microbial basement layer in the middle, and a regulating layer in the center ^{69,70}. To further colonize new surfaces, biofilms will enter the last stage, the dispersion state, either actively via cells regaining motility and leaving the biofilm, or passively by shear stress through liquid flow, which will, in turn, create openings in the biofilms to facilitate better nutrient availability 71 72.

The intricacy of these steps in themselves opens possibilities for targeting specific steps of adhesion and maturation, with the most prominent one being the deterring of bacteria from initial adhesion by modifying the surface of contact.

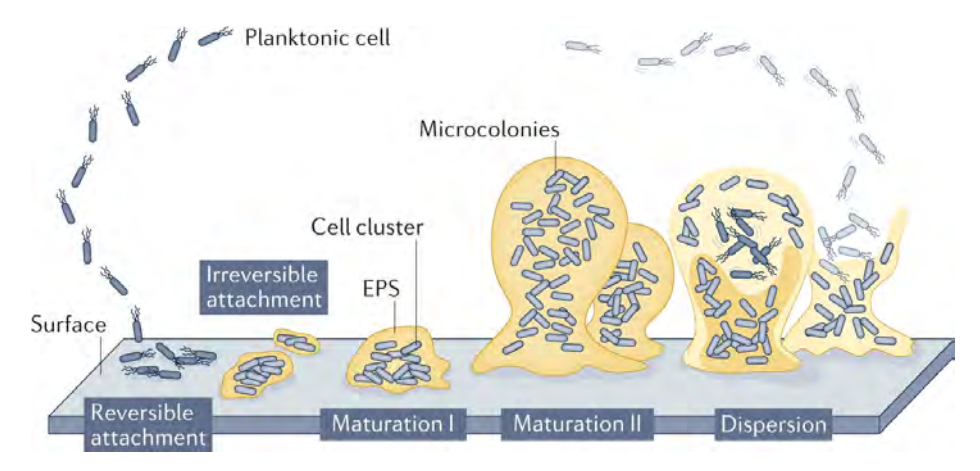


Figure 3. Maturation stages of a biofilm separated into reversible attachment, irreversible attachment which is followed by maturation stages I and II with the final step leading to the dispersion of new cells for purposes of colonizing new areas, reprinted with permission ².

1.5 Surface coatings as Antifouling agents

Fouling is described as unwanted adhesion, oftentimes referring to the adhesion of microbes, to any surface 73. It comes as no surprise that the terms "biofilm" and "film" originate from observations on ships, that after short exposures to water, a bacterial slime layer, or film, was found to develop 74. Since then, research has consistently improved its approaches to obstruct any type of fouling, be it in the shipping industry, medical implants and catheters, or medical devices. There have been three main strategies that divide approaches in antifouling research: Surface chemistry, surface topography, and surface architecture (Figure 4) 75.

These strategies have been well employed by nature all around us: blood vessels structured like cobblestones and coated in glycoproteins stop any attachment attempts 76 or pilot whale skin, with a nanoscale roughness just slightly smaller than microbial marine life, making it tough to adhere 77. Combining the strategies mentioned offers coatings the chance for multifaceted mechanisms to effectively hinder any fouling and stop biofilms from even forming.

Utilizing polymers as fouling-resistant coatings was long based on poly(ethylene glycol), which is still now considered the golden standard amongst this class, but new research is showing issues when it comes to immunogenic responses and stability issues caused by autoxidation 78 79 80.

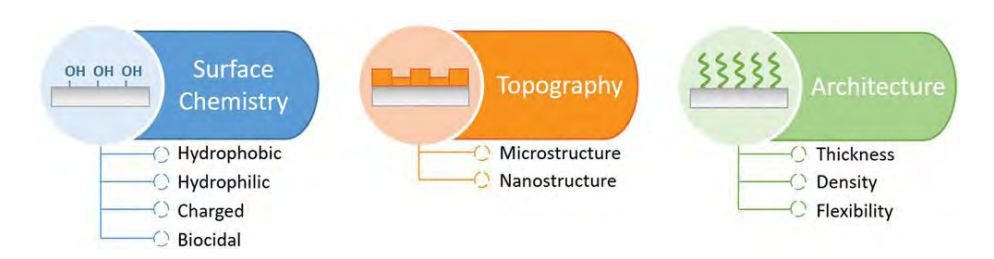


Figure 4. Strategies to create antifouling surface coatings, by changing the surface chemistry, topography, or architecture, adapted from Maan et al. 75.

Zwitterionic materials are moving more into the spotlight as a new class of antifouling polymers, owing largely to their efficiency in creating hydration layers as well as tunable properties such as pH or temperature responsiveness 81,82,83. Zwitterionic polymers possess a charge-neutral ionic system, with a positive and negative charge on one monomer residue 84,85. This allows for the capturing of water molecules by stronger ion-dipole interactions, which have been shown to be stronger compared to PEG. 82 All this creates a non-desirable surface for bacteria to grow on, where initial attachment, which in part is mediated by electrostatic forces and hydrophobic interactions, parameters that are significantly hindered by zwitterionic surface coatings 86. The effectiveness of such materials is demonstrated in many examples. By mimicking a dental coating, Sun et al. fabricated a highly efficient zwitterionic poly(carboxy betaine) polymer, which inhibited the biofilm formation of common oral biofilm-forming species such as S. mutants and P. aeruginosa 87. In an attempt to combine antibiotics with a zwitterionic polymer brush, Hassani et al. found that the native brushes without antibiotics had significantly better antifouling effectiveness, showing that these types of coating by themselves offer a great platform to deter biofilm growth and stop subsequent infections 88.

1.6 Nanoparticle-based strategies to combat biofilms

Treating established biofilms has become a great challenge in the medical field due to their obstinance and intrinsic resistance 89. Biofilms as a cause for infections make up around 80% of infections and can occur on any tissue, implant, or wound ⁹⁰ ⁹¹. Common antibiotics often fail at fully eradicating biofilms due to the specific mode of action, which gives bacteria a high selective pressure to form resistance.

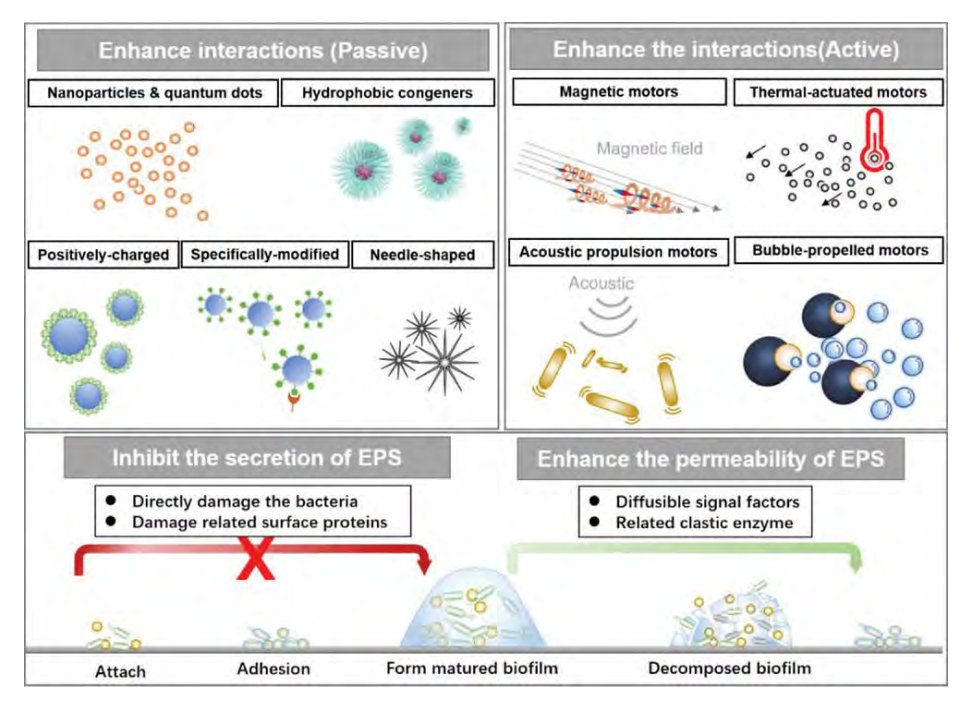


Figure 5. The versatility of nanoparticle systems to combat biofilms. Strategies range from passively diffusing nanoparticles to active motion displaying nanomotors, reprinted with permission 92. Copyright (2022) Wiley-VCH GmbH.

Many strategies using nanoparticle-based systems are emerging to effectively combat established biofilms, with great variations in complexity and size, from 10 nm silver nanoparticles to laser-propelled nanomotors (Figure 5) 93 94. The great advantage of using nanoscale structures comes with the adaptability of these, being able to functionalize parts of a nanoparticle to address various scenarios. Using stimuli-responsive systems, two types can be defined: Endogenous and exogenous stimuli-responsive systems.

Endogenous approaches

Bacterial biofilms have a specific microenvironment that differentiates from normal healthy tissue 95. This microenvironment can be used as an endogenous stimulus for controlled drug release 95,96. The most common endogenous stimuli used for antibiofilm NPs are pH and enzymes present in the ECM.

pH-Responsive Nanoparticles

Biofilms are known for their acidic microenvironment with a pH of 5.0-7.0 95. This property can serve as an endogenous trigger for drug release 97. Two types of strategies can be used: 1) drug release upon acidic cleavage and 2) protonation or deprotonation of ionizable groups 95, 98. By using acid-labile chemical bonds, such as hydrazones, acetals, orthoesters, etc., the nanoparticle is disintegrated in acidic environments leading to the release of the encapsulated antibiotic 95, 99.

An example of such pH-responsive nanocarriers is described by Raju et al. who loaded catechins onto zeolitic imidazole frameworks (ZIFs) 100. The ZIF-L framework is disintegrated due to the acidic pH which releases catechin and Zn²⁺ ions. Both have an anti-biofilm activity. Catechin is able to damage the membrane and destabilize the biofilm matrix, while the Zn²⁺ ions are able to impair the swarming ability and the production of exopolysaccharides.

Liu et al. developed mixed-shell polymeric micelles (MSPMs) with hydrophilic PEG and the charge switchable polymer ligand poly(-amino ester) 101. These MPMs have negative surface charges at neutral pH and switch to positive charges in the acidic biofilm microenvironment. This charge change allows them to penetrate and accumulate in S. aureus biofilms and leads to drug release upon attachment to the bacterial surface.

Enzyme-Responsive Nanoparticles

Besides the acidic microenvironment, bacteria also secrete specific enzymes, such as lipase, phosphatase, protease, hyaluronidase, and others 95, 99. These specific enzymes can be used to design enzyme-responsive nanocarriers which release their load upon the enzymatic degradation ¹⁰². Hyaluronic acid (HA) is often used to coat NPs and is degraded by hyaluronidases 99. Wu et al. developed hyaluronidaseresponsive NPs by coating ampicillin-loaded MSNs with lysozyme, HA, and 1,2-ethylamine-modified polyglycerol methacrylate (PGMA) 103. The ampicillin release upon HA degradation gives synergistic antibacterial activity with lysozyme and results in an accelerated wound healing of *S. aureus* infected wounds.

Another example of enzyme-responsive NPs are the lipase-responsive nanoparticles developed by Komnatnyy et al. 104. These NPs consist of an HMBA-linked ChemMatrix polymer to which they covalently bound ciprofloxacin with the use of an azelaic acid linker and were used against P. aeruginosa. The antibiotic is released upon the catalyzed hydrolysis of the anhydride bond by lipases LipA and LipC. Their study shows that these NPs can kill P. aeruginosa within a matter of hours.

Exogenous approaches

Exogenous stimuli-responsive nanoparticles respond to external triggers such as light, temperature, ultrasound, and magnetism. An advantage of these approaches is that the external stimuli are easily controlled 95. These approaches often use metallic inorganic NPs due to their unique magnetic or physicochemical properties 98.

Light-Responsive Nanoparticles

Phototherapy is one of the non-antibiotic therapies that shows great potential as a noninvasive treatment ¹⁰⁵. Several wavelengths of light are used against bacteria, which are ultraviolet (UV, 100 - 400 nm), visible (400 - 800 nm), and near-infrared (NIR, 800 – 2,500 nm) light ¹⁰². Due to the toxicity of UV light and its low tissue penetration, visible and NIR light are more attractive options 95, 106.

Shen et al. developed an amphiphilic block copolymer containing an N-nitrosaminebased nitric oxide (NO) donor for the visible light-mediated NO release 107. These nanoparticles could be co-loaded with the antibiotic ciprofloxacin to effectively eliminate P. aeruginosa biofilms. These NPs showed slow drug release without light irradiation, while this release was greatly enhanced upon irradiation with a wavelength of 410 nm. The NO release promotes the antibacterial activity of ciprofloxacin by dispersing the dense biofilm.

The nanohybrids developed by Bing et al. consist of Ag nanoparticles that are embedded into graphitic carbon nitride (g-C₂N₄) nanosheets ¹⁰⁸. On its own, the q-C₂N, nanosheets have a limited ROS generation ability upon irradiation with visible light. However, the addition of the Ag NPs enhances the photocatalytic effect by facilitating the creation of electron-hole pairs and extending the spectral absorption. These Ag/g-C₂N₄ nanohybrids were effective against *E. coli* and *S. aureus*.

Photothermal Therapy

Photothermal therapy (PTT) is a non-invasive therapeutic method that combines photothermal agents with irradiation to treat bacterial infections ^{97, 109}. NIR light is in this case employed as the preferred light source due to its deeper tissue penetrating ability ¹⁰⁵. The PTT process involves the irradiation of the photothermal agents which subsequently convert this energy into heat by non-radiative relaxation 106. The heat (~50 °C) alone is able to cause bacterial cell death by denaturing proteins on the surfaces, but it can also be used as a release mechanism when the nanoparticles consist of heat-sensitive material 102, 109. An advantage of PTT is that only a few minutes of irradiation suffices for the generation of heat required for the biofilm destruction.[4]

The thermal-responsive nanocarriers developed by Qing et al. undergo a phase change upon irradiation with a NIR laser 110. These nanocarriers use lauric acid which encapsulates the photothermal agent IR780 and the antibiotic imipenem. The phase change damages the nanocarriers which leads to the rapid release of imipenem. This therapy can eradicate MRSA at a significantly lower dose than free imipenem.

García et al. developed MSNs for the PTT against S. aureus 111. The MSNs were coated with Au nanorods which can increase the temperature upon NIR irradiation. The nanoparticles were also embedded with the antibiotic levofloxacin and nitric oxide donors via heat-liability linkers. Upon the increase of the temperature by the Au nanorods, release of levofloxacin and NO is increased, increasing the antimicrobial activity of this system 3-fold.

Photodynamic Therapy

Another light-based approach is photodynamic therapy (PDT). PDT contains three important elements: photosensitizers (PS), light, and oxygen ¹⁰⁵. Upon irradiation with the appropriate wavelength, the PSs generate cytotoxic ROS, which includes superoxides, hydroxyl radicals, and singlet oxygen 97, 109. The generated ROS is able to rapidly kill bacteria without the development of drug resistance 109. The PS-containing nanoparticles are able to improve their stability and blood circulation, which leads to an enhanced photodynamic antimicrobial effect at the infection site.[45]

Li et al. have developed a smart antimicrobial nanohybrid by encapsulating lanthanide-doped upconversion nanoparticles and a methylene blue photosensitizer in silica NPs that are coated with lysozyme and a mixture of HA and poly-L-lysine (referred to as HP), abbreviated as UCMB-LYZ-HP ¹¹². This nanohybrid involves several mechanisms that help in bacterial cell death. First, the nanohybrid is absorbed onto the bacterial surface and produces local ROS upon laser irradiation. Besides this, the HP layer is degraded which results in the release of lysozyme. They showed that this nanohybrid was an effective treatment against MRSA infections in deep tissue without side effects.

Another example of PDT is developed by Xie et al. who designed DNase functionalized Au nanoclusters for the killing of several bacterial species 113. This system is not only able to have PDT effects, but it also has PTT effects due to the presence of Au nanomaterials. Upon NIR light irradiation (808 nm), the nanoclusters are able to increase the temperature to 24.1 to 65.3 °C depending on the concentration of the nanoclusters. Upon the same irradiation, these nanoclusters are also able to produce singlet oxygen. Lastly, the DNase molecules present in the nanoclusters are able to degrade the DNA in the bacterial EPS matrix, destroying the structure of the bacterial biofilms and facilitating the access of the nanoclusters to the bacteria.

Sonodynamic therapy

Sonodynamic therapy (SDT) uses sonosensitizers that generate electron transfer upon ultrasound (US) excitement 106. The electron transfer is able to react with water and oxygen to produce ROS. Sonosensitizers are loaded into nanoparticles to improve their hydrophilicity and stability. US stimulation is able to better penetrate tissue and reduce off-target effects in comparison to light stimulation 106, making this an interesting approach for biofilm destruction.

Yu et al. developed an ultrasound-based approach for the treatment of osteomyelitis that is caused by MRSA 114. This treatment consists of an Au nanorod-actuated Pt single-atom doped porphyrin metal-organic framework with a red blood cell membrane. This complex enhances the sonocatalytic activity of porphyrin by the presence of the Au nanorod and the monoatomic Pt.

Pourhajibagher et al. developed metal oxide nanoparticles (MONPs) that have synergistic biocidal effects upon ultrasound irradiation 115. These NPs contained a mixture of ZnO and TiO₃ which produce ROS upon ultrasound irradiation. This ROS production was 2-fold higher than the homologous ZnO NPs and TiO₃ NPs in S. mutans biofilm. In addition, these NPs led to decreased cell viability, metabolic activity, gene expression levels of virulence factors, and significant inhibition in biofilm growth.

Magnetic-Responsive Nanoparticles

The last endogenous approach to consider is the one involving magnetic-responsive nanoparticles which can be controlled by an external magnetic field. There are two strategies that can be used. One is the magnetic field-induced hyperthermia for drug release, in which magnetic NPs convert the magnetic energy to heat via Neel relaxation and Brownian relaxation 102, 106. The other involves magnetic fieldguided drug targeting which is often used with superparamagnetic iron oxide NPs (SPIONs) 96, 98, 102.

Geilich et al. developed an iron oxide polymersome that co-encapsulated methicillin and hydrophobic SPIONs 116. These nanoparticles are able to penetrate 20 µm thick biofilms upon the introduction of an external magnetic field. In addition, it resulted in a selective antimicrobial activity within the desired region. These polymersomes were able to eradicate the biofilm completely at a much lower concentration than when free methicillin was used.

Li et al. developed novel magnetic nanocomposites by combining selenium (Se) NPs and iron oxide nanoparticles (IONPs) 117. In addition, chitosan was added for the stabilization of both the IONPs and the elemental selenium. The nanocomposites were able to increase the dead bacteria population in S. aureus biofilms by almost 400%, while this was only 51.6 % and 60.0% for SeNPs and IONs, respectively. The anti-biofilm mechanisms involved are the penetration into the biofilm in the presence of an external magnetic field, ROS production, and thiol depletion.

Polymers, defined as chemical compounds of repeating subunits (monomers), offer a versatile toolbox to accomplish these tasks as a platform. Creating a diblock copolymer with a hydrophilic and a hydrophobic segment will create a self-assembled supramolecular structure in an aqueous environment, such as polymersomes 118, 119. The nature of these polymersomes allows for the incorporation of chemical functional handles on the surface, hydrophilic or hydrophobic cargo embedded during the self-assembly process in the membrane spaces, or even the incorporation of other cargo via shape transformation processes 92, 120-122. The ease at which these building blocks can be manipulated and modified allows for intricate systems, such as self-assembled drug-carrying vesicles that disintegrate upon irradiation to release their cargo inside the biofilm 120, or magnetically steered polymersomes that release antibiotics deep inside the biofilm ¹¹⁶. These examples demonstrate the drive in research to create more complex systems with properties such as motile parts, shape transformation, or autonomous motion.

One of the greatest challenges in achieving efficient therapeutic effects is a high accumulation of any therapeutic at the target site. Passively diffusing particles with an antibody will eventually accumulate at the target site, yet equipping nanoparticles with the means of increased motion ups the chances of reaching the target. These so-called nanomotors utilize a fuel source to propel themselves toward a location, oftentimes moving with gradients present or via means of external steering (Figure x). Some of the most studied examples of nanomotors utilize ionic diffusiophoresis, bubble propulsion, or self-thermophoretic effects to overcome Brownian motion and display active motion 123, 124. In ionic diffusiophoresis, found when f.e. using Urease or colloidal AqCl as a motor, the products of the enzymatic reaction generate an electric and pressure gradient as a result of differential diffusion of cations and anions, which pushes the nanoparticle along it 125, 126. Bubble propulsion relies on the mere physical pressure arising from gaseous products, such as H₂ and O₂, catalyzed by enzymes such as Catalase or metals such as platinum 127, 128. Photothermal effects can also induce motion, often described with systems such as metal Janus particles. The asymmetry that occurs in these particles, f.e. a silica particle with half of it covered in an Au layer, causes localized photothermal effects under Near Infrared Light (NIR) resulting in thermal gradients 129, 130.

The conventional nanoparticles discussed above move through the body mainly via systemic circulation, but they can be guided to the infection site using different stimuli 131.

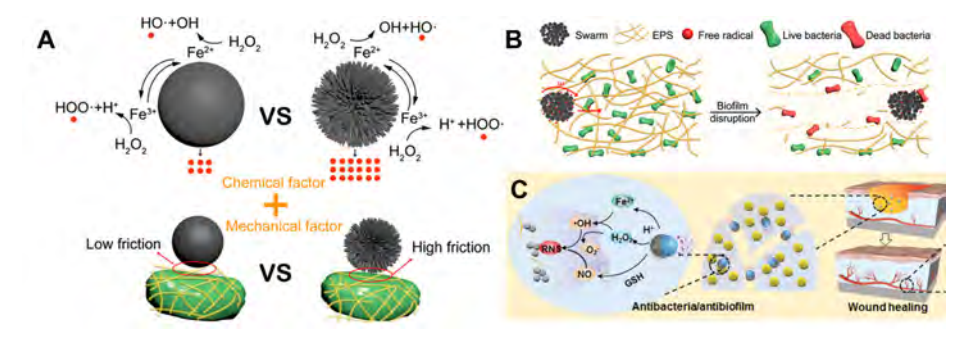


Figure 6. Strategies to combat biofilms using active motion systems. A. System design of magnetically steered nanoparticle which disrupts biofilms via a multifaceted approach (B), including breaking through the ECM and inducing ROS production, reprinted with permission ¹³². Copyright (2021) American Chemical Society. C. Overview of a biofilm penetrating Janus nanomotor, which has increased penetration into the biofilm by O₂ release from one side of the particle consisting of CaO₂, reprinted with permission ¹³³. Copyright (2022) Wiley-VCH GmbH.

(Bio) Chemical Propulsion

(Bio)chemically propelled nanoparticles mainly consist of two components: a catalyst, such as a metal or an enzyme, that is able to convert the fuel into kinetic energy via in situ reactions the inert material which provides the structure 131, 134. These self-propelled NPs generally rely on either the asymmetric surface chemical reactions or bubble formation for the autonomous movement 135. The energy for these self-propelled NPs is usually supplied by H₂O₂, NO, or molecules such as urea and glucose.

Hydrogen Peroxide as fuel

Hydrogen peroxide (H₂O₂) is one of the most extensively used fuels for self-propelled nanoparticles. ¹³⁴ With catalysts such as Au, platinum (Pt), or MnO₂) H₂O₂ is catalytically decomposed to water and oxygen bubbles 136, 137. Especially the heterogeneous catalyst MnO₂ gained scientific attention due to its catalytic activity compared to the noble metal catalyst Pt, low cost, and degradability under acidic conditions 135, 138. Even though H₂O₂ as fuel gives high propulsion speeds, its toxicity to healthy tissue limits the biomedical applications of these H₂O₂-propelled nanoparticles ^{131, 136}.

Wilson et al. designed a Pt-based nanoparticle motor that consists of a polymer stomatocyte that encapsulates Pt NPs 122. This stomatocyte structure were developed to allow for the diffusion of H₂O₂ in and out of the cavity while preventing the escape of the catalytically active Pt NPs. The Pt NPs are able to catalytically decompose H₂O₂ into water and oxygen, propelling the polymer stomatocyte into the direction opposite of the cavity opening. H₂O₂-propelled nanomotors to target biofilms as not yet been investigated.

Urea and/or Glucose as fuel

Enzyme-powered nanoparticles have gained scientific attention due to their catalytic capacity and biocompatibility of natural enzymes^{131, 139}. Mesoporous SiO₃ (mSiO₂) has emerged as a nanoparticle platform due to its rich surface properties and good biocompatibility 135. Initially, these mSiO₂ nanoparticles were anchored with catalase, an alternative for Pt and $MnO_{2^{\prime}}$ to break down $H_{2}O_{2^{\prime}}$, but the concentration of H₂O₂ still caused toxicity within healthy tissue ^{135, 138}. To divert from non-compatible fuels, they developed fully biocompatible nanoparticles based on mSiO₂ with covalently linked enzymes like glucose oxidase (GOx) and urease ^{131, 135}. GOx can be used in a binary enzyme system with catalase as glucose is converted into H₂O₂ by GOx upon which catalase converts this H₂O₂ molecule to water and oxygen for the propulsion 131, 137, 138.

Vilela et al. were able to achieve a highly efficient Urease nanomotor capable of inhibiting biofilms formation of a uropathogenic E. coli strain 140. Coupled with lysozyme, the nanomotors showed high speeds and antimicrobial effectiveness mediated by the production of bicarbonate and ammonia directly at the bacterial cell surface 140.

Nitric Oxide as fuel

Another type of fuel-propelled nanoparticles are NO-propelled NPs. The release of NO produces ROS which are able to disturb cell metabolisms and degrade the EPS of bacterial biofilms. Hence, without the need of antibiotics, NO propelled nanoparticles show excellent antibacterial activity 133.

Yu et al. developed a synergistic photothermal and NO antibacterial nanoparticles 141. This system uses a polydopamine coated iron oxide nanocomposite (Fe₃O₄@PDA) modified with three generation dendritic poly(amidoamine) that is loaded with the NO-donor N-diazeniumdiolate (NONOate). The photoconversion agent Fe₂O₂@ PDA can produce hyperthermia that subsequently accelerates the decomposition of NONOate and the release of NO. With the advantages that come with this nanocomposite, such as high bacteria-separation efficiency, synergistic photothermal and NO bactericidal effects, and photo controllable NO release, this system can efficiently eradicate E. coli and S. aureus biofilms 139, 141.

Fuel-free Propulsion

Besides (bio)chemically propelled nanoparticles, fuel-free propelled NPs have been developed which respond to an applied external field and move freely.^[61] In comparison with the (bio)chemically propelled NPs, these external-field powered NPs have several advantages including the flexible control to motion performance, biocompatibility, and selectivity to the disease site 131, 135, 138. The fuel-free NPs that are discussed here are powered by light, ultrasonic or magnetic fields.

Light-driven Nanoparticles

Light is an environment-friendly and renewable energy source that can activate and propel the light-driven NPs by UV, visible light, NIR, or multiwavelength 136, 137, 139. In order for the light-driven NPs to react to the light field, they are assembled with at least one photoactive material, which can be photocatalytic, photochromic, or photothermal material ¹³⁴. These photoactive materials absorb the light energy and convert it into photocatalytic reactions, photo-isomerization, or photothermal conversion which propels the NPs by introduction of an asymmetric field 131, 134. This asymmetric field can be established by bubble concentration, temperature gradient, deformation, etc 131. Even though the penetration depths (0.5 – 5.0 mm) of the light sources are limited, the light-propelled NPs are suitable candidates for the diagnosis and treatment at near-skin positions 136, 139, 142.

To our knowledge, light-driven nanoparticles for antibiofilm use have not yet been investigated, but there has been work which discusses light-driven micromotors against biofilms. One of these micromotors is described by Ussia et al. where they developed ZnO:Ag micromotors that actively move upon UV irradiation 143. The self-propulsion originates from the asymmetric generation of chemical species in water. The antimicrobial activity originates from the ROS produced by the photogenerated electrons of ZnO, and is even enhanced by the presence of Ag particles. Ussia et al. showed that these NPs are able to eradicate up to 80% of biofilms of MRSA and *P. aeruginosa* in only a few minutes.

Ultrasonic-driven Nanoparticles

Another fuel-free propulsion is induced by high-frequency acoustic waves ^{137, 138}. These US-driven nanoparticles are often bimetallic nanorods which are propelled due to oscillation at one side of the asymmetric nanorod 131, 134, 139. There have been two types of acoustic radiation forces discussed: The primary radiation force is responsible for the NP migration which occurs in a direction perpendicular to the acoustic wave, while the secondary radiation force is responsible for the repulsion between the US-driven NPs ^{131, 139}. US-driven NPs have potential biomedical applications due to their non-hazardous, biocompatible power source 137.

The first example of ultrasonic-driven NPs was demonstrated by Wang et al., who developed Au-Ru bimetallic nanorods which can be propelled, aligned, and assembled by MHz frequency acoustic waves 144. Their observations showed that the shape asymmetry of the nanorods causes directional motion via a mechanism known as self acoustophoresis. This research showed the potential for the use of US-powered nanorods in biologically relevant environments.

Kiristi et al. developed US-powered porous Au nanowires which were modified with lysozyme for bacteria-killing ¹⁴⁵. The nanowires are divided into two sections: a concave section, which is essential for acoustic propulsion, and a porous section which ensures high enzyme loading. Upon ultrasound irradiation, the nanowires showed continuous movement, which was shown to be the driving force for the high bacterial killing efficiency due to the enhanced contact between the lysozyme and the bacterial cell wall, demonstrated by using M. lysodeikticus and E. coli.

Magnetic-driven Nanoparticles

Lastly, magnetic-driven NPs have shown great promise in the biomedical field due to the fact that low strength magnetic fields are harmless to cells and tissues 136, 137 Magnetically driven nanoparticles often contain an asymmetric geometry with helical or flexible structures inspired by common motile systems of microorganisms ^{131, 134, 137}. A rotating magnetic field is able to induce propulsion by rotating the magnetic part of the nanoparticles and oscillating the helical or flexible tail structures ¹³⁸. With the ability of magnetic-driven NPs to approach hardto-reach spaces and permeate deeply into tissue, they are especially interesting for bacterial biofilm killing ¹³⁹. The magnetic-driven NPs developed by Gao et al. are flexible Au/Ag/Ni nanowires that link the Au head and the Ni tail with a weakened Ag bridge ¹⁴⁶. Upon an external rotating magnetic field, the Ni tail starts to rotate which subsequently induces rotation of the Au head. Due to the breakage of the system symmetry, the nanowires are able to move in an axial direction. By tailoring

the length of the Au and Ni segments and modulating the magnetic field, these nanowires can move in a forward or a backward direction. Because the Au/Ag/ Ni nanowires can be mass-produced and functionalized, they are promising for targeted drug delivery.

Ma et al. developed a magneto-nanozyme for the destruction and eradication of S. aureus biofilm 147. This method involved mesoporous iron oxide nanoparticles (MNPs) with polyvalent iron. These MNPs have different functions. One is that these MNPs can assemble into micro swarms and physically destroy the biofilm upon the addition of a rotating magnetic field. The MNPs are also able to produce ROS in the presence of H₂O₂, which is promoted by the physical biofilm destruction. Lastly, they can induce magnetic hyperthermia upon alternating magnetic fields.

(Self-)propelled nanoparticles in in vivo studies

Over the past few years, great strides have been made in the development of nanoparticles as antibacterials against biofilms. The main goal of these nanoparticles is to kill the bacteria while reducing the chance of AMR, which is achieved by either using an anti-biofilm system that does not rely on antibiotics or by reducing the minimal inhibitory concentration of the applied antibiotic ¹³⁹. While it started with nanoparticles as drug carrier systems, propulsion mechanisms are gaining interest. Current research is mainly focused on in vitro studies which unfortunately often neglect the biosafety, tissue infiltration, and immune response at the infection site 139. [65] Even though a lot more research is needed in order to utilize (self)propelled nanoparticles against bacterial biofilms in a clinical setting as therapeutic, more and more examples of successful in vivo studies can be found, highlighting the promising progress this field is making ^{133, 148-150}.

1.7 Light-driven Molecular Rotors

A special class of smart stimuli-responsive nanomaterials has gained much attention after being awarded the Nobel Prize in 2016: Light-activated molecular machines have proven highly efficient in the battle to overcome multidrug resistance in bacteria, with many different types being further investigated and optimized (Figure 7) ¹⁵¹.

Two classes of light-activated molecular rotors can be separated: The Feringa rotor and the HTI-based rotor 153, 154. While the Feringa motor undergoes a 360° rotation via two cycles of photoisomerization and a thermal helical inversion, the HTI-based

rotors switch between the E and Z conformations. One of the biggest differences between the two is the missing of a distinguished rotor and stator part for HTIrotors. Feringa motors will have a stator section at which the rotor head will rotate, while HTI-based rotors will have two sections rotating at the central double-bond 155. Considerable efforts have been made to utilize both these rotors in overcoming multidrug resistance. By permeabilizing the membrane of Extensively Drug-resistant Klebsiella pneumoniae with a Feringa-rotor, Galbadage et al. could resensitize the bacteria to Meropenem, making them antibiotic-susceptible again ¹⁵⁶.

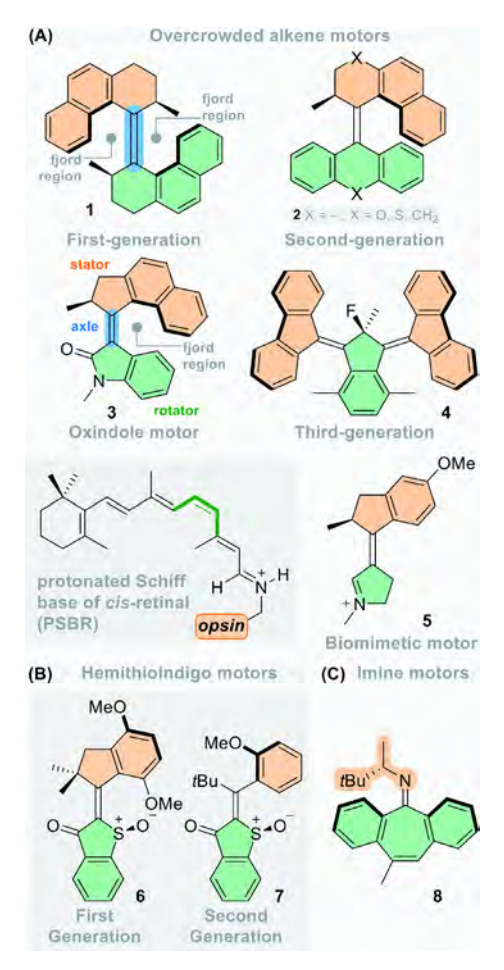


Figure 7. Different types of light-driven motors, such as alkene motors (A), Hemithioindigo motors (B), and Imine Motors (C), adapted from Pooler et al. 152.

In an extensive study conducted by Santos et al. HTI-molecular rotors efficiently eradicated biofilms by Gram-positive and Gram-negative bacteria, overcoming antibiotic-tolerant persister cells without any noticeable formation of resistances 155. The mechanism by which these rotors act on to display such efficient antimicrobial damage has been found to be mediated by the opening of the complete bacterial membrane, with subsequent production of reactive oxygen species 155-157. The challenges such systems face are targeted damage, instead of overall cellular damage, as well as efficient localized accumulation as opposed to passive diffusion throughout an organism.

The complexity of such smart and autonomous nanoparticles as well as advanced surface coatings is constantly increasing, with more and more tasks being taken over by one platform. Research in modifying these systems to become more versatile and effective in eradicating biofilms is still a priority to win the race against multidrug resistance and pathogenic biofilms.

1.8 Thesis Outline

As reviewed above, bacterial biofilms in their complexity offer many angles of attack to effectively combat them. By understanding the various mechanisms underlying biofilm formation, maturation, and structure, novel polymer-based systems can be tailored to offer approaches that go away from standard antibiotic-using systems. Targeting bacterial adhesion can be done by coating a surface with antifouling materials. In chapter 2, novel zwitterionic polymers of the poly(ylide) class will be evaluated for their use as an antifouling coating. By characterizing the ability to repel biomolecules often attributed to the initial adhesion of, for example, blood serum molecules, further assessment of biofilm growth inhibition was performed. Initial hypotheses relied on the increased hydration layer coupled with a general inhibition of growth by membrane damage, yet further experiments utilizing poly(ylide) variations highlighted the potential for a more unique mechanism with various genetic markers being upregulated. Although effective in repelling bacteria and inhibiting biofilm formation, challenging already propagated biofilms became the focus of chapter 3, where self-assembled porous polymersomes were modified to act as a silver ion-releasing sponge. Silver nanoparticles and nanoclusters were synthesized inside of the polymersomes. Successful compartmentalization was verified by FFF-MALS. This creates a compartmentalized system capable of slowly releasing the silver ions, exhibiting bactericidal properties. Biofilms were challenged under flow conditions where both systems effectively eradicated biofilms with higher efficiency than pure silver nanoparticles and clusters. Furthermore, the high cytocompatibility of nanocluster systems promoted these as the ideal candidate.

Exploiting the self-assembled structures of polymersomes even more, chapter 4 modifies polymersomes with a rotating unit to damage bacterial cells via opening of the membrane. The hemithioindigo motor was covalently attached to the surface of polymersomes after which these were incubated with biofilms. Under light activation, the rotors showed effective killing of cells inside of the biofilms by permeabilizing the membrane and turning it more rigid. Genetic characterization revealed a multifaceted response array bacteria used to adapt to this stress such as genes involved in membrane repair responses that were upregulated after exposure to light. Additionally, a self-lysis mechanism was found to be activated, paired with an increase in quorum sensing. Putting these two together revealed a cascade-like self-lysis, an attempt to fortify the biofilm from further attacks. Since polymersomes were able to infiltrate the biofilms, this signal surged through the whole biofilm, turning it into a "death" signal to cells that did not experience direct contact with the drilling unit. The ability for nanoparticles to navigate toward the target via active motion is a desirable feature in nanomedicine. This is most often done utilizing physiochemical gradients produced by the target. The guorum sensing apparatus has been shown to create gradients inside of biofilms, which the nanoparticle system in **chapter 5** attempts to use as an active propellant and signal to detect biofilms. By shape-transforming polymersomes, stomatocytes with the quorum-quenching enzyme Acylase were produced. These showed enhanced motion when exposed to the quorum-sensing molecules of the homoserine lactone class. In various chemotactic studies, these systems showed accumulation towards the biofilms and were able to effectively quench and shutdown the quorum sensing apparatus on a genetic level. To conclude this thesis, chapter 6 provides an overview coupled with some future outlook on how this research can serve as a foundation for biofilm targeting and combating therapeutics.

The presented thesis ultimately aims to expand the toolbox of polymer-based antibiofilm systems with smart, autonomous moving, and stimuli-responsive systems. We believe that the research comprised in these projects offers versatile platforms to further develop multitasking capable nanoparticles and surface coatings to combat pathogenic biofilms and overcome arising problems of antibiotic resistance.

1.9 References

- (1) Sauer, K.; Camper, A. K.; Ehrlich, G. D.; Costerton, J. W.; Davies, D. G. Pseudomonas aeruginosa displays multiple phenotypes during development as a biofilm. Am Soc Microbiol: 2002.
- Sauer, K.; Stoodley, P.; Goeres, D. M.; Hall-Stoodley, L.; Burmølle, M.; Stewart, P. S.; Bjarnsholt, T. (2) The biofilm life cycle: expanding the conceptual model of biofilm formation. Nature Reviews Microbiology 2022, 20 (10), 608-620. DOI: 10.1038/s41579-022-00767-0.
- (3) Cendra, M. d. M.; Torrents, E. Pseudomonas aeruginosa biofilms and their partners in crime. Biotechnology Advances **2021**, 49, 107734. DOI: https://doi.org/10.1016/j.biotechadv.2021.107734.
- Almblad, H.; Rybtke, M.; Hendiani, S.; Andersen, J. B.; Givskov, M.; Tolker-Nielsen, T. High levels (4) of cAMP inhibit Pseudomonas aeruginosa biofilm formation through reduction of the c-di-GMP content. Microbiology 2019, 165 (3), 324-333.
- (5) Jennings, L. K.; Dreifus, J. E.; Reichhardt, C.; Storek, K. M.; Secor, P. R.; Wozniak, D. J.; Hisert, K. B.; Parsek, M. R. Pseudomonas aeruginosa aggregates in cystic fibrosis sputum produce exopolysaccharides that likely impede current therapies. Cell Reports 2021, 34 (8), 108782. DOI: https://doi.org/10.1016/j.celrep.2021.108782.
- Ramphal, R.; Lhermitte, M.; Filliat, M.; Roussel, P. The binding of anti-pseudomonal antibiotics to (6) macromolecules from cystic fibrosis sputum. Journal of Antimicrobial Chemotherapy 1988, 22 (4), 483-490. DOI: 10.1093/jac/22.4.483 (acccessed 4/25/2024).
- (7) Chiang, W.-C.; Nilsson, M.; Jensen Peter, Ø.; Høiby, N.; Nielsen Thomas, E.; Givskov, M.; Tolker-Nielsen, T. Extracellular DNA Shields against Aminoglycosides in Pseudomonas aeruginosa Biofilms. Antimicrobial Agents and Chemotherapy 2013, 57 (5), 2352-2361. DOI: 10.1128/ aac.00001-13 (acccessed 2024/04/25).
- Jennings, L. K.; Storek, K. M.; Ledvina, H. E.; Coulon, C.; Marmont, L. S.; Sadovskaya, I.; Secor, P. R.; (8) Tseng, B. S.; Scian, M.; Filloux, A. Pel is a cationic exopolysaccharide that cross-links extracellular DNA in the Pseudomonas aeruginosa biofilm matrix. Proceedings of the National Academy of Sciences 2015, 112 (36), 11353-11358.
- Abriat, C.; Gazil, O.; Heuzey, M.-C.; Daigle, F.; Virgilio, N. The Polymeric Matrix Composition of (9)Vibrio cholerae Biofilms Modulate Resistance to Silver Nanoparticles Prepared by Hydrothermal Synthesis. ACS Applied Materials & Interfaces 2021, 13 (30), 35356-35364. DOI: 10.1021/ acsami.1c07455.
- Wang, S.; Zhao, Y.; Breslawec, A. P.; Liang, T.; Deng, Z.; Kuperman, L. L.; Yu, Q. Strategy to combat biofilms: a focus on biofilm dispersal enzymes. npj Biofilms and Microbiomes 2023, 9 (1), 63. DOI: 10.1038/s41522-023-00427-y.
- (11) Whitchurch, C. B.; Tolker-Nielsen, T.; Ragas, P. C.; Mattick, J. S. Extracellular DNA required for bacterial biofilm formation. Science 2002, 295 (5559), 1487-1487.
- (12)Tetz, V. V.; Tetz, G. V. Effect of extracellular DNA destruction by DNase I on characteristics of forming biofilms. DNA and cell biology 2010, 29 (8), 399-405.
- Erskine, E.; MacPhee, C. E.; Stanley-Wall, N. R. Functional amyloid and other protein fibers in the biofilm matrix. Journal of Molecular Biology 2018, 430 (20), 3642-3656.
- Kumar Shukla, S.; Rao, T. S. Dispersal of Bap-mediated Staphylococcus aureus biofilm by proteinase K. The Journal of antibiotics 2013, 66 (2), 55-60.
- (15) Nguyen, U. T.; Burrows, L. L. DNase I and proteinase K impair Listeria monocytogenes biofilm formation and induce dispersal of pre-existing biofilms. International journal of food microbiology 2014, 187, 26-32.

- Daboor, S. M.; Raudonis, R.; Cheng, Z. Characterizations of the viability and gene expression of dispersal cells from Pseudomonas aeruginosa biofilms released by alginate lyase and tobramycin. PLoS One 2021, 16 (10), e0258950.
- Baker, P.; Hill, P. J.; Snarr, B. D.; Alnabelseya, N.; Pestrak, M. J.; Lee, M. J.; Jennings, L. K.; Tam, J.; Melnyk, R. A.; Parsek, M. R. Exopolysaccharide biosynthetic glycoside hydrolases can be utilized to disrupt and prevent Pseudomonas aeruginosa biofilms. Science advances 2016, 2 (5), e1501632.
- (18) Turnbull, L.; Toyofuku, M.; Hynen, A. L.; Kurosawa, M.; Pessi, G.; Petty, N. K.; Osvath, S. R.; Cárcamo-Oyarce, G.; Gloag, E. S.; Shimoni, R.; et al. Explosive cell lysis as a mechanism for the biogenesis of bacterial membrane vesicles and biofilms. Nature Communications 2016, 7 (1), 11220. DOI: 10.1038/ncomms11220.
- Ibáñez de Aldecoa, A. L.; Zafra, O.; González-Pastor, J. E. Mechanisms and regulation of (19)extracellular DNA release and its biological roles in microbial communities. Frontiers in microbiology **2017**, 8, 1390.
- (20)Zweig, M.; Schork, S.; Koerdt, A.; Siewering, K.; Sternberg, C.; Thormann, K.; Albers, S. V.; Molin, S.; van der Does, C. Secreted single-stranded DNA is involved in the initial phase of biofilm formation by N eisseria gonorrhoeae. Environmental microbiology 2014, 16 (4), 1040-1052.
- Campoccia, D.; Montanaro, L.; Arciola, C. R. Tracing the origins of extracellular DNA in bacterial biofilms: story of death and predation to community benefit. Biofouling 2021, 37 (9-10), 1022-1039.
- Schuch, A. P.; Garcia, C. C. M.; Makita, K.; Menck, C. F. M. DNA damage as a biological sensor for environmental sunlight. Photochemical & Photobiological Sciences 2013, 12 (8), 1259-1272.
- (23)Little, J. W. Lysogeny, Prophage Induction, and Lysogenic Conversion. In *Phages*, 2005; pp 37-54.
- Heredia-Ponce, Z.; Secchi, E.; Toyofuku, M.; Marinova, G.; Savorana, G.; Eberl, L. Genotoxic stress (24)stimulates eDNA release via explosive cell lysis and thereby promotes streamer formation of Burkholderia cenocepacia H111 cultured in a microfluidic device. npj Biofilms and Microbiomes **2023**, 9 (1), 96. DOI: 10.1038/s41522-023-00464-7.
- (25)Prentice, J. A.; van de Weerd, R.; Bridges, A. A. Cell-lysis sensing drives biofilm formation in Vibrio cholerae. Nature Communications 2024, 15 (1), 2018. DOI: 10.1038/s41467-024-46399-1.
- (26)Stoodley, P.; Hall-Stoodley, L.; Boyle, J. D.; Jørgensen, F.; Lappin-Scott, H. Community structure and co-operation in biofilms. 2000.
- Quan, K.; Hou, J.; Zhang, Z.; Ren, Y.; Peterson, B. W.; Flemming, H.-C.; Mayer, C.; Busscher, H. J.; van (27)der Mei, H. C. Water in bacterial biofilms: pores and channels, storage and transport functions. Critical Reviews in Microbiology 2022, 48 (3), 283-302. DOI: 10.1080/1040841X.2021.1962802.
- Ju, X.; Chen, J.; Zhou, M.; Zhu, M.; Li, Z.; Gao, S.; Ou, J.; Xu, D.; Wu, M.; Jiang, S. Combating (28)Pseudomonas aeruginosa biofilms by a chitosan-PEG-peptide conjugate via changes in assembled structure. ACS applied materials & interfaces 2020, 12 (12), 13731-13738.
- Forier, K.; Messiaen, A.-S.; Raemdonck, K.; Nelis, H.; De Smedt, S.; Demeester, J.; Coenye, T.: Braeckmans, K. Probing the size limit for nanomedicine penetration into Burkholderia multivorans and Pseudomonas aeruginosa biofilms. Journal of Controlled Release 2014, 195, 21-28. DOI: https://doi.org/10.1016/j.jconrel.2014.07.061.
- Rooney, L. M.; Amos, W. B.; Hoskisson, P. A.; McConnell, G. Intra-colony channels in E. coli function (30)as a nutrient uptake system. The ISME journal 2020, 14 (10), 2461-2473.

- Flemming, H. C.; Wingender, J. The biofilm matrix. Nat Rev Microbiol 2010, 8 (9), 623-633. DOI: 10.1038/nrmicro2415 From NLM.
- Flemming, H.-C.; van Hullebusch, E. D.; Neu, T. R.; Nielsen, P. H.; Seviour, T.; Stoodley, P.; (32)Wingender, J.; Wuertz, S. The biofilm matrix: multitasking in a shared space. Nature Reviews Microbiology 2023, 21 (2), 70-86. DOI: 10.1038/s41579-022-00791-0.
- Jo, J.; Price-Whelan, A.; Dietrich, L. E. P. Gradients and consequences of heterogeneity in biofilms. Nature Reviews Microbiology 2022, 20 (10), 593-607. DOI: 10.1038/s41579-022-00692-2.
- Stewart, P. S.; Franklin, M. J. Physiological heterogeneity in biofilms. *Nature Reviews Microbiology* (34)**2008**, 6 (3), 199-210.
- Scheidweiler, D.; Bordoloi, A. D.; Jiao, W.; Sentchilo, V.; Bollani, M.; Chhun, A.; Engel, P.; de Anna, P. Spatial structure, chemotaxis and guorum sensing shape bacterial biomass accumulation in complex porous media. Nature Communications 2024, 15 (1), 191. DOI: 10.1038/s41467-023-44267-y.
- Hollmann, B.; Perkins, M.; Chauhan, V. M.; Aylott, J. W.; Hardie, K. R. Fluorescent nanosensors reveal dynamic pH gradients during biofilm formation. npj Biofilms and Microbiomes 2021, 7 (1), 50. DOI: 10.1038/s41522-021-00221-8.
- (37) Mukherjee, S.; Bassler, B. L. Bacterial quorum sensing in complex and dynamically changing environments. Nature Reviews Microbiology 2019, 17 (6), 371-382. DOI: 10.1038/s41579-019-0186-5.
- Narla, A. V.; Borenstein, D. B.; Wingreen, N. S. A biophysical limit for quorum sensing in biofilms. (38)Proceedings of the National Academy of Sciences 2021, 118 (21), e2022818118.
- Li, Z.; Nair, S. K. Quorum sensing: How bacteria can coordinate activity and synchronize their (39)response to external signals? Protein Science 2012, 21 (10), 1403-1417. DOI: https://doi. org/10.1002/pro.2132.
- (40) Waters, C. M.; Bassler, B. L. Quorum sensing: cell-to-cell communication in bacteria. Annu. Rev. Cell Dev. Biol. 2005, 21, 319-346.
- Solano, C.; Echeverz, M.; Lasa, I. Biofilm dispersion and quorum sensing. Current opinion in microbiology **2014**, 18, 96-104.
- Papenfort, K.; Bassler, B. L. Quorum sensing signal-response systems in Gram-negative bacteria. *Nature Reviews Microbiology* **2016**, *14* (9), 576-588.
- Malgaonkar, A.; Nair, M. Quorum sensing in Pseudomonas aeruginosa mediated by RhIR is regulated by a small RNA PhrD. Scientific Reports 2019, 9 (1), 432. DOI: 10.1038/s41598-018-36488-9.
- (44) Lee, J.; Zhang, L. The hierarchy quorum sensing network in Pseudomonas aeruginosa. Protein & cell **2015**, 6 (1), 26-41.
- (45)Kiratisin, P.; Tucker, K. D.; Passador, L. LasR, a transcriptional activator of Pseudomonas aeruginosa virulence genes, functions as a multimer. Journal of bacteriology 2002, 184 (17), 4912-4919.
- (46)Schertzer, J. W.; Boulette, M. L.; Whiteley, M. More than a signal: non-signaling properties of quorum sensing molecules. TRENDS in Microbiology 2009, 17 (5), 189-195.
- (47)Lee, J.; Wu, J.; Deng, Y.; Wang, J.; Wang, C.; Wang, J.; Chang, C.; Dong, Y.; Williams, P.; Zhang, L.-H. A cell-cell communication signal integrates quorum sensing and stress response. Nature Chemical Biology 2013, 9 (5), 339-343. DOI: 10.1038/nchembio.1225.
- Qin, S.; Xiao, W.; Zhou, C.; Pu, Q.; Deng, X.; Lan, L.; Liang, H.; Song, X.; Wu, M. Pseudomonas (48)aeruginosa: pathogenesis, virulence factors, antibiotic resistance, interaction with host, technology advances and emerging therapeutics. Signal Transduction and Targeted Therapy **2022**, 7 (1), 199. DOI: 10.1038/s41392-022-01056-1.

- (49) Gambello, M. J.; Kaye, S.; Iglewski, B. H. LasR of Pseudomonas aeruginosa is a transcriptional activator of the alkaline protease gene (apr) and an enhancer of exotoxin A expression. Infection and immunity **1993**, 61 (4), 1180-1184.
- (50)Jayaseelan, S.; Ramaswamy, D.; Dharmaraj, S. Pyocyanin: production, applications, challenges and new insights. World J Microbiol Biotechnol 2014, 30 (4), 1159-1168. DOI: 10.1007/s11274-013-1552-5 From NLM.
- (51) Tuon, F. F.; Dantas, L. R.; Suss, P. H.; Tasca Ribeiro, V. S. Pathogenesis of the Pseudomonas aeruginosa biofilm: a review. Pathogens 2022, 11 (3), 300.
- Carterson, A. J.; Morici, L. A.; Jackson, D. W.; Frisk, A.; Lizewski, S. E.; Jupiter, R.; Simpson, K.; Kunz, (52)D. A.; Davis, S. H.; Schurr, J. R. The transcriptional regulator AlgR controls cyanide production in Pseudomonas aeruginosa. Journal of bacteriology 2004, 186 (20), 6837-6844.
- Cody, W. L.; Pritchett, C. L.; Jones, A. K.; Carterson, A. J.; Jackson, D.; Frisk, A.; Wolfgang, M. C.; (53)Schurr, M. J. Pseudomonas aeruginosa AlgR controls cyanide production in an AlgZ-dependent manner. Journal of bacteriology 2009, 191 (9), 2993-3002.
- (54)Rather, M. A.; Saha, D.; Bhuyan, S.; Jha, A. N.; Mandal, M. Quorum Quenching: A Drug Discovery Approach Against Pseudomonas aeruginosa. Microbiological Research 2022, 264, 127173. DOI: https://doi.org/10.1016/j.micres.2022.127173.
- Rather, M. A.; Gupta, K.; Mandal, M. Inhibition of biofilm and quorum sensing-regulated (55)virulence factors in Pseudomonas aeruginosa by Cuphea carthagenensis (Jacq.) Macbr. Leaf extract: An in vitro study. Journal of Ethnopharmacology 2021, 269, 113699.
- (56)Zhou, L.; Zhang, Y.; Ge, Y.; Zhu, X.; Pan, J. Regulatory mechanisms and promising applications of quorum sensing-inhibiting agents in control of bacterial biofilm formation. Frontiers in microbiology **2020**, 11, 589640.
- (57)Utari, P. D.; Setroikromo, R.; Melgert, B. N.; Quax, W. J. PvdQ quorum quenching acylase attenuates Pseudomonas aeruginosa virulence in a mouse model of pulmonary infection. Frontiers in cellular and infection microbiology **2018**, 8, 119.
- (58)Khoshbakht, R.; Panahi, S.; Neshani, A.; Ghavidel, M.; Ghazvini, K. Novel approaches to overcome Colistin resistance in Acinetobacter baumannii: Exploring quorum quenching as a potential solution. Microbial Pathogenesis 2023, 182, 106264. DOI: https://doi.org/10.1016/j. micpath.2023.106264.
- Mayer, C.; Muras, A.; Parga, A.; Romero, M.; Rumbo-Feal, S.; Poza, M.; Ramos-Vivas, J.; Otero, A. Quorum sensing as a target for controlling surface associated motility and biofilm formation in Acinetobacter baumannii ATCC® 17978TM. Frontiers in microbiology 2020, 11, 565548.
- Fong, J.; Zhang, C.; Yang, R.; Boo, Z. Z.; Tan, S. K.; Nielsen, T. E.; Givskov, M.; Liu, X.-W.; Bin, W.; Su, H. Combination therapy strategy of quorum quenching enzyme and quorum sensing inhibitor in suppressing multiple quorum sensing pathways of P. aeruginosa. Scientific reports 2018, 8 (1), 1155.
- Song, Y.; Wang, R.; Pan, Y.; Fang, D.; Tian, Y.; Zhou, S. An integrated quorum quenching biocatalytic nanoplatform for synergistic chemo-photothermal eradication of P. aeruginosa biofilm infections. Acta Biomater 2023, 171, 532-542. DOI: 10.1016/j.actbio.2023.09.021 From NLM.
- Wafaa, H. The Role of Biofilm Exopolysaccharides on Biocontrol of Plant Diseases. In *Biopolymers*, (62)Magdy, E. Ed.; IntechOpen, 2010; p Ch. 14.
- Rather, M. A.; Gupta, K.; Mandal, M. Microbial biofilm: formation, architecture, antibiotic (63)resistance, and control strategies. Braz J Microbiol 2021, 52 (4), 1701-1718. DOI: 10.1007/s42770-021-00624-x From NLM.
- (64)Banerjee, P.; Singh, M.; Sharma, V. Biofilm formation: a comprehensive review. Int J Pharm Res Health Sci 2015, 3 (2), 556-560.

- Römling, U.; Galperin, M. Y.; Gomelsky, M. Cyclic di-GMP: the first 25 years of a universal bacterial second messenger. Microbiology and Molecular Biology Reviews 2013, 77 (1), 1-52.
- Wood, D. W.; Gong, F.; Daykin, M. M.; Williams, P.; Pierson 3rd, L. N-acyl-homoserine lactone-(66)mediated regulation of phenazine gene expression by Pseudomonas aureofaciens 30-84 in the wheat rhizosphere. Journal of bacteriology 1997, 179 (24), 7663-7670.
- (67)Bagge, N.; Hentzer, M.; Andersen, J. B.; Ciofu, O.; Givskov, M.; Høiby, N. Dynamics and spatial distribution of β-lactamase expression in Pseudomonas aeruginosa biofilms. Antimicrobial agents and chemotherapy 2004, 48 (4), 1168-1174.
- (68)Wood, S.; Kirkham, J.; Marsh, P.; Shore, R.; Nattress, B.; Robinson, C. Architecture of intact natural human plaque biofilms studied by confocal laser scanning microscopy. Journal of Dental Research 2000, 79 (1), 21-27.
- Rabin, N.; Zheng, Y.; Opoku-Temeng, C.; Du, Y.; Bonsu, E.; Sintim, H. O. Biofilm formation (69)mechanisms and targets for developing antibiofilm agents. Future medicinal chemistry 2015, 7 (4), 493-512.
- (70)Zhao, X.; Zhao, F.; Wang, J.; Zhong, N. Biofilm formation and control strategies of foodborne pathogens: food safety perspectives. RSC advances 2017, 7 (58), 36670-36683.
- (71) Rumbaugh, K. P.; Sauer, K. Biofilm dispersion. Nature Reviews Microbiology 2020, 18 (10), 571-586. DOI: 10.1038/s41579-020-0385-0.
- (72) Costerton, J. W.; Stewart, P. S.; Greenberg, E. P. Bacterial biofilms: a common cause of persistent infections. science 1999, 284 (5418), 1318-1322.
- (73)Magin, C. M.; Cooper, S. P.; Brennan, A. B. Non-toxic antifouling strategies. *Materials today* **2010**,
- (74) Høiby, N. A short history of microbial biofilms and biofilm infections. APMIS 2017, 125 (4), 272-275. DOI: https://doi.org/10.1111/apm.12686.
- Maan, A. M. C.; Hofman, A. H.; de Vos, W. M.; Kamperman, M. Recent Developments and Practical Feasibility of Polymer-Based Antifouling Coatings. Advanced Functional Materials 2020, 30 (32), 2000936. DOI: https://doi.org/10.1002/adfm.202000936.
- Hamilos, M.; Petousis, S.; Parthenakis, F. Interaction between platelets and endothelium: from pathophysiology to new therapeutic options. Cardiovascular diagnosis and therapy 2018, 8 (5), 568.
- Baum, C.; Meyer, W.; Stelzer, R.; Fleischer, L. G.; Siebers, D. Average nanorough skin surface of the (77)pilot whale (Globicephala melas, Delphinidae): considerations on the self-cleaning abilities based on nanoroughness. Marine Biology 2002, 140 (3), 653-657. DOI: 10.1007/s00227-001-0710-8.
- (78)Yang, W. J.; Neoh, K.-G.; Kang, E.-T.; Teo, S. L.-M.; Rittschof, D. Polymer brush coatings for combating marine biofouling. Progress in Polymer Science 2014, 39 (5), 1017-1042.
- Krishnan, S.; Weinman, C. J.; Ober, C. K. Advances in polymers for anti-biofouling surfaces. (79)Journal of Materials Chemistry 2008, 18 (29), 3405-3413.
- (80)Cao, Z.; Jiang, S. Super-hydrophilic zwitterionic poly (carboxybetaine) and amphiphilic non-ionic poly (ethylene glycol) for stealth nanoparticles. Nano Today 2012, 7 (5), 404-413.
- (81) Blackman, L. D.; Gunatillake, P. A.; Cass, P.; Locock, K. E. S. An introduction to zwitterionic polymer behavior and applications in solution and at surfaces. Chemical Society Reviews 2019, 48 (3), 757-770, 10.1039/C8CS00508G. DOI: 10.1039/C8CS00508G.
- (82) Eng, Y. J.; Nguyen, T. M.; Luo, H.-K.; Chan, J. M. W. Antifouling polymers for nanomedicine and surfaces: recent advances. Nanoscale 2023, 15 (38), 15472-15512, 10.1039/D3NR03164K. DOI: 10.1039/D3NR03164K.

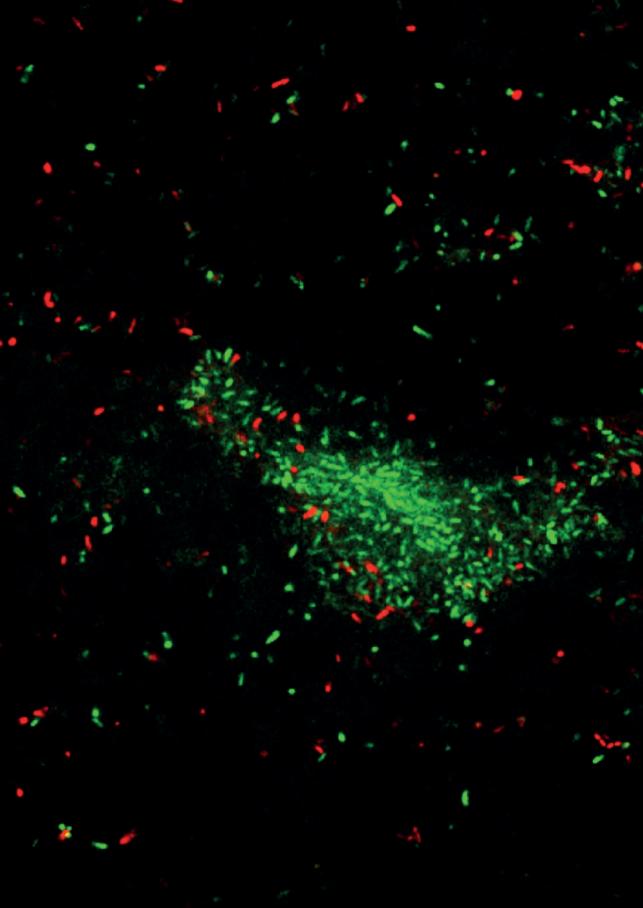
- Nikam, S. P.; Chen, P.; Nettleton, K.; Hsu, Y. H.; Becker, M. L. Zwitterion Surface-Functionalized Thermoplastic Polyurethane for Antifouling Catheter Applications. Biomacromolecules 2020, 21 (7), 2714-2725. DOI: 10.1021/acs.biomac.0c00456 From NLM.
- (84)Laschewsky, A.; Rosenhahn, A. Molecular Design of Zwitterionic Polymer Interfaces: Searching for the Difference. Langmuir 2019, 35 (5), 1056-1071. DOI: 10.1021/acs.langmuir.8b01789.
- (85) Chen, Z. Surface Hydration and Antifouling Activity of Zwitterionic Polymers. Langmuir 2022, 38 (15), 4483-4489. DOI: 10.1021/acs.langmuir.2c00512.
- Chen, S.; Li, L.; Zhao, C.; Zheng, J. Surface hydration: Principles and applications toward low-(86)fouling/nonfouling biomaterials. Polymer 2010, 51 (23), 5283-5293.
- Sun, F.; Hung, H.-C.; Yan, W.; Wu, K.; Shimchuk, A. A.; Gray, S. D.; He, W.; Huang, X.; Zhang, H. (87)Inhibition of oral biofilm formation by zwitterionic nonfouling coating. Journal of Biomedical Materials Research Part B: Applied Biomaterials 2021, 109 (10), 1418-1425. DOI: https://doi. org/10.1002/jbm.b.34801.
- (88) Hassani, M.; Kamankesh, M.; Rad-Malekshahi, M.; Rostamizadeh, K.; Rezaee, F.; Haririan, I.; Daghighi, S. M. Biomaterials coated with zwitterionic polymer brush demonstrated significant resistance to bacterial adhesion and biofilm formation in comparison to brush coatings incorporated with antibiotics. Colloids Surf B Biointerfaces 2024, 234, 113671. DOI: 10.1016/j. colsurfb.2023.113671 From NLM.
- Gupta, P.; Sarkar, S.; Das, B.; Bhattacharjee, S.; Tribedi, P. Biofilm, pathogenesis and prevention—a journey to break the wall: a review. Archives of microbiology 2016, 198, 1-15.
- (90)Jamal, M.; Ahmad, W.; Andleeb, S.; Jalil, F.; Imran, M.; Nawaz, M. A.; Hussain, T.; Ali, M.; Rafiq, M.; Kamil, M. A. Bacterial biofilm and associated infections. Journal of the chinese medical association **2018**, *81* (1), 7-11.
- Arciola, C. R.; Campoccia, D.; Montanaro, L. Implant infections: adhesion, biofilm formation and immune evasion. Nature Reviews Microbiology 2018, 16 (7), 397-409. DOI: 10.1038/s41579-018-0019-y.
- (92)Lv, X.; Wang, L.; Mei, A.; Xu, Y.; Ruan, X.; Wang, W.; Shao, J.; Yang, D.; Dong, X. Recent Nanotechnologies to Overcome the Bacterial Biofilm Matrix Barriers. Small 2023, 19 (6), 2206220. DOI: https://doi.org/10.1002/smll.202206220.
- Zhang, J.; Xu, Q.; Li, H.; Zhang, S.; Hong, A.; Jiang, Y.; Hu, N.; Chen, G.; Fu, H.; Yuan, M. Self-powered electrodeposition system for sub-10-nm silver nanoparticles with high-efficiency antibacterial activity. The Journal of Physical Chemistry Letters 2022, 13 (29), 6721-6730.
- Ji, X.; Yang, H.; Liu, W.; Ma, Y.; Wu, J.; Zong, X.; Yuan, P.; Chen, X.; Yang, C.; Li, X. Multifunctional parachute-like nanomotors for enhanced skin penetration and synergistic antifungal therapy. ACS nano 2021, 15 (9), 14218-14228.
- (95)Huang, Y.; Zou, L.; Wang, J.; Jin, Q.; Ji, J. Stimuli-responsive nanoplatforms for antibacterial applications. WIREs Nanomedicine and Nanobiotechnology 2022, 14 (3), e1775. DOI: https://doi. org/10.1002/wnan.1775.
- (96)Zhang, Y.; Lin, S.; Fu, J.; Zhang, W.; Shu, G.; Lin, J.; Li, H.; Xu, F.; Tang, H.; Peng, G.; et al. Nanocarriers for combating biofilms: Advantages and challenges. Journal of Applied Microbiology 2022, 133 (3), 1273-1287. DOI: https://doi.org/10.1111/jam.15640.
- Xiu, W.; Shan, J.; Yang, K.; Xiao, H.; Yuwen, L.; Wang, L. Recent development of nanomedicine for the treatment of bacterial biofilm infections. VIEW 2021, 2 (1), 20200065. DOI: https://doi. org/10.1002/VIW.20200065.
- Canaparo, R.; Foglietta, F.; Giuntini, F.; Della Pepa, C.; Dosio, F.; Serpe, L. Recent Developments in Antibacterial Therapy: Focus on Stimuli-Responsive Drug-Delivery Systems and Therapeutic Nanoparticles. Molecules 2019, 24 (10). DOI: 10.3390/molecules 24101991 From NLM.

- Wang, Z.; Liu, X.; Duan, Y.; Huang, Y. Infection microenvironment-related antibacterial nanotherapeutic strategies. Biomaterials 2022, 280, 121249. DOI: 10.1016/j. biomaterials.2021.121249 From NLM.
- (100) Raju, P.; Arivalagan, P.; Natarajan, S. One-pot fabrication of multifunctional catechin@ZIF-L nanocomposite: Assessment of antibiofilm, larvicidal and photocatalytic activities. Journal of Photochemistry and Photobiology B: Biology 2020, 203, 111774. DOI: https://doi.org/10.1016/j. jphotobiol.2019.111774.
- (101) Liu, Y.; Busscher, H. J.; Zhao, B.; Li, Y.; Zhang, Z.; van der Mei, H. C.; Ren, Y.; Shi, L. Surface-Adaptive, Antimicrobially Loaded, Micellar Nanocarriers with Enhanced Penetration and Killing Efficiency in Staphylococcal Biofilms. ACS Nano 2016, 10 (4), 4779-4789. DOI: 10.1021/acsnano.6b01370.
- (102) Hong, Q.; Huo, S.; Tang, H.; Qu, X.; Yue, B. Smart Nanomaterials for Treatment of Biofilm in Orthopedic Implants. Front Bioeng Biotechnol 2021, 9, 694635. DOI: 10.3389/fbioe.2021.694635 From NLM.
- (103) Wu, Y.; Long, Y.; Li, Q.-L.; Han, S.; Ma, J.; Yang, Y.-W.; Gao, H. Layer-by-Layer (LBL) Self-Assembled Biohybrid Nanomaterials for Efficient Antibacterial Applications. ACS Applied Materials & Interfaces 2015, 7 (31), 17255-17263. DOI: 10.1021/acsami.5b04216.
- (104) Komnatnyy, V. V.; Chiang, W.-C.; Tolker-Nielsen, T.; Givskov, M.; Nielsen, T. E. Bacteria-Triggered Release of Antimicrobial Agents. Angewandte Chemie International Edition 2014, 53 (2), 439-441. DOI: https://doi.org/10.1002/anie.201307975.
- (105) Hu, D.; Zou, L.; Gao, Y.; Jin, Q.; Ji, J. Emerging nanobiomaterials against bacterial infections in postantibiotic era. VIEW 2020, 1 (3), 20200014. DOI: https://doi.org/10.1002/VIW.20200014.
- (106) Jia, B.; Du, X.; Wang, W.; Qu, Y.; Liu, X.; Zhao, M.; Li, W.; Li, Y.-Q. Nanophysical Antimicrobial Strategies: A Rational Deployment of Nanomaterials and Physical Stimulations in Combating Bacterial Infections. Advanced Science 2022, 9 (10), 2105252. DOI: https://doi.org/10.1002/ advs.202105252.
- (107) Shen, Z.; He, K.; Ding, Z.; Zhang, M.; Yu, Y.; Hu, J. Visible-Light-Triggered Self-Reporting Release of Nitric Oxide (NO) for Bacterial Biofilm Dispersal. Macromolecules 2019, 52 (20), 7668-7677. DOI: 10.1021/acs.macromol.9b01252.
- (108) Bing, W.; Chen, Z.; Sun, H.; Shi, P.; Gao, N.; Ren, J.; Qu, X. Visible-light-driven enhanced antibacterial and biofilm elimination activity of graphitic carbon nitride by embedded Ag nanoparticles. Nano Research 2015, 8 (5), 1648-1658. DOI: 10.1007/s12274-014-0654-1.
- (109) Zhao, Y.; Chen, L.; Wang, Y.; Song, X.; Li, K.; Yan, X.; Yu, L.; He, Z. Nanomaterial-based strategies in antimicrobial applications: Progress and perspectives. Nano Research 2021, 14 (12), 4417-4441. DOI: 10.1007/s12274-021-3417-4.
- (110) Qing, G.; Zhao, X.; Gong, N.; Chen, J.; Li, X.; Gan, Y.; Wang, Y.; Zhang, Z.; Zhang, Y.; Guo, W.; et al. Thermo-responsive triple-function nanotransporter for efficient chemo-photothermal therapy of multidrug-resistant bacterial infection. Nature Communications 2019, 10 (1), 4336. DOI: 10.1038/s41467-019-12313-3.
- (111) García, A.; González, B.; Harvey, C.; Izquierdo-Barba, I.; Vallet-Regí, M. Effective reduction of biofilm through photothermal therapy by gold core@shell based mesoporous silica nanoparticles. Microporous and Mesoporous Materials 2021, 328, 111489. DOI: https://doi. org/10.1016/j.micromeso.2021.111489.
- (112) Li, Z.; Lu, S.; Liu, W.; Dai, T.; Ke, J.; Li, X.; Li, R.; Zhang, Y.; Chen, Z.; Chen, X. Synergistic Lysozyme-Photodynamic Therapy Against Resistant Bacteria based on an Intelligent Upconversion Nanoplatform. Angewandte Chemie International Edition 2021, 60 (35), 19201-19206. DOI: https://doi.org/10.1002/anie.202103943.

- (113) Xie, Y.; Zheng, W.; Jiang, X. Near-Infrared Light-Activated Phototherapy by Gold Nanoclusters for Dispersing Biofilms. ACS Applied Materials & Interfaces 2020, 12 (8), 9041-9049. DOI: 10.1021/ acsami.9b21777.
- (114) Yu, Y.; Tan, L.; Li, Z.; Liu, X.; Zheng, Y.; Feng, X.; Liang, Y.; Cui, Z.; Zhu, S.; Wu, S. Single-Atom Catalysis for Efficient Sonodynamic Therapy of Methicillin-Resistant Staphylococcus aureus-Infected Osteomyelitis. ACS Nano 2021, 15 (6), 10628-10639. DOI: 10.1021/acsnano.1c03424.
- (115) Pourhajibagher, M.; Bahador, A. Synergistic biocidal effects of metal oxide nanoparticlesassisted ultrasound irradiation: Antimicrobial sonodynamic therapy against Streptococcus mutans biofilms. Photodiagnosis and Photodynamic Therapy 2021, 35, 102432. DOI: https://doi. org/10.1016/j.pdpdt.2021.102432.
- (116) Geilich, B. M.; Gelfat, I.; Sridhar, S.; van de Ven, A. L.; Webster, T. J. Superparamagnetic iron oxideencapsulating polymersome nanocarriers for biofilm eradication. Biomaterials 2017, 119, 78-85. DOI: 10.1016/j.biomaterials.2016.12.011 From NLM.
- (117) Li, S.; Chang, R.; Chen, J.; Mi, G.; Xie, Z.; Webster, T. J. Novel magnetic nanocomposites combining selenium and iron oxide with excellent anti-biofilm properties. Journal of Materials Science 2020, 55 (3), 1012-1022. DOI: 10.1007/s10853-019-04019-0.
- (118) Discher, B. M.; Won, Y.-Y.; Ege, D. S.; Lee, J. C.; Bates, F. S.; Discher, D. E.; Hammer, D. A. Polymersomes: tough vesicles made from diblock copolymers. Science 1999, 284 (5417), 1143-1146.
- (119) Meier, W.; Nardin, C.; Winterhalter, M. Reconstitution of channel proteins in (polymerized) triblock copolymer membranes. Angewandte Chemie International Edition 2000, 39 (24), 4599-4602.
- (120) Duan, Y.; Zhang, M.; Shen, Z.; Zhang, M.; Zheng, B.; Cheng, S.; Hu, J. Photoresponsive Vesicles Enabling Sequential Release of Nitric Oxide (NO) and Gentamicin for Efficient Biofilm Eradication. Macromolecular Rapid Communications 2021, 42 (18), 2000759. DOI: https://doi. org/10.1002/marc.202000759.
- (121) Rijpkema, S. J.; Langens, S. G. H. A.; van der Kolk, M. R.; Gavriel, K.; Toebes, B. J.; Wilson, D. A. Modular Approach to the Functionalization of Polymersomes. Biomacromolecules 2020, 21 (5), 1853-1864. DOI: 10.1021/acs.biomac.9b01734.
- (122) Wilson, D. A.; Nolte, R. J. M.; van Hest, J. C. M. Autonomous movement of platinum-loaded stomatocytes. Nature Chemistry 2012, 4 (4), 268-274. DOI: 10.1038/nchem.1281.
- (123) Safdar, M.; Khan, S. U.; Jänis, J. Progress toward Catalytic Micro- and Nanomotors for Biomedical and Environmental Applications. Advanced Materials 2018, 30 (24), 1703660. DOI: https://doi. org/10.1002/adma.201703660.
- (124) Arqué, X.; Andrés, X.; Mestre, R.; Ciraulo, B.; Ortega Arroyo, J.; Quidant, R.; Patiño, T.; Sánchez, S. Ionic Species Affect the Self-Propulsion of Urease-Powered Micromotors. Research (Wash D C) 2020, 2020, 2424972. DOI: 10.34133/2020/2424972 From NLM.
- (125) Brown, A.; Poon, W. Ionic effects in self-propelled Pt-coated Janus swimmers. Soft matter 2014, 10 (22), 4016-4027.
- (126) Ibele, M. E.; Lammert, P. E.; Crespi, V. H.; Sen, A. Emergent, collective oscillations of self-mobile particles and patterned surfaces under redox conditions. ACS nano 2010, 4 (8), 4845-4851.
- (127) Ismagilov, R. F.; Schwartz, A.; Bowden, N.; Whitesides, G. M. Autonomous movement and selfassembly. Angewandte Chemie International Edition 2002, 41 (4), 652-654.
- (128) Serra-Casablancas, M.; Di Carlo, V.; Esporrín-Ubieto, D.; Prado-Morales, C.; Bakenecker, A. C.; Sánchez, S. Catalase-Powered Nanobots for Overcoming the Mucus Barrier. ACS Nano 2024, 18 (26), 16701-16714. DOI: 10.1021/acsnano.4c01760.

- (129) Huschka, R.; Zuloaga, J.; Knight, M. W.; Brown, L. V.; Nordlander, P.; Halas, N. J. Light-Induced Release of DNA from Gold Nanoparticles: Nanoshells and Nanorods. Journal of the American Chemical Society 2011, 133 (31), 12247-12255. DOI: 10.1021/ja204578e.
- (130) Xuan, M.; Wu, Z.; Shao, J.; Dai, L.; Si, T.; He, Q. Near Infrared Light-Powered Janus Mesoporous Silica Nanoparticle Motors. Journal of the American Chemical Society 2016, 138 (20), 6492-6497. DOI: 10.1021/jacs.6b00902.
- (131) Sun, Z.; Hou, Y. Micro/Nanorobots as Active Delivery Systems for Biomedicine: From Self-Propulsion to Controllable Navigation. Advanced Therapeutics 2022, 5 (7), 2100228. DOI: https:// doi.org/10.1002/adtp.202100228.
- (132) Dong, Y.; Wang, L.; Yuan, K.; Ji, F.; Gao, J.; Zhang, Z.; Du, X.; Tian, Y.; Wang, Q.; Zhang, L. Magnetic Microswarm Composed of Porous Nanocatalysts for Targeted Elimination of Biofilm Occlusion. ACS Nano 2021, 15 (3), 5056-5067. DOI: 10.1021/acsnano.0c10010.
- (133) Xie, S.; Huang, K.; Peng, J.; Liu, Y.; Cao, W.; Zhang, D.; Li, X. Self-Propelling Nanomotors Integrated with Biofilm Microenvironment-Activated NO Release to Accelerate Healing of Bacteria-Infected Diabetic Wounds. Advanced Healthcare Materials 2022, 11 (19), 2201323. DOI: https://doi. org/10.1002/adhm.202201323.
- (134) Luo, M.; Feng, Y.; Wang, T.; Guan, J. Micro-/Nanorobots at Work in Active Drug Delivery. Advanced Functional Materials 2018, 28 (25), 1706100. DOI: https://doi.org/10.1002/adfm.201706100.
- (135) Liu, W.; Chen, X.; Lu, X.; Wang, J.; Zhang, Y.; Gu, Z. From Passive Inorganic Oxides to Active Matters of Micro/Nanomotors. Advanced Functional Materials 2020, 30 (39), 2003195. DOI: https://doi. org/10.1002/adfm.202003195.
- (136) Wang, B.; Kostarelos, K.; Nelson, B. J.; Zhang, L. Trends in Micro-/Nanorobotics: Materials Development, Actuation, Localization, and System Integration for Biomedical Applications. Advanced Materials 2021, 33 (4), 2002047. DOI: https://doi.org/10.1002/adma.202002047.
- (137) Guix, M.; Weiz, S. M.; Schmidt, O. G.; Medina-Sánchez, M. Self-Propelled Micro/Nanoparticle Motors. Particle & Particle Systems Characterization 2018, 35 (2), 1700382. DOI: https://doi. org/10.1002/ppsc.201700382.
- (138) Wang, S.; Liu, X.; Wang, Y.; Xu, D.; Liang, C.; Guo, J.; Ma, X. Biocompatibility of artificial micro/ nanomotors for use in biomedicine. Nanoscale 2019, 11 (30), 14099-14112, 10.1039/ C9NR03393A. DOI: 10.1039/C9NR03393A.
- (139) Zhang, Z.; Wang, L.; Chan, T. K. F.; Chen, Z.; Ip, M.; Chan, P. K. S.; Sung, J. J. Y.; Zhang, L. Micro-/ Nanorobots in Antimicrobial Applications: Recent Progress, Challenges, and Opportunities. Advanced Healthcare Materials 2022, 11 (6), 2101991. DOI: https://doi.org/10.1002/ adhm.202101991.
- (140) Vilela, D.; Blanco-Cabra, N.; Eguskiza, A.; Hortelao, A. C.; Torrents, E.; Sanchez, S. Drug-Free Enzyme-Based Bactericidal Nanomotors against Pathogenic Bacteria. ACS Applied Materials & Interfaces 2021, 13 (13), 14964-14973. DOI: 10.1021/acsami.1c00986.
- (141) Yu, S.; Li, G.; Liu, R.; Ma, D.; Xue, W. Dendritic Fe3O4@Poly(dopamine)@PAMAM Nanocomposite as Controllable NO-Releasing Material: A Synergistic Photothermal and NO Antibacterial Study. Advanced Functional Materials 2018, 28 (20), 1707440. DOI: https://doi.org/10.1002/ adfm.201707440.
- (142) Ruggiero, E.; Alonso-de Castro, S.; Habtemariam, A.; Salassa, L. Upconverting nanoparticles for the near infrared photoactivation of transition metal complexes: new opportunities and challenges in medicinal inorganic photochemistry. Dalton Transactions 2016, 45 (33), 13012-13020, 10.1039/C6DT01428C. DOI: 10.1039/C6DT01428C.

- (143) Ussia, M.; Urso, M.; Dolezelikova, K.; Michalkova, H.; Adam, V.; Pumera, M. Active Light-Powered Antibiofilm ZnO Micromotors with Chemically Programmable Properties. Advanced Functional Materials 2021, 31 (27), 2101178. DOI: https://doi.org/10.1002/adfm.202101178.
- (144) Wang, W.; Castro, L. A.; Hoyos, M.; Mallouk, T. E. Autonomous Motion of Metallic Microrods Propelled by Ultrasound. ACS Nano 2012, 6 (7), 6122-6132. DOI: 10.1021/nn301312z.
- (145) Kiristi, M.; Singh, V. V.; Esteban-Fernández de Ávila, B.; Uygun, M.; Soto, F.; Aktaş Uygun, D.; Wang, J. Lysozyme-Based Antibacterial Nanomotors. ACS Nano 2015, 9 (9), 9252-9259. DOI: 10.1021/ acsnano.5b04142.
- (146) Gao, W.; Sattayasamitsathit, S.; Manesh, K. M.; Weihs, D.; Wang, J. Magnetically Powered Flexible Metal Nanowire Motors. Journal of the American Chemical Society 2010, 132 (41), 14403-14405. DOI: 10.1021/ja1072349.
- (147) Ma, X.; Wang, L.; Wang, P.; Liu, Z.; Hao, J.; Wu, J.; Chu, G.; Huang, M.; Mair, L. O.; Huang, C.; et al. An electromagnetically actuated magneto-nanozyme mediated synergistic therapy for destruction and eradication of biofilm. Chemical Engineering Journal 2022, 431, 133971. DOI: https://doi. org/10.1016/j.cej.2021.133971.
- (148) Peng, J.; Xie, S.; Huang, K.; Ran, P.; Wei, J.; Zhang, Z.; Li, X. Nitric oxide-propelled nanomotors for bacterial biofilm elimination and endotoxin removal to treat infected burn wounds. Journal of Materials Chemistry B 2022, 10 (22), 4189-4202, 10.1039/D2TB00555G. DOI: 10.1039/ D2TB00555G.
- (149) Zhou, D.; Zhang, Z.; Qiu, B.; Zhang, D.; Xie, S.; Huang, K.; Li, X. Ultrasound-Activated Persistent Luminescence Imaging and Bacteria-Triggered Drug Release for Helicobacter pylori Infection Theranostics. ACS Applied Materials & Interfaces 2022, 14 (23), 26418-26430. DOI: 10.1021/ acsami.2c04683.
- (150) Arqué, X.; Torres, M. D. T.; Patiño, T.; Boaro, A.; Sánchez, S.; de la Fuente-Nunez, C. Autonomous Treatment of Bacterial Infections in Vivo Using Antimicrobial Micro- and Nanomotors. ACS Nano 2022, 16 (5), 7547-7558. DOI: 10.1021/acsnano.1c11013.
- (151) Service, R. F. Chemistry Nobel heralds age of molecular machines. American Association for the Advancement of Science: 2016.
- (152) Pooler, D. R. S.; Lubbe, A. S.; Crespi, S.; Feringa, B. L. Designing light-driven rotary molecular motors. Chemical Science 2021, 12 (45), 14964-14986. DOI: https://doi.org/10.1039/d1sc04781g.
- (153) Feringa, B. L. The art of building small: from molecular switches to molecular motors. The Journal of organic chemistry **2007**, 72 (18), 6635-6652.
- (154) Guentner, M.; Schildhauer, M.; Thumser, S.; Mayer, P.; Stephenson, D.; Mayer, P. J.; Dube, H. Sunlight-powered kHz rotation of a hemithioindigo-based molecular motor. Nat Commun 2015, 6, 8406. DOI: 10.1038/ncomms9406 From NLM.
- (155) Santos, A. L.; van Venrooy, A.; Reed, A. K.; Wyderka, A. M.; García-López, V.; Alemany, L. B.; Oliver, A.; Tegos, G. P.; Tour, J. M. Hemithioindigo-Based Visible Light-Activated Molecular Machines Kill Bacteria by Oxidative Damage. Adv Sci (Weinh) 2022, 9 (30), e2203242. DOI: 10.1002/ advs.202203242 From NLM.
- (156) Galbadage, T.; Liu, D.; Alemany, L. B.; Pal, R.; Tour, J. M.; Gunasekera, R. S.; Cirillo, J. D. Molecular Nanomachines Disrupt Bacterial Cell Wall, Increasing Sensitivity of Extensively Drug-Resistant Klebsiella pneumoniae to Meropenem. ACS Nano 2019, 13 (12), 14377-14387. DOI: 10.1021/ acsnano.9b07836.
- (157) Santos, A. L.; Liu, D.; Reed, A. K.; Wyderka, A. M.; van Venrooy, A.; Li, J. T.; Li, V. D.; Misiura, M.; Samoylova, O.; Beckham, J. L.; et al. Light-activated molecular machines are fast-acting broadspectrum antibacterials that target the membrane. Science Advances 2022, 8 (22), eabm2055. DOI: doi:10.1126/sciadv.abm2055.



Chapter 2

Zwitterionic Polymeric Ylides with Minimal Charge Separation open a New Generation of Antifouling and Bactericidal Materials

Berking, B. B.; Karagrigoriou, D.; Poulladofonou, G.; Wilson, D. A.; Neumann K. * (* corresponding Author)

This Chapter has been published in:

Berking, B. B.; Poulladofonou, G.; Karagrigoriou, D.; Wilson, D. A.; Neumann, K *. Zwitterionic Polymeric Sulfur Ylides with Minimal Charge Separation Open a New Generation of Antifouling and Bactericidal Materials. Angewandte Chemie International Edition 2023, 62 (41), e202308971. Karagrigoriou, D.; Berking, B. B.; Wang, Q.; Sánchez-Cerrillo, D. M.; Galimberti, D. R.; Wilson, D. A *.; Neumann, K *. Unveiling the Antifouling Potential of Stabilized Poly(phosphorus ylides). ACS Macro Letters 2023, 12 (12), 1608-1613.

Institude for Molecules and Materials, Radboud University, Heyendaalseweg 135, 6525 AJ, Nijmegen, Netherlands

Abstract

Zwitterionic polymers are widely employed hydrophilic building blocks for antifouling coatings with numerous applications across a wide range of fields, including but not limited to biomedical science, drug delivery and nanotechnology. Zwitterionic polymers are considered as an attractive alternative to polyethylene glycol because of their biocompatibility and effectiveness to prevent formation of biofilms. To this end, zwitterionic polymers are classified in two categories, namely polybetaines and polyampholytes. Yet, despite a fundamental interest in driving the development of new antifouling materials, the chemical composition of zwitterionic polymer remains severely limited. Here, we show that poly(sulfur vlides) that belong to the largely overlooked class of poly(vlides), effectively prevent the formation of biofilms from pathogenic bacteria. While surface energy analysis reveals strong hydrogen-bond acceptor capabilities of poly(sulfur ylide), membrane damage of pathogenic bacteria induced by poly(sulfur ylides) indicates toxicity towards bacteria while not affecting eucaryotic cells. Further modifying the chemical nature of these ylides provides us with a toolbox of antifouling polymers with synergistic effects that offer distinct advantages over polyethylene glycol. We expect that our findings will pave the way for the development of a range of ylidebased materials with antifouling properties that have yet to be explored, opening new directions at the interface of chemistry, biology, and material science.

2.1 Introduction

Non-specific adsorption of biomolecules and microorganisms on surfaces results in the formation of biofilms, which display a major threat for numerous medical applications 1, 2. Biofilms make up the majority of organised microbial life, and it is estimated that 65% of hospital acquired infections originate from biofilms. This inevitably results in more rigorous antibiotic treatments due to the high level of resistance displayed by this type of bacterial organization ³. Biofilmassociated infections on implanted and indwelling devices, including prosthetic joints, catheters, valves and endotracheal tubes, are predominantly caused by contamination with opportunistic bacteria from patients' skin, or during early stages of wound healing due to circulation of pathogens in the bloodstream 4,5. The subsequent attachment followed by irreversible adhesion to these surfaces leads to a reservoir of bacteria consistently acquiring more cells throughout the process of infection (Figure 1A) ^{6, 7}. Besides medical implants, the effectiveness of nanomedicinal devices is affected by non-specific adhesion of organic and biological materials. For example, non-specific adsorption of serum-proteins onto surfaces of drug nano-carriers triggers recognition by the innate immune system and leads to rapid clearance 8, 9. Thus, the circulation half-life of drug delivery devices – a critical parameter in drug delivery device design – is closely related to the undesired and non-specific adsorption of biomolecules.

Therefore, when developing new generations of medical devices with enhanced efficiency and safety profile, a crucial aspect is to provide structural barriers that eliminate the risk of biofilm formation. Hydration layer on surfaces is considered a key factor for preventing the undesired adsorption of biomolecules by introducing energetic and physical barriers (Figure 1A) 10, 11. The replacement of water from densely packed hydration layers is however an energetically unfavoured process. For inducing hydration layers, polyethylene glycol (PEG) was frequently used because of its strong hydrophilic nature and biocompatibility ^{12, 13}. Yet, recent reports suggest that PEG displays complex behaviour, for example enabling insertions of chemical anchors, something undesired when developing antifouling coatings 14. Additionally, issues concerning the immunotoxicity and occurrence of PEG-specific antibodies, 15-17 led to the development and frequent use of zwitterionic materials that display not only equally or superior abilities to induce hydration layers but also offer enhanced chemical versatility 18. Zwitterionic materials are often fabricated from hydrophilic polybetaines, which are well-defined polymers containing a stoichiometric amount of positive and negative charges, although the charges are separated by hydrophobic carbon spacer 19. These zwitterionic polymers - mimicking naturally occurring phosphorylcholine - have found widespread applications as antifouling coatings and have been established as an alternative to PEG. In contrast to PEG, which forms hydration layers due to hydrogen bonds, zwitterionic polymers are believed to form hydration layers based on their stronger electrostatic interactions 20.

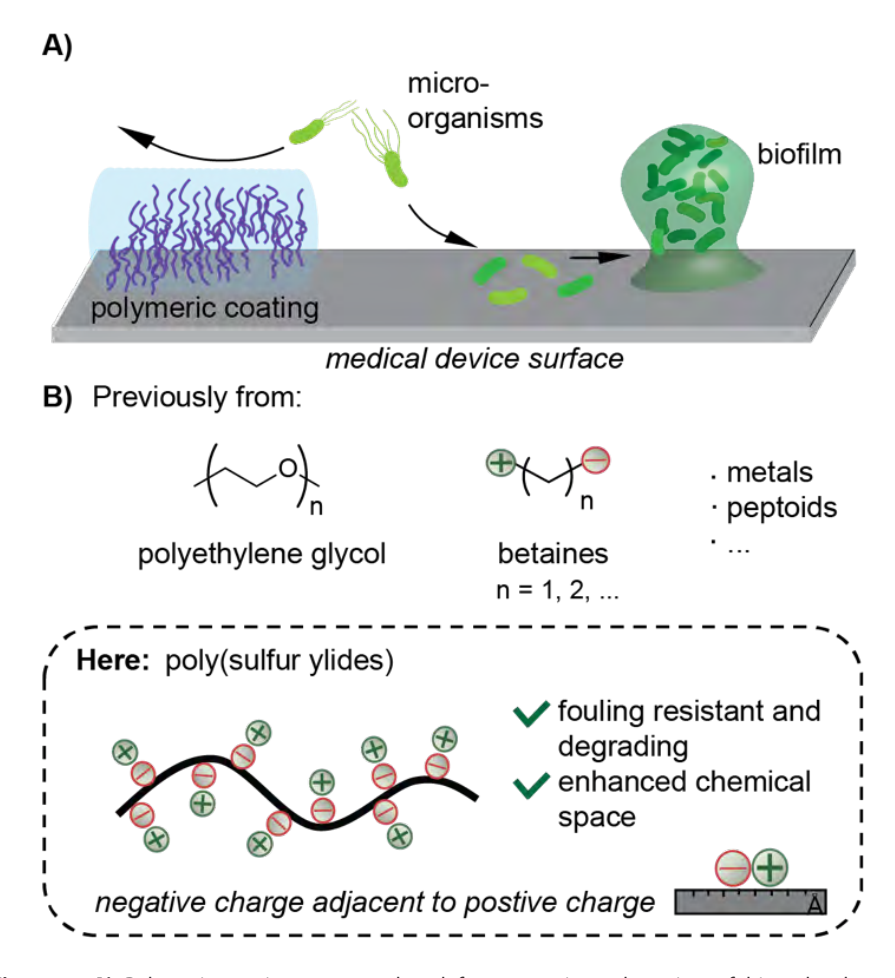


Figure 1. A) Polymeric coatings are employed for preventing adsorption of biomolecules and microorganisms, thus minimizing the risk of biofilm formation. B) Typically, polymers for antifouling coatings are made from polyethylene glycol, polybetaines or metal nanoparticles. Here, we report poly(sulfur ylides) as a structurally new scaffold for the design of antifouling polymers.

During the last decade, the development of new forms of zwitterionic structures has been subject of significant research to meet the increased demand for advanced materials with (bio)medical applications 21, 22. While many innovative materials have been reported by employing new betaine- and ampholyte-based scaffolds, their limited structural diversity and chemical space hinder the discovery and wider development of entirely new zwitterionic materials. For example, it was shown that the hydration effect is enhanced with a decreased linker length between the positive and negative charge, a structural requirement that simply cannot be fulfilled with existing polybetaine scaffolds ^{23, 24}. In strong contrast, ylides own a unique structural feature by displaying a positive charge directly adjacent to a negative charge (Figure 1B). In pioneering work, Li et al established N-oxides as biomimetic material with ultralow antifouling in mice models ²⁵. While this first report on the antifouling behaviour of N-oxides confirms that ylides display antifouling properties, the restricted structural diversity and chemical space of N-oxides severely limit the wider development of new generations of materials. One can imagine that the use of sulfur-vlides, in which the negative charge is localized on a carbon and the positive charge on a sulfur residue, 26 would open a variety of possibilities and applications in the field of antifouling materials and biomaterials. Due to the large and unexplored chemical space provided by sulfur-ylides, we envision that this structurally new class of zwitterionic polymers would significantly expand the chemical toolbox available for the fabrication of antifouling materials. However, to this end, the biological properties of sulfur ylide-derived materials and their ability to act as antifouling building blocks remains elusive, which can be attributed to the scarcity of existing ylide-based materials.

Here, we demonstrate that sulfur ylides, a recently reported new class of zwitterionic polymers, display strong antifouling properties. Our results indicate that the antifouling behaviour is caused by a synergistic effect from induced hydration layers and inhibition of bacterial growth. To the best of our knowledge, this is the first report on the antifouling properties of sulfur ylide-derived materials, and we envision that our findings will pave the way for the design of new advanced materials based on poly(ylides).

2.2 Results and Discussion

2.2.1 Poly(sulfur ylides) for hydrophilic coatings

Inspired by recent reports that a decreased linker length between positive and negative charges within zwitterionic headgroups leads to enhanced hydration effects, we envisioned that sulfur ylide-derived zwitterionic polymers could efficiently promote the formation of hydration layers. Notably, in strong contrast to betaines, ylides display a positive charge directly adjacent to a negative charged carbon, a unique structural feature that cannot be accessed by existing betainederived structures. For our studies, we utilized poly(sulfur ylides), which we recently reported as a new class of remarkably stable and easily accessible zwitterionic polymers.²⁵ Here, we report for the first time a homopolymeric poly(sulfur ylide) P(SY) 1, which was accessed from ylide monomer 2 via reversible additionfragmentation cain-transfer (RAFT) polymerisation (Figure 2A). As a non-degradable polymer backbone, polystyrene was chosen in order to guarantee prolonged stability of the coatings even when incubated under biological conditions. Monitoring of the polymerisation via ¹H-NMR revealed pseudo-first order kinetic, which is characteristic for a controlled polymerisation (supporting information). The controlled nature of the polymerisation allowed us to target P(SY) 1 with a moderate length ($X_n = 48$ and $M_n = 11$ kDa).

At the onset of our research, we intended to confirm our hypothesis that zwitterionic poly(sulfur ylides) are capable of modulating surface properties by inducing hydrophilicity. Water contact angle is a common measure to determine the hydrophilicity of coatings. Indeed, employing P(SY) 1 as a coating on a glass surface and determining a contact angle of 45°, provided first evidence that sulfur ylides effectively induce hydrophilicity to even more polar surfaces such as glass (Figure 2B). To prove this finding further, homopolymeric P(SY) 1 coated surfaces were compared with coatings consisting of recently reported copolymers poly(styrene-co-sulfur ylide) that displayed a varying fraction of styrene (F_c) and sulfur ylide (F_{sv}) . Analysis of the contact angle revealed a clear trend, namely increasing hydrophilicity with increasing molar fraction $F_{\rm sy}$ of sulfur ylide. Conversely, enhancing the molar fraction of styrene within copolymers resulted in a more hydrophobic surface.

While the obtained water contact angles offer initial insights into the on-surface characteristics of poly(sulfur ylides), a more critical assessment of the on-surface chemistry is required for understanding potential interactions of microorganism with solid surfaces. For this purpose, we performed a surface energy component analysis for P(SY) 1 coated surfaces using the method reported by van Oss (ESI).²⁸ In brief, we determined a surface energy = 52.4 mJ m⁻² for the homopolymer P(SY) 1 and a Lewis-base component = 31.2 mJ m^{-2} (Figure 2C).

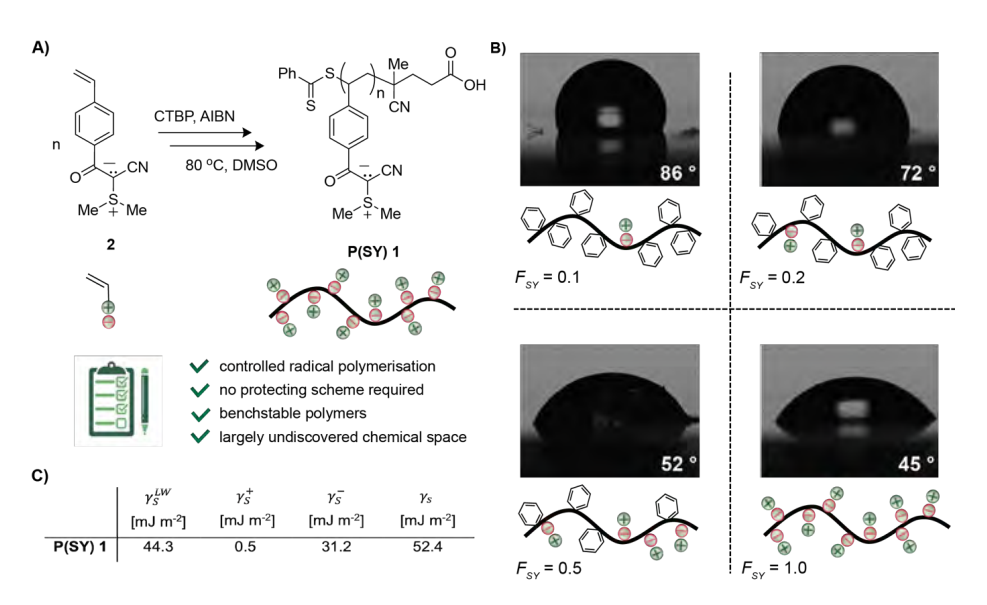


Figure 2. A) P(SY) 1 was accessed using RAFT agent CTBP (4-cyano-4-(thiobenzoylthio)pentanoic acid) and AIBN with an average degree of polymerisation of $X_{z} = 48$. The polymerisation was carried out in DMSO at 80 °C. **B)** Homopolymer P(SY) **1** ($F_{(SY)} = 1.0$) displayed a contact angle of 45°. P(SY) **1** was compared to previously reported copolymers displaying a varying fraction F of sulfur ylide and styrene units. The figure was partly created with biorender. C) Surface energy data calculated for P(SY) coated surfaces at room temperature; = the Liftshitz/van der Waals component, = Lewis-acid component of solid; Lewis-base component of solid and = total surface energy of surface. Measurements and analysis were conducted by Neumann and Karagrigoriou.

The Lewis-base component is an indicator for the capability of surfaces to accept hydrogen-bonding and is often employed as a measure for hydration layer.²⁹ Both, the surface energy and Lewis-base component compare to those that are reported for antifouling surfaces in literature, and indicate that sulfur ylides have the ability to induce hydrogen binding on surfaces.^{30,31} Finally, we tested the temperatureand salt-responsiveness of poly(sulfur ylides). This is because many zwitterionic polymer display such environmental responsiveness. Yet, in the case of P(SY) 1, we did not observe any stimuli-effect by neither temperature or salt concentration. While for many applications, such responsiveness would be desired, we believe that the absence of such stimuli-responsiveness offers also advantages, for example a more robust coating for medical applications.

A crucial requisite of antifouling coatings is to prevent non-specific adsorption of plasma proteins. This is because bacterial adhesion is often promoted by coating of the abiotic surface with bodily fluids, resulting in a thin protein layer formed within nanoseconds, eventually enabling an increasing adhesiveness of pathogenic microbes to the surface.³² A prominent factor in elevating levels of adhesiveness is fibrinogen. Therefore, we sought to investigate the ability of both, small moleculebased sulfur ylides, and poly(sulfur ylides) to prevent the adhesion of fibrinogen. For this study, we envisioned that it is somewhat more reliable to immobilize sulfur ylides covalently onto the surface.

For allowing such covalent attachment, we chose to employ amine-coated polystyrene surfaces, which offered the possibility to immobilize carboxylic acid bearing sulfur vlides via formation of amide bonds. Due to their size and structural dynamics, polymers have been shown to induce hydration layers more efficiently compared to small molecules, thus we turned our attention first to poly(sulfur ylides) and their ability to prevent adhesion of human plasma fibringgen. Homopolymer P(SY) 1 was coupled to amine-coated polystyrene surfaces via the terminal carboxylic acid that conveniently was introduced by the utilized RAFT agent CTBP. Further, for enabling dosage-dependent activity comparison, a coating from a random copolymer P(S-co-SY) 3 was prepared, consisting out of styrene (w% = 50) and sulfur ylide (w% = 50), respectively. The high control over molecular weight offered by RAFT polymerization allowed us to access a comparable degree of polymerization of P(S-co-SY) **3** ($X_n = 51$) vs P(SY) **1** ($X_n = 48$). Finally, a sample was prepared in which carboxylic acid terminated PEG was immobilized onto amine-coated surfaces. The amount of adhered fibrinogen was determined by incubation of these coated surfaces with fibrinogen from human plasma (2 mg/mL) in PBS for 2 hours and subsequent fluorescent labelling. When comparing P(SY) 1 and P(S-co-SY) 3, the homopolymer displays a significantly enhanced capability to prevent adhesion of fibrinogen (Figure 3). This finding is in accordance with the determined water contact angle that suggests an enhanced hydration effect by homopolymeric P(SY) 1. While comparison of P(SY) 1 to PEG yielded no statically significant difference, nonfunctionalized polystyrene (PS) surfaces displayed a highly significant increase by 3-fold levels of fibrinogen adhered to the surface (Figure 3).

Next, a small molecule bearing sulfur ylide was immobilized onto the amine-coated surface and its ability to prevent fibrinogen adhesion was investigated. We have chosen dimethyl sulfide-derived ylide SY 4 as a representative small moleculebearing ylide, which was accessed in three steps (SI) and immobilized onto the surface using EDAC and NHS.

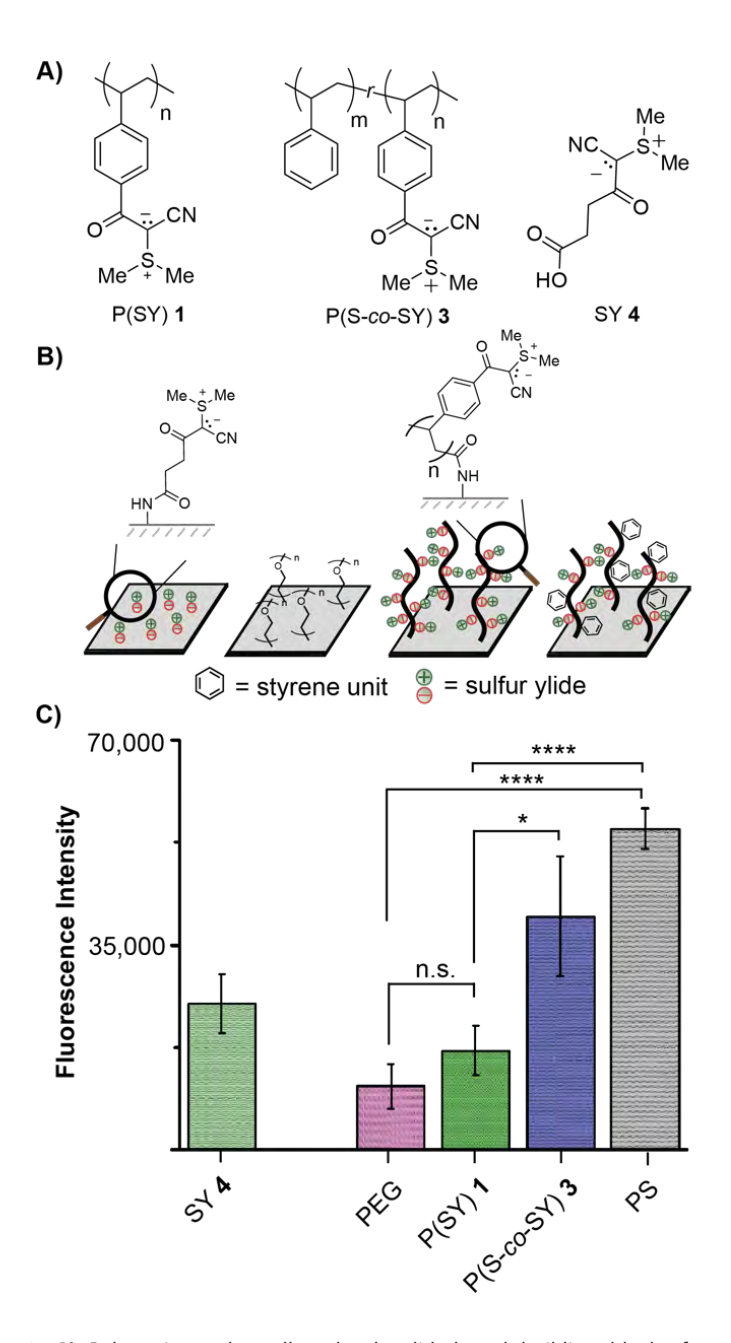


Figure 3. A) Polymeric- and small molecule ylide-based building blocks for surface coatings B) Polystyrene surface was modified with P(SY) 1, ylide bearing small molecule 4, P(S-co-SY) 3 containing 50 w% ylide residues and PEG as a reference. C) Fibrinogen adherence onto polymer coated surfaces displays significantly reduced interaction of the protein with homopolymer P(SY) 1 and PEG compared to co polymer P(S-co-SY) 3 and PS. Experiments were carried out in replicates of eight and analysed with unpaired t.test, p < 0.001.

After treatment with fibrinogen and subsequent fluorescent labelling, SY 4 treated samples displayed less fibringen adhesion compared to P(S-co-SY) 3 and PS, but increased adhesion levels in comparison with the homopolymer P(SY) 1 and PEG. We attributed these differences to the improved ability of polymers to form thicker hydration layers. Encouraged by the unprecedented findings that sulfur ylide containing zwitterionic polymers prevent fibringen adhesion, we turned our attention to inhibition of biofilms that are formed by microorganisms. To assess the production of biomass caused by bacterial cells (Pseudomonas aeruginosa) adhered to the surface, a conventional crystal violet assay was employed. Biomass was quantified after 4 hours with and without pre-treatment with fibrinogen. Bacterial cells effectively colonized copolymer P(S-co-SY) 3 and PS surfaces, with significant lower amount of biomass observed in P(SY) 1 and PEG (Figure 4). Although PEG-coated surfaces displayed a lower amount of biomass in the absence of fibrinogen, when pre-treated with fibrinogen a statistically significant increase in biomass production was observed, whereas biomass production for P(SY) 1 coated samples were not affected by pre-treatment with fibrinogen. Additionally, we incubated the coatings with bacteria in human AB blood serum to simulate more complex conditions and obtained a similar trend.

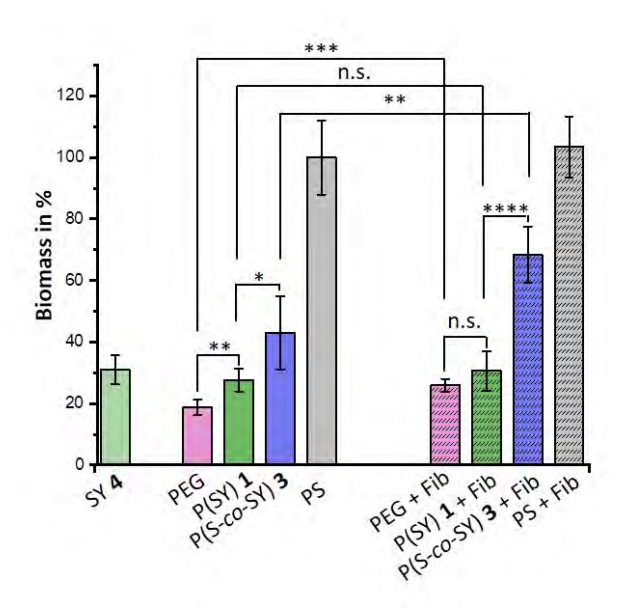


Figure 4. Biomass production upon biofilm formation is significantly decreased when incubated with PEG and P(SY) **1.** Fibrinogen adherence before bacterial incubation significantly increased biomass in PEG yet failed to have an effect on P(SY) **1.** Experiments were carried out with 6-14 replicates and analysed with unpaired t.test, p < 0.05. namely that P(SY) **1** and PEG coatings significantly prevent the adhesion of bacteria (SI, Figure 1).

Increased biomass after fibringen pre-treatment was also detected for copolymer P(S-co-SY) 3, while PS stayed on an already highly elevated level. Since pathogenicity and reinfection is dependent on cell viability in biofilms, bacterial viability on the previously analysed surface coatings was conducted and assessed by a Live/Dead assay, employing Syto9 and Propidium Iodide stain, respectively (Figure 5 A). P(SY) 1 coated samples showed significantly decreased viability of surface-associated bacteria compared to copolymer 3 and PS. When comparing biomass production and the viability of cells on fibrinogen pre-treated PEG samples, one can observe that although biomass is decreased, a significant level of cell viability is detected. This is particularly true when compared with P(SY) 1, where biomass, as well as viability, are at decreased levels. This raises the question of hostile to favourable surfaces. The hostile environment provided by sulfur ylides could be explained by a mechanism that is referred to as killing on contact ²⁷. This hypothesis was further assessed by evaluating the cytotoxicity of P(SY) 1 in solution (SI Figure 2).

To avoid self-assembly of polymers, a reduced concentration of 0.1 mg/ml was utilized for growth inhibition assays (SI Figure 9). Bacteria grown in a forced planktonic state over 24 hours show significantly reduced growth when exposed to P(SY) 1, compared to PEG and pure BHI Broth medium (Figure 5 B), explaining reduced viability as observed in the Live/Dead assay. To further elucidate a potential killing by contact mechanism and an associated toxicity effect caused by P(SY) 1, an uptake assay was performed. Images taken after 4 h indicate that Cy3 labelled P(SY) 1 was internalized (Figure 5 C). Both, the cellular uptake of P(SY) 1 and cytotoxicity in solution at already low concentration indicate that poly(sulfur ylides) provide a hostile environment for bacterial cells that attach. The observed toxicity towards bacterial cells made us wonder if the ylide displays a general cytotoxic structural motif. In literature, cytotoxicity studies of carbon-centred ylides are absent, which can be explained by the typical high reactivity associated with ylides.

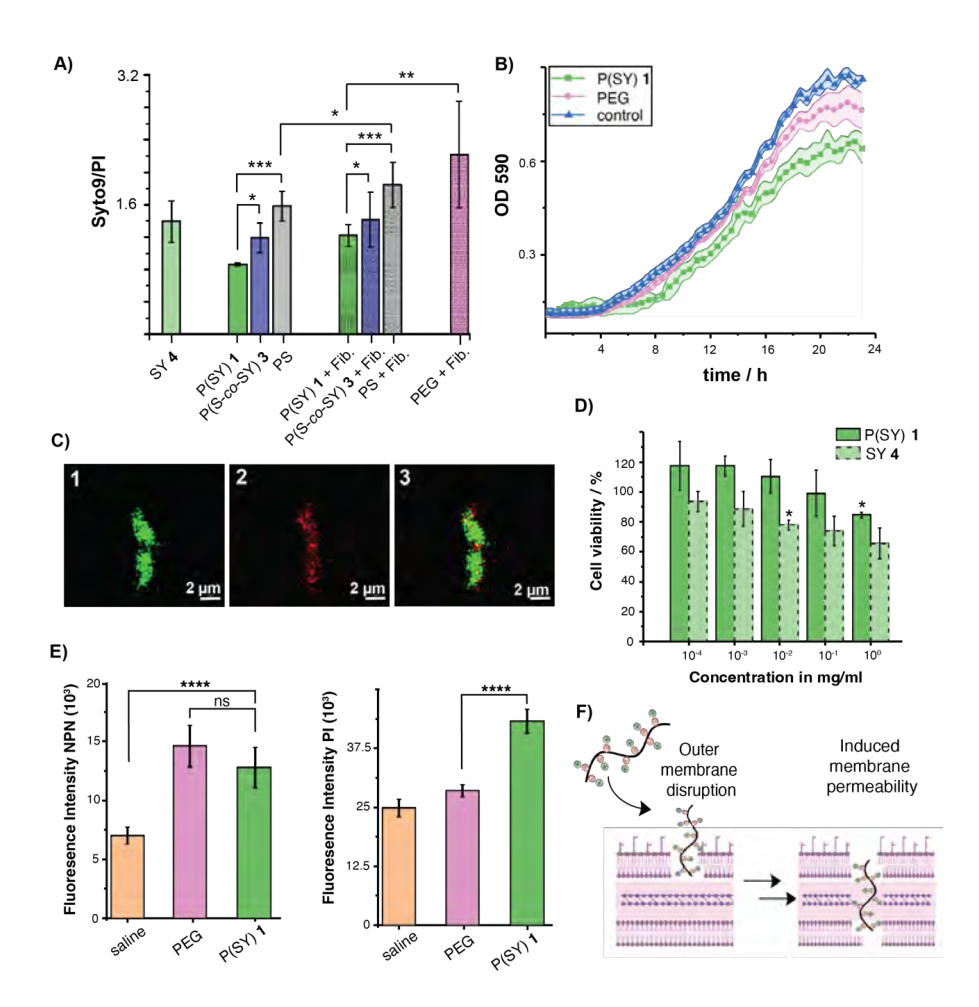


Figure 5. A) Viability of biofilms are significantly decreased when grown on P(SY) **1** compared to copolymer P(S-co-SY) **3** and PS. Experiments were carried out with 3-8 replicates and analysed with unpaired t.test, p < 0.05. **B)** P(SY)**1** (0.1 mg/ml) decreases planktonic growth when in solution compared to PEG and only medium. **C)** Bacteria stained with Syto9 (C 1) show uptake of Cy3 labelled P(SY) **1** (C 2) and merged image (C 3). Scale bar represents 2 μ m. **D)** Cytotoxicity studies of ylide bearing polymer P(SY)**1** and small molecule SY **4** in HEK 293 cells for 72 h. Variance was determined with f.test and the correct t.test against the control samples ($p \le 0.01$, p = 5). **E)** NPN-assay with pseudomonas aeruginosa and polymers (0.1 mg/mL). Pl-uptake assays with pseudomonas aeruginosa and polymers (0.1 mg/mL). Experiments were carried out with 6 replicates and analysed with unpaired t.test, p < 0.0.5. **F)** Postulated mechanism of interaction of bacterial membrane and poly(sulfur ylide). Parts of figure were created with BioRender.com.

For that reason, we carried out cytotoxicity studies with human HEK 293 cells for both, ylide bearing polymer P(SY) 1 and small molecule ylide 4. For P(SY) 1 no cytotoxic effect was observed even at high micromolar concentration after incubation for 72 h (Figure 5 D). While the small molecule ylide is also displaying overall only a low level of cytotoxicity, a decrease in cell viability was observed at a much lower concentration of 40 μM. We hypothesized that the small molecule is preferable taken up by cells and therefore has a larger impact on the cell viability. A similar trend was observed when performing cytotoxicity with NIH/3T3 and CHO cells indicating that ylide bearing polymer P(SY) 1 is not affecting the cellular membrane of human cells (SI, Figure 3-5)Next, we turned our attention again towards the interaction between poly(sulfur ylides) and gram-negative bacterial membranes. For gaining a better understanding, we incubated *Pseudomonas* aeruginosa together with P(SY) 1 and subsequently visualized outer membrane disruption. This was done by using 1-N-phenylnaphthylamine, a small molecule fluorescent probe that allows to visualise outer membrane permeability and disruption ²⁸. While a somewhat increased level of fluorescence was detected, no statical significant difference to polyethylene glycol was observed (Figure 5 E). Both, PEG and P(SY) 1 display not more than a 2-fold increase in fluorescence, which is considerably lower than values typically observed for outer-membrane damage ^{29, 30}. Next, bacterial cells were incubated with P(SY) **1** or PEG (0.1 mg/mL) and subsequently stained with propidium iodide. Here, a significant difference was observed between poly(sulfur ylide) and polyethylene glycol, namely that P(SY) 1 induces total membrane permeability, while PEG is not promoting the uptake of propidium iodide, indicating an intact cellular membrane. These results can be either explained by i) a cytotoxic effect of poly(sulfur ylides) resulting in membrane damage, or by ii) active membrane damage as a result from poly(sulfur ylide) insertion. Taken together, this reveals a mechanism which goes beyond a sole repelling effect caused by hydration layer. Based on our results, we hypothesize that initial adhesion is vastly prevented by a strong hydration effect; yet, in the event of successful adhesion, bacteria are exposed to a hostile and highly unfavourable surface. In contrast, PEG coatings display antifouling properties due to their repellent nature and are not hostile 31. To further confirm this hypothesis, we treated P. aeruginosa and E. coli with varying concentrations of P(SY) 1 and observed that both cell types were affected at higher concentration, whereas P. aeruginosa was affected already at lower concentration (0.01 mg/mL) (SI Figure 2). A trend emerges when comparing the cytotoxicity assays of bacterial and mammalian cells, namely that the polymeric sulfur ylides display bactericidal activity while not affecting eukaryotic cells.

To further explore the biocompatibility of sulfur ylides with eukaryotic cells, we intended to grow fibroblast NIH/3T3 cells on sulfur ylide-derived coatings along with two control groups featuring PEG- and collagen-coated surfaces. We observed that fibroblasts grown on PEG-coated surfaces exhibited reduced cell density and displayed a rounded morphology (Figure 6, SI Figure 7). In stark contrast, fibroblasts grown on polymeric ylides, and collagen-coated surfaces displayed the typical elongated shape of fibroblasts.

Our findings suggest that poly(sulfur ylides) not only serve as a new replacement for PEG-derived materials but also provide an additional antifouling mechanism by creating a selective toxic environment for those bacterial cells that overcome the initial hydration barrier, Importantly, this mechanism seems not to be affecting mammalian cells.

Selective toxicity towards bacterial cells over human cells is often attributed to a so-called 'amphiphilic balance,' which we believe might also apply to the polymeric sulfur ylide reported here 32, 33. While the polystyrene backbone displays strong hydrophobicity, the sulfur ylide residues exhibit hydrophilic properties. This structural feature enables initial binding to the bacterial cell membrane via electrostatic attraction, followed by the insertion of the hydrophobic part into the membrane core, ultimately resulting in membrane permeabilization ³³. To gain a better understanding of the structure-properties relation of these materials, as well as expand the chemical space, multiple different ylide-based materials were examined for their antifouling effects. We began by investigating a stabilized phosphorus ylide, namely poly(trimethyl phosphorus ylides) (P(TMPY)), which we compared to a P(DMAPS), a widely used zwitterionic polymer considered efficient in use as an antifouling coating 34,35.

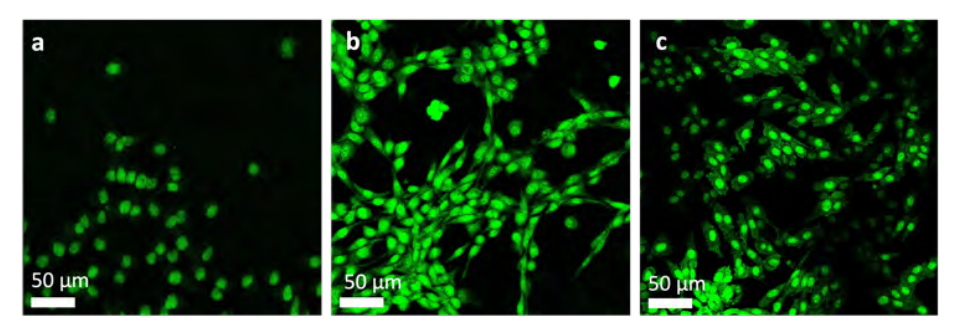


Figure 6. NIH3T3 cells seeded on coated glass slides with A) PEG, B) P(SY) 1 and C) collagen. After 24 h, cells were stained with Syto9 and images were taken with confocal microscopy.

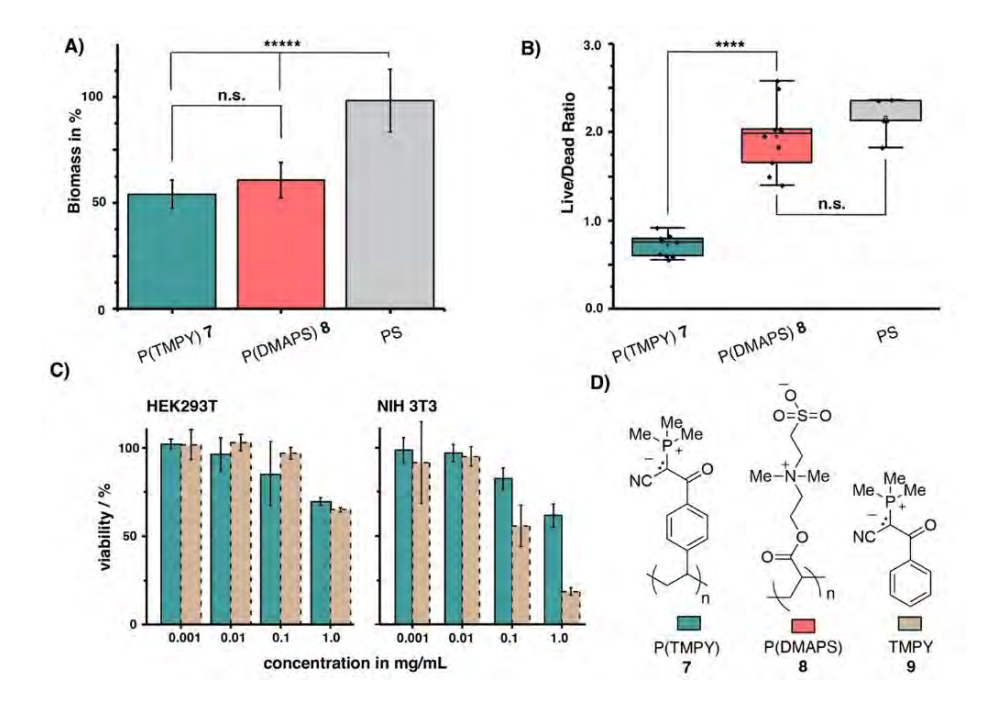


Figure 7. A) Biomass formation upon incubation with Pseudomonas aeruginosa (4 h, 37 °C) on surfaces covalently coated with zwitterionic P(TMPY) 7 and P(DMAPS) 8 alongside the reference of polystyrene. B) Live/dead ratio was determined by applying Syto9 and PI stain upon incubation of samples with Pseudomonas aeruginosa (4 h, 37 °C). C) Cytotoxicity was determined by incubating HEK293T and NIH 3T3 cells with polymeric phosphorus ylide 7 or small molecule analogue 9 for 72 h at 37 °C. **D)** Structures of P(TMPY) 7, P(DMAPS) 8, and small molecule TMPY 9.

We evaluated these coatings in their ability to prevent the accumulation of biomass upon incubation with Pseudomonas aeruginosa. Both coatings displayed a significant decrease in biomass in comparison to simple polystyrene surfaces, while the difference between P(TMPY) 7 and P(DMAPS) 8 was statistically not significant. In contrast, when determining the ratio of viable and dead cells, a significant difference was observed. Surfaces coated with poly(betaine) 8 and untreated polystyrene displayed a majority of viable cells without statistical significance; yet, poly(phosphorus ylide)-coated surfaces exhibited a majority of dead cells (Figure 7 A and B). These results indicate that poly(phosphorus ylides) behave in a similar way than poly(sulfur ylides) by preventing biofilm formation with a combination of hydration layer and toxicity toward bacterial cells. For many applications, selective toxicity toward bacterial cells is desirable, for example, for implants or other biomedical devices. For that reason, we determined the effect of polymeric phosphorus ylides on mammalian cell lines. Three cell lines, HEK293T, NIH3T3, and CHO, representing human 195 embryonic kidney, mouse fibroblasts, and epithelial ovarian cell lines, respectively, were incubated with P(TMPY) 7 and small molecule analogue 9 for 72 h (Figure 7 and SI Figure 6). At lower concentrations, no cytotoxicity was observed for either of the phosphorus ylide species. Whereas small molecule phosphorus ylide 9 became cytotoxic for fibroblast cells. At a higher concentration of 1 mg/mL, P(TMPY) 7 only displayed reduced viability (60% viability). The difference in toxicity between polymeric ylide 7 and small molecule 9 could be related to enhanced cellular uptake of the small molecule. Notably, the ylides do not seem to affect CHO cells. Taken together, we have introduced poly(phosphorus ylides) as a readily available and versatile class of zwitterionic polymers bearing acyl/nitrile-stabilized carbon ylide-residues. We hypothesize that the principle of 'amphiphilic balance' may be applicable to the here reported poly(phosphorus ylides) and explains the preferential toxicity to bacterial cells over mammalian cells ^{32, 36}. While ylide residues possess hydrophilic characteristics, the polystyrene backbone exhibits significant hydrophobicity. This structural attribute facilitates an initial interaction with the bacterial membrane through electrostatic attraction, with subsequent insertion of the hydrophobic component into the cell membrane, which ultimately leads to membrane permeabilization ³³.

Since some of the previous effects could be related to the hydrophobic styrene backbone, we investigated the effects of changing the backbone to a watersoluble acrylamide backbone, while keeping the sulfur ylide group, resulting in Poly(Acrylamide Sulfur Ylide), namely P(AmSY) (Synthesized and characterized by Neumann and Karagrigoriou).

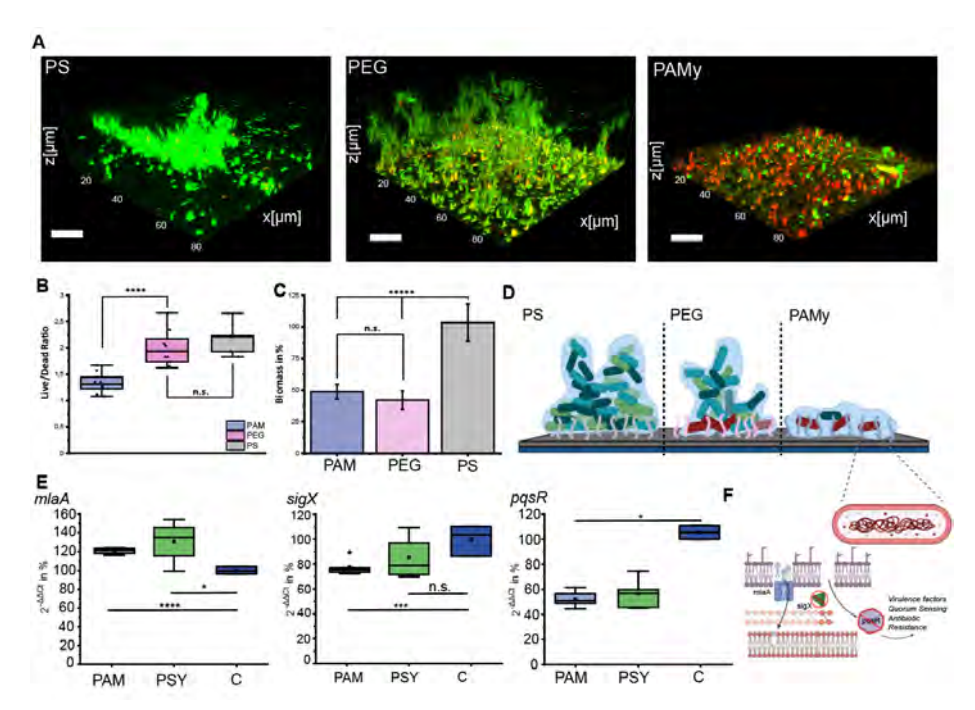


Figure 8. Effects of P(AmSY) and PSY on biofilms. Confocal images A) of biofilms grown on Polystyrene, PEG and P(AmSY), scale bars are set at 20 µm. Live Dead ration B) of biofilms, quantified via Biofilm Viability Checker from confocal images and Biomass C) measured using Crystal Violet assay. Statistical significance was assessed via f.test and one-sided t.test with $p \le 0.01$. D) Schematic overview of different biofilm growth development on the three tested surfaces, gRT-PCR analysis E) of genes mlaA, siqX and pqsR. Statistical significance was assessed via f.test and one-sided t.test with p ≤ 0.05 . F) Graphical overview of molecular response to PAMy, upregulation of mlaA for outer membrane lipid transfer following outer membrane damage, disruption of sigX and pqsR, leading to beneficial effects for biofilm treatment.

To visualize the possible effects P(AmSY) has in biofilm formation, glass surfaces functionalized with PEG, PS and P(AmSY) were prepared and incubated with bacteria to allow for biofilm growth. Confocal images reveal fully formed biofilms with complex pores formed for PS and PEG, while bacteria grown on P(AmSY) were unable to form biofilms above one or two cell layers, with the majority of cells being non-viable (Figure 8A). This effect is quantified via a Live/Dead ratio calculation, revealing a significantly less viable population on P(AmSY) when compared to PEG and PS. Expectedly, biomass for P(AmSY) is significantly reduced. Although confocal images show functional biofilms for PEG, overall Biomass when quantified is still reduced when compared to PS. We hypothesize that, while PS offers an ideal surface, PEG only inhibits the initial attachment, with little effect on viability as previously hypothesized. This effect can then be overcome with accumulating biomass and allow for biofilm overgrowth Figure (8A and C). The underlying genetic responses which P(AmSY) activates were compared to P(SY)1, which we discussed previously. Since P(SY)1 was shown to cause membrane damage, we analyzed the transcript levels of the outer membrane lipoprotein MlaA after 4 hours of exposure. The Mla (maintenance of outer membrane lipid asymmetry) apparatus has been shown to aid in outer membrane lipid asymmetry, with MlaA effectively removing mislocalized glycerophospholipids from the OM ^{37, 38}. In both P(AmSY) and P(SY)1, mlaA transcripts are significantly increased when compared to the non-treated control, indicating the disturbance of the outer membrane by both polymers, Many genetic responses and adaptations in P. aeruginosa are controlled transcriptional regulators called sigma factors ³⁹. Amongst these sigma factors, Sigx, also referred to as $\sigma(22)$, is a main regulator when it comes to the response to cell wall envelope stress, as well as production of virulence factors such as alginate 40,41. We observe that upon exposure Sigx transcription levels are significantly decreased for P(AmSY) treatment, yet do not significantly changer for P(SY)1. Sigx has been shown to be upregulated upon exposure to most cell wall targeting compounds, so the decrease in transcriptional activity seems guite counterintuitive. Some data suggests, that decreasing sigX has resulted in higher baseline biofilm formation, so one plausible hypothesis would be a potential feedback loop, in which the downregulation is meant to compensate for the lack of biofilm formation 42. Other work highlights the connection between the loss of SigX and membrane fluidity and integrity 43. Considering this observation, we believe that there is an underlying mechanistic difference in how P(SY)1 and P(AmSY) interact with the membrane due to the difference in chemical nature. A big hurdle when combating biofilms are secreted virulence factors, allowing for adaptation of the bacterial population to adverse effects, the host immune system, and other parameters dictating the infection cycle 44. The pseudomonas quinolone signal (pgs) system is a main contributor to the excretion of such virulence factors, as well as a core regulator of the quorum sensing network, which governs biofilm growth and dispersion 45, 46. The adverse effects of both Pamy and PS significantly decrease the transcription levels of pask, which stands at the top of the pgs system, by controlling the production of the pgs signal molecule, as well as activating excretion of toxins and other pathways 47, 48. The inhibition of the pgs system is a highly desirable effect, due to the direct consequence this has on biofilm virulence, persister cells, and overall viability, all being negatively affected by shutting down this network 48,49.

2.3 Conclusion

For decades, poly(ethylene glycol) was frequently referred to as the golden standard for (bio) medical applications. Rising concerns about the safety profile and the chemical reactivity, forced researchers to identify alternative materials with zwitterionic polymers being among the most popular ones. To this end, the vast majority of zwitterionic materials is based on polybetaines and polyampholytes; yet, the chemical space and accessibility of both polybetaines and polyampholytes are severely limited. Here, we demonstrate – for the first time – that poly(sulfur ylides) efficiently induce hydration layers and prevent the adhesion of both, biomolecules and pathogenic bacteria. Our results show that poly(sulfur ylides) exhibit strong antifouling properties that are comparable to poly(ethylene glycol), effectively preventing the adhesion of both biomolecules and pathogenic bacteria. In strong contrast to PEG, our results indicate that poly(sulfur ylide) are not only preventing the formation of biofilms by surface hydration but also display a hostile environment for bacterial growth while not affecting mammalian cells. This effect is translated when altering the chemical composition of the polymers, by exchange of the sulfur ylide by a stabilized phosphorus ylide, or by removal of the styrene backbone for a water-soluble acrylamide backbone. We believe ylides to hold significant impact on pioneering novel coatings to deter biofilm formation in clinical settings.

2.4 Acknowledgments

This work was funded by Radboud University (start-up-package), B. B. and D. W. acknowledge financial support from Ministry of Education, Culture and Science (Gravitation program 024.001.035). We would like to thank the NMR facility at Radboud university for their support. We like to thank Dr. Robert Jansen and Prof. Dr. Laura van Niftrik for the access to ML2 facilities and for their help. We thank Helene Amatdjais-Groenen for support in SEC analysis.

2.5 Experimental and Supplementary Information

All polymers were synthesized and characterized by the Neumann group. Surface energy analysis and contact angle measurements were conducted by the Neumann group. Coated slides and well plates were prepared and provided by the Neumann group as well.

Fibrinogen Adhesion

To circumvent potential change of Fibrinogen surface properties via fluorescent labeling, Fibrinogen was first adhered to the modified surface and labeled afterwards. Fibrinogen (0.5 mg/ml) was dissolved in PBS (Thermo Scientific, end concentrations: 150 mM NaCl, 100 mM NaPO $_{\alpha}$, pH 7.4) and added to the wells (100 μ l). After 2 hours at room temperature, wells were gently washed with PBS (150 mM NaCl, 100 mM NaPO₄, pH 8.4) three times after which Alexa Fluor 647 (stock solution: 100 μg in 100 μl DMF) was added in PBS (150 mM NaCl, 100 mM NaPO₄, pH 8.4, 40 µl into 4 ml) and left at room temperature for 2 more hours to allow binding of dye to Fibrinogen. Wells were washed three more times and adsorption was measured with a microplate reader at $\lambda = 562$ nm in a Tecan Spark M10 plate reader.

Biofilm formation

All experiments were conducted with *P. aeruginosa* ATCC 10145. An overnight culture was inoculated from a 50% Glycerol Stock and grown in BHI broth for 24 hours at 37 °C. The OD was monitored and diluted into BHI broth to a working solution with an OD of 0.005 which was used for inoculating wells.

Live/Dead Assay

96 well plates with various modified surfaces were inoculated with 100 µl of bacterial solution in BHI broth (OD 0.005) and incubated for 4 hours at 37 °C to allow for adhesion and biofilm formation. After 4 hours, all wells were gently washed three times with 1x PBS buffer (pH 7.4) to remove planktonic cells. BacLight stain (Molecular Probles) containing Syto9 and Propidium Iodide was used to create a suitable working solution: for Syto9 a final concentration of c = 11.1 nM and for Propidium Iodide a final concentration of c = 66.6 nM in PBS (150 mM NaCl, 100 mM NaPO₄ mM, pH 7.4). Wells were stained for 10 minutes and washed three times with PBS (150 mM NaCl, 100 mM NaHPO₄, pH 7.4). Fluorescence intensity was measured at λ_{ex} = 485 nm, λ_{em} = 535 nm and λ_{ex} = 300 nm, λ_{em} = 632 nm, respectively, with a bandwidth of 20 nm, 30 flashes and an Integration time of 40 µs using a Tecan Spark M10 plate reader.

Crystal Violet Stain

96 well plates with various modified surfaces were inoculated with 100 ul of bacterial solution in BHI broth (OD 0.005) and incubated for 4 hours at 37 °C to allow for adhesion and biofilm formation. After 4 hours, all wells were gently washed three times with 1x PBS buffer (pH 7.4) to remove planktonic cells and subsequently stained for 10 minutes with 0.01 % Crystal violet in water (w/v). CV solution was then removed, and wells washed three times with PBS buffer before

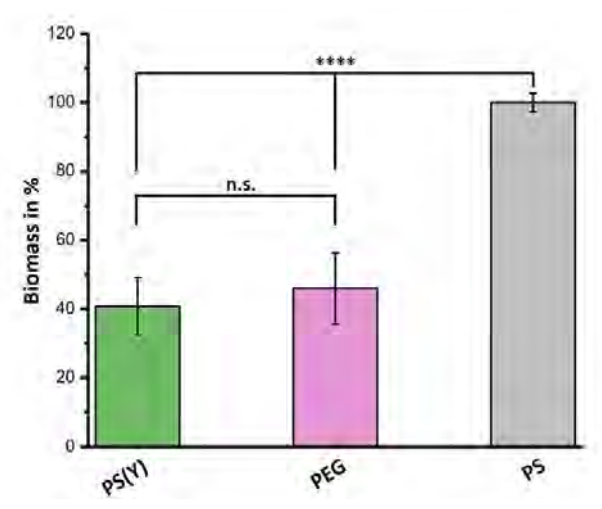
letting the well plate dry overnight fpr analysis. Stained biomass was resolubilized in 30% Acetic acid in distilled water (v/v) and transferred to a new clear bottom well plate. Absorbance was measured at 590 nm in a Tecan Spark M10 plate reader.

Assessing Bacterial adhesion onto Fibrinogen treated surfaces

100 µl Sterile Fibrinogen solution (0.5 mg/ml) was added to pretreated wells and left at room temperature for 2 hours after which wells were gently washed three times with PBS (150 mM NaCl, 100 mM NaPO, pH 7.4). 100 µl of P. aeruginosa in BHI broth (Final OD 0.005) were seeded into each well and left to incubate 4 hours at 37 °C. Afterwards wells were washed three times to remove planktonic cells and either stained with L/D stain or Crystal violet as previously described.

Bacterial Growth in Human Serum

To challenge the Ylide surface coating Bacteria were incubated in Human AB Serum (Sigma Aldrich). 96 well plates with PEG and PSY coated surfaces were inoculated with 100 µl of bacterial solution in Human AB Serum broth (OD 0.005) and incubated for 4 hours at 37 °C to allow for adhesion and biofilm formation. After 4 hours, all wells were gently washed three times with 1x PBS buffer (pH 7.4) to remove planktonic cells and subsequently stained for 10 minutes with 0.01 % Crystal violet in water (w/v). CV solution was then removed, and wells washed three times with PBS buffer before letting the well plate dry for analysis. Stained biomass was resolubilized in 30 % Acetic acid in distilled water (v/v) and transferred to a new clear bottom well plate. Absorbance was measured at 590 nm in a Tecan Spark M10 plate reader.



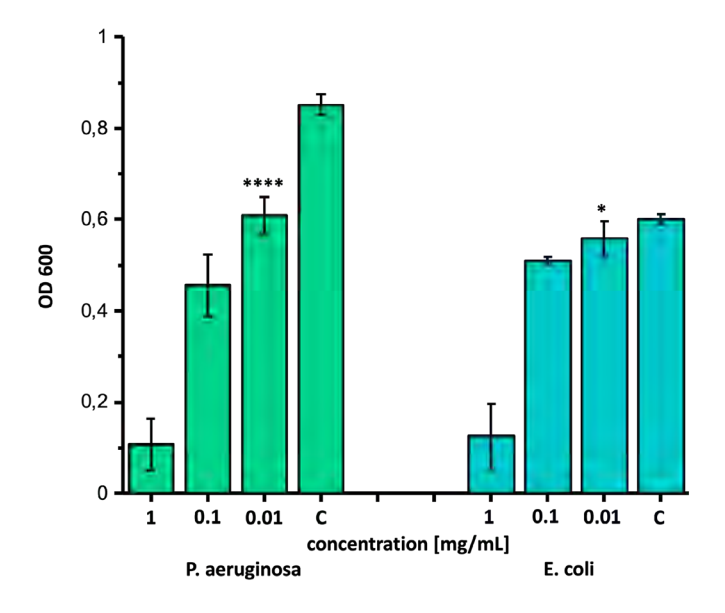
Supplementary Figure 1. Both PEG and PSY-coated surfaces show significantly decreased biomass compared to Polystyrene (PS). Experiments were carried out in 15 replicates and analyzed with an unpaired t. test, p < 0.05.

Growth Curve

An overnight culture of P. aeruginosa was diluted to a final OD of 0.01 in BHI broth with 0.04 % Tyloxapol to prevent aggregation and Biofilm formation. PEG and P(SY) 1 (Stock 100 mg/ml in DMF) were added to final concentrations of 0.1 mg/ml. 100 µl of bacterial solution with Polymers were added to a clear 96 well plate (Greiner) and measured every 30 minutes in a Tecan Spark M10 Plate reader at an OD 600. Temperature was set to 29 °C.

Toxicity towards Bacterial Cells

E. coli BL21 DE3 and P. aeruginosa overnight cultures were diluted to an OD of 0.01 in BHI supplemented with Tyloxapol 0.04%. Bacterial solution was mixed with varying concentrations of P(SY) 1 (1.0, 0.1, 0.01 mg/mL) and added to a clear wellplates. Absorbance at 600 nm was immediately measured to get a baseline, before returning the plate back into the incubator for 24 hours at 37 °C. Afterwards absorbance was measured again at 600 nm and data analysed by subtracting the last OD from the baseline to retrieve an OD increase after 24 hours.



Supplementary Figure 2. Cytotoxicity studies of polymer P(SY) 1 with E. coli and P. aeruginosa. Cells were incubated for 24 h upon treatment with polymer.

Uptake assay

100 µl Cy3 labelled P(SY) 1 was mixed with 400 µl of *P. aeruginosa* solution (OD 0.1) in PBS (150 mM NaCl, 100 mM NaPO, pH 7.4) and incubated at 10 °C and 350 rpm in a Thermoshaker for 5 hours. Bacteria were pelleted at 5000 rcf for 10 minutes and washed in PBS (150 mM NaCl, 100 mM NaPO, pH 7.4) three times before. To visualize bacteria, they were staining with Syto 9 c = 11.1 nM, in PBS (150 mM NaCl, 100 mM NaPO, pH 7.4) for 10 minutes pelleted at 5000 rcf for 10 minutes and washed in PBS (150 mM NaCl, 100 mM NaPO, pH 7.4) three times before being transferred into a ibidi µ slide 18 well (Ibidi). Imaging was done on a SP8x Confocal Laser scanning system using a 63x/ 1.40 Oil Objective (0.14 mm). Lasers were set at $\lambda_{PX} = 470$ nm, $\lambda_{\rm em}$ = 500-520 nm and $\lambda_{\rm ex}$ = 550 nm, $\lambda_{\rm em}$ = 620-700 nm, using HyD Detectors. Images were later analysed with Imaris.

Inner and outer membrane permeability

NPN Assay

Outer membrane permeability was assessed via NPN assay derived from the previously described protocol by Munquia et. al. with minor changes (Munquia J, LaRock DL, Tsunemoto H, Olson J, Cornax I, Pogliano J, Nizet V. J Mol Med (Berl). 2017 Oct; 95(10):1127-1136.).

Bacteria were grown overnight and diluted to an OD of 0.1 with 0.1 mg/ml of Ylide or PEG solution, or 0.9% saline supplemented with 0.04% of Tyloxapol in PBS (150 mM NaCl, 100 mM NaPO $_{\rm A}$ mM, pH 7.4) with 0.04 % of Tyloxapol and incubated for 30 minutes in the fridge. To each well 90 µl of bacterial solution and 10 µl of a stock of 120 µM NPN in PBS was added resulting in a final NPN concentration of 12 μ M. Samples were immediately measured at $\lambda_{ev} = 350$ nm, $\lambda_{em} = 420$ nm in a Tecan Spark M10 Plate reader.

PI Stain for inner membrane damage

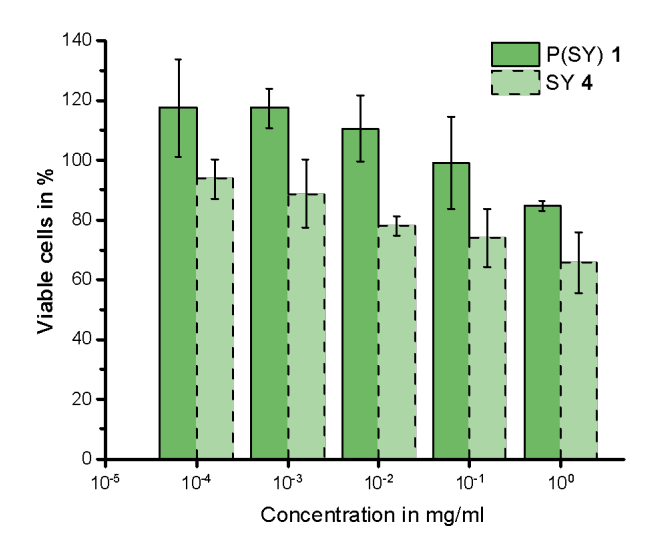
Bacteria were grown overnight, spun down at 5000 rcf for 10 minutes and diluted to an OD of 0.1 in using a 0.1 mg/ml of Ylide or PEG solution, or 0.9% saline supplemented with 0.04% of Tyloxapol. The samples were incubated for 30 minutes in the fridge and subsequently stained with a Propidium Iodide solution at final concentration of c = 66.6 nM for 15 minutes.

Samples were spun down 3x at 5000 rcf for 10 minutes to remove unbound Propidium Iodide and washed into PBS (150 mM NaCl, 100 mM NaPO₄ mM, pH 7.4)

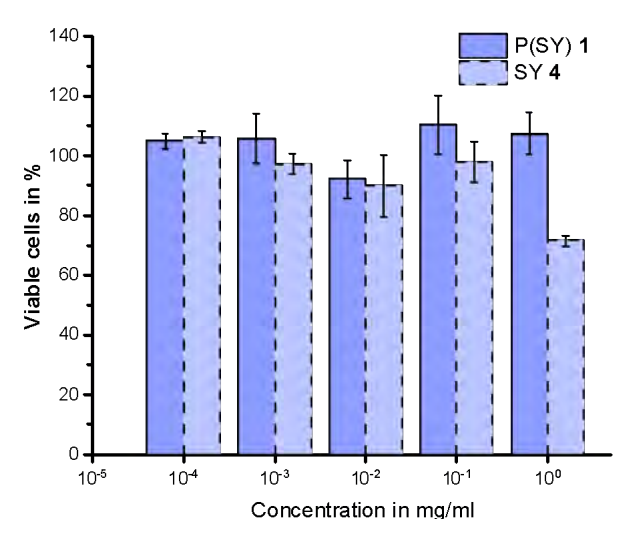
and added to a 96 wellplate. Samples were measured in 8 replicates at λ_{ex} = 485 nm, λ_{em} = 530 nm in a Tecan Spark M10 Plate reader.

Cytotoxicity assays

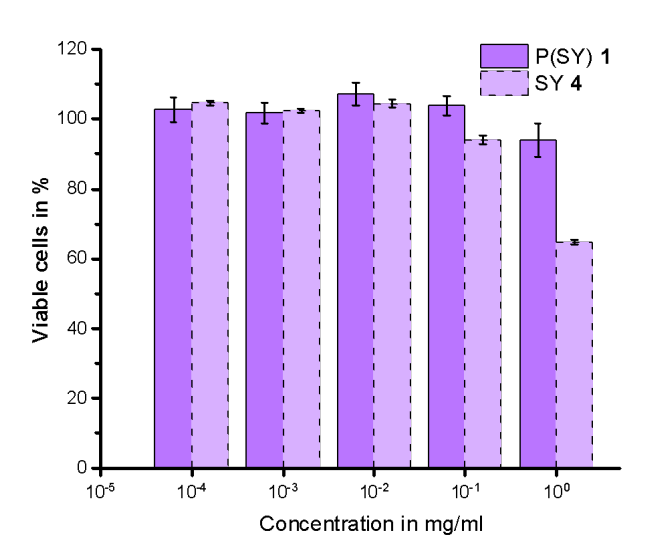
HEK293T, Chinese Hamster Ovarian (CHO) and NIH 3T3 cells were cultured in DMEM medium supplemented with 10% FBS. After cells reached a confluence of around 50 %, they were rinsed with 1x PBS three times and detached with 4 ml Trypsin for 3 minutes. Trypsin was quenched by adding 8 ml of DMEM medium. The cells were transferred to a 15 ml falcon and spun down 5 minutes at 0.3 rcf. The supernatant was discarded, and cells seeded with DMEM complete medium in a 96 well plate at a density of 4.0 to 4.5 x 10^4 cells/ml and incubated for 24 hours at 37 °C with $5 \% CO_2$. Afterwards, varying concentrations of polymer in DMEM complete medium were added to the wells and left to further incubate at 37 °C and $5 \% CO_2$ for 72 hours. $10 \mu l$ of CCK8 (Sigma Aldrich) was added to the wells, incubated for 3 hours and the absorbance measured at 450 nm.



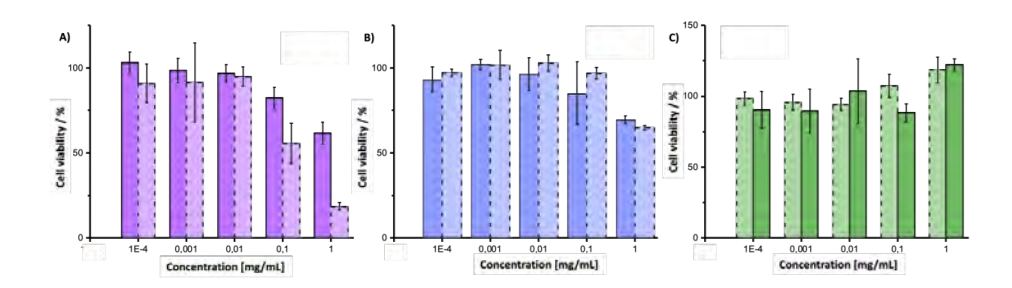
Supplementary Figure 3. Cytotoxicity studies of polymer P(SY) **1** and small molecule ylide SY **4** with HEK293 cells. Cells were incubated for 72 h upon treatment with polymer or small molecule. Variance was determined with f test and the correct t.test against the control samples utilized, $p \le 0.01$, n = 5.



Supplementary Figure 4. Cytotoxicity studies of polymer P(SY) 1 and small molecule ylide SY 4 with NIH3T3 cells. Cells were incubated for 72 h upon treatment with polymer or small molecule. Variance was determined with f test and the correct t.test against the control samples utilized, $p \le 0.01$, n = 5.



Supplementary Figure 5. Cytotoxicity studies of polymer P(SY) 1 and small molecule ylide SY 4 with CHO cells. Cells were incubated for 72 h upon treatment with polymer or small molecule. Variance was determined with f test and the correct t.test against the control samples utilized, $p \le 0.01$, n = 5.



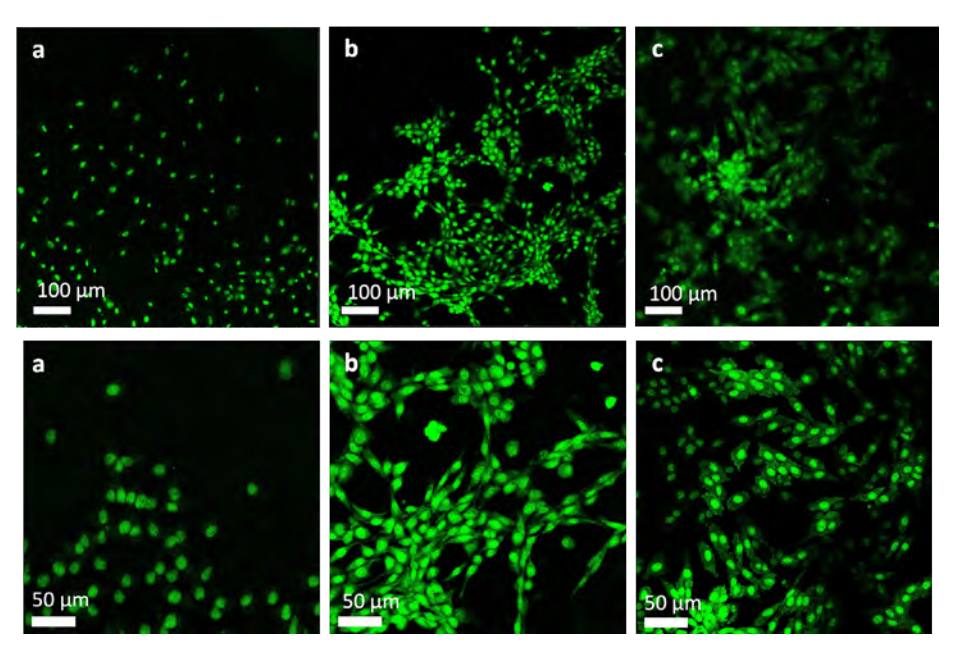
Supplementary Figure 6. Cytotoxicity of mammalian cells after 72 h incubation with P(TMPY) 7 (solid line) and small molecule analogue 9 (patterned line) A) NIH 3T3 B) HEK 293 C) CHO.

Analysis of cell adhesion via confocal microscopy

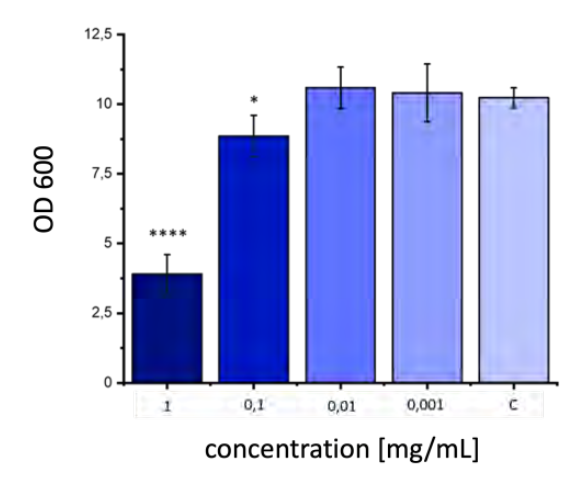
Amine coated glass (obtained from PolyAn) slides were covalently modified with PEG and P(SY) 1. As an additional reference, collagen (Bornstein and Traub Type I, powder, obtained from Sigma Aldrich) was coated on glass slides. To analyze cell adhesion, 100 µl NIH 3T3 cells in DMEM medium were seeded at a density of 5 x 10⁴ cells/ml in silicon molds on top of functionalized glass slides and grown for 24 hours. The medium was removed, and cells were gently washed with PBS before staining with Syto9 in PBS (final concentration of c = 11.1 nM) for 20 minutes and subsequently washing three more times with PBS. The molds were then removed and cells covered with a 1.5 Coverslip with a drop of PBS for imaging. Imaging was conducted on a SP8x Confocal Laser scanning system using a 10x/ 0.40 and a 20x/ 0.40 Air objectives. Lasers were set at $\lambda_{av} = 470$ nm, $\lambda_{am} = 500-520$ nm. Images were later analysed with Imaris.

Bacterial Cytotoxocity assay

An overnight culture was prepared as described above with the addition of 0.04 % Tyloxapol. After 24 hours bacteria were adjusted to an OD of 0.01 in various concentrations of P(AmSY). 100 µl of bacterial-polymer solution were added into 96 well plates and left to incubate for 24 hours at 37°C. Afterwards, the OD was measured using a Tecan Spark M10 plate reader at 600 nm. Experiments were carried out in replicates of n=7-9.



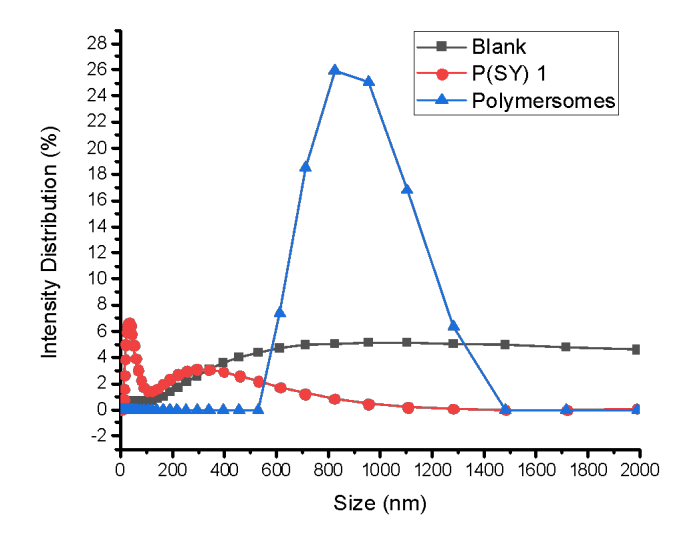
Supplementary Figure 7. NIH3T3 cell growth on a) PEG, b) PSY 1 and c) collagen coated glass slides. Cells were stained with Syto9. Images were taken with confocal.



Supplementary Figure 8. Growth factors of planktonic bacteria in the presence of 1 to 0.001 mg/ml over 24 hours. Samples were conducted in replicates of 10. P value \leq 0.01.

DLS measurements

Dynamic light scattering experiments were performed for determining whether P(SY) 1 forms aggregates at the concentration used for cytotoxicity studies (c = 0.1 mg/mL). Dynamic light scattering experiments were carried out on a Malvern Zetasizer Nano S equipped with a He-Ne (633 nm, 4 mW) laser and an Avalanche photodiode detector at an angle of 173°. No larger aggregates were observed and only noise signal was recorded as can be seen when comparing to a blank consisting of MilliQ (Figure 13). As a reference, polystyrene-PEG polymersomes were added to confirm sensitivity of the measurements.



Supplementary Figure 9. P(SY) 1 was dissolved in water (c = 0.1 mg/mL). Dynamic light scattering revealed that there are no larger aggregates present that might influence cytotoxicity studies.

Confocal Microscopy

Various coated slides were prepared to assess biofilm growth. For this, silicon culture inserts were reversibly mounted on the slides, creating a reservoir which allowed for biofilm growth. Previously prepared bacterial solution diluted to an OD of 0.1 was then seeded into these reservoirs and left to incubate for 24 hours. Afterwards the biofilms were cleaned with PBS before being stained with Live Dead stain. Syto9 and Propidium lodide were used to create a suitable working solution: for Syto9 a final concentration of c = 11.1 nM and for Propidium lodide a final concentration of c = 66.6 nM in PBS (150 mM NaCl, 100 mM NaPO4mM, pH 7.4).

Biofilms were stained for 10 minutes and washed three times with PBS (150 mM NaCl, 100 mM NaHPO., pH 7.4). The silicone culture inserts were then removed and a coverslip glued over the biofilm populated areas with instant glue. Imaging was conducted using an SP8x AOBS-WLL confocal laser scanning microscope. Lasers were set at $\lambda ex = 470 \text{ nm}$, $\lambda em = 500-520 \text{ nm}$ and $\lambda ex = 560 \text{ nm}$, $\lambda em = 620-670 \text{ nm}$. Images were later analysed with Imaris.

RNA Extraction

Bacteria harvested from an overnight culture were diluted to an OD of 0.1 in the different treatments all prepared in BHI broth and left to incubate at 37°C for 4 hours. The total RNA was extracted from the biofilms using the RNeasy Kit of OIAGEN. Bacteria were spun down and pellets resuspended in 1x PBS and RNA protect reagent in a 1 to 2 ration. The samples were transferred into bead-beating tubes and the cells were lysed by 0.1mm Zirconia/silica beads in the BeadBug 6 bead homogenizer for 3 cycles of 30 seconds on and off at 4000rpm. Following the lysis, the lysate was transferred to the RNeasy Mini Spin Column and placed in 2 mL collection tubes. The columns were centrifuged at ≥8000x g for 15 sec. and the flow-through was discarded and the collection tube was reused. This step was repeated until all lysate was processed. Then to wash the spin column membrane 700µl Buffer RW1 was added and centrifuged at ≥8000x g for 15 sec. The flow-through was discarded and the columns were placed in new collection tubes. Subsequently, 500µl Buffer RPE was added and centrifuged at ≥8000x g for 15 sec. This step was repeated once more with 500µl Buffer RPE and centrifuged at ≥8000x g for 2 min. to ensure the removal of ethanol. The spin columns were then transferred to new 1.5 ml collection tubes, and 30-50µl of Rnase-free water was added directly to the membrane. The columns were then centrifuged at ≥8000x g for 1 min. to elute the Rather concentration and purity of the RNA were determined by the Nanodrop 1000™ spectrophotometer. Additionally, an Agarose Gel electrophoresis was conducted to verify presence of 16s RNA

cDNA Synthesis

For the cDNA synthesis, the RNA was treated with DNase to remove genomic DNA. This was done using the DNase I Amplification Grade by Invitrogen™. The following was added to an RNase-free PCR-strips on ice: 500 ng total RNA, 1µl 10X DNase I Reaction Buffer, 1μL DNase I Amplification Grade (1U/μl) and DEPC-treated water to 10µL. Then the PCR strips were incubated for 15 min. at room temperature. Then 1µl of 25 mM EDTA was added to inactivate the DNase I. Lastly, the RNA samples were incubated for 10 min. at 65°C. cDNA was synthesized using the SuperScript™ II Reverse Transcriptase by Invitrogen™. To each DNase-treated RNA 9µl of the following mix were added: 1µl random primers (250 ng/µl), 1µl 10mM dNTP's, 4µl 5X 1st Strand Buffer, 1µl 0.1M DTT, 1µl RNaseOUT™ (10 U/µl), 0.5µl Superscript II (200 U/µl) and 0.5µl DEPC-treated water. Mixed and incubated for 10 min. at 25°C followed by another incubation of 50 min. at 42°C and the reaction was inactivated by heating it for 15 min. at 70°C. After the cDNA synthesis, the cDNA was purified using the QIAquick PCR Purification Kit of QIAGEN. This was done according to the manufacturer's instructions. Following purification, the cDNA concentration was measured with the Qubit[™] 4 Fluorometer using the 1X High Sensitivity dsDNA assay.

gRT-PCR

gRT-PCR was performed using the iQ SYBR Green Supermix by Bio-Rad. Each reaction contains 10µL iQ SYBR Green Supermix, 2µL (10µM) forward primer, 2µL (10µM) reverse primer, 1ng cDNA and DEPC-treated water to a final volume of 20µL. The primers that were used are listed in Table x.

The gRT-PCR was performed in a Bio-Rad C1000 Touch Thermal Cycler using the following protocol: 95°C for 30 seconds, 95°C for 30 seconds, 60°C for 10 seconds and 72°C for 20 seconds (repeat 39X). Followed by a melt-curve analysis from 58°C to 95°C at a 0.5°C/cycle melt rate. The relative gene expression was calculated using the 2- $\Delta\Delta$ CT method, where all Ct values were normalized to the housekeeping genes gyrA and recA. All samples were carried out in replicates of n=3.

Table 1. Primer design for all genes of interest. Primers were designed using Primer3 and verified via Blast.

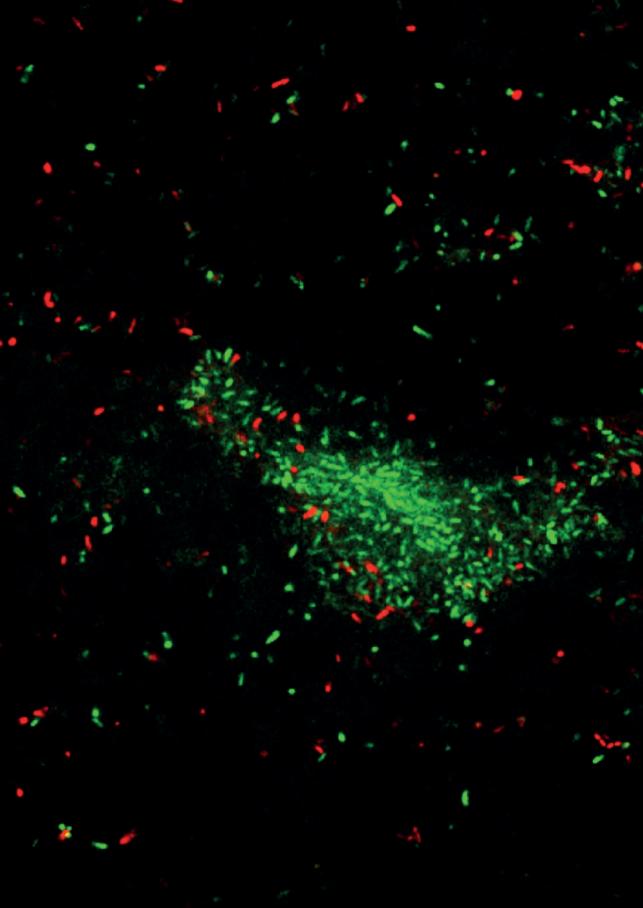
Gene of Interest	Forward Sequence (5'->3')	Reverse Sequence (5'->3')
mlaA	GCATCAACCGTCCCATCTTC	GGTTGTTGGCCAGGTTCTTC
sigX	CAAGCGCCGATTGATGGATG	TCAACCTTCGGCGACTTCTC
pqsR	CCAATTACCGGCAGATCAGC	TCGTAGAGTTCGCTGAGGAC
recA	GAAGTTCTACGCCTCGGTCC	GTTCTTCACCACCTTGACGC
gyrA	ATGGAGGTGATCCGTGAGGA	TTCTTCACGGTACCGAAGGC

2.6 References

- 1. Meyers, S. R.; Grinstaff, M. W., Biocompatible and bioactive surface modifications for prolonged in vivo efficacy. Chem Rev 2012, 112 (3), 1615-32.
- 2. Donlan, R. M., Biofilms: microbial life on surfaces. Emerg Infect Dis 2002, 8 (9), 881-90.
- 3. Assefa, M.; Amare, A., Biofilm-Associated Multi-Drug Resistance in Hospital-Acquired Infections: A Review. Infect Drug Resist 2022, 15, 5061-5068.
- 4. Ciofu, O.; Moser, C.; Jensen, P.; Høiby, N., Tolerance and resistance of microbial biofilms. Nat Rev Microbiol 2022, 20 (10), 621-635.
- 5. Zimmerli, W., Clinical presentation and treatment of orthopaedic implant-associated infection. Journal of Internal Medicine 2014, 276 (2), 111-119.
- 6. Tande, A. J.; Patel, R., Prosthetic joint infection. Clin Microbiol Rev 2014, 27 (2), 302-45.
- 7. Arciola, C. R.; Campoccia, D.; Montanaro, L., Implant infections: adhesion, biofilm formation and immune evasion. Nature Reviews Microbiology 2018, 16 (7), 397-409.
- 8. Grabbe, S.; Landfester, K.; Schuppan, D.; Barz, M.; Zentel, R., Nanoparticles and the immune system: challenges and opportunities. Nanomedicine (Lond) 2016, 11 (20), 2621-2624.
- 9. Cai, R.; Chen, C., The Crown and the Scepter: Roles of the Protein Corona in Nanomedicine. Advanced Materials 2019, 31 (45), 1805740.
- 10. Del Grosso, C. A.; Leng, C.; Zhang, K.; Hung, H. C.; Jiang, S.; Chen, Z.; Wilker, J. J., Surface hydration for antifouling and bio-adhesion. Chem Sci 2020, 11 (38), 10367-10377.
- 11. Chen, S.; Li, L.; Zhao, C.; Zheng, J., Surface hydration: Principles and applications toward lowfouling/nonfouling biomaterials. Polymer 2010, 51 (23), 5283-5293.
- 12. Pelaz, B.; del Pino, P.; Maffre, P.; Hartmann, R.; Gallego, M.; Rivera-Fernández, S.; de la Fuente, J. M.; Nienhaus, G. U.; Parak, W. J., Surface Functionalization of Nanoparticles with Polyethylene Glycol: Effects on Protein Adsorption and Cellular Uptake. ACS Nano 2015, 9 (7), 6996-7008.
- 13. Knop, K.; Hoogenboom, R.; Fischer, D.; Schubert, U. S., Poly(ethylene glycol) in drug delivery: pros and cons as well as potential alternatives. Angew Chem Int Ed Engl 2010, 49 (36), 6288-308.
- 14. Zhang, S.; Li, W.; Luan, J.; Srivastava, A.; Carnevale, V.; Klein, M. L.; Sun, J.; Wang, D.; Teora, S. P.; Rijpkema, S. J.; Meeldijk, J. D.; Wilson, D. A., Adaptive insertion of a hydrophobic anchor into a poly(ethylene glycol) host for programmable surface functionalization. Nature Chemistry 2023, 15 (2), 240-247.
- 15. Chen, B. M.; Cheng, T. L.; Roffler, S. R., Polyethylene Glycol Immunogenicity: Theoretical, Clinical, and Practical Aspects of Anti-Polyethylene Glycol Antibodies. ACS Nano 2021, 15 (9), 14022-14048.
- Kozma, G. T.; Shimizu, T.; Ishida, T.; Szebeni, J., Anti-PEG antibodies: Properties, formation, testing 16. and role in adverse immune reactions to PEGylated nano-biopharmaceuticals. Adv Drug Deliv Rev **2020**, 154-155, 163-175.
- 17. Zhang, P.; Sun, F.; Liu, S.; Jiang, S., Anti-PEG antibodies in the clinic: Current issues and beyond PEGylation. J Control Release 2016, 244 (Pt B), 184-193.
- 18. Blackman, L. D.; Gunatillake, P. A.; Cass, P.; Locock, K. E. S., An introduction to zwitterionic polymer behavior and applications in solution and at surfaces. Chem Soc Rev 2019, 48 (3), 757-770.
- 19. Jiang, S.; Cao, Z., Ultralow-Fouling, Functionalizable, and Hydrolyzable Zwitterionic Materials and Their Derivatives for Biological Applications. Advanced Materials 2010, 22 (9), 920-932.
- 20. Qu, K.; Yuan, Z.; Wang, Y.; Song, Z.; Gong, X.; Zhao, Y.; Mu, Q.; Zhan, Q.; Xu, W.; Wang, L., Structures, properties, and applications of zwitterionic polymers. ChemPhysMater 2022, 1 (4), 294-309.

- Brown, M. U.; Triozzi, A.; Emrick, T., Polymer Zwitterions with Phosphonium Cations. J Am Chem Soc 2021, 143 (17), 6528-6532.
- 22. Zhang, L.; Cao, Z.; Bai, T.; Carr, L.; Ella-Menye, J.-R.; Irvin, C.; Ratner, B. D.; Jiang, S., Zwitterionic hydrogels implanted in mice resist the foreign-body reaction. Nature Biotechnology 2013, 31 (6), 553-556.
- 23. Shao, Q.; He, Y.; White, A. D.; Jiang, S., Difference in hydration between carboxybetaine and sulfobetaine. J Phys Chem B 2010, 114 (49), 16625-31.
- Schönemann, E.; Koc, J.; Karthäuser, J. F.; Özcan, O.; Schanzenbach, D.; Schardt, L.; Rosenhahn, 24. A.; Laschewsky, A., Sulfobetaine Methacrylate Polymers of Unconventional Polyzwitterion Architecture and Their Antifouling Properties. Biomacromolecules 2021, 22 (4), 1494-1508.
- 25. Li, B.; Jain, P.; Ma, J.; Smith, J. K.; Yuan, Z.; Hung, H.-C.; He, Y.; Lin, X.; Wu, K.; Pfaendtner, J.; Jiang, S., Trimethylamine <i>N</i>-oxide–derived zwitterionic polymers: A new class of ultralow fouling bioinspired materials. Science Advances 2019, 5 (6), eaaw9562.
- Kaiser, D.; Klose, I.; Oost, R.; Neuhaus, J.; Maulide, N., Bond-Forming and -Breaking Reactions at 26. Sulfur(IV): Sulfoxides, Sulfonium Salts, Sulfur Ylides, and Sulfinate Salts. Chem Rev 2019, 119 (14), 8701-8780.
- 27. Zander, Z. K.; Becker, M. L., Antimicrobial and Antifouling Strategies for Polymeric Medical Devices. ACS Macro Letters 2018, 7 (1), 16-25.
- 28. Helander, I. M.; Mattila-Sandholm, T., Permeability barrier of the gram-negative bacterial outer membrane with special reference to nisin. Int J Food Microbiol 2000, 60 (2-3), 153-61.
- 29. Muheim, C.; Götzke, H.; Eriksson, A. U.; Lindberg, S.; Lauritsen, I.; Nørholm, M. H. H.; Daley, D. O., Increasing the permeability of Escherichia coli using MAC13243. Sci Rep 2017, 7 (1), 17629.
- 30. Saito, H.; Sakakibara, Y.; Sakata, A.; Kurashige, R.; Murakami, D.; Kageshima, H.; Saito, A.; Miyazaki, Y., Antibacterial activity of lysozyme-chitosan oligosaccharide conjugates (LYZOX) against Pseudomonas aeruginosa, Acinetobacter baumannii and Methicillin-resistant Staphylococcus aureus. PloS one 2019, 14 (5), e0217504.
- 31. Uneputty, A.; Dávila-Lezama, A.; Garibo, D.; Oknianska, A.; Bogdanchikova, N.; Hernández-Sánchez, J. F.; Susarrey-Arce, A., Strategies applied to modify structured and smooth surfaces: A step closer to reduce bacterial adhesion and biofilm formation. Colloid and Interface Science Communications **2022**, 46, 100560.
- 32. Cuthbert, T. J.; Hisey, B.; Harrison, T. D.; Trant, J. F.; Gillies, E. R.; Ragogna, P. J., Surprising Antibacterial Activity and Selectivity of Hydrophilic Polyphosphoniums Featuring Sugar and Hydroxy Substituents. Angew Chem Int Ed Engl 2018, 57 (39), 12707-12710.
- Palermo, E. F.; Lienkamp, K.; Gillies, E. R.; Ragogna, P. J., Antibacterial Activity of Polymers: Discussions 33. on the Nature of Amphiphilic Balance. Angew Chem Int Ed Engl 2019, 58 (12), 3690-3693.
- 34. Jiang, H.; Wang, X. B.; Li, C. Y.; Li, J. S.; Xu, F. J.; Mao, C.; Yang, W. T.; Shen, J., Improvement of Hemocompatibility of Polycaprolactone Film Surfaces with Zwitterionic Polymer Brushes. Langmuir **2011**, 27 (18), 11575-11581.
- 35. Blackman, L. D.; Fros, M. K.; Welch, N. G.; Gengenbach, T. R.; Qu, Y.; Pasic, P.; Gunatillake, P. A.; Thissen, H.; Cass, P.; Locock, K. E. S., Dual Action Antimicrobial Surfaces: Alternating Photopatterns Maintain Contact-Killing Properties with Reduced Biofilm Formation. Macromolecular Materials and Engineering **2020,** 305 (10), 2000371.
- Sambhy, V.; Peterson, B. R.; Sen, A., Antibacterial and hemolytic activities of pyridinium polymers 36. as a function of the spatial relationship between the positive charge and the pendant alkyl tail. Angewandte Chemie 2008, 47 7, 1250-4.

- Kaur, M.; Mingeot -Leclercq, M. P., Maintenance of bacterial outer membrane lipid asymmetry: insight into MlaA. BMC Microbiology 2024, 24 (1), 186.
- 38. Abellón-Ruiz, J.; Kaptan, S. S.; Baslé, A.; Claudi, B.; Bumann, D.; Kleinekathöfer, U.; van den Berg, B., Structural basis for maintenance of bacterial outer membrane lipid asymmetry. Nature microbiology 2017, 2 (12), 1616-1623.
- 39. Potvin, E.; Sanschagrin, F.; Levesque, R. C., Sigma factors in Pseudomonas aeruginosa. FEMS Microbiol Rev 2008, 32 (1), 38-55.
- 40. Blanka, A.; Schulz, S.; Eckweiler, D.; Franke, R.; Bielecka, A.; Nicolai, T.; Casilag, F.; Düvel, J.; Abraham, W.-R.; Kaever, V.; Häussler, S., Identification of the Alternative Sigma Factor SigX Regulon and Its Implications for Pseudomonas aeruginosa Pathogenicity. Journal of Bacteriology 2014, 196 (2), 345-356.
- 41. Wood, L. F.; Ohman, D. E., Use of cell wall stress to characterize σ 22 (AlgT/U) activation by regulated proteolysis and its regulon in Pseudomonas aeruginosa. Molecular microbiology 2009, 72 (1), 183-201.
- 42. Yaeger, L. N.; Ranieri, M. R. M.; Chee, J.; Karabelas-Pittman, S.; Rudolph, M.; Giovannoni, A. M.; Harvey, H.; Burrows, L. L., A genetic screen identifies a role for oprF in Pseudomonas aeruginosa biofilm stimulation by subinhibitory antibiotics. npj Biofilms and Microbiomes 2024, 10 (1), 30.
- Fléchard, M.: Duchesne, R.: Tahrioui, A.: Bouffartiques, E.: Depayras, S.: Hardouin, J.: Lagy, C.: 43. Maillot, O.; Tortuel, D.; Azuama, C. O.; Clamens, T.; Duclairoir-Poc, C.; Catel-Ferreira, M.; Gicquel, G.; Feuilloley, M. G. J.; Lesouhaitier, O.; Heipieper, H. J.; Groleau, M.-C.; Déziel, É.; Cornelis, P.; Chevalier, S., The absence of SigX results in impaired carbon metabolism and membrane fluidity in Pseudomonas aeruginosa. Scientific Reports 2018, 8 (1), 17212.
- Qin, S.; Xiao, W.; Zhou, C.; Pu, Q.; Deng, X.; Lan, L.; Liang, H.; Song, X.; Wu, M., Pseudomonas 44. aeruginosa: pathogenesis, virulence factors, antibiotic resistance, interaction with host, technology advances and emerging therapeutics. Signal Transduction and Targeted Therapy **2022,** 7 (1), 199.
- 45. Mukherjee, S.; Bassler, B. L., Bacterial guorum sensing in complex and dynamically changing environments. Nature Reviews Microbiology 2019, 17 (6), 371-382.
- 46. Malgaonkar, A.; Nair, M., Quorum sensing in Pseudomonas aeruginosa mediated by RhIR is regulated by a small RNA PhrD. Scientific Reports 2019, 9 (1), 432.
- 47. Xiao, G.; Déziel, E.; He, J.; Lépine, F.; Lesic, B.; Castonguay, M. H.; Milot, S.; Tampakaki, A. P.; Stachel, S. E.; Rahme, L. G., MvfR, a key Pseudomonas aeruginosa pathogenicity LTTR-class regulatory protein, has dual ligands. Molecular microbiology 2006, 62 (6), 1689-1699.
- 48. Allegretta, G.; Maurer, C. K.; Eberhard, J.; Maura, D.; Hartmann, R. W.; Rahme, L.; Empting, M., Indepth Profiling of MvfR-Regulated Small Molecules in Pseudomonas aeruginosa after Quorum Sensing Inhibitor Treatment. Frontiers in Microbiology 2017, 8.
- Que, Y.-A.; Hazan, R.; Strobel, B.; Maura, D.; He, J.; Kesarwani, M.; Panopoulos, P.; Tsurumi, 49. A.; Giddey, M.; Wilhelmy, J., A quorum sensing small volatile molecule promotes antibiotic tolerance in bacteria. PLoS One 2013, 8 (12), e80140



Chapter 3

Porous Polymersomes as Carriers for Silver Nanoparticles and Nanoclusters: Advantages of Compartmentalization for Antimicrobial Usage

Bela B. Berking, Lucía Mallen-Huertas, Sjoerd J. Rijpkema, and Daniela A. Wilson* (* corresponding Author)

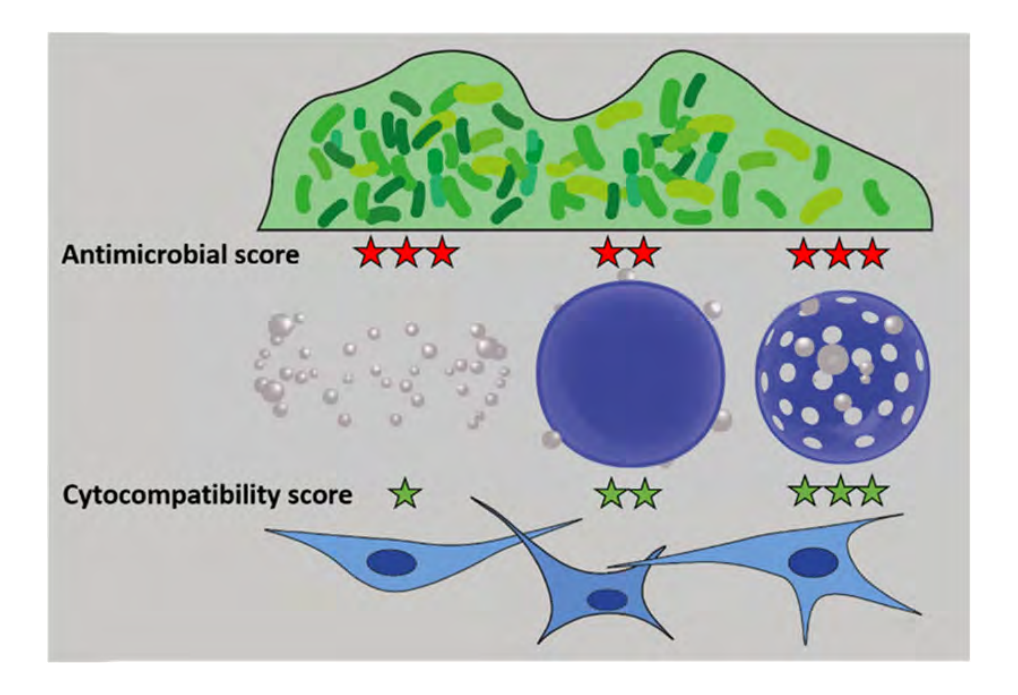
This chapter has been published:

Bela B. Berking, Lucía Mallen-Huertas, Sjoerd J. Rijpkema, and Daniela A. Wilson, "Porous Polymersomes as Carriers for Silver Nanoparticles and Nanoclusters: Advantages of Compartmentalization for Antimicrobial Usage"

Biomacromolecules 2023 24 (12)

Abstract

The global threat to public health posed by antibiotic-resistant bacterial infections requires the exploration of innovative approaches. Nanomaterials, particularly silver nanoparticles (AgNPs) and nanoclusters (AgNCs), have emerged as potential solutions to address the pressing issue of a bacterial healthcare crisis. However, the high cytotoxicity levels and low stability associated with AgNPs and AgNCs limit their applicability. To overcome these challenges, AgNCs and AgNPs were synthesized in the presence of porous polymersomes, resulting in a compartmentalized system that enhances stability, reduces cytotoxicity, and maintains high antimicrobial activity. The encapsulated particles exhibit a distribution of silver components on both the surface and the core, which is confirmed through analysis of surface charge and center of mass. Moreover, our investigation demonstrates improved stability of the nanoparticles and nanoclusters upon entrapment in the porous system, as evidenced by theg ion release assay. The antimicrobial effectiveness of porous polymersomes containing AgNPs and AgNCs was demonstrated by visualizing biofilms and quantifying penetration depth. Furthermore, cytotoxicity studies showed that compartmentalizing increases cell compatibility for AgNC based systems, showcasing the many advantages this system holds.



3.1 Introduction

According to the World Health Organization (WHO), antibiotic resistance poses a significant threat to public health worldwide¹. It not only causes extended hospital stays and higher medical expenses but also increased mortality rates². Immunocompromised patients, including those with autoimmune diseases, cancer, diabetes, or HIV, are particularly vulnerable to antibiotic resistance³. In fact, in 2019 alone, there were 4.95 million deaths globally associated with antimicrobial resistance (AMR) with 1.27 million directly attributable to AMR4. The financial burden is concerning as well, resistance to antibiotics is estimated to cost more than 300 billion dollars annually by 20505.

This issue is aggravated by the ability of resistant pathogens to form biofilms, consortiums of microorganisms that form a protective matrix of extracellular material. This matrix, known as the extracellular matrix (ECM), consists of exopolysaccharides, extracellular DNA, and proteins⁶. Its primary function is to provide integrity and protection against antimicrobials and the host's immune system. Remarkably, the ECM can prevent the penetration of positively charged antibiotics through interaction with its components⁷. Additionally, the transfer of genes associated with antibiotic resistance occurs at a high rate⁸. Consequently, bacteria in biofilms exhibit a 10- to 1000-fold increase in antibiotic resistance in comparison to bacteria in planktonic state⁹.

In medical settings, bacteria in biofilms have been found in living tissues and on the surface of medical devices leading to nosocomial infections that increase the risk of complications in patients with underlying conditions^{6,10}. Notably, common pathogens belong to the ESKAPE group, which includes the ubiquitous Pseudomonas aeruainosa, which is an opportunistic bacterium often associated with cystic fibrosis, chronic wounds, keratitis, and medical device colonization⁶. P. aeruginosa is responsible for 10-15% of global infections and frequently contributes to upper respiratory tract infections and catheter-associated urinary tract infections.

P. aeruginosa is characterized by forming biofilms that provide both structural support and drug resistance¹¹. The biofilm's structural integrity mainly relies on extracellular proteins and exopolysaccharides. Interestingly, exopolysaccharides also play a role in antibiotic resistance. P. aeruginosa's ECM consists of three main exopolysaccharides: Psl, Pel, and alginate. While Psl and Pel serve as the primary structural components of the biofilm, it has been observed that Psl interacts electrostatically with antibiotics, leading to their sequestration within the matrix¹². In addition, the presence of alginate contributes to the formation of mucoid biofilms which result in more persistent infections¹¹.

The inability to treat infections caused by antibiotic-resistant bacteria highlights the need for alternative therapeutic approaches. Among these, nanomaterials are promising alternatives for combating bacterial infections¹³. Unlike traditional antibiotics, nanoparticles (NPs) may simultaneously target the cell wall and intracellular components via physical interaction¹⁴, generation of reactive oxygen species (ROS)¹⁵, and ion release¹⁶. This multifaceted and simultaneous attack poses a significant challenge for bacteria to develop resistance against them.

Nanoparticles (NPs) have been studied as both delivery platforms and antimicrobial agents. Silver nanoparticles (AqNPs) have gathered considerable attention due to their versatile antimicrobial properties and their ability to overcome resistance mechanisms. Various studies have already explored the use of AqNPs with different sizes and chemical composition, either encapsulated within delivery systems or employed directly¹⁷⁻²⁵. However, challenges arise when their application involves cellular interactions, as silver nanoparticles often exhibit high cytotoxicity upon direct contact with mammalian cells 17,26-30.

Nanoclusters (NCs) represent the next generation of antimicrobials. Silver nanoclusters (AgNCs) exhibit advantageous characteristics compared to nanoparticles, such as a surface layer enriched with silver ions and a higher surface area-to-volume ratio^{31,32}, facilitating an accelerated release of silver ions. Moreover, their small size enables them to effectively penetrate the cellular membrane and interact with microbial components^{33,34}. However, nanoclusters tend to be unstable in physiological conditions³⁵.

To address the challenges associated with both nanoparticles and nanoclusters, the utilization of carriers may be a solution. Encapsulation offers the possibility to mitigate the high cytotoxicity levels observed with AgNPs, as it reduces direct contact with cellular membranes. Furthermore, encapsulation can enhance the stability of AgNCs, shielding them from oxidation, aggregation, and loss of antimicrobial activity.

Carriers have previously demonstrated their effectiveness in reducing the adverse effects of both AgNPs and AgNCs^{18,35}. Mesoporous silica nanoparticles (MSN) have shown improved antibacterial activity by preventing the aggregation of silver particles and reducing cytotoxicity. In this study, we investigate the use of polymersomes as carriers for encapsulating AgNPs and AgNCs. Polymersomes are self-assembled vesicles formed by amphiphilic copolymers, known for their excellent stability and biocompatibility with tissues and cells³⁶. Moreover, the surface of polymersomes can be easily and readily functionalized using various chemical handles^{37,38}, making them promising candidates for encapsulating AgNPs and AgNCs and to further compartmentalize this system for multifunctionality.

3.2 Results and Discussion

Crosslinked polymersomes were prepared using the method previously described by Rijpkema et al. 39. AgNPs and AgNCs were synthesized according to Yan et. al. (2018)¹⁷ and Liu et al. (2019)³⁵ and checked for size, surface charge, UV-Vis and TEM (S1). To investigate the impact of encapsulation in polymersomes two samples were prepared, namely 70% and 100% crosslinked polymersomes. Both samples exhibited uniform distribution and displayed a peak at approximately 400 nm in DLS-Zetasizer (Figure 1A,B, S2), which is consistent with the employed method³⁹. To determine the pore size of the 70% crosslinked polymersomes, TEM images were analyzed using ImageJ (Figure 1 C). The average pore size was 28nm (± 9nm), which aligns with earlier studies³⁹. On the other hand, no visible pores were observed on the surface of the 100% crosslinked polymersomes (Figure 1 D), indicating that neither AgNPs nor AgNCs would be able to penetrate the core and be encapsulated.

The fully assembled systems, comprised of porous 70-CL AgNP or AgNCs and 100-CL AgNP and AgNCs, were subjected to size and surface charge analysis (Figure 1A). The porous polymersomes 70-CL showed peaks at around 400 nm, aligning with the observed size for empty 70-CL polymersomes ³⁹. 100-CL AgNC shifted in size to around 660 nm while 100-CL AgNP displayed another peak at around 25 nm. This indicates that nanoclusters have formed on the outer side of the polymersomes, sticking to the membrane, and even "breaking" off and going back into solution in the case of 100 CL- AgNP.

The surface charge of polymersomes can provide more information on particles accumulating around the shells or on the inside of carriers due to shifts in zetapotential. Silver ions and particles on the outer shell increased the surface charge of non-porous polymersomes (Figure 1B), while porous polymersomes retained a charge close to that of their empty counterpart. This data suggests that AgNCs and AgNPs were successfully formed in the inner compartment of porous polymersomes.

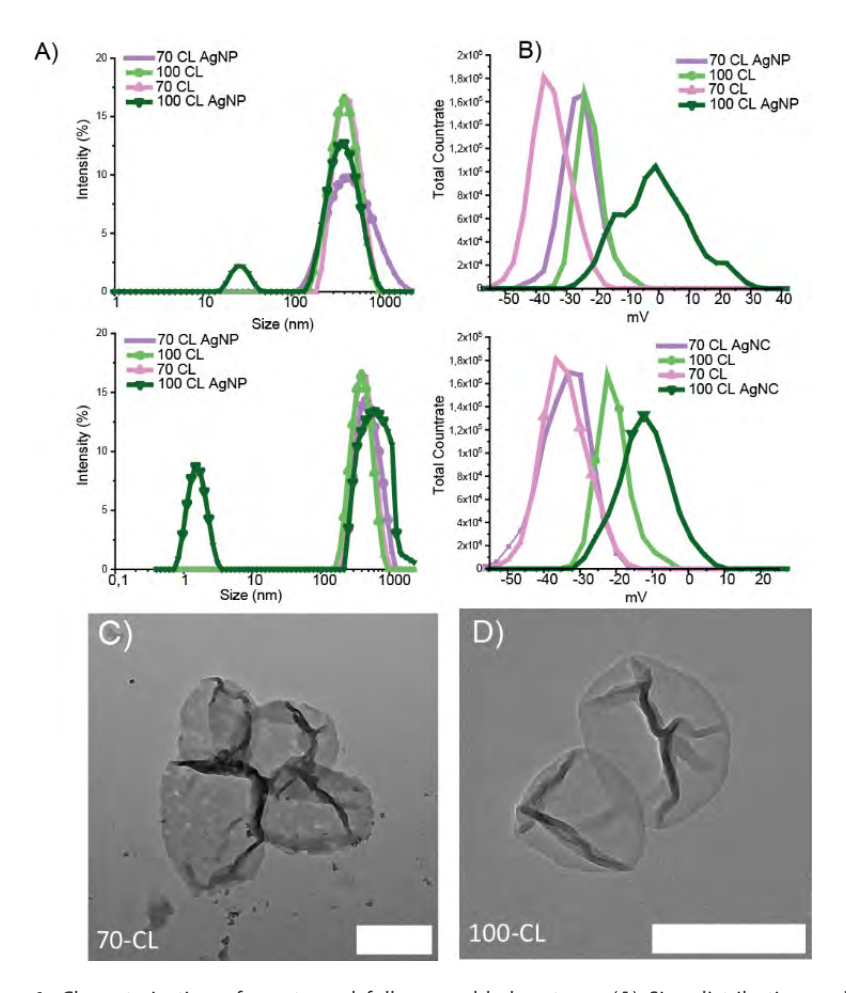


Figure 1. Characterization of empty and fully assembled systems. **(A)** Size distribution and **(B)** surface charge of AgNP and AgNC systems as determined by DLS-Zetasizer. TEM images of 70-CL **(C)** and 100-CL **(D)**.

To further study the morphology of the fully assembled system, TEM was employed (Figure 2). AgNPs and AgNCs can be seen covering both 70-CL and 100-CL polymersomes with clustering of AgNCs on the surface of 100-CL. Determining the inner or outer location of silver is difficult with this technique, which is why additionally FFF as well as total silver content serve as proof of compartmentalized and non-compartmentalized polymersomes.

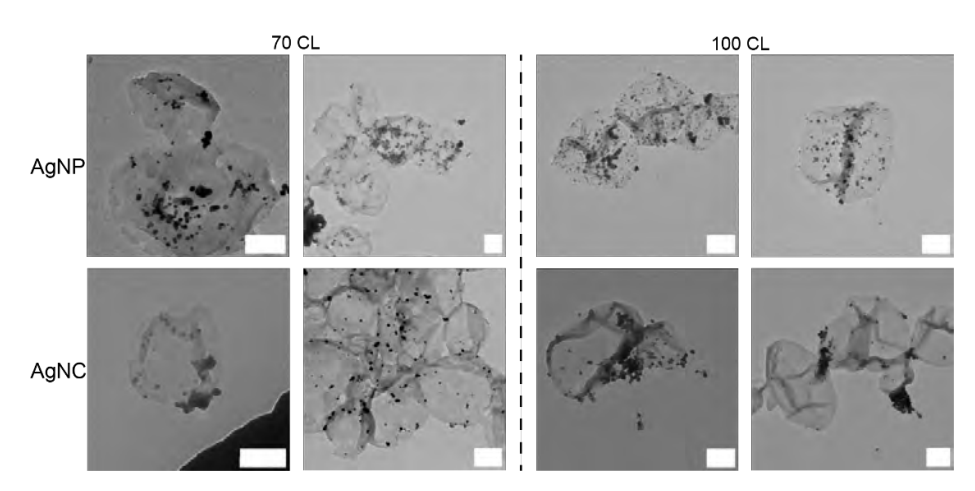


Figure 2. TEM analysis of systems comprised of 70-CL (left side) and 100-CL (right side) polymersomes containing AgNPs (upper row) or AgNCs (lower row). Scale bar represents 200 nm.

Center of mass, or radius of gyration (Rg)/ hydrodynamic radius (Rh), has been previously used to determine the loading of carriers with various cargo following the general idea of increased Rg/Rh when loaded (Figure 3A) 40-45. Spherical particles will have the Rg located at the surface of the particle, matching the Rh, causing the center of mass to equal 143. When Rg becomes lower due to loading of cargo in the center of a polymersomes, the center of mass will become smaller 44. Due to the nucleation of silver nanoparticles and nanoclusters in the core of 70-CL, a decrease in $R_{\rm a}/R_{\rm h}$ is observed (Figure 3B, S3), whereas the increase of mass on the outer surface of 100-CL increases the R_a/R_h compared to the native particles (Figure 3B, S3). Conclusive evidence of a compartmentalized system containing silver cargo is therefore given.

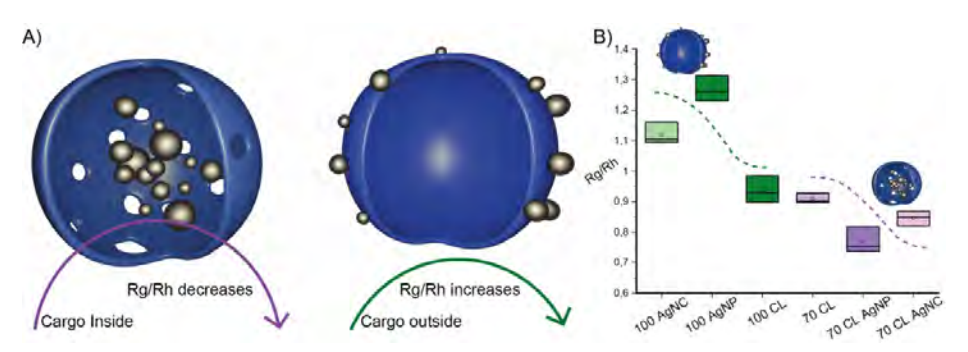


Figure 3. FFF-MALS characterization of cargo location. A) Overview of Rg/Rh value response to cargo inside or outside of the polymersomes as can be seen in experimental data (B).

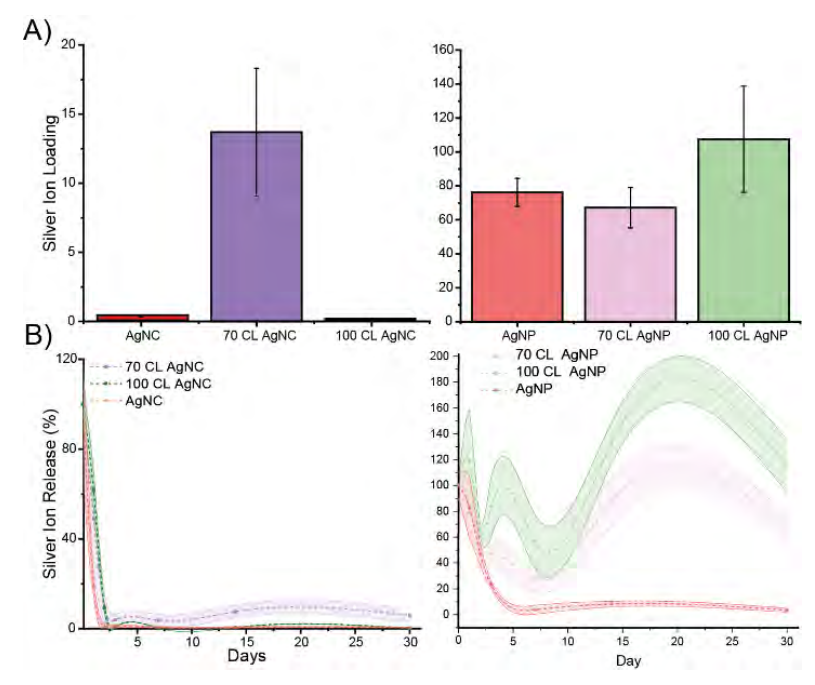


Figure 4. ICP-MS analysis of total silver content in AgNP and AgNC systems (**A**), and silver ion release over 30 days in % relative to day 0 (**B**)

Total silver content of the different systems was measured to showcase different silver retaining capabilities (Figure 4A). 70-CL AgNC showed significantly higher Ag+ ion count compared to 100-CL and pure AgNCs, indicating increased nucleation in the core as well as the retaining of formed particles. Contents of AgNP system show no statistically significant differences in Ag levels, exposing a failed retainment of silver from 70-CL polymersomes. To investigate the potential of polymersomes in enhancing the stability of silver particles and clusters, an ion release assay was conducted (Figure 4B). Remarkably, both 70-CL and 100-CL polymersomes loaded with AqNPs demonstrated sustained stability throughout the experiment (Figure 4B, S4), while the ion content of AqNCs exhibited a rapid decrease at the onset of the experiment. Previous studies have shown a substantial decline in AgNPs within the initial 72-hour period, followed by a stabilization phase 17. Notably, the presence of both 70-CL and 100-CL polymersomes contributed to the improved stability of silver nanoparticles. We propose that the protective nature of polymersomes, likely through encapsulation, may account for this effect. We observe though that nucleation at the membrane of 100-CL polymersomes and subsequent attachment is followed by slower disintegration of AgNPs. We hypothesize that interaction with the polymersome membrane leaves less surface area of AgNPs to interact with the harsh dissolving environment, resulting in prolonged ion release.

Silver nanocluster systems displayed a massive reduction of ions due to their unstable nature within the first three days, for both 100-CL AgNCs and AgNCs, a substantial reduction of 140-fold and 105-fold, respectively. On the contrary, the release of silver ions from 70-CL AgNCs remains relatively stable over time. Notably, the silver release from 70-CL AgNCs is significantly higher compared to both AgNCs and 100-CL AgNCs after 14 and 30 days. These findings highlight the unique capability of 70-CL polymersomes in preventing the rapid oxidation of silver within nanoclusters by utilizing the core as a protective compartment and allowing for sustained release of ions for antimicrobial purposes.

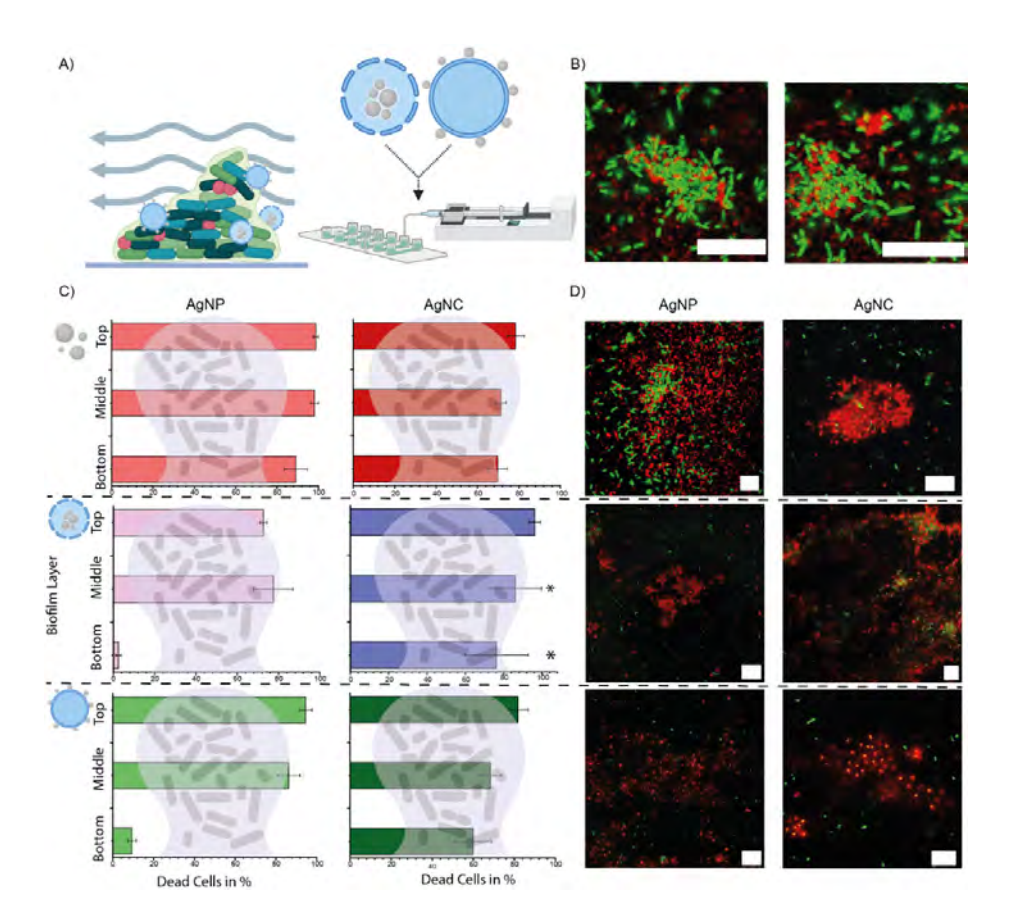


Figure 5. Antimicrobial activity of all systems in P. aeruginosa. A. Overview of experimental setup with flow. B) Accumulation of empty polymersomes (red channel) in biofilms (green channel) under flow. C) Quantified viability across top, middle, and bottom biofilm layers, derived from confocal images (D).

Effects of empty polymersomes were studied under flow conditions (Figure 5A) to confirm adherence to the biofilm (Figure 5B) as well as rule out cytotoxic effects from only polymersomes (Figure S5). Antimicrobial activity assays were performed to study the effects of polymersomes with AgNPs and AgNCs on P. aeruginosa biofilms in a flow environment, mimicking a more natural as well as challenging environment for antimicrobials (Figure 5C, 5D, S6). After exposure, the bacteria in the biofilms were analyzed for their cell wall integrity utilizing confocal laser scanning microscopy, indicating viablity of bacteria throughout the biofilms. To further gain insight into the effectiveness of the systems, the analysis of single biofilms was split into bottom, middle and top layers of the biofilm. All samples showed high antimicrobial activity on the top layers, yet different effectiveness was observed for the middle and bottom laver (Figure 5C).

The efficacy of AqNPs on the bottom layer was found to be ineffective for both 70-CL and 100-CL systems, with eradication rates of only 2.45% \pm 1.3 and 9.38% ± 2.04, respectively. Conversely, AgNCs, including both 70-CL and 100-CL, demonstrated notable eradication of the bottom layer, with rates of 76.22% ± 16.51 and 59.98% ± 8.8, respectively. Interestingly, there were no significant differences observed in the efficacy on the bottom layer between 70-CL AgNCs and pure AgNCs, whereas 100-CL AgNC exhibited significantly lower efficiency in eradicating the bottom layer as well as the middle layer, putting the compartmentalized system on the same antimicrobial level as pure AgNCs. To rule out effects of the different capping agents on the antimicrobial effects, biofilms were exposed to citrate, glutathione in the concentrations used for silver particle synthesis (Figure S7). No effects were observed when comparing to the negative control (PBS), unlike the positive control Polymyxin B, a broad range antibiotic, which showed a significant decrease in viability. Antimicrobial effects observed by fully assembled systems are therefore to be attributed to released silver, not the capping agents.

The great challenge in combating biofilms has been disrupting the bottom layer, where often dormant cells are found. Ideally, particles should exhibit high antimicrobial activity across all three layers, namely the top, middle, and bottom. While the addition of a carrier hinders this activity in the case of AgNPs, 70-CL AgNCs do not impede antimicrobial efficacy, potentially due to sustained release of ions and prolonged protection of the AgNCs in the core of polymersomes, whereas 100-CL AgNCs suffer from immediate dissolution.

An optimal system is expected to have high cytocompatibility, so high doses can be administered without fear of damaging healthy cell tissue. Both 70-CL and 100CL AgNPs significantly decreased cell viability. On the other hand, no significant differences were found between 70-CL and 100-CL AgNCs, and the control (Figure 6a, S8). To further investigate, concentrations of AgNC systems used for antimicrobial assays were increased 10 and 100-fold. While pure AgNCs and 100-CL AgNCs guickly deteriorate the viability of cells, 70-CL AgNC retained excellent cytocompatibility (Figure 6b).

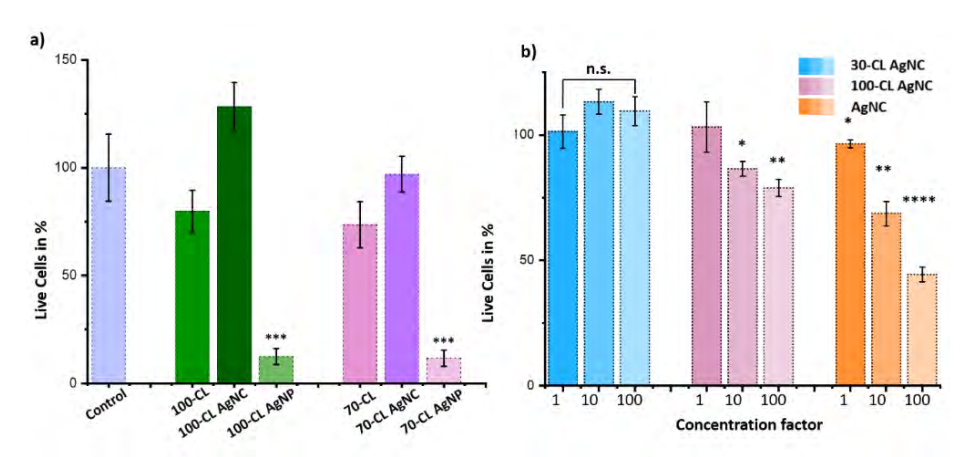


Figure 6. Cell cytotoxicity. a) After treatment with 70-CL AgNP, 100-CL AgNP, 70-CL AgNC, and 100-Cl AgNC. b) After treatment with different concentrations of AgNC, 70-CL AgNC, and 100-CL AgNC. Experiments were carried out in replicates of 5-10, unpaired t. Test with $p \le 0.05$ was conducted to determine statistical significance.

Previous studies have consistently demonstrated the adverse effects of silver particles and ions on various systems within the human body, such as the respiratory, digestive, and reproductive systems^{30,46}. Nevertheless, the application of silver nanoparticles has shown promise in mitigating cell cytotoxicity due to their protective outer layer⁴⁷. However, the presence of citrate hinders cell viability in these nanoparticles⁴⁸. In contrast, silver nanoclusters possess an outer layer composed of glutathione, a naturally occurring non-toxic compound in the human body. Remarkably, recent research has illustrated that the cell viability of silver nanoclusters is four times higher compared to silver ions, further highlighting their potential as a safer alternative³⁵.

To further investigate the effect of AgNCs on cell cytotoxicity, the concentration of AgNCs, 100-CL AgNCs, and 70-CL AgNCs was increased by 10- and 100-fold (Figure 6b). Notably, even a 10-fold increase in the concentration of AgNCs resulted in significant cytotoxicity. Moreover, when the concentration of 100-CL AgNCs was increased by 10-fold, clear indications of cytotoxicity were observed. Surprisingly,

in the case of 70-CL AgNCs, even a 100-fold increase in concentration did not lead to an increase in cell cytotoxicity. These findings provide robust evidence that 70-CL AgNCs are non-toxic to human cells, even at concentrations 100 times higher than those previously employed for antimicrobial purposes. Therefore, higher doses of 70-CL AgNCs can be utilized to enhance antibacterial activity without compromising cell cytotoxicity. We hypothesize that the reduced contact of AgNC with the cell membranes decreases the cytotoxicity observed, whereas systems with direct contact led to significant damage.

Antibiotic resistance has rendered traditional antibiotics obsolete, highlighting the development of new strategies to effectively combat infections caused by these microorganisms. This research focuses on the utilization of encapsulated silver nanoparticles and nanoclusters as potential antimicrobial agents. The high antimicrobial activity coupled with minimal cytotoxicity exhibited by encapsulated silver nanoclusters makes them highly promising for antimicrobial treatments. However, it is worth noting that these nanoclusters exhibit low stability even when encapsulated. Therefore, it is imperative to dedicate further efforts towards optimizing silver nanoclusters, aiming to preserve their remarkable antimicrobial activity and low cytotoxicity while enhancing their stability. Considering the trend towards a selectivity of 70-CL AgNC, sparing human cells and exhibiting antimicrobial activities, we forsee this system as having great potential in the medical field, f.e. as topical antibiofilm compound after a surgical site infection.

3.3 Conclusion

To summarize, we developed various systems utilizing silver nanoparticles or silver nanoclusters as cargo, either on the surface of crosslinked polymersomes or formed in the core of porous polymersomes, resulting in an ion-releasing compartment. Indepth characterization was used to verify the localization of particles and clusters on and inside the polymersomes. Ion-releasing assays confirmed the hypothesis that entrapping particles in the core enhances stability which in turn significantly increases the antimicrobial effectiveness while allowing the system to have good mammalian cell compatibility. These findings establish the promising prospects of 70-CL AgNCs as an effective and safe antimicrobial treatment, offering a valuable alternative to combat antibiotic resistance by compartmentalization of toxic nanoclusters inside porous polymersomes.

3.4 Materials and Methods

Materials and instrumentation. During these experiments, analytical grade chemicals were used. The preparation and characterization of polymers were conducted as described by Rijpkema et al. (2022)³⁹. Centrifugation steps were performed using an Eppendorf Centrifuge 5430 R. The samples were characterized using various instruments, including the Malvern DLS-ZetaSizer, JEOL JEM-1400 FLASH, Tecan Spark M10 Plate Reader, Wyatt FFF-MALS (Shimadzu HPLC, Damn Heleos-II, Optilab T-rEX, and Eclipse AF4), SP8x AOBS-WLL confocal microscope, and ICP-MS. Data analysis was carried out using the software tools Image J and ASTRA 6.1.

Fabrication of polymersomes. Polymersomes were prepared following the method previously described by Rijpkema et al. (2022)³⁹. Briefly, 10 mg of PEG44-PS178 polymer was dissolved in 1 mL of THF and Dioxane 4:1 organic solvent. The addition of mQ water (0.5 mL) to the solution was carried out using a flow rate of 1 mL/h, with a time delay of 30 minutes. The reaction was guenched by adding 6 mL of mO water, followed by centrifugation at 13000 rpm for 10 minutes. Finally, the sample was cleaned with mQ water three times. For the preparation of polymersomes with Nile Red, 25 µL of a 1 mg/mL Nile Red stock solution was added to the mixture.

Fabrication of crosslinked polymersomes. A modified version of the method previously reported by Rijpkema et al. (2022)³⁹ was employed. To prepare 70% crosslinked polymersomes, the following solution was prepared under dark conditions: 3 mg of PEG44-PS178, 7 mg of crosslinking polymer PEG44P(S-co-4VBA)150, 20 µL of Irgacure, and 1 mL of THF Dioxane (4:1). Subsequently, mQ water (0.5 mL) was added using a flow rate of 1 mL/h, with a 30-minute time delay. The solution was degassed by flushing with argon for 3-5 minutes and then photocrosslinked with UV light at a wavelength of 450 nm for 5 minutes at a light intensity of 70. Afterward, the sample was centrifuged at 10000 rpm for 10 minutes, washed twice with organic solvent THF Dioxane (4:1), and finally, washed with mQ water. For 100% polymersome crosslinking, the same procedure was followed except for using 10 mg of PEG44-P(S-co-4VBA)150 in the initial solution.

Synthesis of silver nanoparticles (AgNP). Silver nanoparticles were synthesized according to Yan et al. (2018)¹⁷. To produce 20 nm particles, a solution containing 100 mM silver nitrate and 100 mM trisodium citrate (TSC) was prepared under continuous stirring. Subsequently, 6 mL of a 5 mM sodium borohydride solution was added to the mixture. The sample was vigorously stirred for 3 hours. Following the stirring process, the sample was centrifuged at 10000 rpm for 10 minutes and subsequently washed twice with mQ water.

Synthesis of AgNP in polymersomes post-self-assembly. If polymersomes were included in the preparation, 100 µL was added simultaneously with the 100 mM silver nitrate and 100 mM TSC solution. Subsequently, the samples were washed with mQ water until the supernatant became clear. The resulting pellet was resuspended in 500 uL of mO water and transferred to a 220 nm spin filter. The samples were then centrifuged at 14000 rpm for 10 minutes and washed with an additional 500 µL of mQ water until no pellet remained. Finally, the particles trapped in the membrane were resuspended in 200 uL of mO water and stored overnight in the fridge.

Synthesis of silver nanoclusters (AgNC). AgNCs were synthesized using a modified version of the methodology described by Liu et al. (2019)³⁵. Firstly, a 112mM solution of sodium borohydride was prepared by dissolving 4.3 mg of NaBH4 in 200 µL of a 1M NaOH solution. Subsequently, 800 µL of deionized water was added to the solution. In parallel, a mixture of silver nitrate (50 µL, 20 mM) and GSH (100 µL, 20 mM) was prepared in 1.83 mL of mQ water. Both solutions were combined and vigorously stirred for 1 hour. Following that, 20 µL of the 112 mM sodium borohydride solution was added, and the resulting solution was stirred for an additional 5 hours. Finally, the sample was centrifuged at 10000 rpm for 10 minutes.

Synthesis of AqNC in polymersomes post-self-assembly. If polymersomes were included in the preparation, 100 µL was added during the mixing of the solutions 112 mM sodium borohydride, 20 mM silver nitrate, and 20 mM GSH.

Characterization. First, size and surface charge were determined using DLS-Zetasizer. Additionally, Transmission Electron Microscopy (TEM) was employed to visualize all the samples, providing a visual representation of their structures. For a more detailed characterization FFF-MALS was utilized, as it can provide further proof and information regarding the positioning of encapsulated AgNP and AgNC. For this purpose, the detector flow rate was set at 1 ml/min, the focus flow rate at 0.5 ml/min, and the inject flow rate at 0.15 ml/min. UV light with a wavelength of 254 nm was utilized. The solvent used during this process was 20 mM NaNO, + 0.02% NaN₃, and samples were dissolved in mQ water. A regenerative cellulose 10 kDa membrane, obtained from Wyatt, was employed for the FFF-MALS analysis.

Silver release assay. Freshly prepared samples were first normalized using NPN and measured in a plate reader. Subsequently, the samples were centrifuged at 10000 rpm for 10 minutes. Following centrifugation, the supernatant was filtered through a 0.22 µm filter and then diluted 1:5 in mQ water. For analysis, a 1:100 dilution of 65% nitric acid was added. The concentration of silver was determined using ICP-MS on days 0, 1, 2, 3, 7, 14, and 30 to reveal the changes in silver concentration over time.

Antimicrobial activity assay. Pseudomonas aeruginosa was cultured overnight in Brain Heart Infusion (BHI) broth. Afterward, the cultured P. aeruginosa was seeded in μ slides VI 0.5 Glass Bottom (ibidi) and incubated for 3 hours. The flow rate was maintained at 0.4 ml/h using BHI media overnight. The study involved the utilization of various samples, including 70-CL, 100-CL, AgNP, 70-CL AgNP, 100-CL AgNP, AgNC, 70-CL AgNC, and 100-CL AgNC. In order to investigate the particle deposition on the biofilm, polymersomes labeled with Nile Red were employed. All samples were normalized using NPN and measured using a plate reader. Following that, they were injected into the flow at a rate of 0.33 ml/h for 3 hours. Subsequently, a LIVE/ DEAD assay was performed, omitting the addition of propidium iodide during the staining process for the polymersomes labeled with Nile Red. Finally, the stained samples were examined using confocal microscopy.

XTT Assay to assess Toxicity of Capping agents. P. aeruginosa cells were grown overnight and diluted the next day 1:100 in 96 well plated to allow for biofilm formation. The biofilms were incubated for 24 hours at 37 °C and washed three times with PBS to remove planktonic bacteria, after which 100 mM Citrate, 10 mM Glutathione and 20 µg/ml Polymyxin B in PBS were added to the wells and left for 3 hours to incubate. Wells were washed once again and XTT (5 µl per well) was added to the wells and left to incubate for another 2 hours. Afterwards, absorbance was measured at 450 nm using a Tecan Spark M10 Platereader.

Cell cytotoxicity assay. HEK239 cells were cultured in DMEM medium supplemented with 10% FBS for three days. Once the cells reached approximately 60% confluence, they were rinsed three times with 1x PBS, pH 7.4, and detached using 4 ml of Trypsin for 3 minutes. Trypsin was guenched by adding 8 ml of DMEM medium. The cells were then transferred to a 15 ml Falcon tube and centrifuged at 0.3 rcf for 5 minutes. After discarding the supernatant, the cells were seeded in a 96-well plate with DMEM complete medium at a density of 5 x 10⁵ cells/ml and incubated for 24 hours at 37 °C with 5% CO₂. Next, different concentrations of treatments in DMEM complete medium were added to the wells and incubated at 37 °C with 5% CO₂ for either 24 or 48 hours. Following the incubation period, 10 µl of CCK8 (Sigma Aldrich) was added to each well and incubated for 3 hours. The absorbance was then measured at 450 nm.

3.5 Acknowledgements

This work was funded by the Ministry of Education, Culture and Science (Gravitation program 024.001.035). B.B. and D.A.W. acknowledges support from the European Research Council (ERC) under the European Union's Horizon 2020 research and innovation programme ERC-CoG 101044434 "SynMoBio". We like to thank Dr. Robert Jansen and Prof. Dr. Laura van Niftrik for the access to ML2 facilities.

3.6 References

- World Health Organization. Antibiotic resistance. www.who.int/news-room/fact-sheets/detail/ 1 antibiotic-resistance (accessed 2023-05-01).
- 2 Cosgrove, S. E. The Relationship between Antimicrobial Resistance and Patient Outcomes: Mortality, Length of Hospital Stay, and Health Care Costs. Clinical Infectious Diseases 2006, 42 (Supplement_2), S82-S89. https://doi.org/10.1086/499406.
- 3 Kamat, S.; Kumari, M. Emergence of Microbial Resistance against Nanoparticles: Mechanisms and Strategies. Front Microbiol 2023, 14. https://doi.org/10.3389/fmicb.2023.1102615.
- Murray, C. J. L.; Ikuta, K. S.; Sharara, F.; Swetschinski, L.; Robles Aguilar, G.; Gray, A.; Han, C.; Bisignano, C.; Rao, P.; Wool, E.; Johnson, S. C.; Browne, A. J.; Chipeta, M. G.; Fell, F.; Hackett, S.; Haines-Woodhouse, G.; Kashef Hamadani, B. H.; Kumaran, E. A. P.; McManigal, B.; Achalapong, S.; Agarwal, R.; Akech, S.; Albertson, S.; Amuasi, J.; Andrews, J.; Aravkin, A.; Ashley, E.; Babin, F.-X.; Bailey, F.; Baker, S.; Basnyat, B.; Bekker, A.; Bender, R.; Berkley, J. A.; Bethou, A.; Bielicki, J.; Boonkasidecha, S.; Bukosia, J.; Carvalheiro, C.; Castañeda-Orjuela, C.; Chansamouth, V.; Chaurasia, S.; Chiurchiù, S.; Chowdhury, F.; Clotaire Donatien, R.; Cook, A. J.; Cooper, B.; Cressey, T. R.; Criollo-Mora, E.; Cunningham, M.; Darboe, S.; Day, N. P. J.; De Luca, M.; Dokova, K.; Dramowski, A.; Dunachie, S. J.; Duong Bich, T.; Eckmanns, T.; Eibach, D.; Emami, A.; Feasey, N.; Fisher-Pearson, N.; Forrest, K.; Garcia, C.; Garrett, D.; Gastmeier, P.; Giref, A. Z.; Greer, R. C.; Gupta, V.; Haller, S.; Haselbeck, A.; Hay, S. I.; Holm, M.; Hopkins, S.; Hsia, Y.; Iregbu, K. C.; Jacobs, J.; Jarovsky, D.; Javanmardi, F.; Jenney, A. W. J.; Khorana, M.; Khusuwan, S.; Kissoon, N.; Kobeissi, E.; Kostyanev, T.; Krapp, F.; Krumkamp, R.; Kumar, A.; Kyu, H. H.; Lim, C.; Lim, K.; Limmathurotsakul, D.; Loftus, M. J.; Lunn, M.; Ma, J.; Manoharan, A.; Marks, F.; May, J.; Mayxay, M.; Mturi, N.; Munera-Huertas, T.; Musicha, P.; Musila, L. A.; Mussi-Pinhata, M. M.; Naidu, R. N.; Nakamura, T.; Nanavati, R.; Nangia, S.; Newton, P.; Ngoun, C.; Novotney, A.; Nwakanma, D.; Obiero, C. W.; Ochoa, T. J.; Olivas-Martinez, A.; Olliaro, P.; Ooko, E.; Ortiz-Brizuela, E.; Ounchanum, P.; Pak, G. D.; Paredes, J. L.; Peleg, A. Y.; Perrone, C.; Phe, T.; Phommasone, K.; Plakkal, N.; Ponce-de-Leon, A.; Raad, M.; Ramdin, T.; Rattanavong, S.; Riddell, A.; Roberts, T.; Robotham, J. V.; Roca, A.; Rosenthal, V. D.; Rudd, K. E.; Russell, N.; Sader, H. S.; Saengchan, W.; Schnall, J.; Scott, J. A. G.; Seekaew, S.; Sharland, M.; Shivamallappa, M.; Sifuentes-Osornio, J.; Simpson, A. J.; Steenkeste, N.; Stewardson, A. J.; Stoeva, T.; Tasak, N.; Thaiprakong, A.; Thwaites, G.; Tigoi, C.; Turner, C.; Turner, P.; van Doorn, H. R.; Velaphi, S.; Vongpradith, A.; Vongsouvath, M.; Vu, H.; Walsh, T.; Walson, J. L.; Waner, S.; Wangrangsimakul, T.; Wannapinij, P.; Wozniak, T.; Young Sharma, T. E. M. W.; Yu, K. C.; Zheng, P.; Sartorius, B.; Lopez, A. D.; Stergachis, A.; Moore, C.; Dolecek, C.; Naghavi, M. Global Burden of Bacterial Antimicrobial Resistance in 2019: A Systematic Analysis. The Lancet 2022, 399 (10325), 629-655. https://doi. org/10.1016/S0140-6736(21)02724-0.
- 5 World Bank. Drug-resistant infections a threat to our economic future. www.worldbank.org (accessed 2023-05-01).
- Cendra, M. del M.; Torrents, E. Pseudomonas Aeruginosa Biofilms and Their Partners in Crime. 6 Biotechnol Adv 2021, 49, 107734. https://doi.org/10.1016/j.biotechadv.2021.107734.
- 7 Wilton, M.; Charron-Mazenod, L.; Moore, R.; Lewenza, S. Extracellular DNA Acidifies Biofilms and Induces Aminoglycoside Resistance in Pseudomonas Aeruginosa. Antimicrob Agents Chemother 2016, 60 (1), 544–553. https://doi.org/10.1128/AAC.01650-15.
- 8 Bowler, P.; Murphy, C.; Wolcott, R. Biofilm Exacerbates Antibiotic Resistance: Is This a Current Oversight in Antimicrobial Stewardship? Antimicrob Resist Infect Control 2020, 9 (1), 162. https://doi.org/10.1186/s13756-020-00830-6.

- 9 Prinzi, A.; Rohde, R. E. The role of bacterial biofilms in antimicrobial resistance. American Society for Microbiology, https://asm.org/Articles/2023/March/The-Role-of-Bacterial-Biofilmsin-Antimicrobial-Re#:~:text=The%20role%20of%20biofilms%20in,living%20in%20a%20 planktonic%20state. (accessed 2023-05-01).
- 10 Donlan, R. M. Biofilms: Microbial Life on Surfaces. Emerg Infect Dis 2002, 8 (9), 881–890. https:// doi.org/10.3201/eid0809.020063.
- 11 Yin, R.; Cheng, J.; Wang, J.; Li, P.; Lin, J. Treatment of Pseudomonas Aeruginosa Infectious Biofilms: Challenges and Strategies. Front Microbiol 2022, 13. https://doi.org/10.3389/ fmicb.2022.955286.
- 12 Billings, N.; Ramirez Millan, M.; Caldara, M.; Rusconi, R.; Tarasova, Y.; Stocker, R.; Ribbeck, K. The Extracellular Matrix Component Psl Provides Fast-Acting Antibiotic Defense in Pseudomonas Aeruginosa Biofilms. PLoS Pathog 2013, 9 (8), e1003526. https://doi.org/10.1371/journal. ppat.1003526.
- 13 Seil, I.; Webster, T. J. Antimicrobial Applications of Nanotechnology: Methods and Literature. Int J Nanomedicine 2012, 7, 2767–2781. https://doi.org/10.2147/IJN.S24805.
- 14 Chen, K. L.; Bothun, G. D. Nanoparticles Meet Cell Membranes: Probing Nonspecific Interactions Using Model Membranes. Environ Sci Technol 2014, 48 (2), 873–880. https://doi.org/10.1021/ es403864v.
- 15 Wang, L.; Hu, C.; Shao, L. The Antimicrobial Activity of Nanoparticles: Present Situation and Prospects for the Future. Int J Nanomedicine 2017, Volume 12, 1227-1249. https://doi. org/10.2147/IJN.S121956.
- 16 Dizaj, S. M.; Lotfipour, F.; Barzegar-Jalali, M.; Zarrintan, M. H.; Adibkia, K. Antimicrobial Activity of the Metals and Metal Oxide Nanoparticles. Materials Science and Engineering: C 2014, 44, 278-284. https://doi.org/10.1016/j.msec.2014.08.031.
- 17 Yan, N.; Tang, B. Z.; Wang, W. X. In Vivo Bioimaging of Silver Nanoparticle Dissolution in the Gut Environment of Zooplankton. ACS Nano 2018, 12 (12), 12212-12223. https://doi.org/10.1021/ acsnano.8b06003.
- 18 Tian, Y.; Qi, J.; Zhang, W.; Cai, Q.; Jiang, X. Facile, One-Pot Synthesis, and Antibacterial Activity of Mesoporous Silica Nanoparticles Decorated with Well-Dispersed Silver Nanoparticles. ACS Appl Mater Interfaces 2014, 6 (15), 12038-12045. https://doi.org/10.1021/am5026424.
- 19 Agnihotri, S.; Mukherji, S.; Mukherji, S. Size-Controlled Silver Nanoparticles Synthesized over the Range 5-100 Nm Using the Same Protocol and Their Antibacterial Efficacy. RSC Adv 2014, 4 (8), 3974-3983. https://doi.org/10.1039/c3ra44507k.
- 20 Fereydouni, N.; Zangouei, M.; Darroudi, M.; Hosseinpour, M.; Gholoobi, A. Antibacterial Activity of Chitosan-Polyethylene Oxide Nanofibers Containing Silver Nanoparticles against Aerobic and Anaerobic Bacteria. J Mol Struct 2023, 1274. https://doi.org/10.1016/j.molstruc.2022.134304.
- Geilich, B. M.; Van De Ven, A. L.; Singleton, G. L.; Sepúlveda, L. J.; Sridhar, S.; Webster, T. J. Silver 21 Nanoparticle-Embedded Polymersome Nanocarriers for the Treatment of Antibiotic-Resistant Infections. Nanoscale 2015, 7 (8), 3511–3519. https://doi.org/10.1039/c4nr05823b.
- Manojkumar, K.; Mecerreyes, D.; Taton, D.; Gnanou, Y.; Vijayakrishna, K. Self-Assembly of 22 Poly(Ionic Liquid) (PIL)-Based Amphiphilic Homopolymers into Vesicles and Supramolecular Structures with Dyes and Silver Nanoparticles. Polym Chem 2017, 8 (22), 3497–3503. https://doi. org/10.1039/c7py00453b.
- Saini, R. K.; Gupta, P. K.; Das, K. Plasmon-Molecular Resonance Coupling: Chlorine-P6 Adsorbed 23 on Poly-I-Lysine Stabilized Silver Nanoparticles. J Mol Struct 2012, 1024, 13-17. https://doi. org/10.1016/j.molstruc.2012.05.036.

- 24 Mi, G.; Shi, D.; Wang, M.; Webster, T. J. Reducing Bacterial Infections and Biofilm Formation Using Nanoparticles and Nanostructured Antibacterial Surfaces. Adv Healthc Mater 2018, 7 (13). https://doi.org/10.1002/adhm.201800103.
- 25 Marsich, L.; Bonifacio, A.; Mandal, S.; Krol, S.; Beleites, C.; Sergo, V. Poly-L-Lysine-Coated Silver Nanoparticles as Positively Charged Substrates for Surface-Enhanced Raman Scattering. Langmuir 2012, 28 (37), 13166-13171. https://doi.org/10.1021/la302383r.
- 26 Braydich-Stolle, L. K.; Lucas, B.; Schrand, A.; Murdock, R. C.; Lee, T.; Schlager, J. J.; Hussain, S. M.; Hofmann, M.-C. Silver Nanoparticles Disrupt GDNF/Fyn Kinase Signaling in Spermatogonial Stem Cells. Toxicological Sciences 2010, 116 (2), 577-589. https://doi.org/10.1093/toxsci/kfq148.
- 27 Sung, J. H.; Ji, J. H.; Park, J. D.; Yoon, J. U.; Kim, D. S.; Jeon, K. S.; Song, M. Y.; Jeong, J.; Han, B. S.; Han, J. H.; Chung, Y. H.; Chang, H. K.; Lee, J. H.; Cho, M. H.; Kelman, B. J.; Yu, I. J. Subchronic Inhalation Toxicity of Silver Nanoparticles. Toxicological Sciences 2009, 108 (2), 452–461. https:// doi.ora/10.1093/toxsci/kfn246.
- 28 Sharma, H. S.; Hussain, S.; Schlager, J.; Ali, S. F.; Sharma, A. Influence of Nanoparticles on Blood-Brain Barrier Permeability and Brain Edema Formation in Rats. In Brain Edema XIV; 2010; pp 359-364. https://doi.org/10.1007/978-3-211-98811-4_65.
- 29 Cha, K.; Hong, H.-W.; Choi, Y.-G.; Lee, M. J.; Park, J. H.; Chae, H.-K.; Ryu, G.; Myung, H. Comparison of Acute Responses of Mice Livers to Short-Term Exposure to Nano-Sized or Micro-Sized Silver Particles. Biotechnol Lett 2008, 30 (11), 1893–1899. https://doi.org/10.1007/s10529-008-9786-2.
- Zhang, J.; Wang, F.; Yalamarty, S. S. K.; Filipczak, N.; Jin, Y.; Li, X. Nano Silver-Induced Toxicity 30 and Associated Mechanisms. Int J Nanomedicine 2022, Volume 17, 1851-1864. https://doi. org/10.2147/IJN.S355131.
- 31 Yuan, X.; Setyawati, M. I.; Tan, A. S.; Ong, C. N.; Leong, D. T.; Xie, J. Highly Luminescent Silver Nanoclusters with Tunable Emissions: Cyclic Reduction-Decomposition Synthesis and Antimicrobial Properties. NPG Asia Mater 2013, 5 (2), e39-e39. https://doi.org/10.1038/ am.2013.3.
- Wang, X.; Gao, W.; Xu, W.; Xu, S. Fluorescent Ag Nanoclusters Templated by Carboxymethyl-32 β-Cyclodextrin (CM-β-CD) and Their in Vitro Antimicrobial Activity. Materials Science and Engineering: C 2013, 33 (2), 656–662. https://doi.org/10.1016/j.msec.2012.10.012.
- 33 Buceta, D.; Busto, N.; Barone, G.; Leal, J. M.; Domínguez, F.; Giovanetti, L. J.; Requejo, F. G.; García, B.; López-Quintela, M. A. Ag2 and Ag3 Clusters: Synthesis, Characterization, and Interaction with DNA. Angewandte Chemie International Edition 2015, 54 (26), 7612-7616. https://doi. org/10.1002/anie.201502917.
- 34 Neissa, J.; Pérez-Arnaiz, C.; Porto, V.; Busto, N.; Borrajo, E.; Leal, J. M.; López-Quintela, M. A.; García, B.; Dominguez, F. Interaction of Silver Atomic Quantum Clusters with Living Organisms: Bactericidal Effect of Ag 3 Clusters Mediated by Disruption of Topoisomerase–DNA Complexes. Chem Sci 2015, 6 (12), 6717-6724. https://doi.org/10.1039/C5SC02022K.
- 35 Liu, J.; Li, S.; Fang, Y.; Zhu, Z. Boosting Antibacterial Activity with Mesoporous Silica Nanoparticles Supported Silver Nanoclusters. J Colloid Interface Sci 2019, 555, 470-479. https:// doi.org/10.1016/j.jcis.2019.08.009.
- 36 Mora-Huertas, C. E.; Fessi, H.; Elaissari, A. Polymer-Based Nanocapsules for Drug Delivery, Int J Pharm 2010, 385 (1-2), 113-142. https://doi.org/10.1016/j.ijpharm.2009.10.018.
- 37 Rijpkema, S. J.; Langens, S. G. H. A.; Van Der Kolk, M. R.; Gavriel, K.; Toebes, B. J.; Wilson, D. A. Modular Approach to the Functionalization of Polymersomes. Biomacromolecules 2020, 21 (5), 1853-1864. https://doi.org/10.1021/acs.biomac.9b01734.
- Zhang, S.; Li, W.; Luan, J.; Srivastava, A.; Carnevale, V.; Klein, M. L.; Sun, J.; Wang, D.; Teora, S. P.; 38 Rijpkema, S. J.; Meeldijk, J. D.; Wilson, D. A. Adaptive Insertion of a Hydrophobic Anchor into a

- Poly(Ethylene Glycol) Host for Programmable Surface Functionalization. Nat Chem 2023, 15 (2), 240-247. https://doi.org/10.1038/s41557-022-01090-0.
- 39 Rijpkema, S. J.; Van Egeraat, R.; Li, W.; Wilson, D. A. Photo-Cross-Linking Polymersome Nanoreactors with Size-Selective Permeability. Macromolecules 2022, 55 (13), 5744-5755. https://doi.org/10.1021/acs.macromol.2c00248.
- 40 Bocca, B.; Battistini, B.; Petrucci, F. Silver and Gold Nanoparticles Characterization by SP-ICP-MS and AF4-FFF-MALS-UV-ICP-MS in Human Samples Used for Biomonitoring, Talanta 2020, 220, 121404. https://doi.org/10.1016/j.talanta.2020.121404.
- Jang, M.-H.; Lee, S.; Hwang, Y. S. Characterization of Silver Nanoparticles under Environmentally 41 Relevant Conditions Using Asymmetrical Flow Field-Flow Fractionation (AF4). PLoS One 2015, 10 (11), e0143149. https://doi.org/10.1371/journal.pone.0143149.
- 42 Loeschner, K.; Navratilova, J.; Legros, S.; Wagner, S.; Grombe, R.; Snell, J.; von der Kammer, F.; Larsen, E. H. Optimization and Evaluation of Asymmetric Flow Field-Flow Fractionation of Silver Nanoparticles. J Chromatogr A 2013, 1272, 116-125. https://doi.org/10.1016/j. chroma.2012.11.053.
- 43 Abdelmohsen, L. K. E. A.; Rikken, R. S. M.; Christianen, P. C. M.; van Hest, J. C. M.; Wilson, D. A. Shape Characterization of Polymersome Morphologies via Light Scattering Techniques. Polymer (Guildf) 2016, 107, 445-449. https://doi.org/10.1016/j.polymer.2016.06.067.
- 44 Abdelmohsen, L. K. E. A.; Nijemeisland, M.; Pawar, G. M.; Janssen, G. J. A.; Nolte, R. J. M.; Van Hest, J. C. M.; Wilson, D. A. Dynamic Loading and Unloading of Proteins in Polymeric Stomatocytes: Formation of an Enzyme-Loaded Supramolecular Nanomotor. ACS Nano 2016, 10 (2), 2652-2660. https://doi.org/10.1021/acsnano.5b07689.
- 45 Stauch, O.; Schubert, R.; Savin, G.; Burchard, W. Structure of Artificial Cytoskeleton Containing Liposomes in Aqueous Solution Studied by Static and Dynamic Light Scattering. Biomacromolecules 2002, 3 (3), 565-578. https://doi.org/10.1021/bm0200074.
- Völker, C.; Oetken, M.; Oehlmann, J. The Biological Effects and Possible Modes of Action of 46 Nanosilver, Rev Environ Contam Toxicol 2013, 223, 81-106. https://doi.org/10.1007/978-1-4614-5577-6_4.
- 47 Greulich, C.; Braun, D.; Peetsch, A.; Diendorf, J.; Siebers, B.; Epple, M.; Köller, M. The Toxic Effect of Silver Ions and Silver Nanoparticles towards Bacteria and Human Cells Occurs in the Same Concentration Range. RSC Adv 2012, 2 (17), 6981. https://doi.org/10.1039/c2ra20684f.
- 48 Freese, C.; Uboldi, C.; Gibson, M. I.; Unger, R. E.; Weksler, B. B.; Romero, I. A.; Couraud, P.-O.; Kirkpatrick, C. Uptake and Cytotoxicity of Citrate-Coated Gold Nanospheres: Comparative Studies on Human Endothelial and Epithelial Cells. Part Fibre Toxicol 2012, 9 (1), 23. https://doi. org/10.1186/1743-8977-9-23.

3.7 Supplementary Information

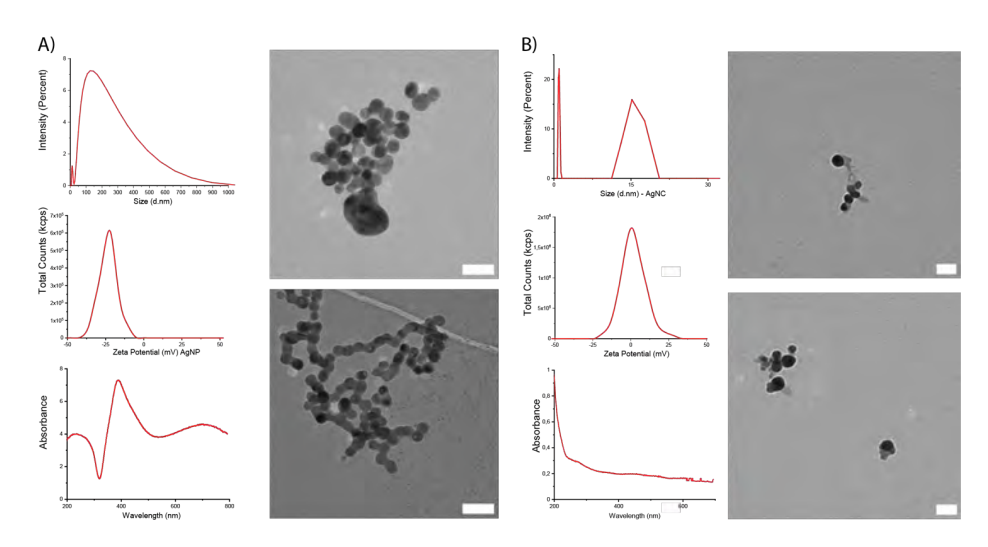


Figure S1. AgNP (A) and AgNC (B) Characterization comprised of DLS, Zeta potential, UV VIS, and TEM. Scale bars set at 50 nm

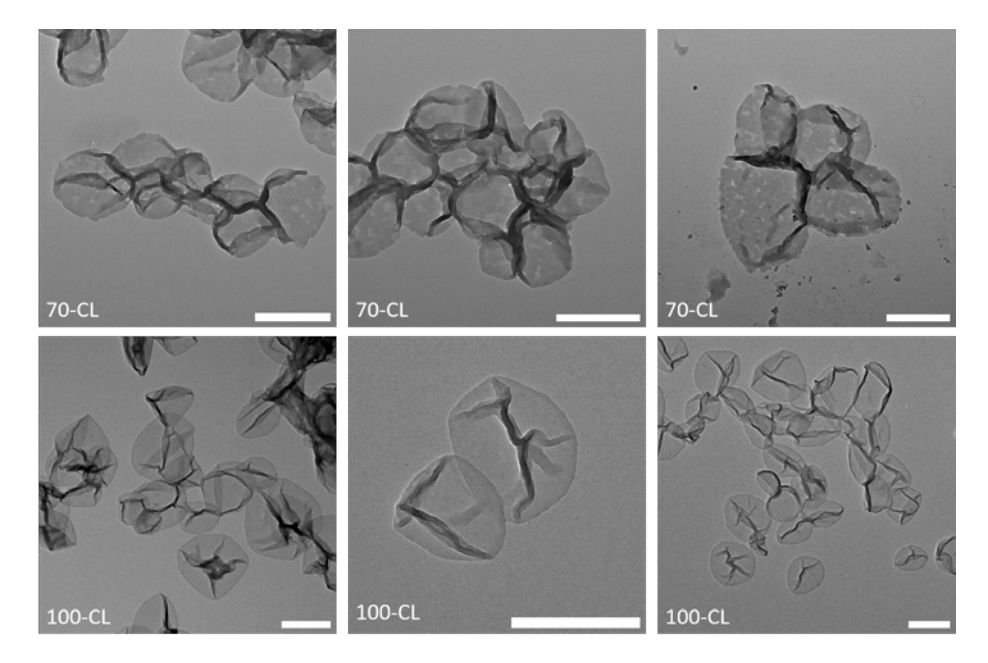


Figure S2. TEM Images of 70-CL and 100-CL Polymersomes. Scale bar 500 nm.

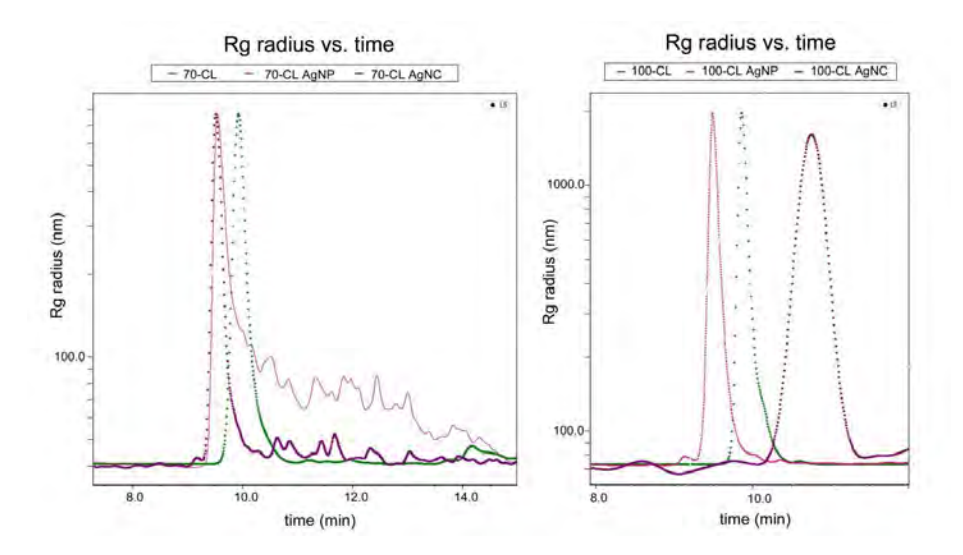


Figure S3. Rg radius (nm) obtained by FFF-MALS

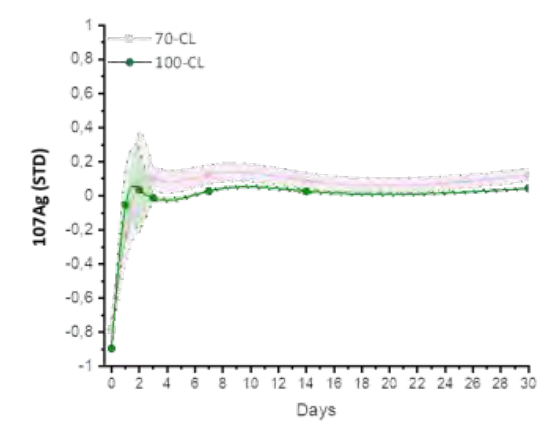


Figure S4. Silver release of empty controls 70-CL and 100-CL determined via ICP-MS over 30 days.

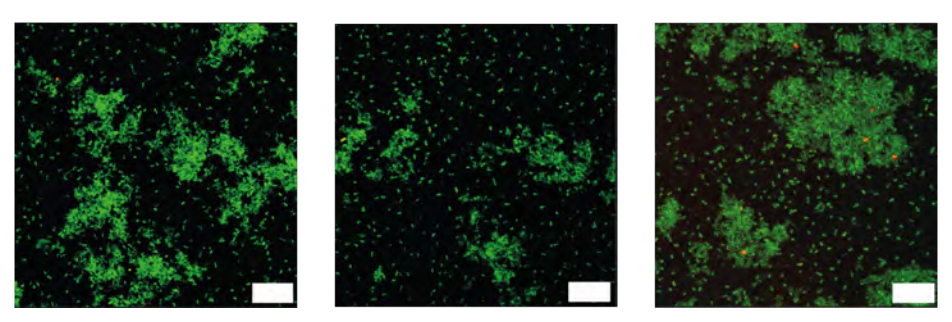


Figure S5. Effect of empty polymersomes on biofilm viability using Live/Dead Assay. Syto9 (Green Channel) representing viable cells, while PI stained cells are non-viable. Scale bar set to 10 µm.

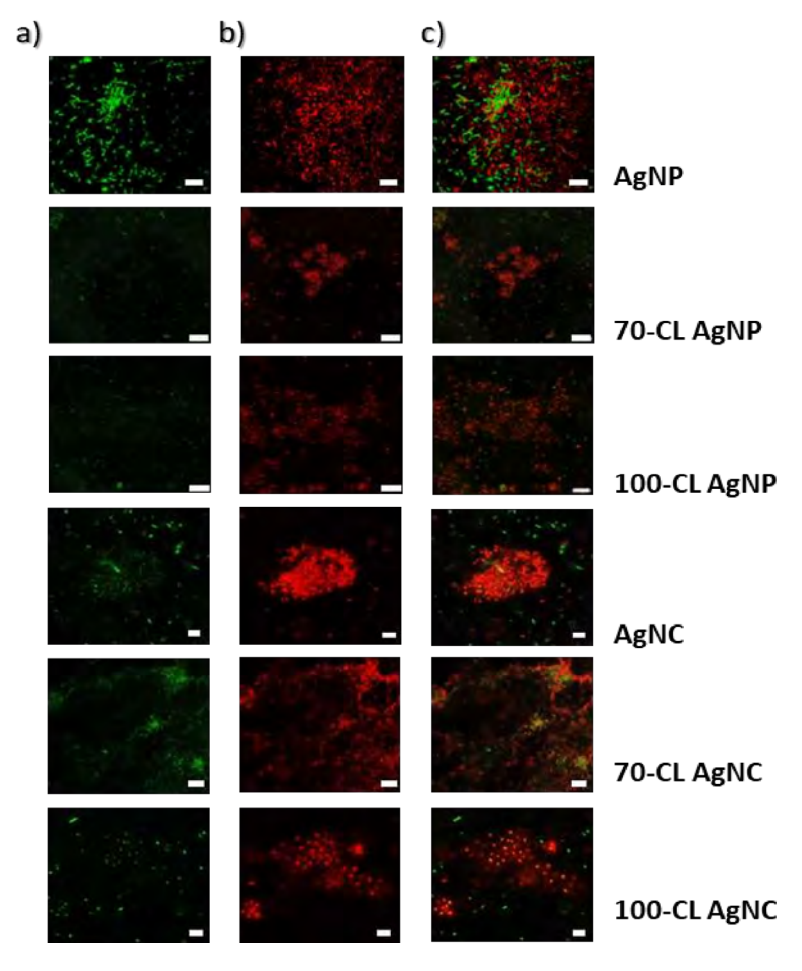


Figure S6. Confocal images of P. aeruginosa biofilms showing (a) live, (b) dead, and (c) merged in response to treatment with AgNPs, 70-CL AgNP, 100-CL AgNP, AgNCs, 70CL AgNC, and 100-CL AgNC. Scale bar 15 µm.

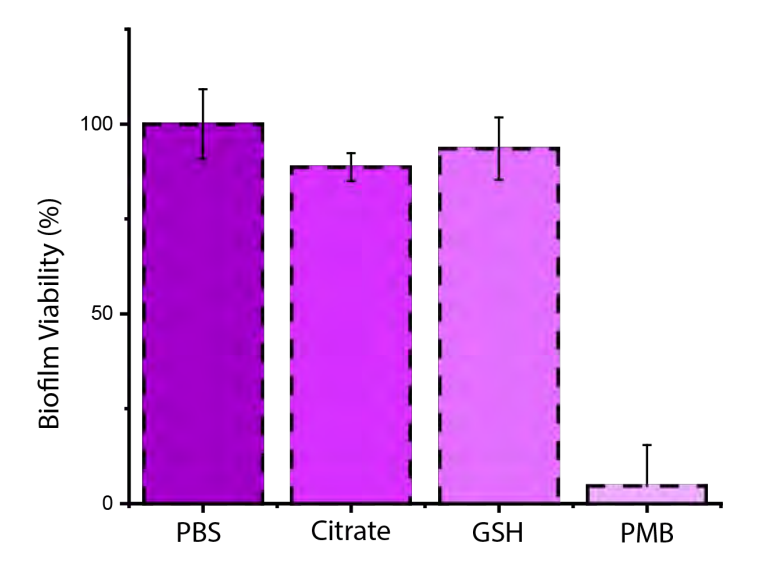


Figure S7. Biofilm viability assay using PBS, Citrate, Glutathione (GSH), and Polymyxin B (PMB)

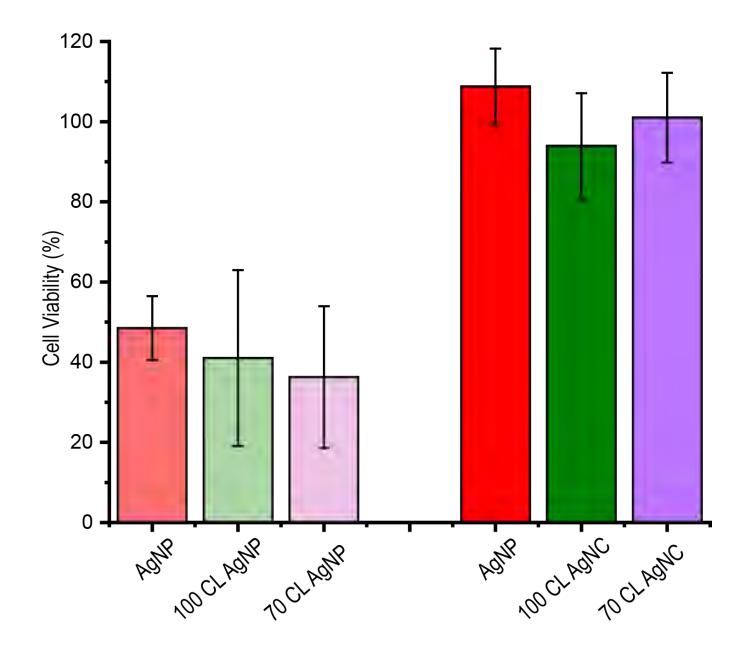
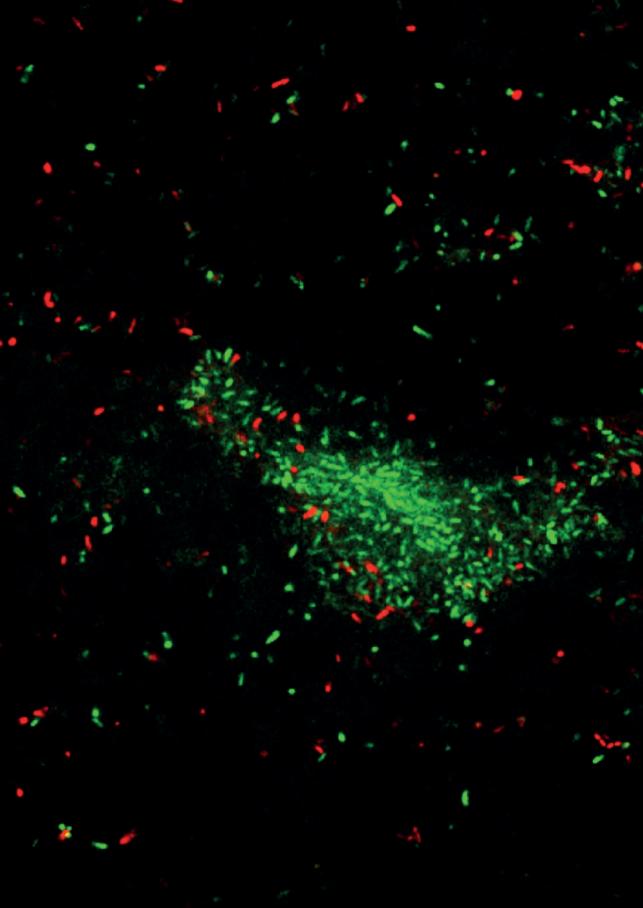


Figure S8. Repetition of cytotoxicity assay.



Chapter 4

Biofilm Disruption from Within: Lightactivated Molecular Drill functionalized Polymersomes bridge the gap between Membrane Damage and Quorum Sensing mediated Cell Death

Bela B. Berking[‡], Sjoerd J. Rijpkema[‡], Bai H. E. Zhang, Arbaaz Sait, Helene Amatdjais-Groenen, Daniela A. Wilson^{*}.

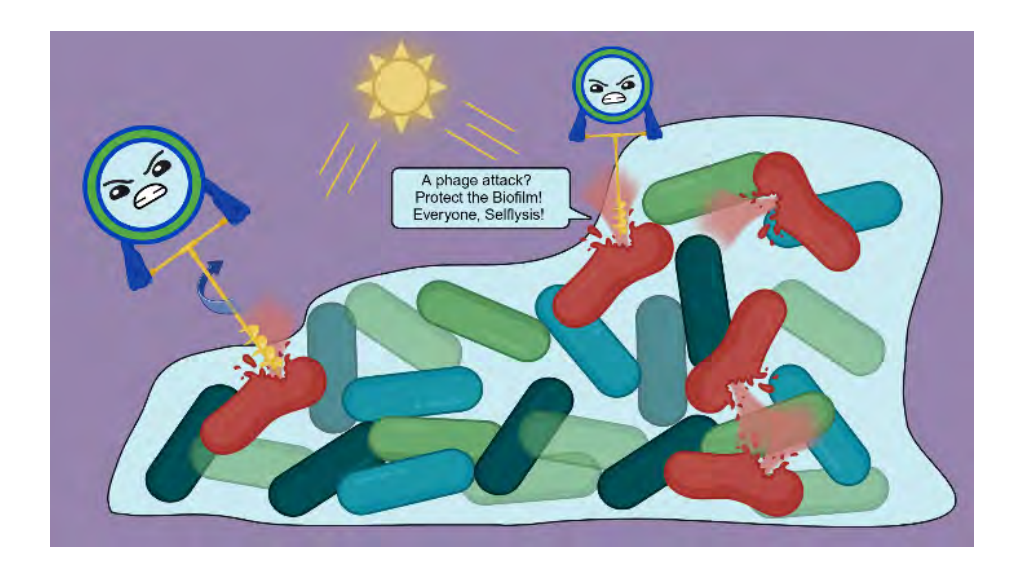
This chapter has been published:

Berking B. B., Rijpkema SJ, Zhang BHE, Sait A, Amatdjais-Groenen H, Wilson DA. Biofilm Disruption from within: Light-Activated Molecular Drill-Functionalized Polymersomes Bridge the Gap between Membrane Damage and Quorum Sensing-Mediated Cell Death.

ACS Biomater Sci Eng. 2024 Aug 23

Abstract

Bacterial biofilms represent an escalating global health concern, with the proliferation of drug resistance and hospital-acquired infections annually. Numerous strategies are under exploration to combat biofilms and pre-empt the development of antibacterial resistance. Among these, mechanical disruption of biofilms and enclosed bacteria presents a promising avenue, aiming to induce membrane permeabilization and consequent lethal damage. Herein, we introduce a hemithioindigo (HTI) motor activated by visible light, capable of disrupting sessile bacteria when integrated into a polymeric vesicle carrier. Under visible light, bacteria exhibited notable outer membrane permeability, reduced membrane fluidity, and diminished viability following mechanical drilling. Moreover, various genetic responses pertaining to the cell envelope were examined via gRT-PCR, alongside the activation of a self-lysis mechanism associated with phage stress, which was coupled to increases in quorum sensing, demonstrating a potential selflysis cascade from within. The multifaceted mechanisms of action, coupled with the energy efficiency of mechanical damage, underscore the potential of this system in addressing challenges posed by pathogenic biofilms.



4.1 Introduction

The emergence of antibiotic-resistant bacterial biofilms represents a mounting health crisis, contributing to elevated mortality rates among hospitalized patients and substantial extensions in hospitalization periods and associated medical expenses. Up to 80% of surgical site infections are estimated to be linked to bacterial biofilms, with persister cells frequently responsible for recurrent infections and the failure of post-antibiotic therapy completion. 1,2

Biofilms are characterized as a sessile group of bacteria embedded in a selfproduced extracellular matrix (ECM). 3 While bacterial biofilms make up the majority of biomass in the microbial world, in a medical setting these coordinated masses can be disruptive to tissue healing and significantly impair the ability of healthy cells to function normally. 45 A common example of a hospital-acquired pathogen is presented by *P. aeruginosa*, an opportunistic Gram-negative rod-shaped bacteria that often colonizes medical devices, open wounds and tissues, and more specifically the lungs of cystic fibrosis patients. ⁶⁷ Biofilm growth on top of these tissues can lead to altered production of cytokines, reduced immune response and in response, inflammation of the tissue, at the expense of the suffering patient. Not only does this impose a burden on patients, hindering the healing process, but it also carries significant economic ramifications, with global estimates reaching up to \$281 billion in 2019.8

A big hurdle in combating bacterial biofilms is the protection given to sessile bacteria by the ECM. 9,10 Consisting of a multitude of biomolecules, including DNA, proteins, lipids, and polysaccharides, as well as active enzymes, this protective shield is able to absorb common antibiotics and shelter bacteria from the host immune system, 11,12,13 The design of novel antimicrobials faces the first challenge when tasked with overcoming this barrier, either by active penetration or by diffusion into the deeper layers of biofilms to ensure sufficient eradication of the complete biofilm. Bacteria have adapted to these attacks with an arsenal of mechanisms such as fortifying the biofilm with increased amounts of eDNA through self-lysis or phage-mediated cell lysis. 14,15 These coordinated responses have been found to lie under partial control of the bacterial communication system, the quorum sensing apparatus, steering these lysis responses in a cascade-like manner through parts of the biofilm. 16

Molecular rotors have been gaining great attention recently due to their promising applications in the medical field. By utilizing intelligent systems with built-in stimuli responsiveness, targets can be manipulated at the flick of a light switch, allowing for the penetration of lipid bilayers. ¹⁷ Molecular rotors have been used to effectively kill cancer cells, fungi, and bacteria, with the main target being penetration of the membrane, leading to increases in reactive oxygen species ROS, leakage of intracellular contents, and overall loss of integrity 18, 19 20. Especially as antimicrobial treatment, these rotors have excellent chances of impacting the global challenge of growing resistance owing to their diverse modes of action. A variety of induced stresses was detected when bacteria were exposed to molecular rotors, showcasing the difficulty that these systems pose to bacteria for gaining resistance. a mechanism that was proven to be not possible for multiple strains tested. ^{20, 21} Examples in literature have been utilizing these novel antimicrobials in a "pure" state, not conjugated to any carrier, which allows for the potential advantage of easier cell wall penetration and distribution. However, this approach restricts these rotors from carrying payloads. Conversely, multiple rotors connected to a particle provides further advantages as they could enhance further biofilm disruption due to stronger synergetic forces over the membrane in addition to sensing capabilities. Incorporating these rotors into polymersomes offers a solution, enabling the attachment of various cargoes to the vesicle through integrated functional handles within or on the polymer membrane or taking advantage of the inner aqueous compartment provided by polymersomes. ²² By decorating a polymersome with a molecular rotor, we would be able to deliver a payload deep inside the biofilm, overcoming the defensive barrier provided by the ECM.

The group of Dube has developed several hemithioindigo (HTI) based rotors. ²³⁻²⁶ Based on their work, we have designed an HTI rotor that can be coupled to polymersomes. HTI motor 10 possesses an azide handle, which allows for the copper-free click binding to polymersomes with dibenzylcyclooctyne (DBCO) handles. A single binding spot was chosen over two to not allow for accidental coupling to two different polymersomes. This enables the polymersome to function as a nano-drill, a capability previously demonstrated with other molecular motors ²⁷ but not yet explored with nanostructures. The integration of this capability with a cargo-carrying polymersome, to the best of our knowledge, has not been attempted before. We fabricated HTI-functionalized polymersomes from supramolecular assemblies based on poly(ethylene glycol)-*b*-polystyrene (PEG-*b*-PS) diblock copolymer (Figure 1) and exposed the biofilms to this system.

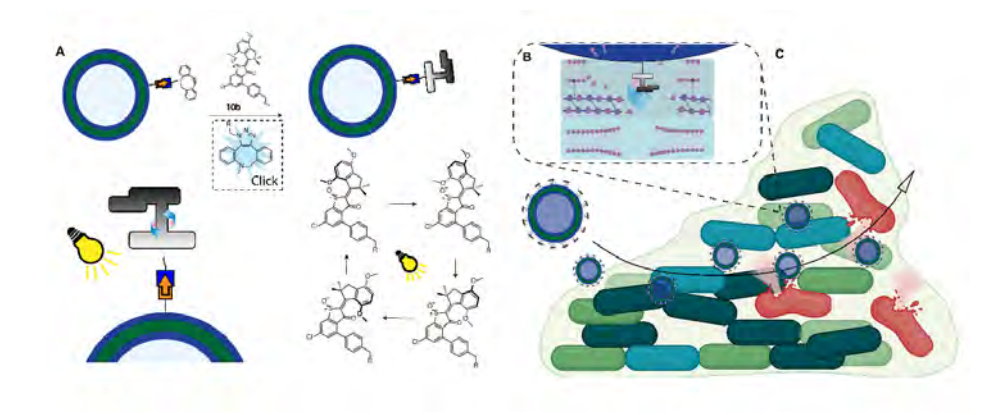


Figure 1. A. System design and conjugation step to fabricate hemithioindigo (HTI) rotor decorated polymersomes with the steps of HTI rotation. **B**, proposed mechanism of membrane-HTI interaction. Outer membrane, peptidoglycan layer as well as the inner membrane of the bacterial cell all become permeabilized and damaged. C. Biofilm infiltration and killing of bacteria via membrane damage. Accumulation of HTI polymersomes in the center of the biofilm results in effective killing of the bacteria, even without direct contact to the cell via quorum sensing cascade.

Upon light activation, HTI-Polymersomes efficiently infiltrated biofilms and eradicated the majority of bacterial cells within them. Furthermore, hydrophobic payloads encapsulated within the polymersomes, as demonstrated by Nile Red, exhibited notable accumulation within the biofilm, suggesting potential for targeted delivery. Detection of loss of membrane fluidity and increased outer membrane permeability of bacteria corroborated the main target of the HTIpolymersomes antimicrobial effect. We set out to investigate potential molecular responses and were able to determine three genetic responses after exposure: the upregulation of the outer membrane homeostasis pathway mlaA (maintenance of outer membrane lipid asymmetry) which upholds the outer membranes lipid asymmetry and flexibility 28, and the upregulation of PA3691, which is linked to a hypothetical protein responsible for a peptidoglycan repair response ²⁹. As a last effort to fortify the biofilm, bacteria activate a self-lysis mechanism via the endolysin lys, which causes the excretion of eDNA 30. We hypothesize that the mechanical damage mimics a phage-like attack and activates a self-lysis signal via quorum sensing, as we detected increases in the quorum sensing apparatus, to fortify the biofilm. We believe that the mechanism goes beyond just opening up the membrane, but rather "tricks" the whole biofilm into a self-lysis response as it would in nature.

4.2 Results and Discussion

Synthesis of the Drill

The synthesis of the azide functionalized HTI motor **10** (Scheme 1) was based on the previous work from the group of Dube^{23, 26}.

Scheme 1. Synthesis of the final products (**10**) starting from commercially available 3,5-dichlorobenzenethiol (**1**) and 4,7-dimethoxy-2,3-dihydro-1H-inden-1-on (**4**). Only the thermodynamically most stable Z isomers are shown for clarity. Only the Z isomer of **7** was used to make **10**. Synthesis and analysis was conducted by S. Rijpkema and H. Amatdjais-Groenen

Starting from the commercially available 3,5-dichlorobenzenethiol 1, we first converted it to the thioacetic acid 2 via a nucleophilic substitution reaction in 93% yield. Then, the acid was converted into the acyl chloride via Vilsmeier reagent 33, after which without purification an intramolecular Friedel-Crafts acylation was performed to make the dichlorinated benzothiophenone 3. Although conversion looked promising with only a small impurity, after purification via column chromatography, only a 50% yield was obtained. In subsequent repetitions, we found that it was also possible to continue with the crude in order to minimize the loss of compound. Commercially available 4.7-dimethoxy-1-indanone 4 was methylated twice in the 2-position using sodium hydride and methyl iodide to give indanone 5 in 85% yield in a fast reaction after purification. The condensation of 3 and 5 using boron trichloride as a Lewis acid then yielded dichlorinated HTI 6 as a mixture of Z and E isomers in 91% combined yield and was completed in less than an hour. Purification of 6 via column chromatography proved to be challenging, as it was found to be unstable on silica. Similarly, NMR spectra of the motors were taken in CD₂Cl₂ instead of the more common CDCl₃, as we found that the isomers were unstable in CDCl₃. However, oxidizing the crude of **6** with sodium perborate also yielded HTI motor $\mathbf{7}$ as a mixture of Z and E isomers without complications. Purification of **7** via column chromatography was possible without stability issues, making it possible to separate the isomers into 31% Z and 39% E. Because the Z isomer is thermodynamically more stable, we used this isomer for the next reaction step. Subsequently, we had to connect a moiety which could attach to the polymersome, for which we used an azide handle. For this, we had to make the azide boronic acid pinacol ester 9 from the commercially available 8 by reaction with sodium azide. This reaction was performed as reported in the literature with a similar yield of 74%.³⁴ A subsequent Suzuki cross-coupling between motor **7** and boronic acid pinacol ester 9 gave the final functionalized HTI motor 10a in 14% and **10b** in 53% yield respectively after purification in only the Z confirmation. Addition on both chloride positions was possible, but a clear preference for **10b** was found. We hypothesize this position is more reactive due to closer proximity to the ketone. We also obtained the double addition product in trace amounts. 10b was then used to bind to the polymersome.

Self-assembly of HTI decorated polymersomes

Polymersomes were self-assembled by slow addition of water over a solution of amphiphilic polymer PEG-b-PS in THF-Dioxane (4:1) using a process we have previously reported ^{22, 35, 36}. Afterwards, **10b** was attached to the polymersomes via a click reaction between the azide and DBCO functional groups overnight. The resulting polymersomes were washed with MeOH 3× to remove excess of **10b**, after which they were resuspended in ultrapure water. Removal of MeOH and excess unbound 10b was verified by NMR (Figure S5-6). We have previously shown the availability and reactivity of the DBCO handles.²² To confirm the binding of **10b** to the polymersomes, we redissolved part of the sample in CD₂Cl₂ and investigated the sample via diffusion NMR. This showed comparable diffusion speeds for both the PEG-b-PS signals and motor signals, whereas uncoupled **10b** has an approximately 10× faster diffusion speed compared to the polymer, indicating successful coupling (Figure S1-S3). Additionally, 1H-13C HMBC spectra before and after binding show a shift of the DBCO alkyne peaks, going from 85 ppm to 137 ppm after binding (Figure S7). After fabrication of HTI-decorated polymersomes, particles were characterized using TEM, dSTORM and DLS (Figure 2). TEM images revealed no morphological changes to the polymersomes before and after binding (Figure 2, A and B). To demonstrate the homogeneity of the HTI drill on the surface, the available handles were crosslinked to a fluorophore in the same way the drill is bound, imitating the binding procedure. Utilizing dSTORM microscopy a surface mapping of the polymersomes reveals evenly distributed handles (Figure 2C and D). This is of importance to understand later mechanisms by excluding the effects of an asymmetric particle. Particle characterization revealed polymersome formation with an average size of around 500 nm for particles with and without the drill (Figure 2E). Zeta potential showed an increase towards a more positive surface charge, which can be linked to the presence of the positively charged HTI drill on the surface (Figure **2F**). Change of the surface charge is a good indication of successful binding and has been previously used to determine surface modification. 35 Furthermore, binding was verified with Diffusion NMR, HTI decorated polymersomes were disassembled to detect HTI molecule presence (Figure S2).

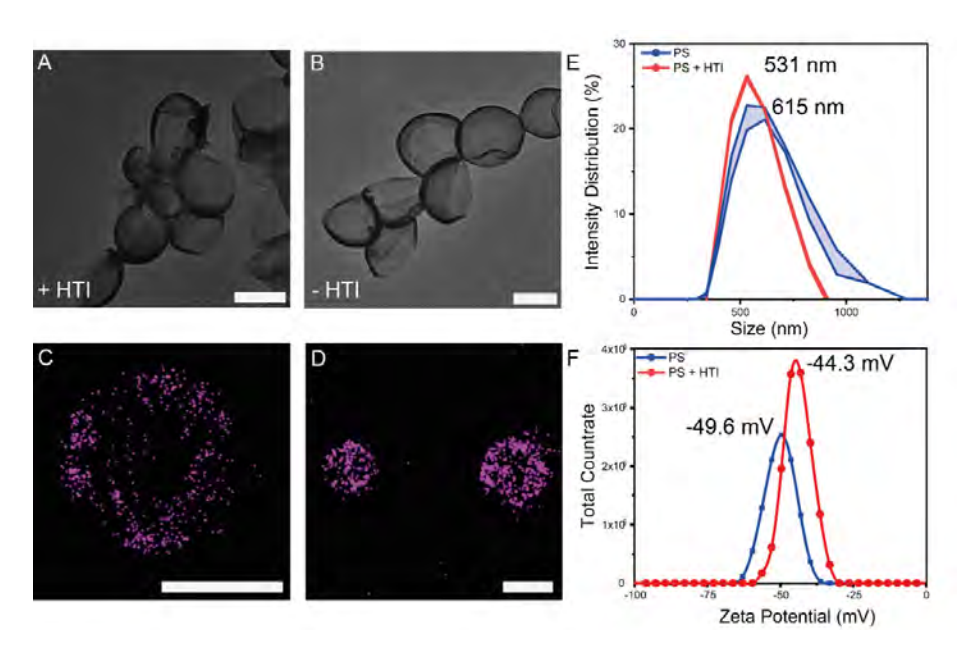


Figure 2. Particle Characterization: TEM of polymersomes with HTI (A) and without (B). Scale bars represent 500 nm. dStorm image of polymersome with AF647 (C-D) scale bar represents 200 nm. Size Analysis (E) of Polymersomes with (red) and without HTI (blue) in nm and Surface charge (F) in mV determined by DLS.

Evaluation of antibiofilm properties

Initial experiments aimed at demonstrating the ability of the Drill system to remove biofilm mass via mechanical damage, so a release of extracellular matrix material was expected. Polysaccharides as well as protein concentrations were determined in the supernatant after exposure. Results indicated no significant increase in ECM components in the supernatant, which imply that the activated HTI drill did not manage to shred off the ECM (Figure S4). By visualizing biofilms after exposure, it became evident that the structure of the biofilms remained intact, as can be seen in orthogonal slices of exposed biofilms (Figure 3A and 3B). Structures of the ECM still reach heights of more than 10 µM. Although structurally intact, a significant amount of bacteria in the biofilm suffered membrane damage, visible by Live/Dead staining. In a rescue experiment, we resuspended the bacteria previously exposed to the HTI polymersomes and mock treatments in media and let them grow in a forced planktonic state for 12 hours (Figure 3C and D). All treatments were able to recover and reached close to stationary phase after 12 hours, while the HTI polymersome-treated biofilms under light exposure did not recover (Figure 3D). This raises the question of polymersome infiltration into the biofilm and subsequent bacterial damage. At around 500 nm, HTI decorated polymersomes are capable of infiltrating water channels and pores which have been known to stretch through the biofilm, although at this size only a small percentage would be expected to diffuse into the biofilms. ³⁷ When visualizing biofilms after exposure to fluorescent HTI polymersomes (Magenta colored), accumulation can be seen in the center areas of the biofilm (Blue colored) (Figure 3E). DBCO decorated control polymersomes can be seen remaining on the outer area of the biofilms with just a few individual particles having diffused into the biofilms (**Figure 3F**). We hypothesize that upon contact, the HTI polymersomes can push themselves forward into the biofilm via rotational force of the HTI drill, damaging bacteria in the process (**Figure 3G**).

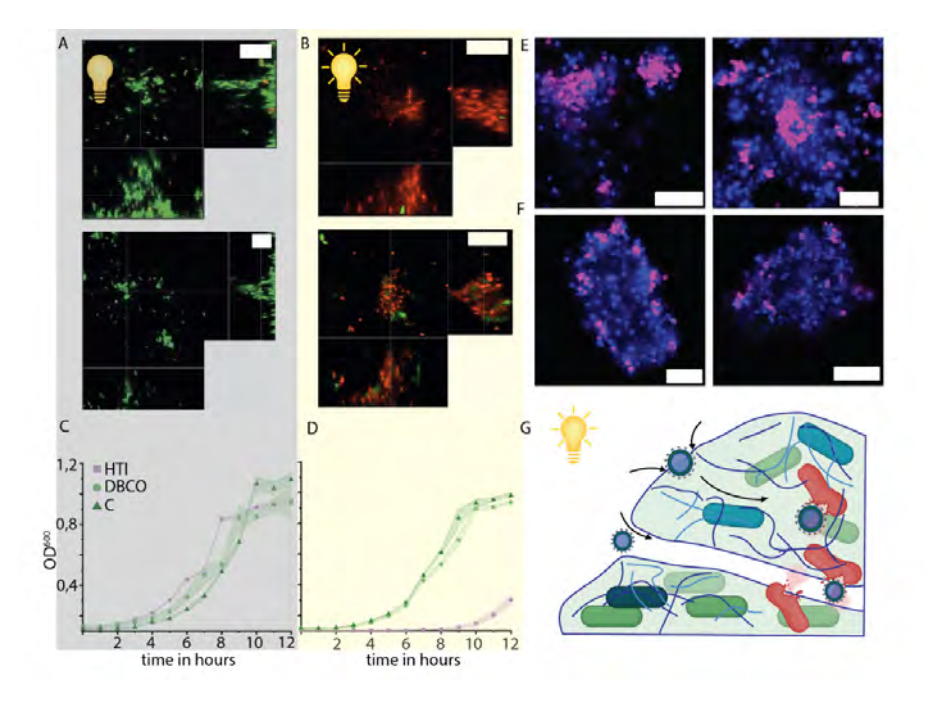


Figure 3. Confocal microscopy of biofilms exposed to HTI decorated polymersomes without (**A**) and with (**B**) subsequent light activation. Scale bars represent 10 μ m. Recovery of bacteria after exposure to HTI in the dark (**C**) and under light (**D**) determined by OD₆₀₀ measurements over 12 hours, n= 6-9. HTI polymersomes (magenta) infiltrate biofilms (blue) (**E**) while DBCO Polymersomes remain on the outer edge of biofilms (**F**). Scale bars represent 10 μ m. Potential mechanisms of biofilm infiltration (**G**) by pushing through ECM or passing through pores.

The delivery of cargo into the biofilm is an advantageous property that we envisioned for this system to have. Using a nanoparticle over only the molecular rotor allows for more modifications but also stronger mechanical forces over the bacterial membrane. In Figure 3E, the Nile Red used to label polymersomes is embedded inside the layers during self-assembly, a method used previously to

deliver f.e. doxorubicin. 38 Utilizing a different hydrophobic antibiotic, the same effect could be achieved. Due to the different compartments polymersomes offer, hydrophilic drug entrapments would also be possible. 39

To assess potential harmful effects on eukaryotic cells, we conducted cytotoxicity studies using Chinese Hamster Ovarian (CHO) cells and Hek cells. Remarkably we did not detect any decrease in cell viability when exposing cells to HTI polymersomes under light (Figure 4A). Additionally, the light control experiments show, that light itself is not strong enough to damage healthy cells and consequentially healthy tissue.

Assessment of bacterial membrane damage

It has been previously shown that one of the main modes of action by molecular rotors is disruption and damaging of the membrane (Figure 4B). ^{20, 21} Subjecting biofilms to membrane-sensitive probes such as N-phenyl-naphthylamine (NPN) and 1,6-diphenyl-1,3,5-hexatriene (DPH) allowed to better quantify the damage inflicted and show the light-activated mechanism of membrane damage even when bacteria are fortified in their biofilms (Figure 4C).

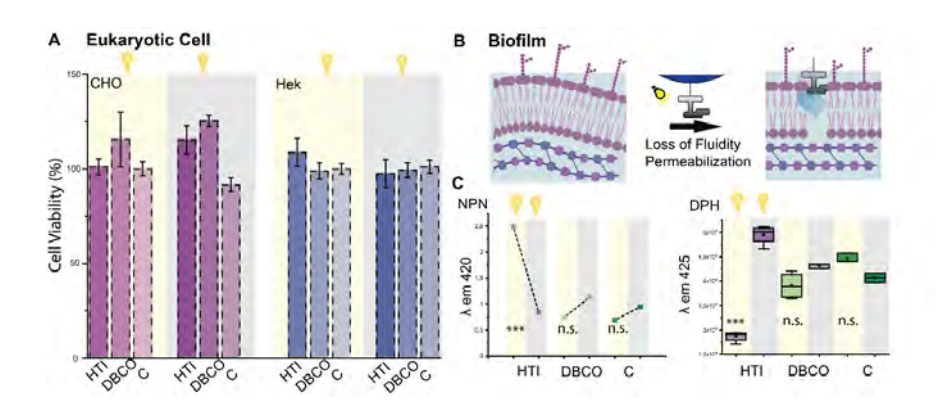


Figure 4. Effects of HTI-polymersomes on eukaryotic cells vs. biofilms. A Cytotoxicity studies of HTI-Polymersomes, DBCO-Polymersomes and controls under light and dark using CHO and Hek cells. N=8, significance tested with two-sided t.test, yet no significant decrease in viability was detected. (B) Outer membrane permeability and membrane fluidity determined by NPN and DPH. Schematic overview of changed membrane properties after exposure to HTI-polymersomes, verified experimentally (C) with NPN and DPH probes. Experiments were conducted in 4-8 biological replicates, $p \le 0.01$.

NPN assays have been widely utilized to showcase an increase in the permeability of the outer membrane (OM). 40 When biofilms are exposed to HTI-decorated polymersomes, yet kept from light exposure, the OM remains at similar levels of permeability as the controls (Figure 4B). Activating the HTI drill results in a significant increase in the permeability of the OM, indicating membrane damage by insertion and opening of the OM. This results in the loss of membrane integrity as well as fluidity, which was demonstrated by the probe DPH. Light-activated damage decreased the fluidity of the membrane, turning it more rigid, an effect of the membrane damage and lipid bilayer destruction (Figure 4B). 41

Genetic Analysis

We hypothesized that bacteria would activate various molecular responses to handle the damage inflicted, protect the biofilm, and adapt to further stressors of such kind, as they would in a natural setting. Analysis of various genes was achieved by monitoring transcript levels after exposure (**Figure 5**).

Responsible for maintaining outer membrane homeostasis is the Mla System. MlaA has been shown to increase outer membrane integrity when being activated, which has been studied in the case of membrane-targeting antibiotics and by deletion studies. 42, 43 When exposed to the HTI-polymersomes under light activation, this apparatus is significantly upregulated, as a response to outer membrane damage and loss of fluidity, as previously demonstrated (Figure 4B), an attempt to reorganize the lipid composition by trafficking phospholipids to increase membrane resilience via lipid asymmetry. ^{28,44} Following the outer membrane, the HTI-polymersomes encounter the peptidoglycan layer, where the hypothetical protein PA3691 has been attributed the role of peptidoglycan repair by upregulation under membrane damage ^{29,45}, which can be seen in Figure 5B under light activation. *P. aeruginosa* has been shown to undergo a self-lysis mechanism to fortify the biofilm using DNA under external stressors such as strong light and mechanical damage. 30, 46 This type of response has also been observed when biofilms experience a phage attack, where the outer laver will self-lyse to protect the inner laver, a mechanism believed to be sensing mediated and induced by the surrounding damaged cells as a cascade-like reaction. ¹⁶ Considering the combination this system uses, utilizing light as fuel to exert mechanical damage, self-lysis is a viable explanation for the observed structurally intact biofilms, with nonviable bacteria in them. To monitor this mechanism, the responsible lysing protein Lys (PA0629) was chosen to be analysed via qRT-PCR. Since we have already demonstrated damage to the outer membrane, the way is paved for this endolysin to open the membrane to release material to fortify the biofilm. Transcript levels can be seen increasing for the treated biofilms and control biofilms, although HTI-exposed biofilms have higher transcript levels, which is due to the combination of light and mechanical damage.

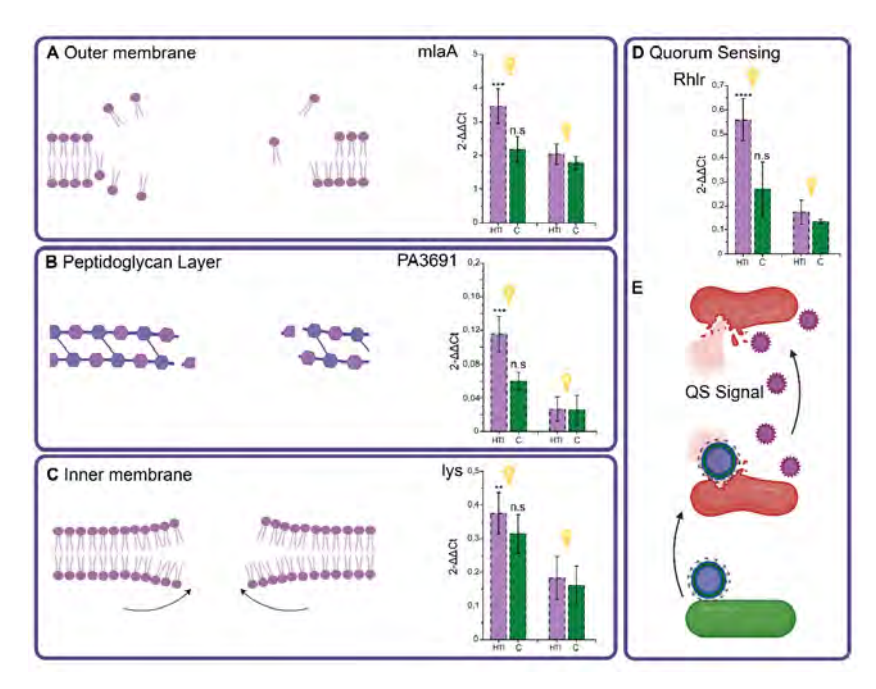


Figure 5. Analysis of membrane marker genes mlaA, PA3691 and lys for outer membrane (A), Peptidoglycan layer (B), and Inner membrane (C) as well as Rhlr to monitor quorum sensing (QS) (D). Genes were analyzed via qRT-PCR in three biological replicates, $p \le 0.01$. (E) Proposed mechanism of quorum sensing mediated lysis after exposure to HTI-polymersomes. The initial membrane damage triggers guorum sensing response which affects bacteria even without HTI-polymersome contact.

Looking back at the intact biofilms previously visualized with confocal microscopy (Figure 3B), a reasonable explanation for this is partial lysis of the bacteria in order to increase the stability of the biofilm and protect it from further attacks. In the event of bacteriophage attacks, sensing-mediated lysis has been shown to occur in Vibrio cholerae biofilms as means of biofilm formation or protection. We set out to investigate a correlation between the quorum sensing of biofilms after treatment as a potential trigger to cause cascade-like self-lysis, even when bacteria were not directly in contact with an HTI-polymersome. The RhIr gene, a main protagonist in the quorum sensing apparatus, was significantly upregulated after treatment (Figure 5D), thus demonstrating a potential link between the previously described self-lysis after HTI-polymersome exposure. We believe that the internalization of HTI-polymersomes shown to occur (Figure 3E) causes a phage-like attack, that, unlike in nature, happens in the center and the outer layer of the biofilm as opposed to just from the outer layer. This attack triggers a QS-mediated self-lysis of bacteria, resulting in the death of the biofilm from within. Bacteria which have come into contact with HTI polymersomes undergo membrane damage which causes an

increase in produced quorum-sensing molecules. This signal cascade then causes bacteria to self-lyse even when they have not come directly into contact with HTI-polymersomes (Figure 5E). This highly conserved lysis response could mean a certain specificity towards bacteria in which the HTI-polymersomes act, which is further supported by cytotoxicity studies demonstrating no adverse effects on Chinese hamster Ovarian cells and Hek cells (Figure 4A). These findings pave the way for further exploring HTI-polymersomes in more complex environments such as in-vivo studies to efficiently eradicate pathogenic biofilms.

4.3 Conclusion

In conclusion, this study has demonstrated the development of HTI-decorated polymersomes as an effective strategy for combatting bacterial biofilms. Through various experiments, we confirmed the successful infiltration of polymersomes into biofilms, leading to bacterial sensing and killing via a sensing-drill and kill mechanism. Our mechanistic investigations revealed that membrane permeabilization and loss of fluidity are key modes of action, while further a selflysis "death" signal propagated via quorum sensing, allows for further damage of the biofilm killing the bacteria from within the biofilm. While the HTI-decorated polymersomes did not break apart the ECM of the biofilm, this in fact turned into an advantage as we anticipate it would prevent a strong immune response for in vivo applications. Genetic analysis further illustrated the diverse responses bacteria employ to survive stress induced by light-activated HTI-polymersomes, including outer membrane and peptidoglycan repair. These findings highlight the multitude of potential targets for antibacterial interventions, crucial for overcoming the current issues of antibiotic resistance. By leveraging a fuel-free system, we anticipate that light-activated rotors will emerge as a sustainable alternative to existing antibiofilm approaches. The ability to turn the bacterial signal/sensing apparatus against the entire biofilm makes this a unique approach to killing biofilms from within.

Acknowledgments

The authors thank Dr. Robert Jansen and Prof. Dr. Laura van Niftrik for the access to ML2 facilities. BB and D.A.W. acknowledges support from the European Research Council (ERC) under the European Union's Horizon 2020 research and innovation programme ERC-CoG 101044434 "SynMoBio". We acknowledge support from the Ministry of Education, Culture and Science (Gravitation program 024.001.035).

Author Contributions

B.B.B. and S.J.R. derived the concept. S.J.R and H.A.G. synthesized the HTI molecule and conducted NMR. B.Z.H.E. and B.B.B conducted the genetic analysis. A.S. and B.B.B conducted confocal microscopy, B.B.B. wrote the initial version of the manuscript. D.A.W. supervised the entire study and contributed to the final version of the manuscript.

4.4 Experimental Section

General preparation of polymersomes with DBCO handles. Modified from a previous report 31, a general procedure is described: MeO-PEG-b-PS (8 mg) and DBCO-PEG-b-PS (2 mg) were dissolved in a mixture of THF and 1,4-dioxane (1 mL, 4:1 v/v) in a 15 mL capped vial with a magnetic stir bar. After dissolving the solution for 0.5 h at 21 °C, a syringe pump equipped with a syringe and a needle was used to deliver ultrapure water at a rate of 1 mL/h for 0.5 h via a rubber septum, while vigorously stirring the mixture (900 rpm). The appearance of a cloudy suspension indicated the formation of the polymersomes. Upon finishing the water addition, 8 mL of ultrapure water was added to the suspension, which ensured a rapid quenching of the PS domain within the bilayer of the polymersomes. The polymersomes were spun down via centrifuge (10 min, 10.000 rpm) and washed with ultrapure water a total of three times.

Click Reaction on DBCO-PEG-b-PS Polymersomes. DBCO-PEG-b-PS polymersomes (10 mg, 20% functionalized) were diluted in MeOH (2 mL). An excess of 10b in MeOH (100 µL,1 mg/mL) was added to the solution and the mixture was stirred for 16 h in the dark. The polymersomes were washed (3x with ultrapure water) by centrifugation to remove the methanol and excess of 10b, and were resuspended in ultrapure water.

Particle Characterization. Size and surface charge were determined using a DLS Zetasizer blue (Malvern). Samples were diluted to 0.01 mg/ml polymer concentration and measured. Transmission Electron Microscopy (TEM) was conducted on a JEOL JEM-1400 FLASH running at 120 kV. Samples were airdried overnight on a copper grid.

dSTORM microscopy. To show HTI drill binding on the surface dSTORM superresolution microscopy was conducted on ONI nanoimager. Polymersomes with 20% DBCO handle availability were incubated with AlexaFluor 647-N₃ for 16 h for binding. Channel Slides carrying Avidin surface coating were provided by ONI. Polymersomes were incubated with a anti-PEG antibody. Polymersomes were then gently flown through the channel to be captured on the surface. Unbound particles were washed away before the dSTORM buffer was added to the channel. Samples were imaged using a 647 laser utilizing 3000 frames acquisition.

Biofilm experiments. The Overnight culture was inoculated in 6 mL of Brain Heart Infusion (BHI) by adding 5 µL of P. aeruginosa ATCC 10145, 50% Glycerol Stock and incubated overnight at 37 °C. The next day, the resulting culture was diluted to an OD of 0.001 and was seeded into wells of a 96-, or 12-well plates for biofilms to grow. The plate was incubated at 37 °C for 2 h after which the medium was refreshed to remove the bulk of the planktonic cells. The plate was then returned to the incubator for overnight incubation to allow for biofilm formation. After allowing biofilm formation for 24 h, the medium was carefully aspirated and the wells were washed 3 times with 1x PBS. Polymersomes were added at 0.1 mg/ml to the wells, resulting in the addition of 10 µl to 100 µl of PBS in the wells. 10 µl of ultrapure water was added to the control wells to mimick the slight dilution of the PBS buffer. Half of the plate was wrapped in aluminum foil to cover the wells (no light exposure control) while the other half was exposed to a 450 nm laser for 2 h to activate the polymersomes. The well-plate was placed on ice during the laser exposure to slow down bacterial metabolism and prevent further biofilm production as well as prevent heating effects. After 2 h, the wells were carefully aspirated, and experiments conducted as described below.

Confocal Microscopy. Imaging was conducted using an SP8x AOBS-WLL confocal laser scanning microscope. Syto9 and Propidium lodide were used to create a suitable working solution: for Syto9 a final concentration of c = 11.1 nM and for Propidium lodide a final concentration of c = 66.6 nM in PBS (150 mM NaCl, 100 mM NaPO4mM, pH 7.4). Biofilms were stained for 10 minutes and washed three times with PBS (150 mM NaCl, 100 mM NaHPO₄, pH 7.4. Lasers were set at λ ex = 470 nm, λ em = 500-520 nm and λ ex = 560 nm, λ em = 620-670 nm. Images were later analysed with Imaris.

Period acid-Schiff assay. Based on a known method, the PAS assay was carried out using the solutions collected after treatment of the biofilms to quantify the exopolysaccharides released due to the drilling. 175 μ L of 0.5% periodic acid (in 5% acetic acid) was added to wells of 96-well plate. 25 μ L of the collected samples were then added to the wells and left to incubate for 30 min. 100 μ L of Schiff's reagent was then added to the wells and left to incubate overnight. Absorbance

measurements were then taken at 544 nm with the Spark multimode microplate reader (Tecan).

Bradford assay. To assess if an increased amount of protein could be detected in the supernatant after HTI exposure, which could be a result of ECM damage, a Bradford assay was conducted. 40 µL of Bradford reagent was added to 20 µL of the collected samples in a 96-well plate. Ultrapure water was then added to make up a final volume of 200 µL. Absorbance measurements were taken at 595 nm with the Spark multimode microplate reader (Tecan).

NPN Assay. To assess outer membrane permeability the fluorescent probe n-phenyl-1-Napthylamine (NPN) was used. Biofilms were left to form over 24-hour incubation time after which various treatments were conducted as described before. Wells were gently washed three times with PBS before adding NPN solution to a final concentration of 12 µM. Parallel to NPN, Syto9 was added to normalize wells in terms of biomass to acquire a more accurate comparison. Wells were measured at λex= 320 nm, λem= 420 for NPN and λex= 450 nm, λem= 550 for Syto9

Membrane Fluidity Assay. Membrane fluidity assay was performed as previously described 32. Biofilms were left to form over 24-hour incubation time after which various treatments were conducted as described before. Wells were gently washed three times with 1x PBS, Using a cell scraper all material was scraped off the wells and centrifuged for 10 minutes at 6000 rcf to collect cells. The supernatant was removed and the cells were fixed in 0.37% Glutaraldehyde for 30 minutes. Bacteria were then frozen in liquid nitrogen for 5 minutes, thawed and resuspended in 0.6 mM DPH solution and measured at λ ex= 350 nm, λ em= 425.

RNA Extraction. Following irradiation, the total RNA was extracted from the biofilms using the RNeasy Kit of QIAGEN. The media was removed from the biofilm and washed once with 1x PBS. Before scraping the biofilm of the wells, 1 volume of 1x PBS and 2 volumes of RNA protect bacteria reagent were added to each well. The samples were then scraped and transferred into bead-beating tubes and the cells were lysed by 0.1mm Zirconia/silica beads in the BeadBug 6 bead homogenizer for 3 cycles of 30 seconds on and off at 4000rpm. Following the lysis, the lysate was transferred to the RNeasy Mini Spin Column and placed in 2 mL collection tubes. The columns were centrifuged at ≥8000x g for 15 sec. and the flow-through was discarded and the collection tube was reused. This step was repeated until all lysate was processed. Then to wash the spin column membrane 700µl Buffer RW1 was added and centrifuged at ≥8000x g for 15 sec. The flow-through was discarded and the columns were placed in new collection tubes. Subsequently, 500μ l Buffer RPE was added and centrifuged at $\geq 8000x$ g for 15 sec. This step was repeated once more with 500μ l Buffer RPE and centrifuged at $\geq 8000x$ g for 2 min. to ensure the removal of ethanol. The spin columns were then transferred to new 1.5 ml collection tubes, and $30-50\mu$ l of Rnase-free water was added directly to the membrane. The columns were then centrifuged at $\geq 8000x$ g for 1 min. to elute the RNA.

The concentration and purity of the RNA were determined by the Nanodrop 1000[™] spectrophotometer. The absorbance ratio A260/280 served as a measure of protein contamination, while the ratio A260/230 served as a measure of contamination of polysaccharides, phenols and salts. Additionally, an Agarose Gel electrophoresis was conducted.

cDNA Synthesis. For the cDNA synthesis, the RNA was treated with DNase to remove genomic DNA. This was done using the DNase I Amplification Grade by Invitrogen™. The following was added to an RNase-free PCR-strips on ice: 500 ng total RNA, 1µl 10X DNase I Reaction Buffer, 1µL DNase I Amplification Grade (1U/µl) and DEPC-treated water to 10uL. Then the PCR strips were incubated for 15 min. at room temperature. Then 1µl of 25 mM EDTA was added to inactivate the DNase I. Lastly, the RNA samples were incubated for 10 min. at 65°C. cDNA was synthesized using the SuperScript™ II Reverse Transcriptase by Invitrogen™. To each DNase-treated RNA 9µl of the following mix were added: 1µl random primers (250 ng/µl), 1µl 10mM dNTP's, 4µl 5X 1st Strand Buffer, 1µl 0.1M DTT, 1µl RNaseOUT™ (10 U/µl), 0.5µl Superscript II (200 U/µl) and 0.5µl DEPC-treated water. Mixed and incubated for 10 min. at 25°C followed by another incubation of 50 min. at 42°C and the reaction was inactivated by heating it for 15 min. at 70°C. After the cDNA synthesis, the cDNA was purified using the QIAquick PCR Purification Kit of QIAGEN. This was done according to the manufacturer's instructions. Following purification, the cDNA concentration was measured with the Qubit™ 4 Fluorometer using the 1X High Sensitivity dsDNA assay.

qRT-PCR. qRT-PCR was performed using the iQ SYBR Green Supermix by Bio-Rad. Each reaction contains 10 μ L iQ SYBR Green Supermix, 2 μ L (10 μ M) forward primer, 2 μ L (10 μ M) reverse primer, 1ng cDNA and DEPC-treated water to a final volume of 20 μ L. The primers that were used are listed in Table x.

The qRT-PCR was performed in a Bio-Rad C1000 Touch Thermal Cycler using the following protocol: 95°C for 30 seconds, 95°C for 30 seconds, 60°C for 10 seconds and 72°C for 20 seconds (repeat 39X). Followed by a melt-curve analysis from 58°C

to 95°C at a 0.5°C/cycle melt rate. The relative gene expression was calculated using the 2-ΔΔCT method, where all Ct values were normalized to the housekeeping genes gyrA and recA

Table 1. Primer design for all genes of interest. Primers were designed using Primer3 and verified via Blast.

Gene of Interest	Forward Sequence (5'->3')	Reverse Sequence (5'->3')
mlaA	GCATCAACCGTCCCATCTTC	GGTTGTTGGCCAGGTTCTTC
PA3691	TCGAGATGAAGTCCGCTCAG	GCATCCTTCACGGCTTTCTG
lys	ATGAAACTGACCGAGCAGCA	TGTGTCGATCTCCCTCTCGT
recA	GAAGTTCTACGCCTCGGTCC	GTTCTTCACCACCTTGACGC
gyrA	ATGGAGGTGATCCGTGAGGA	TTCTTCACGGTACCGAAGGC
rhIR	CTCCTCGGAAATGGTGGTCT	TTCTGGGTCAGCAACTCGAT

Cytotoxicity studies. HEK293T, Chinese Hamster Ovarian (CHO) cells were cultured in DMEM medium supplemented with 10% FBS. After cells reached a confluence of around 50 %, they were rinsed with 1x PBS three times and detached with 4 ml Trypsin for 3 minutes. Trypsin was quenched by adding 8 ml of DMEM medium. The cells were transferred to a 15 ml falcon and spun down 5 minutes at 0.3 rcf. The supernatant was discarded, and cells seeded with DMEM complete medium in a 96 well plate at a density of 4.0 to 4.5 x 10⁴ cells/ml and incubated for 24 hours at 37 °C with 5 % CO2. Afterwards, HTI-polymersomes, DBC O polymersomes were added to the wells and either subjected to light exposure or not. 10 µl of CCK8 (Sigma Aldrich) was added to the wells, incubated for 3 hours and the absorbance measured at 450 nm to determine viability. Experiments were carried out in replicates of 8.

- Edmiston, C. E., Jr.; McBain, A. J.; Roberts, C.; Leaper, D., Clinical and microbiological aspects of biofilm-associated surgical site infections. Adv Exp Med Biol 2015, 830, 47-67.
- Schulze, A.; Mitterer, F.; Pombo, J. P.; Schild, S., Biofilms by bacterial human pathogens: Clinical relevance - development, composition and regulation - therapeutical strategies. *Microb Cell* 2021, 8 (2), 28-56.
- Sauer, K.; Stoodley, P.; Goeres, D. M.; Hall-Stoodley, L.; Burmølle, M.; Stewart, P. S.; Bjarnsholt, T.,
 The biofilm life cycle: expanding the conceptual model of biofilm formation. *Nature Reviews Microbiology* 2022, 20 (10), 608-620.
- 4. Flemming, H. C.; Wuertz, S., Bacteria and archaea on Earth and their abundance in biofilms. *Nat Rev Microbiol* **2019**, *17* (4), 247-260.
- 5. Muhammad, M. H.; Idris, A. L.; Fan, X.; Guo, Y.; Yu, Y.; Jin, X.; Qiu, J.; Guan, X.; Huang, T., Beyond Risk: Bacterial Biofilms and Their Regulating Approaches. *Front Microbiol* **2020**, *11*, 928.
- 6. Groeger, S.; Meyle, J., Oral Mucosal Epithelial Cells. Front Immunol 2019, 10, 208.
- 7. Malhotra, S.; Hayes, D., Jr.; Wozniak, D. J., Cystic Fibrosis and Pseudomonas aeruginosa: the Host-Microbe Interface. *Clin Microbiol Rev* **2019**, *32* (3).
- 8. Cámara, M.; Green, W.; MacPhee, C. E.; Rakowska, P. D.; Raval, R.; Richardson, M. C.; Slater-Jefferies, J.; Steventon, K.; Webb, J. S., Economic significance of biofilms: a multidisciplinary and cross-sectoral challenge. *npj Biofilms and Microbiomes* **2022**, *8* (1), 42.
- 9. Flemming, H. C.; Wingender, J., The biofilm matrix. Nat Rev Microbiol 2010, 8 (9), 623-33.
- Pinto, R. M.; Soares, F. A.; Reis, S.; Nunes, C.; Van Dijck, P., Innovative Strategies Toward the Disassembly of the EPS Matrix in Bacterial Biofilms. Front Microbiol 2020, 11, 952.
- 11. Zhao, A.; Sun, J.; Liu, Y., Understanding bacterial biofilms: From definition to treatment strategies. *Front Cell Infect Microbiol* **2023**, *13*, 1137947.
- 12. Ciofu, O.; Moser, C.; Jensen, P. Ø.; Høiby, N., Tolerance and resistance of microbial biofilms. *Nature Reviews Microbiology* **2022**, *20* (10), 621-635.
- 13. Jones, C. J.; Wozniak, D. J., Psl Produced by Mucoid Pseudomonas aeruginosa Contributes to the Establishment of Biofilms and Immune Evasion. *mBio* **2017**, *8* (3).
- 14. Nanda Arun, M.; Thormann, K.; Frunzke, J., Impact of Spontaneous Prophage Induction on the Fitness of Bacterial Populations and Host-Microbe Interactions. *Journal of Bacteriology* **2015**, *197* (3), 410-419.
- Okshevsky, M.; Meyer, R. L., The role of extracellular DNA in the establishment, maintenance and perpetuation of bacterial biofilms. *Critical Reviews in Microbiology* 2015, 41 (3), 341-352.
- 16. Prentice, J. A.; van de Weerd, R.; Bridges, A. A., Cell-lysis sensing drives biofilm formation in Vibrio cholerae. *Nature Communications* **2024**, *15* (1), 2018.
- 17. Klok, M.; Boyle, N.; Pryce, M. T.; Meetsma, A.; Browne, W. R.; Feringa, B. L., MHz unidirectional rotation of molecular rotary motors. *J Am Chem Soc* **2008**, *130* (32), 10484-5.
- Ayala Orozco, C.; Liu, D.; Li, Y.; Alemany, L. B.; Pal, R.; Krishnan, S.; Tour, J. M., Visible-Light-Activated Molecular Nanomachines Kill Pancreatic Cancer Cells. ACS Applied Materials & Interfaces 2020, 12 (1), 410-417.
- Santos, A. L.; Beckham, J. L.; Liu, D.; Li, G.; van Venrooy, A.; Oliver, A.; Tegos, G. P.; Tour, J. M., Visible-Light-Activated Molecular Machines Kill Fungi by Necrosis Following Mitochondrial Dysfunction and Calcium Overload. *Advanced Science* 2023, 10 (10), 2205781.

- 20. Santos, A. L.; van Venrooy, A.; Reed, A. K.; Wyderka, A. M.; García-López, V.; Alemany, L. B.; Oliver, A.; Tegos, G. P.; Tour, J. M., Hemithioindigo-Based Visible Light-Activated Molecular Machines Kill Bacteria by Oxidative Damage. Adv Sci (Weinh) 2022, 9 (30), e2203242.
- 21. Santos, A. L.; Liu, D.; Reed, A. K.; Wyderka, A. M.; van Venrooy, A.; Li, J. T.; Li, V. D.; Misiura, M.; Samoylova, O.; Beckham, J. L.; Ayala-Orozco, C.; Kolomeisky, A. B.; Alemany, L. B.; Oliver, A.; Tegos, G. P.; Tour, J. M., Light-activated molecular machines are fast-acting broad-spectrum antibacterials that target the membrane. Science Advances 2022, 8 (22), eabm2055.
- 22. Rijpkema, S. J.: Langens, S. G. H. A.: van der Kolk, M. R.: Gavriel, K.: Toebes, B. J.: Wilson, D. A., Modular Approach to the Functionalization of Polymersomes. Biomacromolecules 2020, 21 (5), 1853-1864.
- 23. Guentner, M.; Schildhauer, M.; Thumser, S.; Mayer, P.; Stephenson, D.; Mayer, P. J.; Dube, H., Sunlight-powered kHz rotation of a hemithioindigo-based molecular motor. Nat. Commun. **2015,** 6 (1), 8406.
- 24. Wilcken, R.; Schildhauer, M.; Rott, F.; Huber, L. A.; Guentner, M.; Thumser, S.; Hoffmann, K.; Oesterling, S.; de Vivie-Riedle, R.; Riedle, E.; Dube, H., Complete Mechanism of Hemithioindigo Motor Rotation. J. Am. Chem. Soc. 2018, 140 (15), 5311-5318.
- 25. Uhl, E.; Thumser, S.; Mayer, P.; Dube, H., Transmission of Unidirectional Molecular Motor Rotation to a Remote Biaryl Axis. Angew. Chem., Int. Ed. 2018, 57 (34), 11064-11068.
- Hoffmann, K.; Mayer, P.; Dube, H., A hemithioindigo molecular motor for metal surface 26. attachment. Org. Biomol. Chem. 2019, 17 (7), 1979-1983.
- 27. Liu, D.; García-López, V.; Gunasekera, R. S.; Greer Nilewski, L.; Alemany, L. B.; Aliyan, A.; Jin, T.; Wang, G.; Tour, J. M.; Pal, R., Near-Infrared Light Activates Molecular Nanomachines to Drill into and Kill Cells. ACS Nano 2019, 13 (6), 6813-6823.
- Babu, M.; Bundalovic-Torma, C.; Calmettes, C.; Phanse, S.; Zhang, Q.; Jiang, Y.; Minic, Z.; Kim, 28. S.; Mehla, J.; Gagarinova, A.; Rodionova, I.; Kumar, A.; Guo, H.; Kagan, O.; Pogoutse, O.; Aoki, H.; Deineko, V.; Caufield, J. H.; Holtzapple, E.; Zhang, Z.; Vastermark, A.; Pandya, Y.; Lai, C. C.; El Bakkouri, M.; Hooda, Y.; Shah, M.; Burnside, D.; Hooshyar, M.; Vlasblom, J.; Rajagopala, S. V.; Golshani, A.; Wuchty, S.; J, F. G.; Saier, M.; Uetz, P.; T, F. M.; Parkinson, J.; Emili, A., Global landscape of cell envelope protein complexes in Escherichia coli. Nat Biotechnol 2018, 36 (1), 103-112.
- 29. Lorenz, C.; Dougherty, T. J.; Lory, S., Transcriptional Responses of Pseudomonas aeruginosa to Inhibition of Lipoprotein Transport by a Small Molecule Inhibitor. J Bacteriol 2020, 202 (24).
- 30. Turnbull, L.; Toyofuku, M.; Hynen, A. L.; Kurosawa, M.; Pessi, G.; Petty, N. K.; Osvath, S. R.; Cárcamo-Oyarce, G.; Gloag, E. S.; Shimoni, R.; Omasits, U.; Ito, S.; Yap, X.; Monahan, L. G.; Cavaliere, R.; Ahrens, C. H.; Charles, I. G.; Nomura, N.; Eberl, L.; Whitchurch, C. B., Explosive cell lysis as a mechanism for the biogenesis of bacterial membrane vesicles and biofilms. Nature Communications 2016, 7 (1), 11220.
- Sun, J.; Rijpkema, S. J.; Luan, J.; Zhang, S.; Wilson, D. A., Generating biomembrane-like local curvature in polymersomes via dynamic polymer insertion. Nature Communications 2021, 12 (1), 2235.
- 32. Han, Q.; Yan, X.; Zhang, R.; Wang, G.; Zhang, Y., Juglone Inactivates Pseudomonas aeruginosa through Cell Membrane Damage, Biofilm Blockage, and Inhibition of Gene Expression. Molecules 2021, 26 (19).
- 33. Fujisawa, T.; Mori, T.; Tsuge, S.; Sato, T., Direct and chemoselective conversion of carboxylic acids into aldehydes. Tetrahedron Lett. 1983, 24 (14), 1543-1546.

- White, J. R.; Price, G. J.; Schiffers, S.; Raithby, P. R.; Plucinski, P. K.; Frost, C. G., A modular approach
 to catalytic synthesis using a dual-functional linker for Click and Suzuki coupling reactions.
 Tetrahedron Lett. 2010, 51 (30), 3913-3917.
- Berking, B. B.; Mallen-Huertas, L.; Rijpkema, S. J.; Wilson, D. A., Porous Polymersomes as Carriers for Silver Nanoparticles and Nanoclusters: Advantages of Compartmentalization for Antimicrobial Usage. *Biomacromolecules* 2023, 24 (12), 5905-5914.
- Toebes, B. J.; Cao, F.; Wilson, D. A., Spatial control over catalyst positioning on biodegradable polymeric nanomotors. *Nature Communications* 2019, 10 (1), 5308.
- 37. Forier, K.; Messiaen, A.-S.; Raemdonck, K.; Nelis, H.; De Smedt, S.; Demeester, J.; Coenye, T.; Braeckmans, K., Probing the size limit for nanomedicine penetration into Burkholderia multivorans and Pseudomonas aeruginosa biofilms. *Journal of Controlled Release* **2014**, *195*, 21-28.
- 38. Ferrero, C.; Casas, M.; Caraballo, I., Redox-Responsive Polymersomes as Smart Doxorubicin Delivery Systems. *Pharmaceutics* **2022**, *14* (8).
- 39. Lee, J. S.; Feijen, J., Polymersomes for drug delivery: Design, formation and characterization. *Journal of Controlled Release* **2012**, *161* (2), 473-483.
- Trevors, J. T., Fluorescent probes for bacterial cytoplasmic membrane research. *Journal of Biochemical and Biophysical Methods* 2003, 57 (2), 87-103.
- Marielle, B.; Sarrah, G., Assessment of bacterial membrane fluidity by flow cytometry. *Journal of Microbiological Methods* 2017, 143, 50-57.
- 42. Munguia, J.; LaRock, D. L.; Tsunemoto, H.; Olson, J.; Cornax, I.; Pogliano, J.; Nizet, V., The Mla pathway is critical for Pseudomonas aeruginosa resistance to outer membrane permeabilization and host innate immune clearance. *J Mol Med (Berl)* **2017**, *95* (10), 1127-1136.
- 43. Yero, D.; Díaz-Lobo, M.; Costenaro, L.; Conchillo-Solé, O.; Mayo, A.; Ferrer-Navarro, M.; Vilaseca, M.; Gibert, I.; Daura, X., The Pseudomonas aeruginosa substrate-binding protein Ttg2D functions as a general glycerophospholipid transporter across the periplasm. *Communications Biology* **2021**, *4* (1), 448.
- 44. Bernier, S. P.; Son, S.; Surette, M. G., The Mla Pathway Plays an Essential Role in the Intrinsic Resistance of Burkholderia cepacia Complex Species to Antimicrobials and Host Innate Components. *J Bacteriol* **2018**, *200* (18).
- Wood, L. F.; Ohman, D. E., Use of cell wall stress to characterize sigma 22 (AlgT/U) activation by regulated proteolysis and its regulon in Pseudomonas aeruginosa. *Mol Microbiol* 2009, 72 (1), 183-201.
- Hynen, A. L.; Lazenby, J. J.; Savva, G. M.; McCaughey, L. C.; Turnbull, L.; Nolan, L. M.; Whitchurch, C.
 B., Multiple holins contribute to extracellular DNA release in Pseudomonas aeruginosa biofilms. Microbiology (Reading) 2021, 167 (2).

4.6 Supplementary Introduction

Materials

All PEG polymers with different functional end groups were obtained from AV Chemistry. All other reagents were obtained from commercial sources and were used without purification unless otherwise stated. Solvents were dried by passing over activated alumina columns in a MBraun MB SPS800 under a nitrogen atmosphere and stored under argon. Reactions were carried without the need for an inert atmosphere unless stated otherwise, in which case the reaction was performed under a dry atmosphere of argon. Standard syringe techniques were applied for the transfer of dry solvents and air- or moisture sensitive reagents. Styrene was passed over alumina to remove the inhibitor 4-tert-butylcatechol. Ultrapure water was obtained from a QPOD MilliQ system. HTI molecule synthesis and analysis were conducted by S. Rijpkema and H. Amatdjais-Groenen. NMRs were conducted by S. Rijpkema.

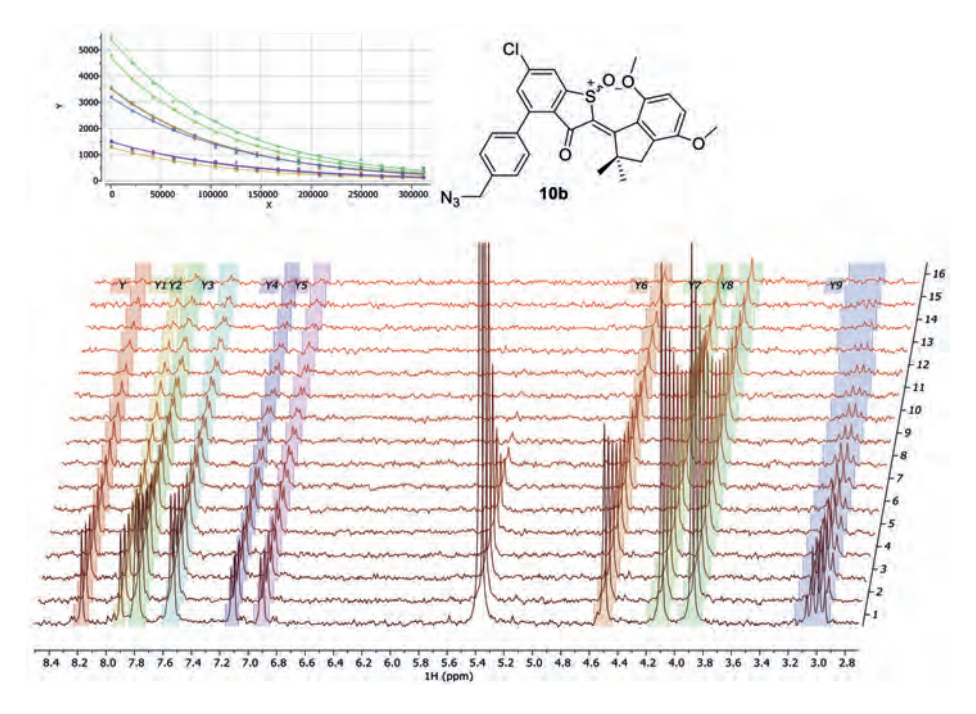


Figure S1. ¹H NMR diffusion spectra (400 MHz, 298 K) of 10b in CD₂Cl₂. Gradient strengths ranged from 5% to 95%. The absolute gradient strength was not calibrated prior to use as a relative comparison was all that was desired. D is the average diffusion coefficient of the molecule. Experiments conducted by S. Rijpkema

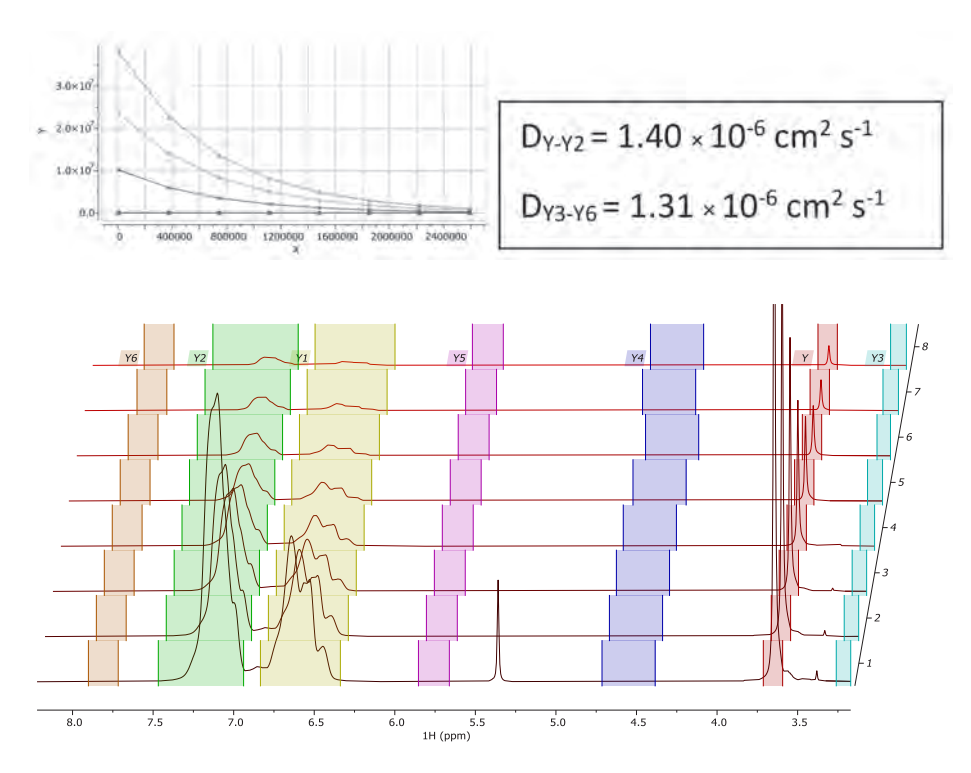


Figure S2. ¹H NMR diffusion spectra (400 MHz, 298 K) of 10b-poly(ethylene glycol)₄₄-b-polystyrene₁₇₆. Gradient strengths ranged from 5% to 95%. The absolute gradient strength was not calibrated prior to use as a relative comparison was all that was desired. $D_{\gamma\gamma}$ is the average diffusion coefficient of the polymer part of the molecule, while D_{y_3,y_6} is the diffusion constant of the **10b** part. The diffusion coefficients are in the same order of magnitude and are ~10x lower than 10b in solution, indicating successful binding. Experiments conducted by S. Rijpkema

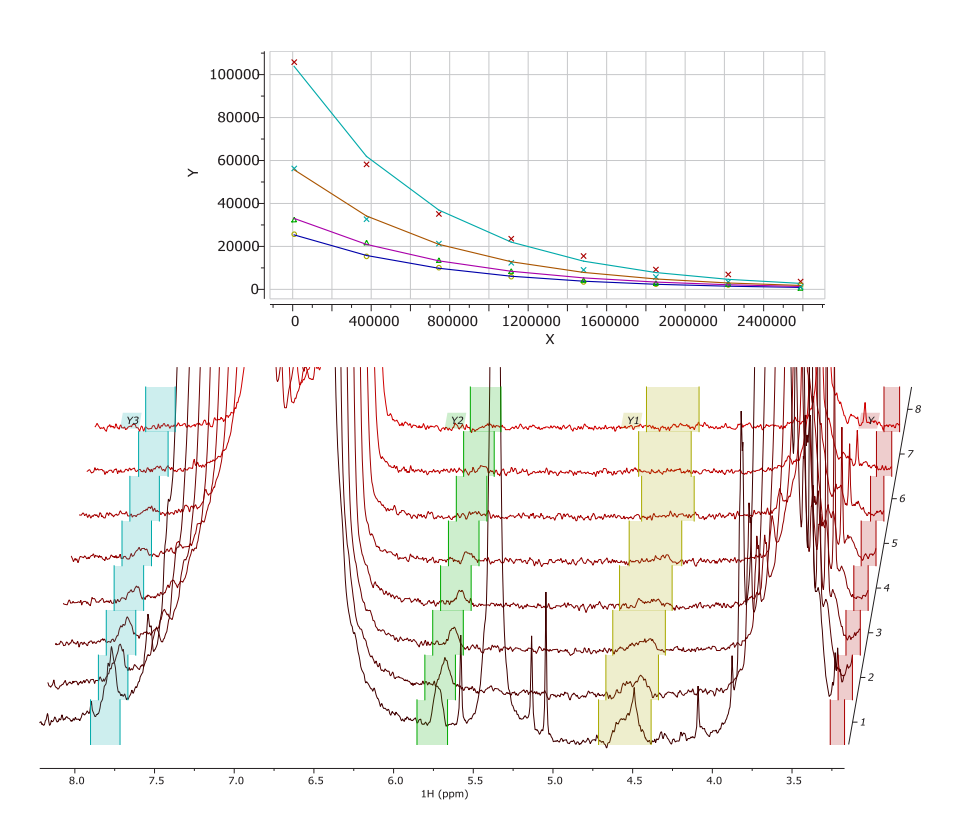


Figure S3. ¹H NMR diffusion spectra (400 MHz, 298 K) of **10b**-poly(ethylene glycol)₄₄-b-polystyrene₁₇₆. Zoomed in on signals from 10b. The absolute gradient strength was not calibrated prior to use as a relative comparison was all that was desired. Gradient strengths ranged from 5% to 95%. Experiments conducted by S. Rijpkema

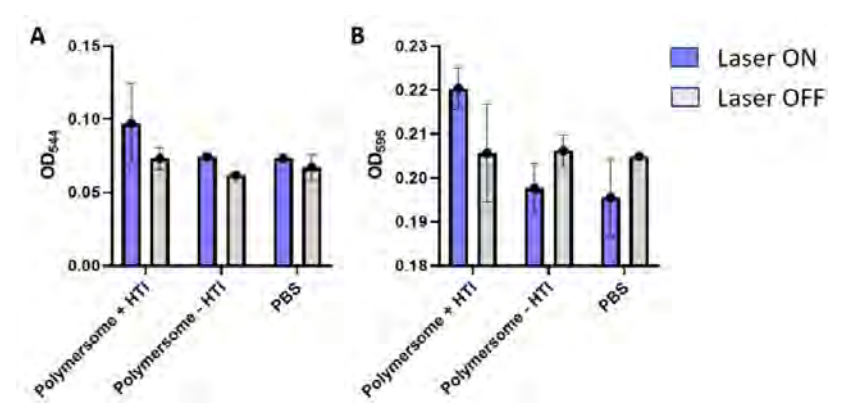


Figure S4. Polysaccharide (A) and Protein (B) content measured in supernatant after various treatments to determine release of ECM material. N = 6-8, no statistical significance could be detected which would indicate release of ECM material.

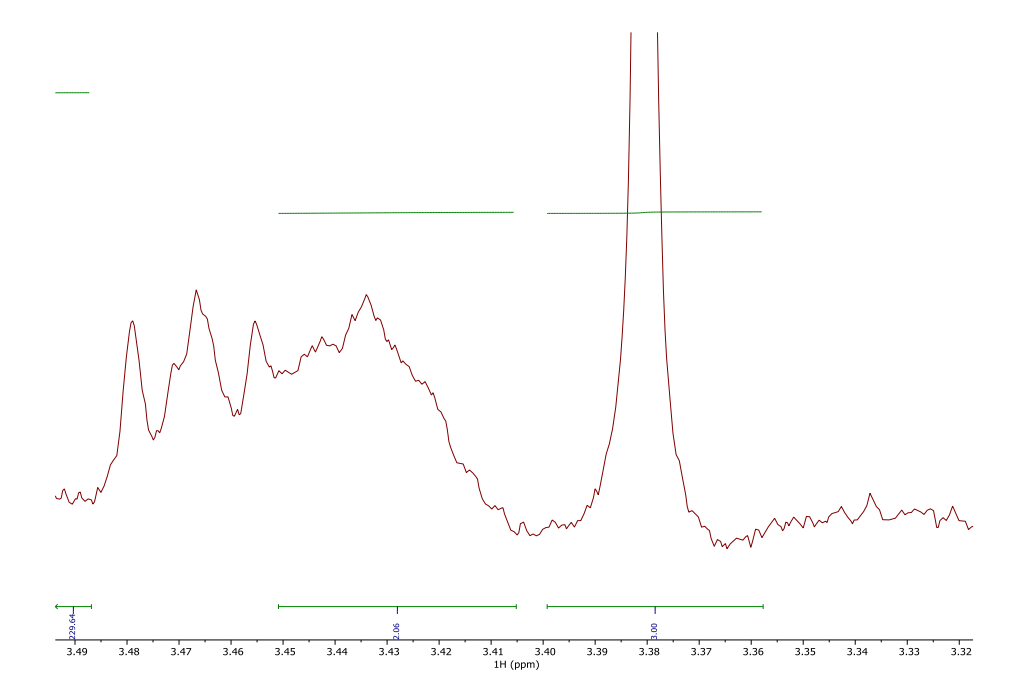


Figure S5. ¹H qNMR spectrum of a 1/3rd 10b-PEG-b-PS polymer and 2/3rd MeO-PEG-b-PS polymer (400 MHz, NS = 128, CD₂Cl₂). In DCM, MeOH is at 3.42 ppm. There is a small peak, which was compared to the MeO-PEG-PS. Based on the 6.67 mg of MeO-PEG-PS measured, we calculated 3.03*10^-7 mol MeO-PEG-PS. This leads to 2.02*10^-7 mol MeOH, which is 6.27 ug of MeOH in the sample. This means that on our total sample of 3.33 mg 10b-PEG-PS, only 0.19% MeOH is present, which is near quantitative removal. Experiments conducted by S. Rijpkema

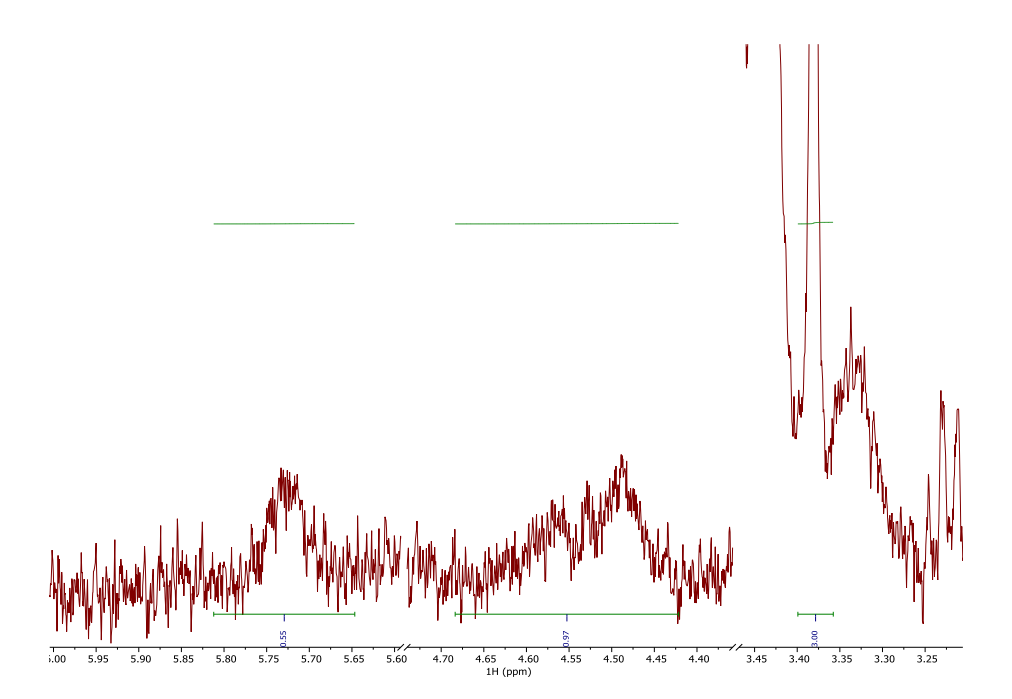


Figure S6. ¹H qNMR spectrum of a 1/3rd 10b-PEG-b-PS polymer and 2/3rd MeO-PEG-b-PS polymer (400 MHz, NS = 128, CD_2CI_2). By integrating the peak of the methoxy from the MeO-PEG-PS to 3, and then integrating 2 signals from the 10b which should be 1 and 2 protons respectively. However, since it's a 2/3 and 1/3 mix, the signals should be half, so 0.5 and 1. We observe integrals of 0.55 and 0.97, aligning with full conversion of the polymer and removal of excess 10b. Experiments conducted by S. Rijpkema

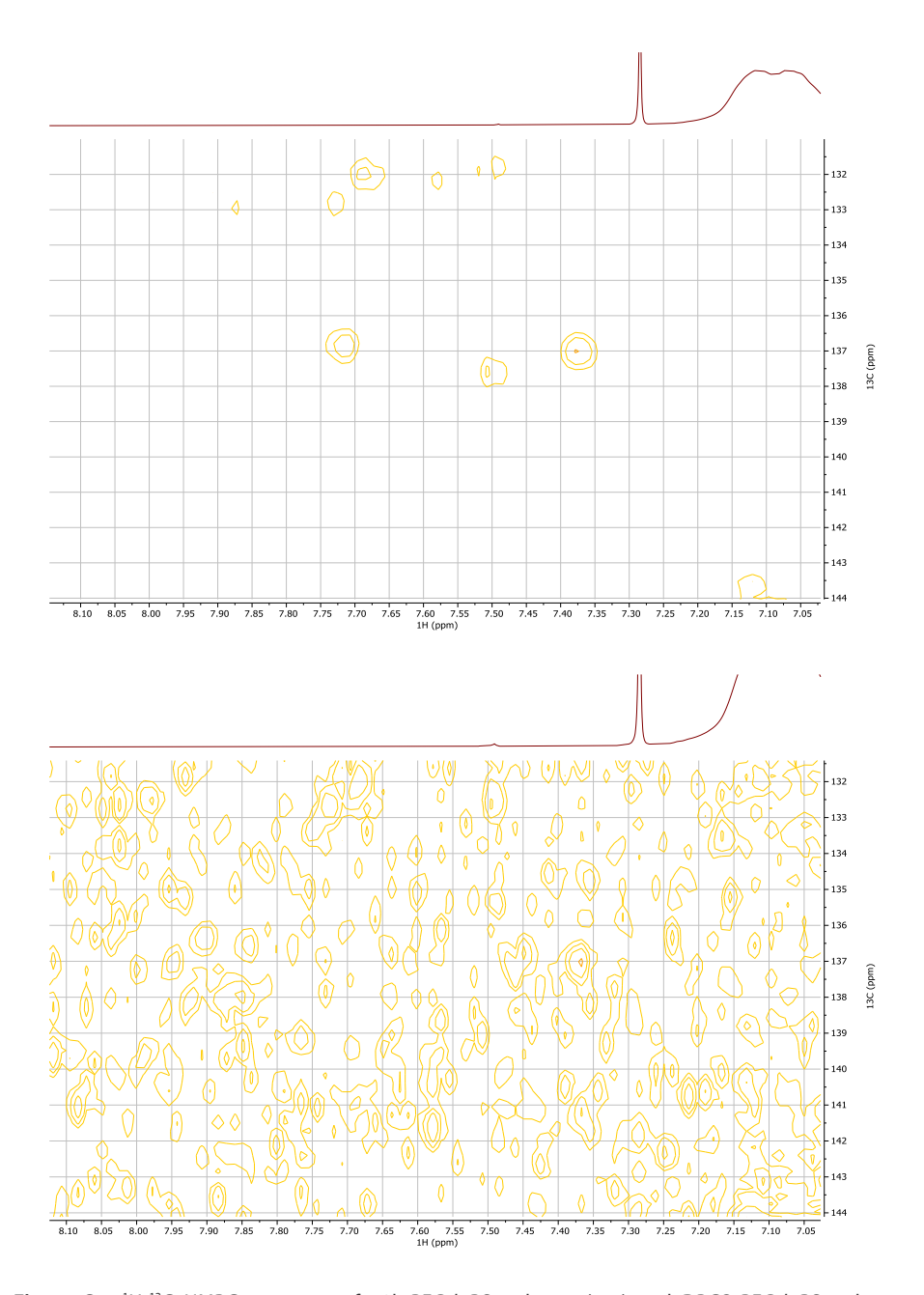
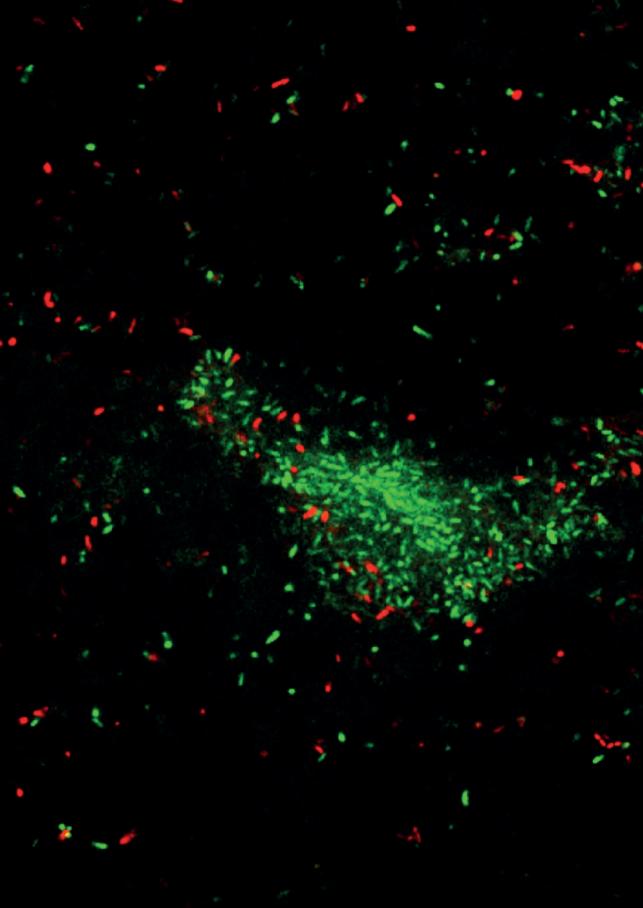


Figure 57. 1 H- 13 C HMBC spectrum of 10b-PEG-*b*-PS polymer (top) and DBCO-PEG-*b*-PS polymer (bottom). 500 MHz, NS = 192, CDCl₃, 128 increments. After performing the click reaction between DBCO of the polymer and N₃ from **10b**, the carbon peaks of the alkyne (85 ppm) shift to azide-bound alkene shifts. These are observed coupling to the aromatic signals of the DBCO at 137.0 and 137.5 ppm. Before the coupling, no signals are observed here above the noise. Experiments conducted by S. Rijpkema



Chapter 5

Quorum Sensing lights the way: Chemotactic Nanomotors target biofilms via quorumquenching mechanism

Bela B. Berking, Laura Herraíz Bentez, Bai H. E. Zhang, Amos Münch, Daniela A. Wilson

Biofilms have traditionally been viewed as uncontrolled proliferations of cells. However, recent discoveries highlight the dynamic processes and adaptability of these microbial communities. Variations in nutrient availability and host responses trigger genetic changes often mediated by quorum-sensing molecules, a class of small molecular transcription factors. Quorum sensing has emerged as a potential target for reducing biofilm viability, growth, and virulence. Despite this, leveraging this natural gradient for active targeting remains unachieved. In this study, we introduce a novel sensing system consisting of enzymatically loaded polymer vesicles capable of navigating towards *Pseudomonas aeruginosa* biofilms via quorum-sensing chemical gradients. These Acylase motors effectively swarm, infiltrate biofilms, and reduce the transcription levels of key quorum-sensing genes. The protective cavity of the stomatocytes shields the enzymes from the biofilm's harsh environment, enhancing quorum quenching efficiency. The accumulation of enzyme-loaded stomatocytes produces a highly effective local quorum quenching effect which silences and shuts down the quorum sensing apparatus on a molecular level.

5.1 Introduction

Microbial biofilms have become one of the most prominent threats to our healthcare systems, with estimated death tolls exceeding those of cancer and diabetes combined by the year 2050 1. Defined as a consortium of cells embedded in a self-produced extracellular matrix, this type of cellular organization has proven more than challenging to combat 2. High intrinsic resistance, shielding from host immune responses, and constant dispersion of new colonizer cells have made these infections a nightmare to deal with 3,4.

Quorum sensing is a means of collective coordination of various actions by the biofilm, induced and guided by various types of extracellular signaling molecules called autoinducers. Quorum sensing in biofilms has been attributed to the steering of biomass production, the dispersion of cells, and the excretion of virulence factors by these small molecules 5. P. aeruginosa has two known main quorum sensing pathways: Las and Rhl. Both of these are steered by the secretion of Acylhomoserine lactones (AHL). These molecules, while produced, will create a gradient, with concentrations up to 1000 times higher inside the center of the biofilm than the planktonic counterpart 6-8. Quorum quenching has emerged as a promising option to decrease biofilm viability and virulence, by either enzymatically cleaving signaling molecules, blocking receptors, or inactivating quorum-sensing molecule production 9. The effects this can have on the biofilm have been shown to be of great significance, shutting down the production of crucial matrix components such as rhamnolipids, pyocyanin, and other exopolysaccharides, reducing host cell pathogenicity and decreasing the production of virulence factors 10, 11. Enzymatic guorum guenching offers a versatile arsenal of enzymes capable of specifically cleaving the different types of quorum-sensing molecules with high efficiency 12. AHL Acylases are able to hydrolyze the amide bond present in AHL molecules, one of the most abundant guorum-sensing molecules present in biofilms formed by P. aeruginosa 13.

While common antibiotics often remain ineffective due to acquired resistance, dormant cells or capturing of antimicrobial compounds via the extracellular matrix, more modern nanoparticle approaches have gained attention as tools to fight these infections, with greater interest laid on systems exhibiting active motion 14, 15.

Recent research has revealed the capability of enzymes to generate motion along concentration gradients ¹⁶. Coupling enzymes to nanoparticles can yield a system capable of following a gradient, either positively or negatively, by mechanisms such as ionic diffusiophoresis or bubble propulsion ¹⁶⁻¹⁸. The use of such nanomotors to combat biofilms has been shown to be highly effective, with the addition of motion allowing for deeper penetration of the biofilm, and external steering of the nanomotors increasing the chance of particle/biofilm interaction ¹⁹⁻²¹. Zheng *et al*, who developed such a system, clearly outlined the challenges that need to be overcome: 1) Use of metal ions which can have unwanted cytotoxic effects, 2) external steering might suffer from poor tissue penetration and poor control, 3) external fuels make the system dependent on constant feeding of fuel from another external source. Taking these challenges together the ideal biofilm targeting nanomotor must rely on a biofilm-produced fuel that steers the nanomotor directly into it ¹⁹.

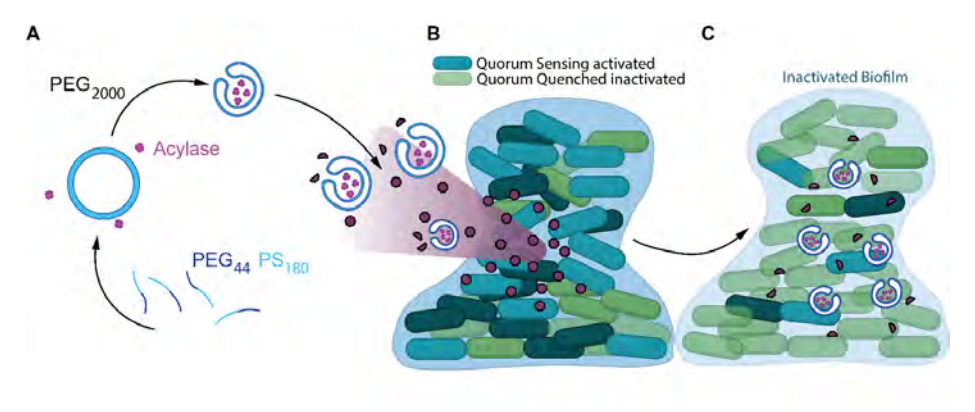


Figure 1. Schematic overview of Acylase motor fabrication by shape transformation via osmotic shock (A), concurrent active targeting of biofilms along the quorum sensing gradient (B) with the accumulation of motors and subsequent quorum quenching (C), resulting in an inactivated state of the biofilm and the decreased transcription of various genes.

To overcome the aforementioned problems, we have designed a polymer-based nanomotor that carries the quorum-quenching enzyme AHL-Acylase protected in the bowl shape of the stomatocytes (Figure 1A). This enzyme utilizes a highly abundant class of quorum-sensing molecules, namely Homoserine lactonebased molecules, to induce enhanced motion along the concentration gradient (Figure 1B). We show selective steering towards biofilm-populated areas and demonstrate biofilm swarming of the nanomotors. Additionally, the quorum quenching effect reduces the activity of the quorum sensing apparatus (Figure 1C) at a molecular level, which has been demonstrated in literature to enhance antibiotic susceptibility and reduce virulence 22, 23. We believe that this system holds significant potential for developing new, precise delivery mechanisms to combat biofilms.

5.2 Results and Discussion

Using shape transformation for the encapsulation of various cargo has been extensively studied and employed for the fabrication of metal nanoparticle or enzyme loaded stomatocytes ^{24, 25}. The process of shape transformation was monitored via DLS and TEM. Stomatocytes showed the typical size range of around 450 nm, and decreased in size compared to before their shape transformation when they are still in the polymersome conformation (Figure 2A). TEM images confirmed the bowl shaped stomatocytes with the characteristic cavity and opening (Figure 2B). Enzyme encapsulation was visualized by fluorescently labelling the AHL enzyme prior to encapsulation and using dSTORM microscopy (Figure 2C and D). The dSTORM images showed a signal that perfectly matched the measured size of Acylase-filled stomatocytes, indicating a fully filled cavity. This was further illustrated by overlaying TEM and dSTORM images, which clearly demonstrated the size match (Figure 2E). The amount of encapsulated enzyme was quantified via SDS-PAGE (Figure S1), and is comparable to previous encapsulation results using this method ²⁴.

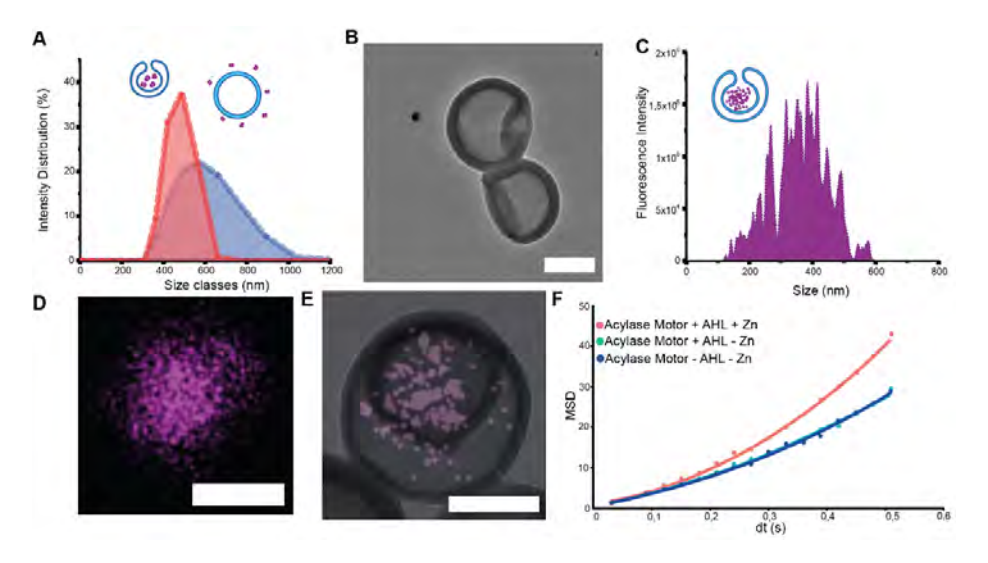
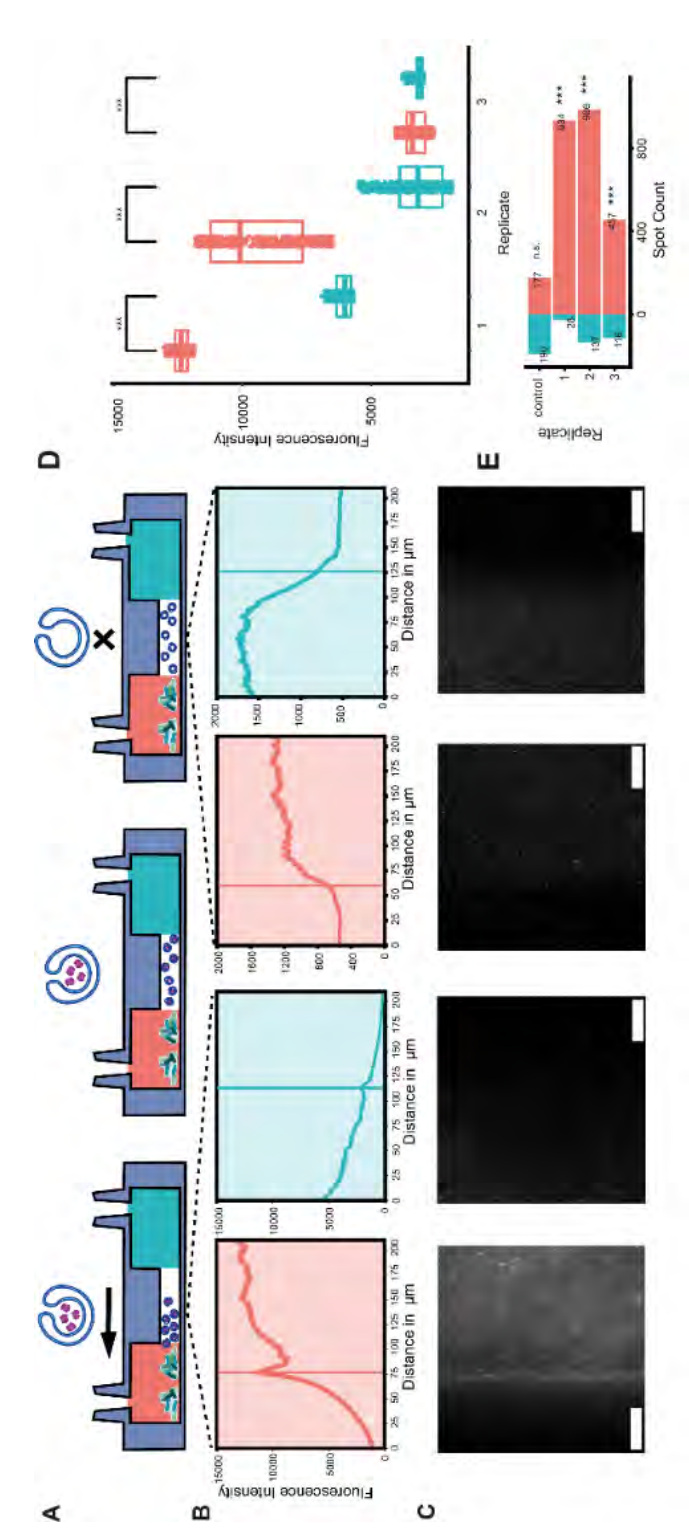


Figure 2. Particle Characterization. Size analysis (A) of Polymersomes (blue) and acylase-containing stomatocytes (red). TEM image of Acylase containing stomatocytes (B). Enzyme encapsulation analysis via dSTORM microscopy via cargo histogram (C), quantified from dSTORM images (D). Overlay of dSTORM image with TEM image to show matching of cargo size to stomatocyte size (E). Scale bars represent 200 nm. (F) Motion analysis of Acylase motors in various conditions, determined via Nanosight by calculation of the mean squared displacement (MSD) over time (dt(s)).

The systems' ability to move via enhanced diffusion was demonstrated by tracking particles and determining the MSD value. Acylase motors lacking fuel as well as the cofactor in solution did not display enhanced motion, while both components present resulted in the parabolic fitting of the curve as an indicator for overcoming the linear fitting present in Brownian motion, displayed as $\langle r^2 \rangle = 4Dt^{26}$ (Figure 2F). A desired effect of enzyme encapsulation was not only enhanced motion, but also a protective function of the enzyme towards the harsh environment of the biofilm.

We hypothesized that the observed enhanced motion of the Acylase motors could lead to a chemotactic behavior following a gradient. To assess this, we used ibidi chemotaxis slides, with one compartment housing 24-hour-old biofilms and the other compartment filled with a mock treatment (Figure 3A). Stomatocytes filled into the inner channel showed accumulation towards the biofilm side after 30 minutes (Figure 3 C and D). The significance of this observation was verified via a spot count by detecting single stomatocytes as well as a generalized quantitative analysis of the fluorescent intensity (Figure 3 D and E). When using empty stomatocytes, no chemotaxis is observed, and fluorescent intensity remains the same for both sides (Figure S2). The chemotaxis and motion of this system could be driven by factors such as substrate-product binding, in and outflow of components via the stomatocyte opening, or a gradient formed around the stomatocytes. Active motion of enzymes using such methods of propulsion have already been studied, for example Urease and RNA Polymerase ^{27, 28}. Since the product from the enzymatic reaction is neither capable of producing ionic diffusiophoresis, nor bubble propulsion, a viable explanation would be the transfer of mechanical force to the surrounding fluids. This has been previously examined as a key driving force in enzymatic motion, and could potentially cause fluid flow around the stomatocytes, propelling them forward ^{29, 30}. Yet, since motion by enzymes is still a topic to be investigated, other theories could also apply, such as non-ionic diffusiophoresis, molarity changes due to the enzymatic reaction, or even interactions of the products from the enzymatic reaction with the PEG layer of the stomatocytes.



remain evenly spread in the channel (A). (B) Plot profiles of the Acylase motor accumulating on the biofilm side (red) vs. the control side (blue) taken from the Figure 3. Chemotaxis analysis of Acylase motors in the vicinity of biofilms. Schematic overview of experimental setup using ibidi chemotaxis slides with matured biofilms on the left side (red) and a negative control made up of PBS buffer (blue). Acylase Motors will display chemotactic behaviour while empty stomatocytes corresponding confocal images below (C) (Scale bar 10 µm). (D) Averaged fluorescence intensity from all replicates, statistical significance determined via a Wilcoxon ranked sum test, p 🛭 0.001 (E) Overall spot count was determined with ImageJ, significance was determined with a Goodness of fit test against the null hypothesis that spot counts were equally distributed across biofilm and control chamber, $p \le 0.001$.

Since the Acylase motors showed chemotactic behavior, we set out to investigate its ability to move into the biofilms. As mentioned previously, quorum-sensing molecules will create gradients inside the biofilm, with higher concentrations located at the center of the biofilm. When added to established biofilms, Acylase motors (Figure 4A, red channel) can be seen accumulating around and inside the biofilm (Figure 4B, white channel), whereas empty stomatocytes have barely interacted with the biofilm, with only a few single stomatocytes being detected (Figure 4C). Going from aqueous media to a more viscous environment has been shown to increase enhanced diffusion of enzymes 31, 32. Since the biofilms' extracellular matrix provides a more viscous environment, a beneficial effect resulting in increased penetration could be expected. The successful infiltration could then result in a quorum quenching effect, which has been shown to occur with this enzyme in biofilms. The hypothesized protective nature of the enzyme by the stomatocytes, which has been observed for other enzymes in the presence of proteases, could allow for prolonged quorum-quenching effects ³³. When investigating two main players of the quorum sensing apparatus, namely rhlR and lasR, exposure to Acylase motors resulted in a significant decrease in transcription levels of both genes, while the non-protected pure enzyme had no effect (Figure 4E and F). After 24 hours, rhlR was still found to be significantly reduced compared to the control, as well as the pure enzyme, while lasR had been reduced in both treatments. These observations show a more rapid quenching effect after 4 hours, explainable by a swarming of the biofilm by the enzyme and protection from ECM-bound proteases, as well as a prolonged effect, at least for rhlR. Lasl, catalyzing the production of N-3-oxo-dodecanoyl-L-homoserine lactone, which binds to LasR to activate it, was significantly reduced after 24 hours ³⁴. Considering the impact on all these main protagonists of the quorum sensing apparatus, significant impacts on the biofilm's viability, growth, and virulence are expected to occur.

We believe that the Acylase-motor acts on a very site-specific local level, quorum quenching directly in the biofilm (Figure 4D). In contrast to this local quenching, the pure enzyme is unable to quench effectively inside the biofilm, possibly due to ECM components inhibiting or cleaving the enzyme, such as proteases, which have been known to be abundant in biofilms ³⁵. Quorum quenching therefore mainly occurs in the surrounding medium (Figure 4D). The usage of enzymes to quench these signaling networks has been extensively studied and has proven to be a valuable tool to mitigate undesirable effects of biofilms, and efficiently decrease virulence, biofilm dispersion and biofilm growth, as well as increase susceptibility to antibiotic treatments ³⁶⁻³⁸. The effect of this can be seen when evaluating a major transcription factor that controls many virulence genes, namely *pqsR* ³⁹. After 24 hours, the

Acylase motor is capable of reducing the transcription levels of pasR significantly by almost 3-fold, which the pure enzyme is unable to achieve. This highlights the effectiveness of the acylase motors in inhibiting various pathways downstream of the quorum sensing apparatus. The potential for enhancing synergistic effects by adding antimicrobial compounds to the surface of the stomatocytes remains unexplored. However, given the versatility and ease of modification this platform provides, incorporating additional cargo is a promising next step.

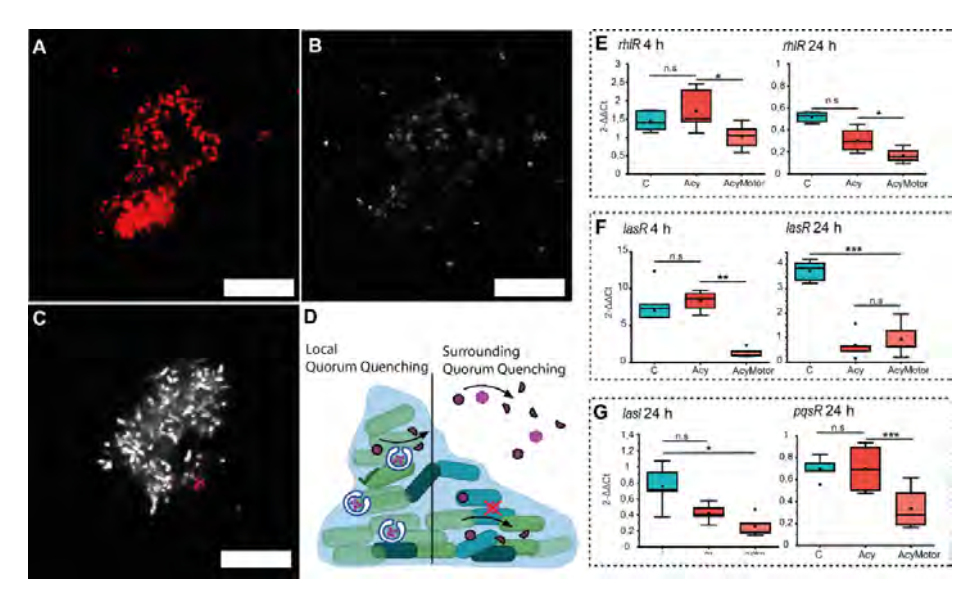


Figure 4. Swarming and quorum quenching of acylase motors. Confocal images of Acylase motors (red channel, A) swarming a biofilm (white channel, B) while empty stomatocytes barely interact with the biofilm (C), scale bars represent 12 μm. Acylase-motor swarming of biofilms induces a highly efficient, local quorum quenching effect, as opposed to pure enzyme quenching only in the surrounding solution (D). Transcription levels of quorum sensing genes rhlr (E) and lasr (F) after 4 and 24 hours of exposure to the pure enzyme (Acy) and Acylase motors (AcyMotor) compared to a control (C), 24-hour local quorum quenching reduces transcription of pasR and lasl (G). Statistical significance was assessed with one-sided t.test and one-way ANOVA p \leq 0.01.

5.3 Conclusion

Smart, autonomously sensing nanomotors represent one of the most promising solutions to many global healthcare challenges. To tackle increasingly difficult biofilm-associated issues, we have developed a biofilm-swarming nanomotor capable of sensing and accumulating within mature biofilms. The rapid swarming of these nanomotors results in a significantly faster local quorum quenching effect compared to quorum quenching enzymes in solution, which only begin to show effectiveness after 24 hours. Additionally, Acylase-motors achieved a reduction of transcript levels of the well-known virulence factor *pqsr*. We believe that such smart nanomotors, which can detect biofilm-produced gradients, will be crucial for precise, active delivery, and more efficient antimicrobial treatment.

5.4 Material and Methods

Fabrication of Acylase Motor

10 mg of poly(ethylene glycol)-b-polystyrene (PEG 44-b-PS180) were weighed and dissolved in 1 mL of a THF/Dioxane (4:1, v/v) solution that was previously prepared. Subsequently, 25 µL of Nile red fluorophore was added to the solution to enable detection for future experiments. Next, 0,5 mL of MilliQ water was added with a syringe at a rate of 1 mL/h and 30 minutes delay while the solution stirred. After that, 700 µL of this solution was transferred into a new vial. 2 mg of acylase I from porcine kidney were dissolved in 100 µL MilliQ water using the vortex mixer and were added to the 700 uL. The resulting solution was stirred for 3 min before creating the osmotic shock by adding 5 µL of (100 mg/mL) PEG 2000. The solution was stirred for 3 min and then guenched by adding 8 mL of 0,1 M phosphatebuffered saline (PBS) with a pH of 7. After this, the samples were spun down 3 times at 10000 rpm for 10 min to remove the remaining solvent and unbound enzyme. The resulting supernatants were discarded and the pellets were resuspended in 500 µL of PBS each time. The 8 tubes were then merged into one Eppendorf tube in order to concentrate, ending up with 1 ml of stomatocytes with a concentration of 10 mg/ml in PBS solution.

Size and TEM

Transmission electron microscopy (TEM) JEOL JEM-1400 FLASH was used to analyze both the size and morphology of the resulting fabricated stomatocytes. For that, 200 μ L of MilliQ water were introduced in a small vial and 5 μ L of the 1 mL solution containing stomatocytes were added. From this solution, 6 μ L were taken to do a TEM sample and let it dry overnight. The average of three size measurements of the vesicles was also analyzed by using Dynamic Light Scattering (DLS) on a Malvern Instruments Zetasizer (ZEN 1600), using a Zetasizer Software (Malvern Instruments).

Nanosight

1 mL of each solution was transferred into three different vials and 4 μ L of the nanomotors (motors fabricated with acylase I or empty stomatocytes when used

as control) were added to each vial for velocity tracking. Next, motors were injected via a syringe into the NanoSight LM10 sample chamber, where the temperature was being monitored. 5 videos of 30 seconds at a frame rate of 30 frames/s were taken, acquired, and analyzed with nanoparticle tracking software (NTA 2.2). With this technique, the speed of each nanomotor is analyzed using their average mean square displacement (MSD).

Bacterial culturing

The Overnight culture was inoculated in 6 mL of Brain Heart Infusion (BHI) by adding 5 µL of P. aeruginosa ATCC 10145, 50% Glycerol Stock and incubated overnight at 37 °C. Bacteria were then diluted to an OD of 0.01 and seeded either into ibidi chemotaxis slides, ibidi 18 well or 6 well culturing plates for 24 hours to allow biofilms to develop.

Chemotaxis

P. aeruginosa overnight culture was incubated for 3 days in the ibidi chemotaxis uslide so the biofilm is developed. The remaining planktonic cells that did not attach to the surface of the slide were removed by adding water softly inside the chambers and pipetting it out carefully. Subsequently, the chambers were filled with a solution containing 1 mM Zn²+ in PBS buffer. Next, 4 µL of the nanomotors were introduced along the middle channel. Nanomotors were observed under the Leica DMi8 widefield microscope with THUNDER fast computational clearing protocol, using LAS X software to obtain images. A drop of water was used in order to be able to visualize the nanomotors with the 63X objective lens.

Confocal

Imaging was conducted using an SP8x AOBS-WLL confocal laser scanning microscope. Syto9 was used to create a suitable working solution: for Syto9 a final concentration of c = 11.1 nM in PBS (150 mM NaCl, 100 mM NaPO4mM, pH 7.4). Biofilms were stained for 10 minutes and washed three times with PBS (150 mM NaCl, 100 mM NaHPO,, pH 7.4. Lasers were set at λ ex = 470 nm, λ em = 500-520 nm and $\lambda ex = 560$ nm, $\lambda em = 620-670$ nm. Images were later analysed with Imaris.

dSTORM Superresolution Microscopy

To show Acylase presence in the cavity of stomatocytes, dSTORM superresolution microscopy was conducted on a ONI nanoimager. Acylase was labelled with AlexaFluor 647-NH, for 16 h for binding, and then encapsulated as previously described. Channel Slides carrying Avidin surface coating were provided by ONI. Stomatocytes were incubated with an anti-PEG antibody. Stomatocytes were then gently flown through the channel to be captured on the surface. Unbound particles were washed away before the dSTORM buffer was added to the channel. Samples were imaged using a 647-laser utilizing 3000 frames acquisition.

RNA Extraction

The total RNA was extracted from the biofilms using the RNeasy Kit of QIAGEN. The media was removed from the biofilm and washed once with 1x PBS. Before scraping the biofilm of the wells, 1 volume of 1x PBS and 2 volumes of RNA protect bacteria reagent were added to each well. The samples were then scraped and transferred into bead-beating tubes and the cells were lysed by 0.1mm Zirconia/silica beads in the BeadBug 6 bead homogenizer for 3 cycles of 30 seconds on and off at 4000rpm. Following the Ivsis, the Ivsate was transferred to the RNeasy Mini Spin Column and placed in 2 mL collection tubes. The columns were centrifuged at ≥8000x g for 15 sec. and the flow-through was discarded and the collection tube was reused. This step was repeated until all lysate was processed. Then to wash the spin column membrane 700µl Buffer RW1 was added and centrifuged at ≥8000x g for 15 sec. The flow-through was discarded and the columns were placed in new collection tubes. Subsequently, 500µl Buffer RPE was added and centrifuged at ≥8000x g for 15 sec. This step was repeated once more with 500µl Buffer RPE and centrifuged at ≥8000x g for 2 min. to ensure the removal of ethanol. The spin columns were then transferred to new 1.5 ml collection tubes, and 30-50ul of Rnase-free water was added directly to the membrane. The columns were then centrifuged at ≥8000x g for 1 min. to elute the RNA. The concentration and purity of the RNA were determined by the Nanodrop 1000™ spectrophotometer. The absorbance ratio A260/280 served as a measure of protein contamination, while the ratio A260/230 served as a measure of contamination of polysaccharides, phenols and salts. Additionally, an Agarose Gel electrophoresis was conducted. Only samples with values in the accepted range were further used for cDNA synthesis.

cDNA Synthesis

For the cDNA synthesis, the RNA was treated with DNase to remove genomic DNA. This was done using the DNase I Amplification Grade by Invitrogen[™]. The following was added to an RNase-free PCR-strips on ice: 500 ng total RNA, 1µI 10X DNase I Reaction Buffer, 1µL DNase I Amplification Grade (1U/µI) and DEPC-treated water to 10µL. Then the PCR strips were incubated for 15 min. at room temperature. Then 1µI of 25 mM EDTA was added to inactivate the DNase I. Lastly, the RNA samples were incubated for 10 min. at 65°C. cDNA was synthesized using the SuperScript[™] II Reverse Transcriptase by Invitrogen[™]. To each DNase-treated RNA 9µI of the following mix were added: 1µI random primers (250 ng/µI), 1µI 10mM dNTP's,

4μl 5X 1st Strand Buffer, 1μl 0.1M DTT, 1μl RNaseOUT™ (10 U/μl), 0.5μl Superscript II (200 U/μl) and 0.5μl DEPC-treated water. Mixed and incubated for 10 min. at 25°C followed by another incubation of 50 min. at 42°C and the reaction was inactivated by heating it for 15 min. at 70°C. After the cDNA synthesis, the cDNA was purified using the QIAquick PCR Purification Kit of QIAGEN. This was done according to the manufacturer's instructions. Following purification, the cDNA concentration was measured with the Qubit[™] 4 Fluorometer using the 1X High Sensitivity dsDNA assay.

aRT-PCR

gRT-PCR was performed using the iQ SYBR Green Supermix by Bio-Rad. Each reaction contains 10μL iQ SYBR Green Supermix, 2μL (10μM) forward primer, 2μL (10µM) reverse primer, 1ng cDNA and DEPC-treated water to a final volume of 20µL. The primers that were used are listed in Table x. The gRT-PCR was performed in a Bio-Rad C1000 Touch Thermal Cycler using the following protocol: 95°C for 30 seconds, 95°C for 30 seconds, 60°C for 10 seconds and 72°C for 20 seconds (repeat 39X). Followed by a melt-curve analysis from 58°C to 95°C at a 0.5°C/cycle melt rate. The relative gene expression was calculated using the 2- $\Delta\Delta$ CT method, where all Ct values were normalized to the housekeeping genes gyrA and recA.

- (1) de Kraker, M. E.; Stewardson, A. J.; Harbarth, S. Will 10 Million People Die a Year due to Antimicrobial Resistance by 2050? PLoS Med 2016, 13 (11), e1002184. DOI: 10.1371/journal. pmed.1002184 From NLM.
- (2) Ali, A.; Zahra, A.; Kamthan, M.; Husain, F. M.; Albalawi, T.; Zubair, M.; Alatawy, R.; Abid, M.; Noorani, M. S. Microbial Biofilms: Applications, Clinical Consequences, and Alternative Therapies. *Microorganisms* 2023, *11* (8). DOI: 10.3390/microorganisms11081934 From NLM.
- (3) Ciofu, O.; Moser, C.; Jensen, P. Ø.; Høiby, N. Tolerance and resistance of microbial biofilms. *Nature Reviews Microbiology* **2022**, *20* (10), 621-635. DOI: 10.1038/s41579-022-00682-4.
- (4) Jones, C.; Wozniak, D. Psl produced by mucoid Pseudomonas aeruginosa contributes to the establishment of biofilms and immune evasion. mBio 8: e00864-17. 2017.
- (5) Mukherjee, S.; Bassler, B. L. Bacterial quorum sensing in complex and dynamically changing environments. *Nature Reviews Microbiology* 2019, 17 (6), 371-382. DOI: 10.1038/s41579-019-0186-5.
- (6) Flemming, H.-C.; Wingender, J.; Szewzyk, U.; Steinberg, P.; Rice, S. A.; Kjelleberg, S. Biofilms: an emergent form of bacterial life. *Nature Reviews Microbiology* 2016, 14 (9), 563-575. DOI: 10.1038/nrmicro.2016.94.
- (7) Charlton, T. S.; De Nys, R.; Netting, A.; Kumar, N.; Hentzer, M.; Givskov, M.; Kjelleberg, S. A novel and sensitive method for the quantification of N-3-oxoacyl homoserine lactones using gas chromatography-mass spectrometry: application to a model bacterial biofilm. *Environmental Microbiology* 2000, 2 (5), 530-541. DOI: https://doi.org/10.1046/j.1462-2920.2000.00136.x.
- (8) De Kievit, T. R.; Gillis, R.; Marx, S.; Brown, C.; Iglewski, B. H. Quorum-sensing genes in Pseudomonas aeruginosa biofilms: their role and expression patterns. *Appl Environ Microbiol* **2001**, *67* (4), 1865-1873. DOI: 10.1128/aem.67.4.1865-1873.2001 From NLM.
- (9) Sikdar, R.; Elias, M. Quorum quenching enzymes and their effects on virulence, biofilm, and microbiomes: a review of recent advances. Expert Rev Anti Infect Ther 2020, 18 (12), 1221-1233. DOI: 10.1080/14787210.2020.1794815 From NLM.
- (10) Rajesh, P. S.; Rai, V. R. Inhibition of QS-regulated virulence factors in Pseudomonas aeruginosa PAO1 and Pectobacterium carotovorum by AHL-lactonase of endophytic bacterium Bacillus cereus VT96. Biocatalysis and Agricultural Biotechnology 2016, 7, 154-163. DOI: https://doi. org/10.1016/j.bcab.2016.06.003.
- (11) Rather, M. A.; Saha, D.; Bhuyan, S.; Jha, A. N.; Mandal, M. Quorum Quenching: A Drug Discovery Approach Against Pseudomonas aeruginosa. *Microbiological Research* **2022**, *264*, 127173. DOI: https://doi.org/10.1016/j.micres.2022.127173.
- (12) Wang, D.; Cui, F.; Ren, L.; Li, J.; Li, T. Quorum-quenching enzymes: Promising bioresources and their opportunities and challenges as alternative bacteriostatic agents in food industry. *Compr Rev Food Sci Food Saf* **2023**, *22* (2), 1104-1127. DOI: 10.1111/1541-4337.13104 From NLM.
- (13) Leadbetter, J. R.; Greenberg, E. P. Metabolism of acyl-homoserine lactone quorum-sensing signals by Variovorax paradoxus. *Journal of bacteriology* **2000**, *182* (24), 6921-6926.
- (14) Zhang, Z.; Wang, L.; Chan, T. K. F.; Chen, Z.; Ip, M.; Chan, P. K. S.; Sung, J. J. Y.; Zhang, L. Micro-/ Nanorobots in Antimicrobial Applications: Recent Progress, Challenges, and Opportunities. Advanced Healthcare Materials 2022, 11 (6), 2101991. DOI: https://doi.org/10.1002/ adhm.202101991.

- Dutt, Y.; Dhiman, R.; Singh, T.; Vibhuti, A.; Gupta, A.; Pandey, R. P.; Raj, V. S.; Chang, C. M.; Priyadarshini, A. The Association between Biofilm Formation and Antimicrobial Resistance with Possible Ingenious Bio-Remedial Approaches. Antibiotics (Basel) 2022, 11 (7). DOI: 10.3390/ antibiotics11070930 From NLM.
- Wang, L.; Hao, X.; Gao, Z.; Yang, Z.; Long, Y.; Luo, M.; Guan, J. Artificial nanomotors: Fabrication, locomotion characterization, motion manipulation, and biomedical applications. Interdisciplinary Materials 2022, 1 (2), 256-280. DOI: https://doi.org/10.1002/idm2.12021.
- Chen, H.; Li, T.; Liu, Z.; Tang, S.; Tong, J.; Tao, Y.; Zhao, Z.; Li, N.; Mao, C.; Shen, J.; et al. A nitricoxide driven chemotactic nanomotor for enhanced immunotherapy of glioblastoma. Nature Communications 2023, 14 (1), 941. DOI: 10.1038/s41467-022-35709-0.
- Ye, Y.; Tong, F.; Wang, S.; Jiang, J.; Gao, J.; Liu, L.; Liu, K.; Wang, F.; Wang, Z.; Ou, J.; et al. Apoptotic Tumor DNA Activated Nanomotor Chemotaxis. Nano Letters 2021, 21 (19), 8086-8094. DOI: 10.1021/acs.nanolett.1c02441.
- Zheng, J.; Wang, W.; Gao, X.; Zhao, S.; Chen, W.; Li, J.; Liu, Y.-N. Cascade Catalytically Released Nitric Oxide-Driven Nanomotor with Enhanced Penetration for Antibiofilm. Small 2022, 18 (52), 2205252. DOI: https://doi.org/10.1002/smll.202205252.
- Ussia, M.; Urso, M.; Dolezelikova, K.; Michalkova, H.; Adam, V.; Pumera, M. Active Light-Powered (20)Antibiofilm ZnO Micromotors with Chemically Programmable Properties. Advanced Functional Materials 2021, 31 (27), 2101178.
- Yuan, K.; Jurado-Sánchez, B.; Escarpa, A. Dual-Propelled Lanbiotic Based Janus Micromotors for Selective Inactivation of Bacterial Biofilms. Angewandte Chemie International Edition 2021, 60 (9), 4915-4924.
- Zhao, X.; Yu, Z.; Ding, T. Quorum-Sensing Regulation of Antimicrobial Resistance in Bacteria. (22)Microorganisms 2020, 8 (3). DOI: 10.3390/microorganisms8030425 From NLM.
- Zhao, X.; Zhong, J.; Wei, C.; Lin, C.-W.; Ding, T. Current perspectives on viable but non-culturable (23)state in foodborne pathogens. Frontiers in Microbiology 2017, 8, 237514.
- Sun, J.; Mathesh, M.; Li, W.; Wilson, D. A. Enzyme-Powered Nanomotors with Controlled Size for Biomedical Applications. ACS Nano 2019, 13 (9), 10191-10200. DOI: 10.1021/acsnano.9b03358 From NLM.
- Wilson, D. A.; Nolte, R. J. M.; van Hest, J. C. M. Autonomous movement of platinum-loaded stomatocytes. Nature Chemistry 2012, 4 (4), 268-274. DOI: 10.1038/nchem.1281.
- Howse, J. R.; Jones, R. A.; Ryan, A. J.; Gough, T.; Vafabakhsh, R.; Golestanian, R. Self-motile colloidal particles: from directed propulsion to random walk. Physical review letters 2007, 99 (4), 048102.
- (27) Yu, H.; Jo, K.; Kounovsky, K. L.; Pablo, J. J. d.; Schwartz, D. C. Molecular Propulsion: Chemical Sensing and Chemotaxis of DNA Driven by RNA Polymerase. Journal of the American Chemical Society 2009, 131 (16), 5722-5723. DOI: 10.1021/ja900372m.
- Zhao, X.; Gentile, K.; Mohajerani, F.; Sen, A. Powering Motion with Enzymes. Accounts of Chemical (28)Research 2018, 51 (10), 2373-2381. DOI: 10.1021/acs.accounts.8b00286.
- Zhao, X.; Dey, K. K.; Jeganathan, S.; Butler, P. J.; Córdova-Figueroa, U. M.; Sen, A. Enhanced Diffusion of Passive Tracers in Active Enzyme Solutions. Nano Letters 2017, 17 (8), 4807-4812. DOI: 10.1021/acs.nanolett.7b01618.

- Lin, X.; He, Y. Study Enhanced Enzyme Diffusion with High-Speed Single Nanoparticle Rotational and Translational Tracking. Analytical Chemistry 2022, 94 (20), 7158-7163. DOI: 10.1021/acs. analchem.2c00363.
- (31) Xu, M.; Ross, J. L.; Valdez, L.; Sen, A. Direct Single Molecule Imaging of Enhanced Enzyme Diffusion. Physical Review Letters 2019, 123 (12), 128101. DOI: 10.1103/PhysRevLett.123.128101.
- Pressé, S. A thermodynamic perspective on enhanced enzyme diffusion. Proceedings of the National Academy of Sciences 2020, 117 (51), 32189-32191. DOI: doi:10.1073/pnas.2022207117.
- (33) Abdelmohsen, L. K. E. A.; Nijemeisland, M.; Pawar, G. M.; Janssen, G.-J. A.; Nolte, R. J. M.; van Hest, J. C. M.; Wilson, D. A. Dynamic Loading and Unloading of Proteins in Polymeric Stomatocytes: Formation of an Enzyme-Loaded Supramolecular Nanomotor. ACS Nano 2016, 10 (2), 2652-2660. DOI: 10.1021/acsnano.5b07689.
- (34) O'Reilly, M.; Dong, S.; Rossi, F.; Karlen, K.; Kumar, R.; Nair, S.; Blackwell, H. Structural and Biochemical Studies of Non-native Agonists of the LasR Quorum-Sensing Receptor Reveal an L3 Loop" Out" Conformation for LasR. Cell Chem Biol 25: 1128-1139. e3. 2018.
- Wang, S.; Zhao, Y.; Breslawec, A. P.; Liang, T.; Deng, Z.; Kuperman, L. L.; Yu, Q. Strategy to combat biofilms: a focus on biofilm dispersal enzymes. npj Biofilms and Microbiomes 2023, 9 (1), 63. DOI: 10.1038/s41522-023-00427-y.
- Khatun, M. A.; Hoque, M. A.; Koffas, M.; Feng, Y. Reducing the virulence of Pseudomonas aeruginosa by using multiple quorum-quenching enzymes. J Ind Microbiol Biotechnol 2023, 50 (1). DOI: 10.1093/jimb/kuad028 From NLM.
- (37)Aslanli, A.; Domnin, M.; Stepanov, N.; Efremenko, E. Synergistic Antimicrobial Action of Lactoferrin-Derived Peptides and Quorum Quenching Enzymes. Int J Mol Sci 2023, 24 (4). DOI: 10.3390/ijms24043566 From NLM.
- (38)Zhong, S.; He, S. Quorum Sensing Inhibition or Quenching in Acinetobacter baumannii: The Novel Therapeutic Strategies for New Drug Development. Front Microbiol 2021, 12, 558003. DOI: 10.3389/fmicb.2021.558003 From NLM.
- Maura, D.; Hazan, R.; Kitao, T.; Ballok, A. E.; Rahme, L. G. Evidence for Direct Control of Virulence and Defense Gene Circuits by the Pseudomonas aeruginosa Quorum Sensing Regulator, MvfR. Scientific Reports **2016**, 6 (1), 34083. DOI: 10.1038/srep34083.

5.6 Supporting Information

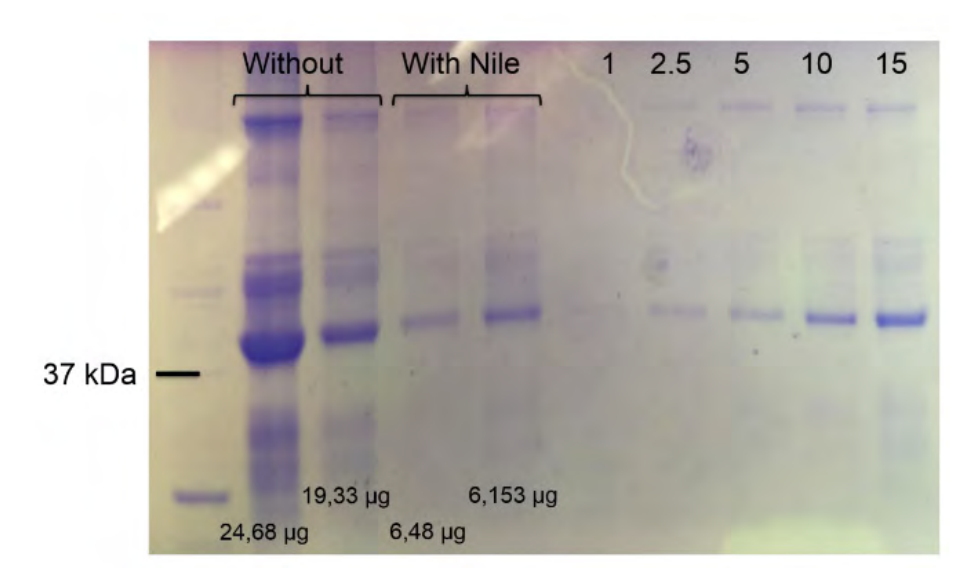
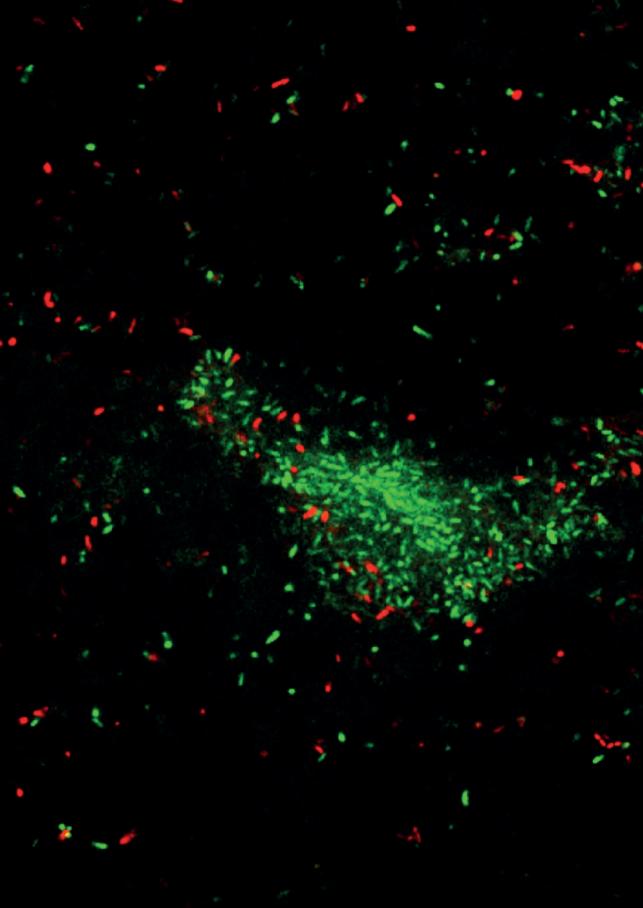


Figure S1. Encapsulation efficiency estimated via SDS-PAGE. Enzyme monomer size has been shown to be located at 42 kDa. Encapsulation efficiency was calculated using ImageJ with the corresponding reference standards ranging from 1-15 µg in the right lanes.



Chapter 6

Summary and Perspectives

6.1 Summary

Polymer-based systems offer a versatile platform to combat pathogenic biofilms. With ease, one can manipulate functional handles on polymersomes, cargo inside of stomatocytes, or the building blocks of polymer surface coatings to achieve a very specific task.

This thesis aimed at expanding the possibilities of such systems, by adding, modifying, and tweaking existing systems to fit their distinctive role in besieging the biofilm.

In **Chapter 1**, we explored the many mechanisms and details of a bacterial biofilm and how these influence and challenge modern therapeutics in overcoming them. We then gave an overview of strategies that are being explored to combat such biofilms, by means of surface coatings quorum quenching, and nanoparticle delivery systems, either passively diffusing or actively moving into the biofilm.

Chapter 2 aimed at characterizing and testing novel ylide-based zwitterionic polymers to prevent bacterial adhesion and subsequent biofilm formation. We found that ylides have strong antifouling properties and offer a hostile environment for bacteria to grow on. Comparing it to the golden standard of antifouling coatings, namely PEG, the hostile environment created by the ylide coating offered distinct advantages to PEG. By modifying the components of the ylide, such as exchanging the styrene backbone or the sulfur for a phosphorus we could exclude any side effects and demonstrate high cytocompatibility to mammalian cells. The effects on bacteria were investigated on a molecular level, membrane damage and subsequent reduction of virulence were key factors accompanying the antifouling mechanisms by the induced hydration layer.

Moving from surface coatings we set out to explore nanoparticle systems, based on previously reported polymeric self-assembled particles.

In **Chapter 3** we created the Swiss cheese of particles: a porous polymersome. By synthesizing silver nanoparticles (AgNPs) and clusters (AgNCs) inside of the compartment, we achieved a longer-lasting silver ion-releasing reservoir. FFF-MALS studies confirmed the successful assembly of silver clusters and nanoparticles inside the compartment, whose releasing properties were then studied using ICP-MS. Exposing biofilms to these porous polymersomes containing AgNPs and AgNCs led to an increase in bacterial mortality in the middle and bottom layers, which the

controls failed to successfully eradicate. AgNCs then proved to be cytocompatible to mammalian cells, offering a promising platform for combating biofilms.

Chapter 4 makes use of light-activated molecular rotors to battle biofilms. By attaching hemithioindigo rotors to the surface of polymersomes, we created a nanoscale drilling platform, which upon light activation infiltrated biofilms and efficiently eradicated them. We found that the membrane undergoes full permeabilization, but we were not convinced this is the only mode of action. By genetic analysis, we uncovered a self-lysis mechanism that is activated upon interaction with the HTI-decorated polymersomes. This self-lysis response is reminiscent of a phage attack, mediated by a lysin protein. The increase in quorum sensing sediments our hypothesis, that this self-lysis response is carried through the biofilm and causes significant self-lysis in the biofilm, even without the HTIpolymersomes direct contact.

In Chapter 5, we challenged the quorum sensing apparatus which biofilms rely on to communicate and coordinate. By encapsulating the guorum guenching enzyme Acylase inside of shape-transformed polymersomes, we generated an Acylase stomatocyte similar to previous enzymatic nanomotors. When exposed to the enzyme's substrate, enhanced motion was observed, which translated to chemotactic behavior when put into a more complex environment with biofilms present. The Acylase motors swarmed the biofilms and subsequently shut down the main protagonists of the quorum sensing network, which we evaluated by genetic analysis. Comparing this to its non-encapsulated counterpart we found that Acylase motors exhibited a more effective local quorum quenching effect which was prolonged, most likely due to the protective benefits the stomatocytes have.

6.2 Perspective

Although we believe that such systems hold great potential, it is always important to be reminded of the challenges these systems must overcome before they can be fully implemented in aiding the battle against biofilms.

The nanoparticle systems we utilized in chapters 3, 4, and 5 are all based on Poly(ethylene glycol)-Polystyrene as a building block. Opting for biodegradable options such as PEG-PLA would help with further in vivo applications ¹. For our research, we have purposely avoided such polymers, since potential accelerated degradation in the biofilm environment would have made studying the fundamental aspects of our systems more difficult. The next step would be to swap PEG-PS for a biodegradable polymer, which would allow for degradation and subsequent clearance. Such building blocks are readily available and have been implemented in comparable systems ².

Although PEG is widely used as a beneficial surface for nanoparticles due to its non-fouling properties, downsides such as adverse immunogenic effects and instability have been reported ³. In **Chapter 2**, we explored a new zwitterionic polymer based on ylides, which could be a suitable alternative. We have proven its effectiveness in repelling serum proteins as well as remaining cytocompatible. Using the investigated zwitterionic polymer as an outer coating for nanoparticles could reduce potential antibody production which is observed in PEG while having excellent stealth capabilities, increasing circulation times.

The silver ion release system we fabricated in **Chapter 3** has proven to be highly efficient in eradicating biofilms, while the Nanocluster variant even stayed cytocompatible. The porous structure of the polymersomes could be utilized to exchange the releasing compound, finetuning the properties to fit other needs. One example would be to use the different microenvironments inside the biofilm to have a more controlled release mechanism. The higher acidity for example could be a great stimulus to control the release, something we hypothesized might accelerate the decomposition of used silver particles but did not experimentally verify.

Chapter 5 explored a motile self-propelled nanomotor, which could navigate and swarm biofilms. The great challenge in a more complex environment is motility competing with liquid flow. Blood flow is multitudes higher than the speeds of most nanomotors, and many examples lack studying of their system in a comparable flow environment ⁴. We believe that it is paramount to further challenge the system in a high flow environment to ensure effectiveness when moving into in-vivo settings.

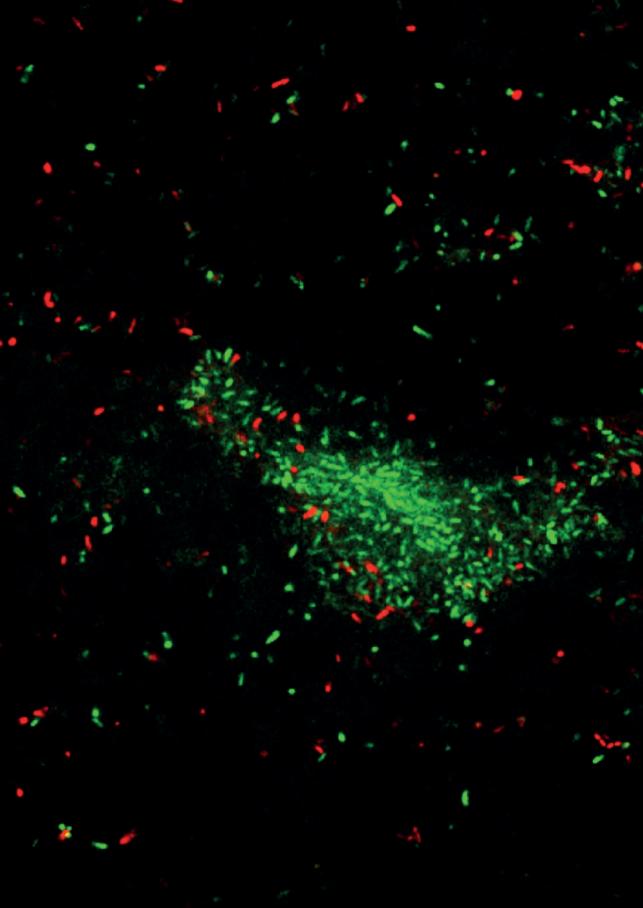
As mentioned previously, in-vivo applications of such nanoparticle systems must take into account how to dispose of nanoparticles once their job is achieved. The clearance capabilities of the human body are highly size-dependent ⁵. Renal clearance has a maximum size of 6 nm for globular proteins ⁶, while slower hepatobiliary clearance was shown to be efficient up to sizes of around 100 nm ^{7,8}. Polymersomes and stomatocytes of similar composition have been scaled down to around 150 nm, which would still make clearance difficult ⁹. Additionally, polymersomes self-assembled are highly stable and will not break down under invivo conditions, which again brings us back to using biodegradable polymers.

One goal was to increase the complexity of polymersome and stomatocyte systems by adding more functionalities to them. A final goal would be to combine some of the systems we explored to create a multifaceted system capable of many different angles of attack. Utilizing the ylides as an outer surface coating of stomatocytes, with acylase encapsulated in the center to create a motile system, and the HTI rotor complimenting the system for enhanced eradication capabilities would result in a highly complex system able to besiege the biofilm

To use the many gradients in a biofilm against it, it is crucial to understanding them. Nanoparticle sensory systems have become a great tool in unraveling the dynamic processes which occur in the biofilm such as fluorescent probes which could track the pH gradients occurring in biofilms under various conditions ¹⁰. The systems used in this thesis show high modularity and potential to become easily modified, which is a crucial aspect for a multisensory system. By fabricating a system which can detect multiple changes in real time, such as pH, aerobic conditions and temperature, novel systems tailored to respond to such stimuli can be designed with even higher specificity and efficiency.

6.3 References

- (1) Tekale, S. U.; Rottenberg, Y.; Ingle, R. D.; Domb, A. J.; Pawar, R. P. Recent developments in biodegradable block copolymers. Polymers for Advanced Technologies 2021, 32 (10), 3877-3899. DOI: https://doi.org/10.1002/pat.5460.
- (2) Toebes, B. J.; Cao, F.; Wilson, D. A. Spatial control over catalyst positioning on biodegradable polymeric nanomotors. Nature Communications 2019, 10 (1), 5308. DOI: 10.1038/s41467-019-13288-x.
- (3) Ibrahim, M.; Ramadan, E.; Elsadek, N. E.; Emam, S. E.; Shimizu, T.; Ando, H.; Ishima, Y.; Elgarhy, O. H.; Sarhan, H. A.; Hussein, A. K.; et al. Polyethylene glycol (PEG): The nature, immunogenicity, and role in the hypersensitivity of PEGylated products. J Control Release 2022, 351, 215-230. DOI: 10.1016/j.jconrel.2022.09.031 From NLM.
- (4) Gao, C.; Wang, Y.; Ye, Z.; Lin, Z.; Ma, X.; He, Q. Biomedical Micro-/Nanomotors: From Overcoming Biological Barriers to In Vivo Imaging. Advanced Materials 2021, 33 (6), 2000512. DOI: https://doi. org/10.1002/adma.202000512.
- (5) Xu, M.; Qi, Y.; Liu, G.; Song, Y.; Jiang, X.; Du, B. Size-Dependent In Vivo Transport of Nanoparticles: Implications for Delivery, Targeting, and Clearance. ACS Nano 2023, 17 (21), 20825-20849. DOI: 10.1021/acsnano.3c05853.
- (6) Choi, H. S.; Liu, W.; Misra, P.; Tanaka, E.; Zimmer, J. P.; Itty Ipe, B.; Bawendi, M. G.; Frangioni, J. V. Renal clearance of quantum dots. Nat Biotechnol 2007, 25 (10), 1165-1170. DOI: 10.1038/ nbt1340 From NLM.
- Souris, J. S.; Lee, C. H.; Cheng, S. H.; Chen, C. T.; Yang, C. S.; Ho, J. A.; Mou, C. Y.; Lo, L. W. Surface (7) charge-mediated rapid hepatobiliary excretion of mesoporous silica nanoparticles. Biomaterials 2010, 31 (21), 5564-5574. DOI: 10.1016/j.biomaterials.2010.03.048 From NLM.
- Zhang, Y.-N.; Poon, W.; Tavares, A. J.; McGilvray, I. D.; Chan, W. C. W. Nanoparticle-liver (8) interactions: Cellular uptake and hepatobiliary elimination. Journal of Controlled Release 2016, 240, 332-348. DOI: https://doi.org/10.1016/j.jconrel.2016.01.020.
- Sun, J.; Mathesh, M.; Li, W.; Wilson, D. A. Enzyme-Powered Nanomotors with Controlled Size for (9)Biomedical Applications. ACS Nano 2019, 13 (9), 10191-10200. DOI: 10.1021/acsnano.9b03358 From NLM.
- (10)Hollmann, B., Perkins, M., Chauhan, V.M. et al. Fluorescent nanosensors reveal dynamic pH gradients during biofilm formation. npj Biofilms Microbiomes 7, 50 (2021).



Appendices

Acknowledgments
List of Publications
Research and Data Management
About the Author

Acknowledgments

I would first like to express my gratitude to my Promoter Prof. dr. Daniela A. Wilson, for giving me this amazing opportunity to conduct my PhD thesis in her department and under her guidance at the Systems Chemistry Department, Radboud University. It was always a great pleasure to brainstorm new ideas together and put amazing research into motion. The freedom I had in shaping my projects together with your input has made for some extraordinary research which has taught me so much over the years. It was awesome to see your excitement about biofilms when learning new things about them, which made me even more excited to research them and find answers. I always enjoyed the biweekly meetings which, after finishing the business side, resulted in some coffee chatter about what the puppies were up to again (Sometimes even with one of them present). I am glad I could learn so much from you and am eager to put all that knowledge to the test in my next steps.

Next I need to thank dr. Kevin Neumann, who joined Radboud in 2021. The antifouling research was something I was never too versed in, but working together with you on testing these ylides taught me a lot of new techniques and approaches and together we got some cool papers published. I greatly appreciate the time you took to have some coffee breaks, discuss science or just chat around a bit, and it was good to be able to speak some German, to make sure I don't fully unlearn it and get too rusty. I am excited to have been part of the beginning of your journey at Radboud and wish you all the best in the future.

I would like to express many thanks to Prof. dr. Laura van Niftrik and dr. Robert Jansen, who gave me the amazing opportunity of being a guest researcher in their microbiology department. Without this friendly opening of doors into their department, this thesis would not have been possible.

Sjoerd Rijpkema, my walking chemistry dictionary, thank you for being an invaluable help to this thesis, and an amazing friend who has always been there to cheer me up and take a little break with me. I think you have had your little NMRobsessed hands mingle in every chapter of this thesis somewhere, and I could not be happier about it. I always knew the day was going to be fun when I saw your backpack at your table.

Then, of course, there is the rest of the Wing 8 group, Jelle, Shauni, Serena, Jiawei, Moussa, Jiabin and Danni, Shaohua, Wei, Sandra, Mingchen, Lotte and Helene, most of you were there even when I was just a young master student, but I remember coming up to all of you with guestions, and you always having the time for a coffee break and to help me out, which was one of the reasons I was excited to start my PhD there, because of this amazing open research atmosphere, that just felt like everybody wanted to help drive each other's research forward.

I want to also thank all the hard-working students I had, Laura, Arbaaz, Lucia and Elisa. You all helped me with the workload and the projects I had, and I had a blast supervising you and seeing you grow in your skills and confidence in the lab.

And of course, it can't always just be work, so I have to thank my Physics buddies, Joost, Robert, Manuel, Fabio, and Tjacco. It was always a pleasure to drop into your office, do some pull-ups, and chat a bit. The same goes for Pieter, having some coffee breaks and enjoying some sun and fresh air during experiments was always a welcome break. Also many thanks to Tierk, Lisa, Pieter K., Levy Lotje, I had so much fun with our Fun-day series, and our hangs were always a great break and recharge.

Although they are 634 km away, in Berlin, my family has been a big support, and for that I would like to express my gratitude. Thank you, Helmuth, Sabine, and Laura for being by my side and supporting me. Also tucked away in Berlin, I would like to thank my dear friends Oliver, Amos, and David as well as Emily, who when I came to visit made sure I regained my strength with some cold beers and Risa chicken. Right in the middle of the route from Nijmegen to Berlin, my thanks go to Kelvin, who I could always visit to regenerate on the countryside, and enjoy some nature in good company.

Lastly, my gratitude goes to my amazing partner, Özden, who has been by my side and ensured I never ran out of delicious Muffins and Tiramisu during my writing periods, and who always had an open ear when I needed to just vent a bit, or go on a forest walk with Beans to get out of the house.

Many thanks to all these amazing people, without whom I would not be where I am today!

List of Publications

Berking, B. B.; Mallen-Huertas, L.; Rijpkema, S. J.; Wilson, D. A. Porous Polymersomes as Carriers for Silver Nanoparticles and Nanoclusters: Advantages of Compartmentalization for Antimicrobial Usage. Biomacromolecules 2023, 24 (12), 5905-5914.

Berking, B. B.; Poulladofonou, G.; Karagrigoriou, D.; Wilson, D. A.; Neumann, K. Zwitterionic Polymeric Sulfur Ylides with Minimal Charge Separation Open a New Generation of Antifouling and Bactericidal Materials. Angewandte Chemie International Edition 2023, 62 (41), e202308971.

Berking B. B., Rijpkema SJ, Zhang BHE, Sait A, Amatdjais-Groenen H, Wilson DA. Biofilm Disruption from within: Light-Activated Molecular Drill-Functionalized Polymersomes Bridge the Gap between Membrane Damage and Quorum Sensing-Mediated Cell Death. ACS Biomater Sci Eng. 2024 Aug 23.

Karagrigoriou, D.; Berking, B. B.; Wang, Q.; Sánchez-Cerrillo, D. M.; Galimberti, D. R.; Wilson, D. A.; Neumann, K. Unveiling the Antifouling Potential of Stabilized Poly(phosphorus ylides). ACS Macro Letters 2023, 12 (12), 1608-1613.

Kumari, J.; Paul, O.; Verdellen, L.; Berking, B.; Chen, W.; Gerrits, L.; Postma, J.; Wagener, F.; Kouwer, P. H. J. Conductive Polyisocyanide Hydrogels Inhibit Fibrosis and Promote Myogenesis. ACS Appl Bio Mater 2024, 7 (5), 3258-3270.

Berking, B. B.; Herraiz Benítez, L.; Zhang B.; Münch A.; Wilson A. D.; Quorum Sensing lights the way: Chemotactic Nanomotors target biofilms via quorum quenching mechanisms. Manuscript in Preparation.

Research and Data management

This thesis research has been carried out in accordance with the research data management policy of the Institute for Molecules and Materials of Radboud University, the Netherlands.

For Chapter 2, please refer to https://www.ncbi.nlm.nih.gov/pmc/articles/ PMC10734299/ and https://onlinelibrary.wiley.com/doi/10.1002/anie.202308971. Data Is stored: CNCZ, Radboud University

For Chapter 3, please refer to https://pubs.acs.org/doi/10.1021/acs.biomac.3c00925. Data Is stored: CNCZ, Radboud University

For Chapter 4, please refer to.Data Is stored: CNCZ, Radboud University

For Chapter 5 Data Is stored: CNCZ, Radboud University

We are happy to share any further relevant data under reasonable request.

About the Author



Bela Berking was born on the 9th of December 1995 in Evanston, Illinois, USA. He obtained is Bachelor of Science (B.Sc.) in Biology from the Freie Universität Berlin where he also completed his Master of Science (M.Sc.) in Molecular Biology and Cell Biology. During his Masters Program Bela participated in a 9 month Erasmus+ program to complete his master thesis at Radboud University. After completing his M.Sc. he started his PhD thesis in the Systems Chemistry department under the supervision of Daniela Wilson, researching novel polymer-based solutions to combat pathogenic biofilms formed by P. aeruginosa.

